



Development of a dual sensor polymer-based system for antibiotic detection in water samples.

Oliver David Jamieson

Doctor of Philosophy

Faculty of Science, Agriculture and

Engineering

Submission 02/2022

Abstract

In April 2019, the UN issued a warning that the overuse of antibiotics could lead to 10 million fatalities annually by 2050. It would also be a significant financial burden as there can be losses of €1.6 billion per single strain of antimicrobial resistant (AMR) bacteria, occurring primarily but not limited to the costs of medical care, hospitalisation, and patient care. Infiltration of antibiotics into groundwater arises from multiple sources; agriculture, highly populated residential areas and pharmaceutical effluents. These leached antibiotics journey to river systems cause selective pressure, thereby giving rise to accelerated AMR development. One route for aiding this issue is to slow the growth rate the emergence of AMR by controlling the levels of antibiotics that gain entry to water systems. To monitor this, a low-cost and reliable sensor platform is needed that can rapidly and on-site identify contaminated areas. Molecularly Imprinted Polymers (MIPs) are synthetic receptors that have potential for specific detection of contaminants in complicated matrices but have found limited commercial applications.

The work within this thesis will explore the rational design of MIPs, their optimisation for a plethora of targets and the investigation of various applications to exploit their favourable characteristics when deployed as sensor platforms. Looking at how these imprinted polymers have been developed and utilised in recent times (primarily 2010-2020) and assessing any limitations encountered. These limitations have holstered MIP use, giving rise to the need for the critical review, which has been carried out in this thesis, on what development is needed to boost their applications to convert them into a mainstream commercial tool.

Most MIP-based sensor systems focus primarily on a single analysis technique. Chapter 3 sees a novel, dual detection system developed which facilitates direct validation of the results and therefore can realise reliable detection of antibiotics in aqueous samples. Fluorescent monomers have been incorporated into the MIP complex allowing for fluorescent analysis as well as thermal, producing a dual sensor platform thus vastly enhancing the reliability of the biosensor.

Two applications of MIPs, that have been deployed as sensors, have been experimentally assessed. A focus on mounting these polymers onto Screen Printed Electrodes (SPEs) and the subsequent thermal analysis will be describe in chapter 4. This work comprised of a comparison of two techniques was carried out to determine the most appropriate method for attaching the polymers to the surface of the SPE, direct polymerisation onto the SPE against dropcasting of MIP particles synthesized by free radical polymerisation on the SPE surface. The direct polymerisation proved to afford MIP-modified SPEs to have higher levels of binding affinity. Chapter 5 explores an investigation into the evolution from small molecule targets to large macromolecules including whole bacteria. This proof-of-concept study saw a yeast mixture used as a target for MIP detection since yeast resembles bacteria in size and shape but does not need to be handled in a certified biosafety lab.

A full evaluation of the work carried out concludes the thesis with an aim to gauge how the work undertaken will contribute to the development of a new division of quantitative sensor platforms. Secondly, the work produced will construct foundations for what is still needed to push the use of MIPs into commercial use to combat the rise in AMR.

Acknowledgments

Throughout this work, I have been mentored and supported by my supervisor Dr Marloes Peeters. Marloes has given me the tools, knowledge and encouragement to carry on working through a city and university change as well as a global pandemic. This work would not have been possible without her constant care and aid, I will forever be grateful for her supervision and friendship.

Dr Katarina Novakovic gave solid guidance and advice throughout my time at Newcastle University and made sure the transition of university was as stress free as possible. Her expertise proved invaluable throughout.

Dr Knut Rurack from BAM Bundesanstalt für Materialforschung und -prüfung offered immense insight and knowledge into the world of fluorescent analysis, which has most certainly promoted the work that was carried out.

The Peeters research group has introduced me to work associates that have aided me significantly throughout my work. Alexander, Jake, Pankaj and Jack have been of great support to me and have offered me great inspiration when I needed it the most.

Dr Emma Foster and Dr Alex Laude from the bioimaging suite gave access and expertise on fluorescent microscopy which proved invaluable to the project.

Appreciation to Manchester Metropolitan University for funding and supporting my first year of the PhD. My colleagues from Manchester Metropolitan University formed a great support network for me and I am immensely grateful for all the help and advice they have given me.

My mother, Vivien, has been of major support throughout my education and is a constant inspiration in my research career. Thank you for backing me through every endeavour and for giving me every opportunity. Brother Mark, thank you for all the calls for support and the constant advice, it was a greatly

valued and appreciated. My father, Maurice, for building my confidence early on and teaching me that perseverance is key, I am indebted to you.

My friends from Manchester, Ireland, and Newcastle alike. All of you have made this possible. From the late-night phone calls, the walks to discuss my work and all the times you were there to support me I thank you endlessly. You have all been so much more important to me during this than you know.

To the Donaldson family who took me in during the pandemic, thank you for sheltering me and helping me keep my family safe during an unforeseen difficult time.

To anyone else who has in anyway helped me with this work, please know I am immensely grateful and thankful for your contribution.

Considerations

The enclosed thesis was carried out through the Covid-19 pandemic. Although the project was completed, it has been impacted. The primary laboratory was closed for over 2 months which stopped all experimentation. Another knock-on effect was the severe limitation on available lab consumables (gloves, glassware etc) due to the diverted supply to aid the pandemic, this meant lab experimentation could only be carried out as and when these resources were available, the limitation on such supplies lasted approximately 6 months. With PPE only sporadically available, experimentation was hindered as and when availability arose, which had a significant effect on experimentation output. A delay in an arranged internship at BAM Bundesanstalt für Materialforschung und –prüfung, under the supervision of Dr Knut Rurack was also experienced. The inability to have access to other lab and the instrumentation within them caused issues with characterisation and analysis of polymers produced, primarily linked to the analysis carried out by the inverted fluorescent microscope which is located in a hospital lab. The pandemic also caused major limitations in regard to conferences and face to face networking

Table of Contents

| | |
|--|-----------|
| Abstract | 2 |
| Acknowledgments | 4 |
| Considerations | 6 |
| Chapter 1. Approaches to the Rational Design of Molecularly Imprinted Polymers Developed for the Selective Extraction or Detection of Antibiotics in Environmental and Food Samples | 20 |
| 1.1 Abstract | 20 |
| 1.2 The Need for Detection of Antibiotic Residues | 21 |
| 1.2.1 Antimicrobial Resistance (AMR) and Its Acceleration through Water Contamination | 21 |
| 1.2.2 Limitations of Current Antibiotic Detection Platforms in Different Media | 25 |
| 1.2.3 Potential of Using MIPs for Antibiotic Detection and Extraction | 27 |
| 1.3. Rational Design of MIPs for Antibiotics | 34 |
| 1.3.1 Computational Modelling | 34 |
| 1.3.2 NMR Techniques Aiding MIP Production | 37 |
| 1.3.3 Isothermal Titration Calorimetry (ITC) | 40 |
| 1.3.4 Infrared Spectroscopy | 41 |
| 1.4 MIP Morphologies | 43 |
| 1.4.1 Use of Copolymers | 43 |
| 1.4.2 Integration of Fluorescent Moiety | 44 |
| 1.4.3 Using Redox Probes to Monitor MIP/Target Binding Phenomena | 48 |
| 1.5 Different MIP Production Methods | 51 |
| 1.5.1 Screen-Printing Techniques | 51 |
| 1.5.2 Electrodeposition of MIP Layers on Transducer Surfaces | 53 |

| | |
|---|-----------|
| 1.5.3 Grafting from/to CoreShell Nanoparticles | 55 |
| 1.5.4 Solid-Phase Imprinting: Immobilization of the Template on a Solid Support | 56 |
| 1.6 Outlook on the Future of Commercial MIP Sensors for Antibiotics | 58 |
| 1.7 Aim of the study | 60 |
| Chapter 2- General Methodologies and Chemicals | 63 |
| 2.1 General Chemicals | 63 |
| 2.2 MIP polymerisation | 64 |
| 2.2.1 Production of polymer microparticles using free radical polymerisation | 65 |
| 2.2.2 Film polymer production | 65 |
| 2.3 Glass cleaning and functionalisation | 66 |
| 2.4 Batch rebinding | 66 |
| 2.5 Fluorescent Analysis | 68 |
| 2.6 HTM analysis | 69 |
| Chapter 3. Development of a dual detection polymer-based sensor for antibiotics in aqueous samples. | 74 |
| 3.1 Abstract | 74 |
| 3.2 Introduction | 74 |
| 3.3 Experimental | 77 |
| 3.3.1 Equipment and Reagents | 77 |
| 3.3.2 Synthesis of Polymers | 77 |
| 3.3.3 Batch rebinding | 80 |
| 3.3.4 HTM analysis | 80 |
| 3.3.5 Fluorescent Analysis | 81 |
| 3.4 Results and Discussion | 84 |
| 3.4.1 Synthesis of MIPs | 84 |
| 3.4.4 Fluorescent Analysis | 89 |

Chapter 4- Functionalisation of Molecularly Imprinted Polymers onto Screen Printed Electrode for the Detection of the Antibiotic Amoxicillin in Aqueous

Samples..... 102

| | |
|---|-----|
| 4.1 Abstract | 102 |
| 4.2 Introduction | 103 |
| 4.3 Experimental | 106 |
| 4.3.1. Equipment and reagents | 106 |
| 4.3.2. MIP and NIP microparticle syntheses | 106 |
| 4.3.3. Batch rebinding experiments evaluated with optical detection | 107 |
| 4.3.4. Thin film polymerization | 108 |
| 4.3.5. Electrochemical deposition of polypyrrole | 108 |
| 4.3.6. Scanning electron microscopy (SEM) | 109 |
| 4.3.7. HTM measurements with MIP-modified SPEs | 109 |
| 4.4 Results | 110 |
| 4.4.1. Batch rebinding results | 110 |
| 4.4.2. Detection of amoxicillin using MIP microparticles | 114 |
| 4.4.3. Detection of amoxicillin using MIP thin films | 116 |
| 4.5 Conclusions | 120 |

Chapter 5- Electropolymerised Molecularly Imprinted Polymers for the Heat-Transfer Based Detection of Microorganisms: A Proof-of-Concept Study using

Yeast 123

| | |
|------------------|-----|
| 5.1 Abstract | 123 |
| 5.2 Introduction | 124 |
| 5.3 Experimental | 126 |

| | |
|---|------------|
| 5.3.1 Reagents | 126 |
| 5.3.2 MIP and NIP syntheses | 127 |
| 5.3.3 HTM measurements of yeast with MIP-modified SPEs | 129 |
| 5.4 Results | 130 |
| 5.4.1 IR and SEM analyses to determine surface structure of MIP-modified SPEs | 130 |
| 5.4.2 Thermal resistance measurements for yeast using MIP-modified SPCEs | 133 |
| 5.4 Conclusions | 138 |
| Chapter 6- General Conclusions and Outlook..... | 141 |
| 6.1 Conference contributions- | 141 |
| 6.2 Scientific journal contribution- | 142 |
| 6.3 Overview of contribution to knowledge | 144 |
| 6.4 Final remarks and future scope | 147 |
| Chapter 7- Appendix | 194 |
| Chapter 8. References..... | 150 |

List of Figures, Tables, Equations and Appendices

List of Figures

Figure 1.1. Routes of entry of antibiotics into the environment. Green arrows displaying antibiotic removal from the environment, red arrows showing the entry routes of antibiotics, and orange arrows explaining that extraction methods are not fully efficient at antibiotic removal. (Selected for front cover of PSSa journal) - 18

Figure 1.2. The several steps of molecular imprinting with a) precomplex with the example template of penicillin G surrounded by crosslinker and generic acrylate functional monomers, b) polymerised MIP, and c) amoxicillin molecule extracted, leaving an empty cavity to be used for rebinding 25

Figure 1.3. Preparation of hollow MIPs using covalent and noncovalent imprinting for an amino acid sequence, demonstrating the “sacrificial spacer” method using $K_2Ti_4O_9$ as a spacer molecule. 27

Figure 1.4. Representation of the increased research in the field via the number of publications including computational methods in MIP design between 2000 and 2019. The data obtained through Web of Science using the keywords “Molecularly Imprinted Polymer,” “MIP,” and “Computational.” 30

Figure 1.5. 1H NMR spectra of 2,4-D with increasing concentration of 4-VP showing changes in the chemical shifts used to rationalise a low crosslinked system that allows for higher levels of specificity and selectivity. 35

| | |
|--|----|
| Figure 1.6. Formation of an MIP layer on the surface of QDs for an antibiotic, sulfadiazine (SDZ). The polymer layer can then have the target extracted, breaking the electron transfer between SDZ and the QDs, which results in a decrease in the fluorescence signal. | 40 |
| Figure 1.7. Flow diagram showing classification of outer- and inner-sphere probes. | 43 |
| Figure 1.8. a) Solid-phase synthesis of nanoMIPs. In this example, a protein is shown as the template molecule. b) Representative TEM of nanoMIPs. | 52 |
| Figure 2.1. In-house designed and printed flow cell stage holder in which inlet and outlet tubes are fastened into position through each clip at either end. | 63 |
| Figure 2.2. Schematic of the flow cell used unless specified (see Chapter 3). An O ring and a copper block is placed on top of the flow cell to create a seal. | 64 |
| Figure 2.3. In-house designed and printed platform to hold the HTM flow cell secure in which the inlet and outlet tubes are fed through the channels at either end. | 65 |
| Figure 2.4. HTM flow cell mounted onto printed holder and placed in the HTM set up couples with an incubator. | 65 |
| Figure 3.1. Structure of a) amoxicillin and b) tetracycline. | 70 |
| Figure 3.2- image of the individual fluorescent microscope set up. | 76 |

Figure 3.3. depiction of the flow cell set up, demonstrating the glass cover slip over the flow chamber to allow for fluorescent analysis. 76

Figure 3.4. Example region of polymer modified glass electrode showing both polymer covered (shown by the white boxes) and uncovered regions (shown by the red box). 78

Figure 3.5. a) specificity and selectivity study of MIP A, showing its binding capabilities compared to that of NIP A and also to other targets and b) the specificity study of MIP T (using 10 mM, 25 mM, 40 mM, 55 mM and 70 mM tetracycline solutions). 80

Figure 3.6. a) Comparison of the thermal resistance of MIP T (black and red) and NIP T (grey and magenta) upon injections of increasing tetracycline solution and b) displaying the dose response curve for MIP T. -82

Figure 3.7. Specificity study of MIP A via fluorescent analysis during the introduction of amoxicillin. 83

Figure 3.8. Specificity of MIP A with 0.03 mM amoxicillin in PBS, displaying the difference in fluorescent intensity exhibition between that of the MIP and the NIP. 84

Figure 3.9. Comparison of target concentration effect on fluorescent intensity produced by MIP A. 85

Figure 3.10. Fluorescent intensity of MIP and NIP T on introduction of PBS and TC (0.25 mM). 88

Figure 3.11. Capture of MIP films polymerised onto functionalised glass. Scores have been cut through the polymer to act as reference points. 89

Figure 3.12. monitoring of fluorescent intensity between MIP and NIP with tetracycline and a PBS control, with guideline for readers eye to follow. 90

Figure 3.13. Selectivity study via fluorescent microscopy of MIP T, comparing the effects of three different solutions on the fluorescent intensity emitted by the polymer, with guideline for readers eye to follow. 92

Figure 4.1. Structures of a) amoxicillin and b) nafcillin showing matching β -lactam ring pharmacophores. 98

Figure 4.2. Binding isotherms of the polymerised MIP/NIPs upon exposure to Amoxicillin solutions in PBS. MIP 1 (filled squares) and NIP 1 (hollow squares), MIP 2 (filled circles) and NIP 2 (hollow circles), and MIP 3 (filled triangles) and NIP 3 (hollow triangles). 105

Figure 4.3. Selectivity batch rebinding of MIP 2 (filled symbols) and NIP 2 (hollow symbols) with amoxicillin (squares) and nafcillin (circles) in PBS. 106

Figure 4.4. **A)** The raw HTM data plot of R_{th} *versus* time for the addition of amoxicillin (1 – 500 nM) in PBS to an SPE functionalized with bulk UV polymerized MIP (red) and NIP (black). **B)** Comparison between the absolute R_{th} values obtained from the HTM for a MIP functionalized SPE (red circles) and NIP functionalized SPE (black). 108

Figure 4.5. **A)** The raw HTM data plot of R_{th} *versus* time for the addition of amoxicillin (1 – 500 nM) in PBS to an SPE functionalized with a direct UV polymerized MIP (red) and NIP (black). **B)** Comparison between the absolute R_{th} values obtained from the HTM for a MIP functionalized SPE (red circles) and NIP functionalized SPE (black). 110

Figure 4.6. A) The raw HTM data plot of R_{th} versus time for the addition of amoxicillin (1 – 500 nM, red) and nafcillin (1 – 500 nM, black) in PBS to an SPE functionalized with a direct UV polymerized MIP. B) Comparison between the absolute R_{th} values obtained from the HTM for a MIP functionalized SPE with additions of amoxicillin (red circles) and nafcillin (black). 111

Figure 5.1. A) FTIR result showing the generation of PPy on the surface of the electrode. B) White light profilometry of the PPy layer generated on the surface of the electrode. 122

Figure 5.2. A) Cyclic voltammograms for the formation of PPy on the surface of the SPCE performed at 100 mV s⁻¹. B) SEM image for the formation of PPy patches on the surface of the SPCE using cyclic voltammetry. C) Chronoamperomogram for the formation of a PPy layer on the surface of an SPCE at +0.98 V vs Ag|AgCl for 100 s. D) SEM image for the formation of a PPy layer on the surface of an SPCE using chronoamperometry. 123

Figure 5.3. A) Schematic diagram of the flow cell used throughout the thermal measurements in this work, comprising of a single thermocouple inserted into a main chamber with a flow inlet and outlet. B) HTM raw data plot of the measured R_{th} versus the time for sequential additions of yeast cells to a MIP-coated SPCE produced using CV. C) Plot of the change in measured R_{th} against the concentration of added yeast cells to a HTM set-up with both a MIP and NIP coated SPE. 125

Figure 5.4. A MIP-modified electrode (prepared with laboratory strain of yeast) was mounted into the HTM set up and stabilised in a standard PBS solution (pH=7.4). While there is some minor drift in the signal, addition of a suspension of yeast (1.0×10^7 CFU/mL) in PBS led to a significant increase in the thermal resistance due to binding of yeast in the activities on the surface. This provided proof-of-concept and in following experiments, yeast from a complex mixture was considered. 126

Figure 5.5. Measurements with the white light profilometer of a MIP-modified electrode after HTM measurements confirmed the presence of yeast on the surface. 127

Figure 5.6. A) Plot of the percentage change in the measured R_{th} against the concentration of added yeast cells to a HTM set-up with both a MIP and NIP coated SPCE using chronoamperometry. B) Plot comparing the percentage change in R_{th} for the MIP platforms produced by chronoamperometry and cyclic voltammetry. Error bars relate to the standard deviation of the experiment. 128

List of Tables

| | |
|--|-----|
| Table 1.1. Summary of commercial MIP based sensors that have been developed. | 23 |
| Table 2.1- General chemicals used throughout the presented thesis. | 57 |
| Table 3.1. Compositions of bulk polymers synthesised in this work. | 72 |
| Table 3.2. compositions for polymers synthesised as thin films. | 73 |
| Table 4.1. The composition of the different MIPs, listing the amount of template, functional monomer, crosslinker monomers, initiator, and porogen used. | 100 |
| Table 4.2. The amount of binding for MIP and NIP at $C_f = 0.5$ mM. | 104 |
| Table 6. 1 Listed research exchanges. | 132 |

List of Equations

Equation 1.1. The binding energy/score (ΔHB) between a template and functional monomer based on heat of formation (ΔH_f). 29

Equation 2.1. C_i is the initial concentration (mM), C_f is the final concentration (mM) and C_b is the concentration bound to the polymer (mM). 61

Equation 2.2. the IF was calculated by dividing the S_b of the MIP by S_b of the NIP at the same C_i .-62

Equation 2.3. Thermal resistance (R_{th}) calculated by dividing the thermal resistance at the solid liquid interface (T_1-T_2) by the input power (P). 66

Equation 2.4. Calculation for the LoD where SD_{blank} = standard deviation of the PBS blank. 66

Equation 3.1. Thermal resistance (R_{th}) calculated by dividing the thermal resistance at the solid liquid interface (T_1-T_2) by the input power (P). 74

Appendices

Appendix A. MIP A fluorescent intensity study with ascorbic acid to act as a radical scavenger, showing significant percentage error. 176

Appendix B. Custom Python script for fluorescent analysis for quantification of Microscope data. 177

| | |
|---|-----|
| Appendix C. Repeat dose response curve of HTM data for MIP T and NIP T with tetracycline solution injections. | 180 |
| Appendix D. SEM image (2000× magnification) of MIP 2 microparticles immobilized onto an SPE using polypyrrole. (B) SEM image (1000× magnification) of thin film of polymer made directly on an SPE. | 181 |
| Appendix E. After polymerisation (1000x zoom), there was clear presence of the yeast on the SPCEs. Different washing strategies were employed, where washing twice with hot water led to full removal of yeast on the surfaces. Washing once was not sufficient whereas washing with organic solvents, such as methanol, led to damaging the polymer layer. | 182 |
| Appendix F. A MIP-modified electrode was exposed to suspensions with increasing concentrations of yeast (from 10^2 to 10^6 CFU/mL) in water. However, at elevated temperature no significant increases were found. | 183 |
| Appendix G. Published paper on the need for detection of antibiotic detection | 177 |
| Appendix H. Published paper on the detection of amoxicillin via MIP modified SPEs. | 239 |
| Appendix I. Published paper on a proof-of-concept yeast sensor based on a MIP modified SPE. | 265 |

**Chapter 1. Approaches to the Rational Design of Molecularly Imprinted Polymers
Developed for the Selective Extraction or Detection of Antibiotics in
Environmental and Food Samples**

**(Published as O. Jamieson *et al.*, *Physica Status Solidi (A) Applications and
Materials Science*, DOI:10.1002/PSSA.202100021)[1]**

1.1 Abstract

The World Health Organisation (WHO) reported antimicrobial resistance (AMR) as a global threat comparable to terrorism and climate change. The use of antibiotics in veterinary or clinical practice exerts a selective pressure, which accelerates the emergence of antimicrobial resistance. Therefore, there is a clear need to detect antibiotic residues in complex matrices, such as water, food, and environmental samples, in a fast, selective, cost-effective, and quantitative manner. Once problematic areas are identified, extraction of the antibiotics can then be carried out to reduce AMR development. Molecularly imprinted polymer (MIPs) are synthetic recognition elements produced through the biomarker of interest being used as a template in order to manufacture tailor-made ligand selective polymeric recognition sites. They are emerging steadily as a viable alternative to natural recognition elements such as antibodies, especially given their low-cost, superior thermal and chemical stability that facilitates on-site detection, simplified manufacturing process, and avoiding the use of animals in the production process. This chapter will see a critical review of literature from primarily 2010–2021 on rational design approaches used to develop MIPs for sensing and extraction of antibiotics, providing an outlook on crucial issues that need to be tackled to bring MIPs for antibiotic sensing to the market.

1.2 The Need for Detection of Antibiotic Residues

1.2.1 Antimicrobial Resistance (AMR) and Its Acceleration through Water Contamination

The word “antibiotic” was first used to coin any small molecule that could hinder the proliferation of microbes. The study and experimentation of penicillin derived from fungi and the discovery of soil bacteria produced antibiotics like tetracycline and chloramphenicol brought with it the age of antibiotics [2]. There is a vast array of different antibiotic families from fluoroquinolones to β -lactams to tetracyclines to name a few [3]. Each antibiotic within the family will possess the characteristic pharmacophore of that type of antibiotic for example the β -lactam ring of penicillin’s. Each pharmacophore is the active backbone of the drug molecule which enables it to interact with its target to a desired effect, in this case the inhibition of bacterial growth [4]. Each antibiotic family interacts with microbes in different ways. Depending on the pharmacophore present, the antibiotic will target a different antigen in different active sites of the bacteria and will inhibit the proliferation of the cell in a different way. For example, β -lactams will target penicillin binding proteins on the surface and hinder cell replication by inhibiting cell wall synthesis. Tetracyclines target the 30S ribosome causing mistranslation of proteins via mismatching the tRNA, this ultimately leads to the inhibition of protein synthesis [5]. The breadth of different antibiotics which can target different bacteria species has revolutionised health care worldwide however the misuse of antibiotics has become an lead to the antimicrobial resistance (AMR) crisis [6]–[8]. In 1945, Alexander Fleming noted in his Nobel prize acceptance speech that the ignorant use of antibiotics would lead to resistance towards them. As he predicted, 2022 saw antibiotic resistance labelled the leading cause of death worldwide [9]. Antibiotics like amoxicillin which are excreted in a 40-80% unmetabolized state, with a half-life of nine days [10] leads to low levels of the pharmaceutical present in the environment. These low concentrations of the antibiotic are non-fatal and allow microbes to grow resistant towards them, through selective pressure. Selective antibiotic pressure is one of the processes in which bacteria colonies are in the presence

of low levels of antibiotics [11]. The bacteria cells multiply which brings about inherent mutations as is natural with most cell replication. These mutations can cause a host of various characteristics and properties, one of which is resistance towards antibiotics. With the antibiotics present in the environment killing off the non-resistant bacteria, only the resistant bacteria are left to replicate and divide. This leads to a colony of resistant bacteria and the process continues leading to the relevel of resistant becoming more significant. This has led to critical implications for the use of antibiotics.

The World Health Organisation (WHO) predicts ten million annual deaths, globally, due to antibiotic-resistant infections, by 2050 [12]. The rise in antimicrobial resistance (AMR) bacteria is therefore considered a global threat. Cassini *et al.* [13], studied deaths linked to drug-resistant infections in Europe and concluded that 700 000 infections in 2015 were related to resistant bacteria, of which 5% were fatal. Similarly, a study by Ventola [14] demonstrated that two million patients in the USA developed hospital-acquired infections (HAIs), of which 99 000 cases proved fatal, a significant proportion of which were also caused by resistant bacteria. In addition to their impact on mortality, these resistant bacteria also pose a serious financial burden. Misurski *et al.* [15], demonstrated that incorrect antibiotic prescription was estimated to be a \$211 million burden, per year, in the USA alone. These costs are ascribed to prolonged hospitalisation, increased morbidity, greater requirement for critical care support, delayed return to the workforce, and consequent economic impact associated with reduced productivity. Moreover, recent events have led to concerns about a new surge in AMR due to the use of antibiotics in patients with COVID-19 [16]. While antibiotics are ineffective against viruses, they can be used in patients with confirmed COVID-19 to prevent or treat secondary bacterial infections: an early study from China showed that secondary infections and HAIs were present in half of all deceased COVID-19 patients [17]. Surprisingly, no current inclusions of antimicrobial stewardship programs (ASPs) in disaster planning or emergency response preparedness efforts have been legislated, but there is a strong drive from the medical and scientific community to integrate ASPs into disaster planning and appoint stewards in a more formal role after the COVID-19 outbreak [18]. Another concerning issue is the possibility of antibiotics leaching into water systems, via the effluents of the pharmaceutical industry, agriculture, and hospitals (Figure 1.1).

However, antibiotics are critical to the continuation of modern-day living so a solution is needed that does not reduce the ability to use them. Behera *et al.* [19], studied the introduction of pharmaceuticals, including antibiotics, into the environment in an industrial city in South Korea. Among the antibiotics screened, standard water treatments achieved antibiotic removal between only 10 and 70%. Sulfamethazine was found to have a removal efficiency below 30%, suggesting that the majority still entered further waterways. Conversely, caffeine, a common contaminant, and a standard indicator molecule, showed a 99% removal efficiency under the same conditions. This exemplifies how using caffeine as an anthropogenic marker [20] may therefore yield false confidence in current purification processes.



Figure 1.1. Routes of entry of antibiotics into the environment. Green arrows displaying antibiotic removal from the environment, red arrows showing the entry routes of antibiotics, and orange arrows explaining that extraction methods are not fully efficient at antibiotic removal. (Selected for front cover of PSSa journal- March 2021 Volume 218. Issue 13) [1]

Effluents from modern-day infrastructure are not the only route of antibiotics into the water systems. Alternative entry routes include livestock feed and excrement. Watanabe *et al.* [21], led a study into the waste outputs of two dairy farms in the USA. It was found that monensin, a polyether antibiotic commonly found in animal feeds, leached into ground water assumedly due to relatively high monensin concentrations found in manure. Tasho *et al.* [22], highlighted that veterinary antibiotic use in livestock and the resulting antibiotic residue in livestock manure can be as high as 216 mg L^{-1} . Given that over 24 million hectares of farming worldwide is conducted organically [23], which equates to a significant amount of natural fertiliser (which has residual levels of antibiotics in from the animal it as sourced from) use, the critical role of agricultural practices in the leaching of antibiotics into the environment is highlighted. Watkinson *et al.* [24], traced the journey of drinking water all the way back to hospital effluent, evaluating the concentration of 28 antibiotics at different stages in Southeast Queensland, Australia. Some antibiotics were detected at concentrations of up to $64.0 \text{ } \mu\text{g L}^{-1}$ in Wastewater Treatment Plant (WWTP) influent, compared with the maximum concentration in the effluent being $3.4 \text{ } \mu\text{g L}^{-1}$. Given that $1 \text{ } \mu\text{g L}^{-1}$ of certain antibiotics was proven to have significantly negative effects on aquatic life [25], it is clear that concentrations of this magnitude are detrimental to the ecology and environment. It was shown that rivers having no effluents from WWTPs in their watershed have a significantly lower residual antibiotic concentration, demonstrating the broader impact of hospital pharmaceutical waste. A study based in Ter River, Spain, by Rodriguez-Mozaz *et al.* [26], incorporated a wider range of antibiotics, showing that fluoroquinolones had the highest residual concentration in hospital effluents up to 14.4 mg L^{-1} , which is most likely due to their enhanced stability compared with other common antibiotics. Both studies show significant presence of antibiotics in water systems from developed countries, portraying that even countries with modern wastewater treatment infrastructure are being impacted by antibiotic presence in water systems. The European Water Framework Directive is a legislative department set up in 2000, to ensure water safety. Carsten von der Ohe *et al.* [27], aimed to improve the existing European Water Framework Directive by classifying chemicals of critical importance in terms of their potential to cause harm. With more in-depth understanding of the harm AMR is causing, improvements to the legislation

can lead to more appropriate restrictions on antibiotic presence in the environment. Despite this, Carvalho *et al.* [28], subsequently noted the lack of relevant regulations regarding the same issue in the European environmental water quality standards. It is therefore of critical concern that carriers of antibiotics, such as meat or milk, and common water micropollutants are regulated; however, unlike in meat (including fish) and milk, there remains limited scrutiny of antibiotics in water systems. A system to accurately measure and follow antibiotics from a variety of media, specifically and critically including aqueous media, must be legislated. The current lack of antibiotic regulation and therefore a need for detection within Europe's waterways could have dire consequences and certainly contribute to exacerbating AMR in the future. Hence, there is a need to identify and more closely monitor waste streams that may contain antibiotics and ultimately enforce new regulations for their processing and removal. However, these testing and analyses methods must be cost effective and financially viable if they are to be broadly implemented.

1.2.2 Limitations of Current Antibiotic Detection Platforms in Different Media

When considering a majority of sensor platforms, a recognition element is required. Naturally existing recognitions elements exist in the form of antibodies which have been used extensively throughout sensor development to date [29], [30]. They work on the basis of a “lock and key” approach where an antibody has a unique active/recognition site that is the complimentary shape of that to the recognition site on a target [31].

Although a vast range of sensors exploit antibodies, other recognition elements exist as do other means of detection. Extensive efforts are required for the research and development of novel detection systems for different families of antibiotics and to be able to do so in different media. Common detection techniques for sensing antibiotics in samples such as muscle and blood serum include biosensors and ELISA [32] however the “gold standard” detection for antibiotics in water is through liquid chromatography-mass spectroscopy (LC-MS). For example, HPLC-MS has been used for detection of antibiotics used in bee keeping in which a vast array of targets could be detected with Limit of Detections (LoD) as low as 0.2 ng g⁻¹ [33]. While highly reliable and powerful, analysis techniques such as LC-MS bring inherent drawbacks

such as the need for elaborate and expensive instrumentation, skilled personnel to carry out and analysis the technique [34]. With other draw backs such as complex sample preparation techniques required, there is a clear need for development of a significantly simpler, onsite sensor platform. Fast onsite detection platforms are currently in existence however they bring with them their own drawbacks. A paper analytical device or PAD, has been developed to detect differences in quality of antibiotics present in water which allow for the detection of a broad range of antibiotics [35]. However, they are purely qualitative, have a short shelf life and have a specific temperature range in which the sensor can be used, critically affecting its level of usefulness. Another PAD has been developed which has quantitative capabilities with low-cost production and mass producible traits [36]. This system was developed for the detection of oxytetracycline and employed the use of cellulose paper coupled with various metal ions such as iron and copper. The primary drawback of a test such as this is this, is its need for a stable pH which when testing in different aqueous environments will be inevitably differing. Although onsite platforms exist, such as the aforementioned examples, a quantitative platform that is mass producible, requires simplistic operation and can be used in various environments is in need. In a study, Khaskheli *et al.* [37], displayed a procedure for the screening of β -lactam antibiotics in milk using a qualitative field disc assay. Despite encouraging results, the biggest drawbacks of the systems were 1) the 24 hr turnaround time and 2) the extensive sample preparation required. The first issue was originally addressed by Knecht *et al.* [38], with the use of an automated microarray for simultaneous detection of ten antibiotics in milk; however, this system required costly infrastructure and apparatus. Wang *et al.* [39], expanded the scope to meat and aquatic products; after these were minced and extracted, ultraperformance liquid chromatography was used to study residual levels in the range of 0.05 ng g^{-1} in meat and $0.2\text{--}5.0 \text{ ng mL}^{-1}$ in milk. A more detailed review of antibiotics detection was released by Pikkemaat [40]. From this work, and the studies provided beforehand, it emerges that the most common analysis technique in the first decade of the 2000s involved microbial screening assays: whilst these are cost effective, they are time-consuming and do not offer quantitative results. Baquero *et al.* [41], gave an oversight as to the main ways in which antibiotics are detected in water samples. Depending on the analyte of interest, common detection systems include electrophoretic and

chromatographic techniques as well as voltammetry and amperometry detection systems. This study shows that several antibiotics can be accurately monitored in a wide range of media and by different detection methods. However, all these techniques required lab environment, time-consuming procedures, and skilled personnel. Smith *et al.* [42], used a commercially available test kit that was modified to enable detection of antibiotics in water systems, trying to optimise the detection. The study provided a qualitative test for antibiotics but lacked the critical quantification. While these in-field testing kits are of promise due to the rapid and on-site detection of antibiotics that will yield more accurate information and simplicity of operation even for nontrained users, further development is still required to increase their commercial usability. Colorimetric bacterial inhibition approaches and lateral flow immunoassays are common for on-site detection of antibiotics. However, colorimetric bacterial inhibition tests require large sample volumes and are limited by poor sensitivity and complex user protocols, whereas lateral flow immunoassays require user intervention for quantifying results [43]. Through this review on literature, a sensor that is quantitative, mass producible, simplistic to operate and can be used in various environments sensor will be considered through the use of MIPs which present a viable alternative whilst overcoming drawbacks of current sensors.

1.2.3 Potential of Using MIPs for Antibiotic Detection and Extraction

MIPs are custom-built, synthetic recognition sites, designed for a specific target molecule [44]. These synthetic receptors can be used in place of antibody-antigen, enzyme-substrate, or ligand-receptor interactions. MIPs indeed can be fabricated to have similar, if not better, affinity and selectivity than their naturally occurring counterparts [45] and crucially when no naturally occurring antibodies exist. The synthesis of MIPs can be accomplished in non-specialist laboratories, with nondedicated equipment, and is often seen as a relatively simple process, whilst also producible by conventional free radical polymerisation. However, its simplicity might be misleading and can mask the fact that it involves multiple and often interdependent variables. The ways in which these affect and change the properties of the resulting polymers are, in fact, quite complex and require a good understanding of molecular recognition

theory, thermodynamics, and polymer chemistry [46]. The concept of MIPs and their potential usefulness in multiple fields of scientific research have been gaining significant interest since the early 1990s when non-covalent imprinting was introduced [47]–[49]. Despite the obvious benefits of MIPs over naturally occurring recognition biomolecules, particularly their increased stability and specificity, as well as their low cost, ease of production, and ability to target molecules for which natural receptors do not exist, [50], [51] they are yet to garner widespread and commercial success. MIPs were initially found to be highly suitable for application in chromatography [52]–[54], especially liquid chromatography [55], [56]. Curti *et al.* [57], developed the first truly functional silica derived-imprinted polymer systems, which subsequently became a common commercial application for MIPs in the chromatography field. Significant advances in imprinting techniques and new synthetic methodologies, along with their excellent recognition specificity and structural predictability, make them a valuable alternative in the recognition systems landscape. This in turn has opened their potential use to a wide variety of applications including that of antibiotic sensing [58], [59].

After the development of a noncovalent fabrication method by Mosbach Arshady and co-workers [60], and modifications thereof, the use of these synthetic ligands has continued to grow. This is evident by the exponential increase in research papers over the past 20 years. To date the use of MIPs has mostly been limited to academic research. Although MIPs have found their way into several commercial markets (Table 1.1), with further exploration, they could be implemented even further. Whitcombe and co-workers [61] stated that MIPs could seize 1–3% of the separation techniques market, worth \$1.19 billion, based predominantly in the chromatography column sector alone. MIPs can be easily synthesised by bulk polymerisation, ground, mechanically sieved, and packed in a column [62]. This method, though crude, is simplistic and versatile. More specifically, monolithic MIP columns have been later prepared directly inside stainless steel columns or capillary columns to solve the problems of non-homogeneous of the binding sites and particle size [63], [64]. High performance liquid chromatography (HPLC) has often seen the use of MIPs as a stationary phase in the racemic resolutions of several species [65] including amino acid derivatives [66], [67] and drugs [68], [69], though often excessive tailing and peak broadening are the

limiting factors for their use and commercialisation for this purpose [70]. Another important area of analytical chemistry, where imprinted polymers have established themselves, is solid-phase extraction (SPE) [70]–[75]. Sigma-Aldrich and Biotage sell MIPs for the highly selective extraction of trace analytes from complex matrices [76]–[78]. Use in commercialisation of MIPs has been limited as their integration into the sensor platforms is not straightforward. In earlier development stages, MIP microparticles prepared by free-radical polymerisation were lacking in affinity and the grafting-on and in situ synthesis techniques were not as refined as they are now [79]–[82].

Table 1.1. Summary of commercial MIP based sensors that have been developed.

| MIP | Company | Description |
|-------------------------------------|------------------------------|--|
| MIPs cartridges for extraction [83] | <i>Acros (SupelMIP)</i> | Solid phase extraction of 14 aminoglycosides (environmental contaminants) in foodstuffs e.g. meat, milk and fish |
| Epitope imprinted MIPs [84] | <i>Aspira Biosystems</i> | Specific and selective uptake of microorganisms |
| MIPs as model drug targets [85] | <i>Semorex Inc.</i> | Incorporation into drug discovery, being used to test drug leads by acting as a synthetic drug target |
| Biotage AFFINILUTE™ MIP Columns | <i>Biotage, MIP Tech AB®</i> | Incorporation of MIPs into Biotage columns to afford significant sample clean up |
| High affinity nanoparticles | <i>MIP Diagnostics</i> | High affinity nanoparticles (nanoMIPs) are produced for extraction and sensing |

A typical MIP synthesis protocol contains a template, one or more functional monomers, a crosslinker monomer, a polymerisation initiator, and a solvent [86]. Figure 1.2 shows a simplistic schematic of the molecular imprinting principle. However, the challenge of designing and synthesising an MIP involves the selection of each of these variables: 1) monomer(s), 2) crosslinker(s), 3) solvent(s), and 4) initiator and the selection of initiation method along with the duration of the polymerisation.

Determination of the appropriate monomer(s) and the optimal stoichiometric ratios of each of the components often requires extensive empirical studies and testing to maximise target recognition [87]. The most common method of fabrication is known as self-assembly or noncovalent imprinting, often chosen for its ease and flexibility. It requires only a small number of synthesis steps, is compatible with a vast majority of target molecules, and template removal is facile post fabrication. The template and the monomers interact through noncovalent interactions and polymerisation takes place with the system (interaction between functional monomer and template) at an equilibrium, although it depends on the choice of reagents and the conditions (temperature, solvent) applied. Interactions at interplay involve hydrogen bonding, ionic interactions, Van der Waals forces, and π - π interactions.

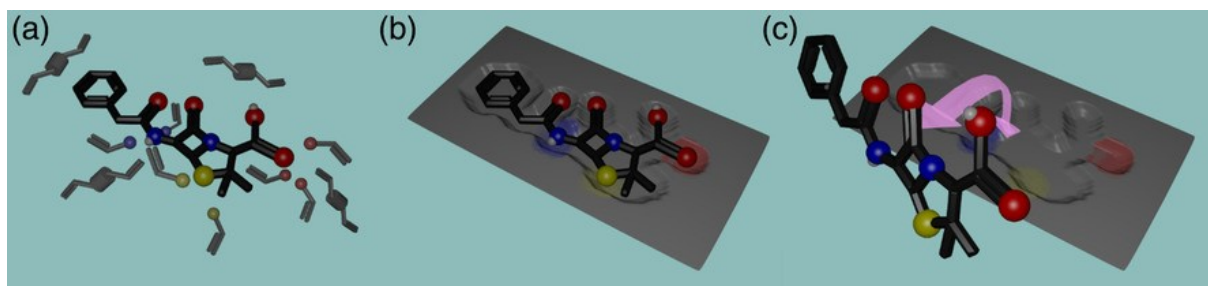


Figure 1.2. The several steps of molecular imprinting with a) precomplex with the example template of penicillin G surrounded by crosslinker and generic acrylate functional monomers, b) polymerised MIP, and c) amoxicillin molecule extracted, leaving an empty cavity to be used for rebinding

MIPs are often synthesised (and optimised) in organic solvents, whereas it has been established that binding characteristics are highly dependent on the solvent. In particular, binding in water is complicated as target molecules can bind in a specific manner to the MIP matrix due to hydrophobic effects [88].

Another drawback is that generally an excess of functional monomers has to be added to increase the chance of binding, which leads to various configurations and heterogeneous binding site distributions [89]. The non-homogeneity of the binding sites in MIPs resulting from noncovalent imprinting is comparable with that of polyclonal antibodies [90]. This is useful when a family of related compounds needs to be screened, such as a class of antibiotics. Especially when not a very precise measure is required, MIP-based sensors have a sizeable advantage over a biosensor that would have to include different antibodies for each analyte. However, though these types of MIPs can work well within a laboratory research setting, their sensitivity, accuracy, and limits of detection are not suitable for commercial devices. A solution to the issue earlier is represented by the covalent method: the functional monomers form a covalent bond with the template, which will be cleaved after the polymerisation process, allowing for the template to be recovered. Covalent fabrication methods yield a homogeneous population of binding sites and minimize nonspecific sites, with selectivity comparable with monoclonal antibodies [45], [91], [92]. Often, the aforementioned reversible bonding uses boronate esters, ketals/acetals, and Schiff bases. Readily reversible condensation reactions are typically chosen to cleave the covalent bond responsible for the interaction, for its extraction to be successful. However, this type of polymerisation introduces an additional step in the fabrication process. Moreover, the covalent strategy poses a major challenge as the covalent bond leads to slow dissociation [61], which limits its practical application, particularly in the area of sensing. Dummy templates, which are very similar to the target molecule, in size and shape but, importantly, are not the exact target, are a useful workaround for this issue. Certain hybrid approaches have emerged, one of which is known as semi-covalent imprinting [93]. Semi-covalent imprinting exploits covalent interactions to form the pre-polymerisation complex between functional monomers and template; however, rebinding to the MIP produced will be solely due to noncovalent interactions that, by nature, will occur with faster kinetics. Another similar imprinting technique is hierarchical imprinting, which uses scaffold molecules, which eventually are eliminated, to produce pores that act as microreactors. This approach is hence termed “sacrificial spacer” method and was first introduced by Klein *et al.* [51], but it has since been used in multiple areas of research. This work demonstrates the preparation of MIP shells, an example of the

sacrificial support approach, with fast absorption kinetics (≈ 10 min) for detection of the antibiotic enrofloxacin (ENR), as shown in Figure 1.3, in fish samples, with limits of detection well below the legal maximum residual level. The $K_2Ti_4O_9$ matrix was chosen because of its nontoxicity, low cost, and easy removal. Silica is indeed another popular choice as sacrificial support as the polymers can be embedded into the pores of the particles.

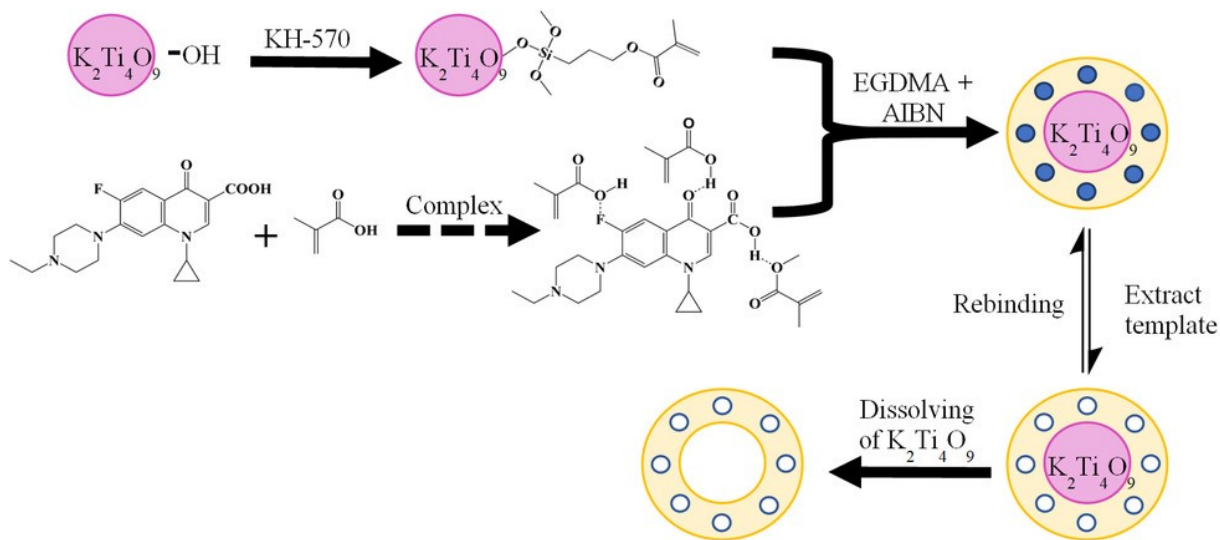


Figure 1.3. Preparation of hollow MIPs using covalent and noncovalent imprinting for an amino acid sequence, demonstrating the “sacrificial spacer” method using $K_2Ti_4O_9$ as a spacer molecule. Adapted with permission [51].

The group of Moreno-Bondi developed MIPs that were able to recognise six cephalosporins below the maximum residual levels set for these antibiotics in raw milk [94]. Silica etching is a more time-consuming process and also involves hazardous chemicals, as the particles were treated with an ammonium hydrogen difluoride mixture for 24 h. A similar approach, where silica beads were functionalised with MIPs according to a procedure introduced by Yilmaz *et al.* [95], was used to synthesise selective recognition elements for structurally related penicillins. This antibiotic pharmacophore, 6-aminopenicillanic acid, acts as a dummy template enabled to detect the entire class of target analytes from milk with high recovery rates. Methacrylic acid (MAA) was already used by Mosbach *et al.* [96], and remains to this date the most commonly utilised, given its ability to serve as H-bond donor and acceptor. Lately, several approaches

have been attempted where combinations of functional monomers have been used to enhance binding affinity [86], [97]–[101]. The approach of using a “dummy” template when discussed earlier is advantageous as it would not involve working with target molecules that are expensive, dangerous, unstable, or toxic [102], [103], while also allowing to detect classes of compounds which can be of particular interest in the case of antibiotics. Many successful cases of epitope imprinting have already been reported [104], [105], as well as computational simulations that use molecular modelling [106], [107] to select the epitope that yields the highest specificity [108]. The recent COVID-19 outbreak has triggered the interest in the epitope approach, considering one could imprint with antigens of the virus or particles with similar size and shape as the virus. The known difficulties in extracting the template led to a problem known as template leaching, which might interfere with the analysis of a given target. While the extraction of residual template molecule is more exhaustive after every use, it might be possible to avoid it with the use of a dummy template [109]. However, this can lead to less-selective binding cavities as a major drawback. A common drawback of MIPs is the difference in sensing performance between lab testing, when samples are spiked with the target analyte, and field testing, when a complex matrix is used. Often, even when state-of-the-art biosensors are utilised, the sample is pre-treated and concentrated to avoid the interference of matrix components. Interestingly, often the separation and removal of unwanted, interfering analytes from a solution is achieved via the use of MIPs in chromatographic methods. Therefore, by using a variety of MIPs in a separation procedure for example solid phase extraction, prior to MIPs sensing of the analyte, may resolve the aforementioned problem. Even with the drawbacks mentioned earlier, noncovalent imprinting, given the reduced number of steps and the ease of template extraction, is often the most widely used method of MIPs fabrication during the development of new sensors. Although sometimes less specific than other MIP methods, specificity of the binding sites can be increased via a low-temperature, light-induced polymerisation process. The synthetic methodology, in contrast, can be chosen depending on the destination of use of the polymer; whereas monolith synthesis and consecutive grinding offers a very simplistic approach, and its use is destined to be abandoned in favour of those able to yield more homogeneous binding sites and a better yield. In the future, methods

that will also ease scalability such as MIP beads, membranes, in situ-prepared monoliths, surface imprinting, and molecularly imprinted monolayers will likely be preferred, as they ease the rebinding kinetics and offer further improvement in the homogeneity of the binding sites.

1.3. Rational Design of MIPs for Antibiotics

1.3.1 Computational Modelling

As mentioned previously, determining the optimal functional monomer, crosslinker monomer, ratios of monomer and crosslinker to target, and solvent for the chosen template is one of the most important considerations when approaching MIP design and often the most time- and resource-consuming task. While this might be a big hindrance in terms of experimental work, such a task lends itself to the use of rational design through computational modelling, offering substantial advantages in both time and cost to the experimental counterpart [110]. The majority of computational modelling in relation to MIP design is centred around the pre-polymerisation complex. The nature of these interactions is a key step in obtaining high-affinity binding sites. With the use of varying computational techniques, these interactions can be investigated and optimised [111]. While the adoption of simple computational methods toward MIP design was first seen toward the end of the 1990s [112], their application toward direct rational design was not fully acknowledged until work by Piletsky *et al.* [113], This work utilised monomer screening, similar to experimental combinatorial screening, to predict the optimal monomer composition. This work, besides many others, considers thermodynamic interactions between template and functional monomer. When the computational program shows increased stability of these interactions, the quality of the template-specific cavity being produced experimentally is usually improved [114]. These energetics-based template-monomer studies are characterised by the determination of binding scores (Equation 1.1), which when compared can identify stronger interactions.

$$\Delta H_b = \Delta H_f \text{Final complex} - (\Delta H_f \text{Monomer} + \Delta H_f \text{Template}) \quad [\text{Equation 1.1}]$$

The energy difference between an independent template and a monomer compared with the final complex, template, and monomer bound by a new bond indicates the strength of this newly formed bond. There has been a considerable decrease in cost and increase in computing power available over the past 20 years. Not only has this increased the number of papers including rational MIP design, but it has also led to the development of more advanced techniques. A search of the available literature (Web of Science) shows a sharp increase in the number of papers since 2000 (Figure 1.4).

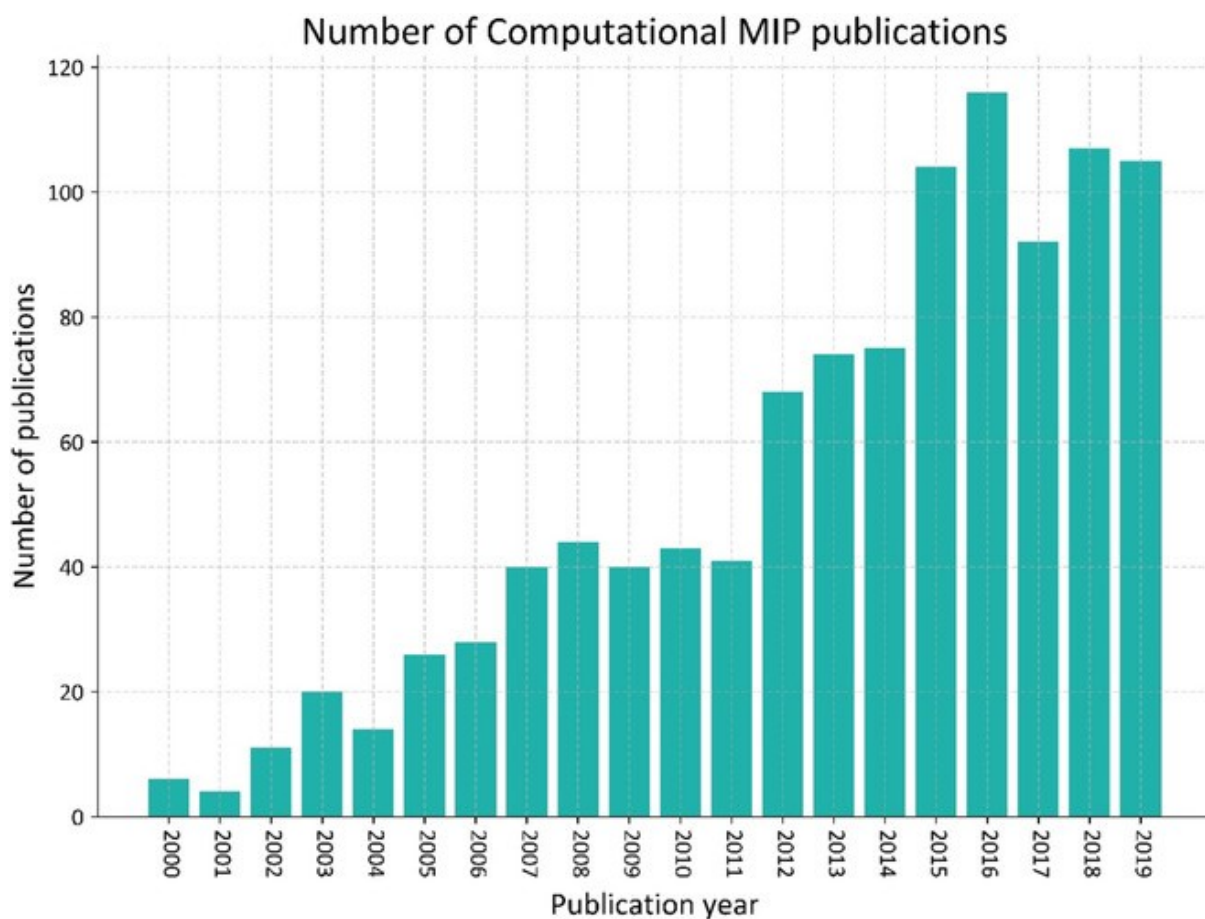


Figure 1.4. Representation of the increased research in the field via the number of publications including computational methods in MIP design between 2000 and 2019. The data obtained through Web of Science using the keywords “Molecularly Imprinted Polymer,” “MIP,” and “Computational.”

Quantum mechanical (QM) techniques, namely, semiempirical methods such as density functional theory (DFT), have become more widespread. QM-based methods offer a more advanced approach to predicting molecular energies. Such energies are calculated through the use of electronic structure-based techniques, allowing for determinations of interaction energies as well as structural predictions. For MIP design, QM methods are mainly used in monomer screening approaches and offer a more accurate method for determining energies for use in Equation (1.1). While many studies consider only template-monomer interactions, many others have investigated this further with more in-depth structural analysis, considering not only changes in ratios but also interactions of both crosslinker monomers and solvent. Again, QM methods have been used in this area, considering interactions of the crosslinker monomer with the template; however, such techniques are still computationally expensive and limited to only a few molecules. Molecular mechanics (MM) and molecular dynamics (MD) are commonly implemented when a more dynamic system is wanting to be defined, with both solvent and larger systems able to be represented. MD techniques allow these interactions to be investigated over time, analysing the motion of individual molecules. MM focuses on the observed properties of these molecules, with bond lengths, angles, and dihedrals along with nonbonding interactions considered. Most commonly, these two methods are used in combination. Specifically, in relation to computational rational design for antibiotics, there have been several papers offering many different techniques outlined previously. A relatively recent paper by Kong *et al.* [115], investigated norfloxacin-imprinted polymers using an MD-based approach. They considered changes in the ratio of functional monomer (MAA) and crosslinker (EGDM) while keeping the solvent (acetonitrile) constant. Computational analysis was completed using radial distribution functions (RDF), which allow for two specific atom pairs to be analysed as a system interacts throughout a simulation. A ratio of 1:8:40 (template: monomer: crosslinker) produced the best pre-polymerisation interactions, namely, the carbonyl to alcohol of norfloxacin to MAA. The experimental rebinding studies also supported the chosen polymer composition ratio, with the computationally predicted composition offering greater rebinding and specificity than the other MIPs analysed. The majority of papers on the subject, however, use the quantum mechanics-based approach, specifically for monomer selection. This

is mainly due to the accuracy of the energies predicted, but also the relative speed and ease when determining template-functional monomer bonds in vacuum. Semiempirical methods, mostly DFT, are used to determine the energies required for Equation 1.1. Such work has been completed for detection of the antibiotics norfloxacin [116], ciprofloxacin [116], [117], ENR [118], and tetracycline [119]. The studies found that the energies derived computationally were consistent with the experimental data produced and that the binding scores generated correlated with the experimental rebinding. The nature of antibiotics, with their relatively small size and presence of multiple, accessible functional groups, makes them a good candidate for computational modelling. Previous work in the area has shown good support for this, with complimentary computational and experimental data. The rational design of MIPs through computational methods is still a growing area of research, with varying approaches and more advanced techniques being developed since its establishment in the early 2000s. Such methods were applied depending on the research, whether that were simple functional monomer predictions using QM or more in-depth structural analysis utilising MD. Already, with many papers showing the ability for strong predictions, the application of such aided design looks set to become commonplace in future MIP production.

1.3.2 NMR Techniques Aiding MIP Production

NMR is an essential technique for structural determination of a wide range of molecules. The plethora of techniques associated with proton and carbon NMR, which allows investigating spatial and electronic interactions between different nuclei, can offer very detailed structural information even in the case of complex molecules. MIPs are composed of crosslinked and macroscopic chains, which complicate the characterisation due to their intractable and insoluble nature. A pioneering NMR study on MIPs was reported by Sellergren, Lepisto, and Mosbach [120]. A ^1H -NMR study combined with results obtained by chromatography, which involved titration of the imprint molecule (phenylalanine anilide) with carboxylic acid, found that the results were consistent with the existence of multimolecular complexes by means of electrostatic and hydrogen-bonding interactions [120]. NMR has been mostly used to determine the extent

of the template to functional monomer association equilibrium in the pre-polymerisation stage; the shift of the relative signals, compared with those of the template and monomer alone, can determine the extent of the interaction. Wang *et al.* used NMR to identify the best template-to-functional monomer ratio [121], a procedure that is often very time-consuming, for the preparation of MIPs for the extraction of a valuable compound. The signals of the protons involved in hydrogen bonding and that of the adjacent carbon were used to gauge the strength. A study by Mattos dos Santos *et al.* reported on the synthesis of MIPs targeting tegafur (an anticancer 5-fluorouracil prodrug) and used $^1\text{H-NMR}$ titration to study solution association between tegafur and 2,6-bis(acrylamido)pyridine (BAAPy) [122]. This confirmed the formation of a 1:1 complex of template and functional monomer, in MIPs being prepared using stoichiometric imprinting. Interestingly, an affinity constant of $574 \pm 15 \text{ M}^{-1}$ in CDCl_3 was calculated using a previous work by Fielding, who reviewed the topic with a section dedicated to diffusion experiments [123]. Hydrophobic effects and their contribution to the selectivity of the resulting MIP were investigated with NMR spectroscopy by O'Mahony *et al.* to identify the interactions occurring in the pre-polymerisation mixture [124]. Sánchez-González *et al.* used $^1\text{H-NMR}$ and, importantly as it represents a novelty, nuclear overhauser effect (NOE) to study the pre-polymerisation interaction between the cocaine template and the functional monomers MAA and ethylene dimethacrylate; in particular, 1D selective NOE experiments were conducted to assess MAA-cocaine and EDMA-cocaine hydrogen-bonding interactions, which were contextually confirmed by *in silico* studies [125]. Commonly, the most time-consuming step is the quest to identify the most appropriate functional monomer(s). Konishi and coworkers addressed this using $^1\text{H-NMR}$ to evaluate the influence of several monomers on the potentiometric performance of histamine-imprinted polymer-modified sensors [126]. Not only was $^1\text{H-NMR}$ able to assess the interaction between histidine and acrylamide (AA) and atropic acid (AT) and MAA, but it was even possible to see the influence of its imidazole ring on the pyridine ring of 4-vinylpyridine (4-VP). The nature of MIPs makes their characterisation usually harder, but solid-state NMR has been shown to evaluate the degree of the binding of the template when the interactions are strong. Andersson *et al.* used this technique to optimise the template-functional monomer proportion [127]. Simple $^{13}\text{C-NMR}$ alone had not been used for the

evaluation of the template-functional monomer interaction, until Zhang *et al.* [128], reported a study where it was utilised to evaluate the interactions between antibiotic erythromycin (ERY) and a set of functional monomers, with the choice of MAA as the optimal one. The rational binding sites were predicted based on chemical shifts changes in ERY structure. DFT theoretical calculations of Lewis basicity of the O/N atoms located at the sites proposed by a sequence regarding their interaction force confirmed its reliability. Solid-state NMR was used by Annamma *et al.*, to design a 2,4-dichlorophenoxyacetic (2,4-D) acid-imprinted polymer with 4-vinylpyridine (4-VP) as the functional monomer [129], intriguingly showing the effect of increasing concentrations of 4-VP on the equilibrium; see Figure 1.5.

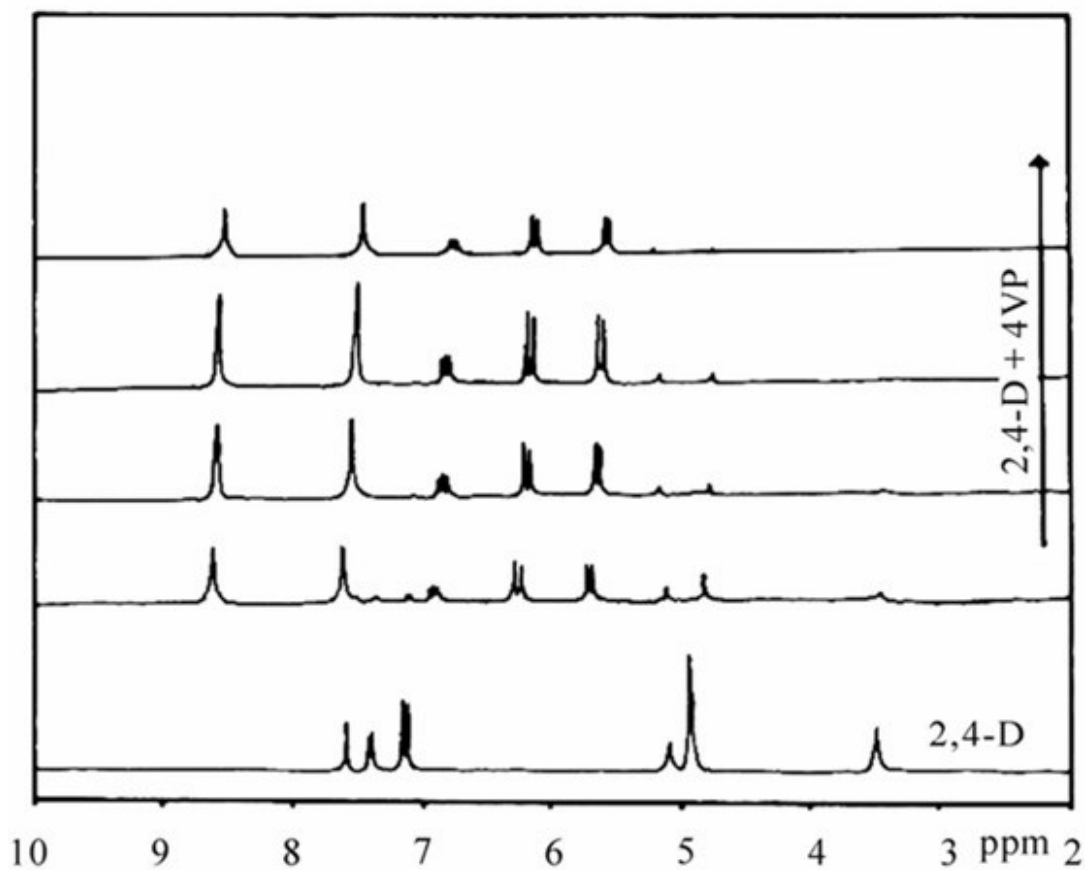
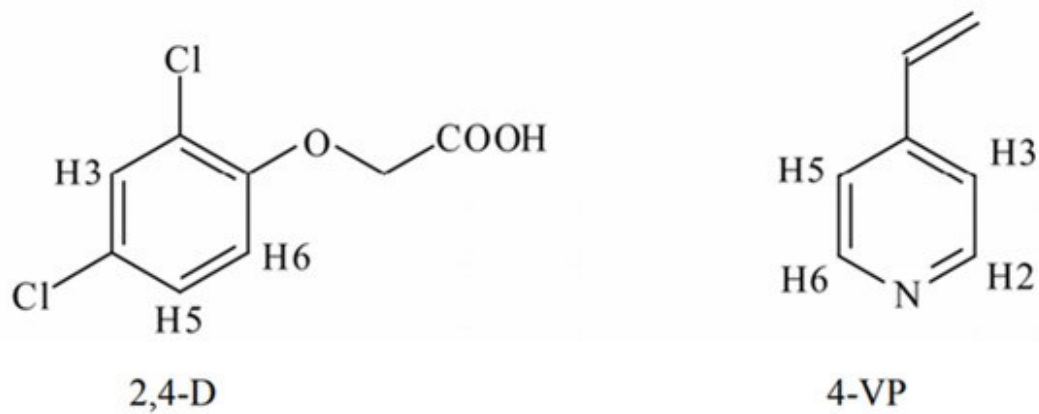


Figure 1.5. ^1H NMR spectra of 2,4-D with increasing concentration of 4-VP showing changes in the chemical shifts used to rationalise a low crosslinked system that allows for higher levels of specificity and selectivity. Reproduced with permission [129].

1.3.3 Isothermal Titration Calorimetry (ITC)

Isothermal titration calorimetry (ITC) is a microcalorimetry technique that measures the heat released or absorbed during a chemical reaction, generally used to determine binding affinity, enthalpy changes, and stoichiometry of interactions between molecules in solutions [130]. The advantage of this technique is that no immobilization or modification of the starting reagents is required. In addition, ITC has the ability to detect changes in the low mK range that corresponded to noncovalent interactions such as hydrogen bonds [131]. However, ITC is not widely available in laboratories and requires expensive instrumentation, which limits the application in the field of MIPs [132]. To the best of knowledge, there have been no reports about the use of ITC for the characterisation or rational design for MIPs produced for antibiotics. There are few reports in literature about using ITC to determine binding affinity of MIPs for small molecules [133], [134] and predicting the optimum ratio of target-to-functional monomer [135], [136]. Due to ITC providing thermodynamic data, it gives fundamental insight into the binding mechanism of MIPs that has been proven strongly dependent on pH [137], [138], showing that pH can be a considerable variable in achieving optimum MIP function. Considering ITC is routinely used in biomedical research including enzyme kinetics, it might play a crucial role in optimising MIPs for antibiotic detection and understanding the influence of external parameters (T, pH, etc.) on binding to polymers.

1.3.4 Infrared Spectroscopy

Infrared (IR) spectroscopy is ubiquitously used in laboratories as it is versatile, offers fast and straightforward analysis, and is inexpensive. The main disadvantage of IR is that it is difficult to analyse complex mixtures or aqueous solutions, as the corresponding spectra provides only limited information about individual peaks of chemicals of interest. Therefore, IR is not routinely used to study interactions in the pre-polymerisation complex prior to MIP formation as the stretching frequency of hydrogen bond donors or acceptors is generally in the same range as that of the solvent peaks [139]. However, IR measurements can also be collected from solid particles and this method of IR can provide useful information about the resulting solid MIP on the expected performance of the material as the peak intensity of the carbonyl group provides quantitative information about the amount of polymer present on the

surface [139]. Thin films of poly(N-isopropylacrylamide) revealed systematic changes in IR peaks associated with the amide bond, that could serve to bind molecules via hydrogen bonding. In addition, the study also demonstrated that the molecular architecture can significantly vary depending on what solvent was used to cast the film [140]. IR measurements are fast and straightforward and therefore have scope for this technique to be used for high-throughput screening of performance of solid polymeric materials. MIP materials are often heavily crosslinked and have limited solubility, which can complicate characterisation. IR is often used on solid materials to establish the presence of the polymer on surfaces and determine whether the template has been fully removed from the MIP cavities. Chen *et al.*, reported on the separation of tetracycline antibiotics from egg and tissue samples using magnetic MIPs as the solid phase [139]. Peaks from the carbonyl and hydroxyl group of the polymer were present in the recorded IR spectra, which confirmed presence of the polymer on the magnetic particles. Wei *et al.* developed dual-imprinted MIPs for the rapid determination of amphenicol antibiotics in water, serum, and food samples. The presence of the polymer was verified with IR measurements. Furthermore, IR spectra of the reference non-molecularly imprinted polymer (NIP) and its corresponding MIP were compared and significant frequency shifts in the peak corresponding to methacrylic acid were observed [141]. It was hypothesized that the observed shift in this peak was due to hydrogen bond interactions between functional monomer and target. A similar approach was followed by the group from Mizaikoff and coworkers [142] that developed gravimetric sensors for detection of the antimalarial drug artemether. Upon inspecting the IR spectra of the polymers, a spectral shift of the peaks corresponding to the carboxyl groups of methacrylic acid to the shorter wavelength was reported. Besides these peaks, there was also a distinct intensity change at a wavelength of 3000 cm^{-1} that was attributed to additional interactions of functional monomers with the template. Over recent years, there has been a move toward the use of the aforementioned “dummy” templates in Section 1.3, which avoid the use of high-cost or toxic target molecules. Zhang *et al.*, used a simple sugar, raffinose, as a dummy template to develop MIPs for antiglycoside antibiotic detection [143]. This molecule resembles the size and shape of the antibiotic of interest and is able to selectively extract six antibiotics from the family of antiglycoside antibiotics from environmental samples. In research by Liu *et*

al. [144], roxithromycin was used as an example of a macrolide antibiotic to develop MIPs for the extraction of this entire family of macrolides. The interesting aspect of this work was that a simple wooden tip was used, that makes it extremely suitable for work in developing countries. IR was used to monitor extraction of the template from the MIP cavities. IR measurements are fast and straightforward and, as shown via the earlier example, can be applicable for high-throughput screening for the performance of MIPs.

1.4 MIP Morphologies

In the early years of imprinting, the most common approach involved free radical polymerisation, often achieved using azobisisobutyronitrile (AIBN). The reason this method is often used is due to its simplicity as it can either be initiated with UV light or increasing the temperature; unfortunately, given the fast chain propagation and the fact that the associated termination reactions are irreversible, it yields inhomogeneous cavities and a wide particle size distribution [145]. This results in MIPs with heterogeneous binding sites, with cavities directly on the surface and others that are partly inaccessible, which hinder mass transfer and limit selectivity. This problem has been addressed with the use of controlled polymerisation techniques including reversible addition fragmentation chain transfer (RAFT) polymerisation [146], [147], ring-opening metathesis polymerisation [148], and atom transfer radical polymerisation (ATRP) [149], which led to particles uniform in size with homogeneous binding sites. In this section, I will review a couple of methodologies which improve upon sensor specificity.

1.4.1 Use of Copolymers

One way to improve upon the specificity and selectivity of MIPs is the inclusion of more than one functional monomer, resulting in what is referred to as a co-polymer [150], [151]. Chullasat *et. al.*, [152] demonstrated an amoxicillin detection system using a copolymer along with quantum dots (QDs). The resulting system proved capable of detecting amoxicillin in complex media such as milk and honey with a LoD of $0.14 \mu\text{g L}^{-1}$, outcompeting the HPLC standards it was tested against. It was also shown that the use of copolymer MIPs can increase the accuracy of results against modern, industrial detection systems

but also decrease the time taken and reduce the need for expensive infrastructure. Tunc *et al.* [153], demonstrated optimising copolymer MIPs through synthesis and comparative testing. This provided insights into optimum monomer selection for the theophylline-imprinted monomers; however, planning monomer selection via rational design, e.g., computational modelling, would lend aid as to which monomers to evaluate. Valtchev *et al.* [154], tested a vast range of MIPs, including six co-functional monomer polymers. The study resulted in the synthesis of many significantly optimised MIPs for the detection of the antibiotic sulfamethoxazole in wastewater. Although this type of “trial by error” study is not time efficient, it does give certain, quantified values to the efficiencies of all the MIPs tested and shows the positive impact that using copolymers can have. Wang *et al.* [155], developed inorganic-organic co-functional monomer-imprinted polymers for fluoroquinolones in milk and observed an LoD in the ng/mL range, which exceeds the standards required by the EU. As sample matrices as complex as milk have benefited from the use of copolymers, the eventual use of copolymers for detection in other sample matrices, especially simple matrices such as water, would have presumptive benefits.

1.4.2 Integration of Fluorescent Moiety

The phenomenon of fluorescent emission is a type of radioactive decay, during such examples where a molecule discards excitation energy in the form of a photon. Fluorescence, unlike phosphorescence, occurs rapidly, ceasing within nanoseconds to milliseconds of the extinguishment of the excitement radiation. An electron is excited from the ground state energy level to an excited triple state, through internal conversion (IC) and vibrational relaxation, the excited electron drops to an excited single state. Once the source of excited radiation stops, the electron drops back down to ground state energy. Fluorescence is equivalent to the energy difference between the eigenstates and is always less than that of the exciting photons due to the energy lost via the IC and vibrational relaxation [156]. Fluorescence of a sample can be easily influenced in terms of the intensity increasing or the fluorescence being quenched. Fluorescence enhancement is primarily due to nonradiative deactivation of non-aggregated fluorophore molecules and hindrance of excitonic interactions by the dissociation of aggregates [157]. Fluorescent enhancement is

commonly observed when a process called aggregation induced emission (AIE) is in effect. [158]. AIE is a process by which electrons are increasingly excited through the interaction of fluorophores aggregating together, hence aggregation induced emission. AIE has been used actively as process to induce fluorescent intensity changes that can be monitored as an analysis technique in MIPs [159]–[161]. Enhancement can also be caused by processes such as Plasmon-enhanced fluorescence in which the excitation power that is absorbed by the fluorophore leads to an increase to the collective electron oscillations to the excited state which therefore produces an increase in the fluorescent emission [162]. Fluorescence quenching can occur through a plethora of different process. Photobleaching is the most common source of fluorescence quenching. Photostability of organic fluorophores is low relative to inorganic fluorophores. The loss of reoccurring cycles of electron excitement to produce a fluorescent signal is a form of photodegradation called photobleaching. Photobleaching can be caused by a number of different factors primarily to do with the environment of the fluorophore, for example the intensity of light it is exposed to and the length of time it is exposed to the light [163]. Interactions with a fluorophore and water can itself lead to quenching via the hydrogen bonds that form between the fluorophore and a water molecule. These hydrogen bonds entail a charge transfer from the fluorophore to the water molecules which causes less oscillations of electrons to the excited state in the dye molecule resulting in a quenching of fluorescence [164]. Fluorescence resonance energy transfer or FRET is another major pathway of fluorescence quenching. FRET describes the process of non-radioactively transfers energy from a fluorophore (donor) to an acceptor fluorophore. This can occur when the distance between the two molecules is less than 1Å- to 100Å and that the donor fluorescence spectrum overlaps sufficiently with the absorption spectrum of the acceptor molecule [165]. FRET is commonly exploited as process for fluorescence detection especially in the field of MIPs [166]–[168].

Fluorescence detection of antibiotics has been a crucial analytical tool for many years because of its versatility, simplicity, and accuracy [169]–[171]. It can be used across a range of different recognition elements, including MIPs. However, it often requires the introduction of a secondary molecule to either bind to the target [172] or serve as a competitor [173] for a measurable fluorescent response to be obtained.

Recent studies, therefore, have looked to develop MIPs, which are inherently fluorescent by introducing certain elements into the polymer itself [174], [175]. This reduces the number of preparation steps needed to analyse samples and allows for the polymer to be adapted to a variety of targets. There have been two primary focuses to achieve this functionality: QDs embedded within or surrounded by the polymer matrix or a fluorescent moiety copolymerised into the backbone [176], [177]. These integrated QDs and fluorophores typically rely on energy or electron transfer from the target molecule to achieve their fluorescence change (Figure 1.6). This transfer is strongest when the target rebinds into the imprinted sites as this is in closest proximity to the fluorescence element that can be achieved.

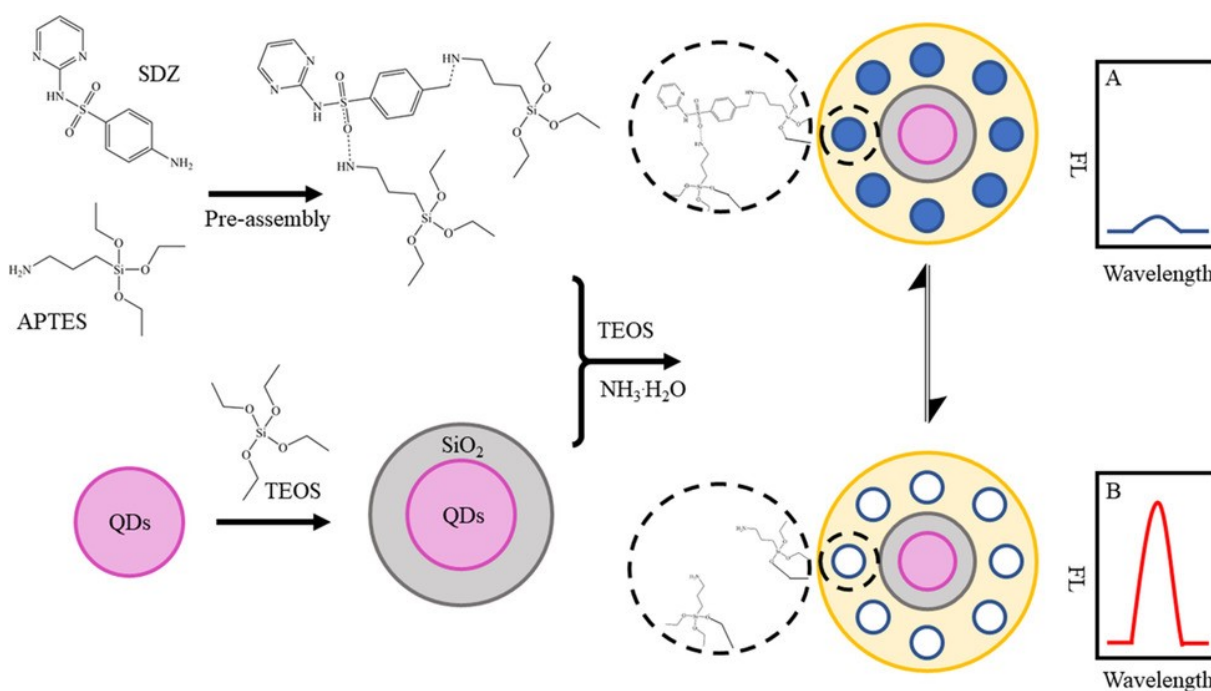


Figure 1.6. Formation of an MIP layer on the surface of QDs for an antibiotic, sulfadiazine (SDZ). The polymer layer can then have the target extracted, breaking the electron transfer between SDZ and the QDs, which results in a decrease in the fluorescence signal. Reproduced with permission [177].

Fluorescence quenching is most commonly seen in both cases, although enhancement can be facilitated by tailoring the molecular system to achieve specific interactions upon rebinding [80]. Shi *et al.* utilised CdSe QDs to introduce fluorescence into a bulk MIP for kanamycin [178]. An increase in fluorescence was seen for both NIP and MIP upon addition of kanamycin, with a greater increase seen for the latter.

The fluorescence response was greatly influenced by composition, pH, temperature, and required optimisation. The system was able to detect kanamycin with a detection limit of $0.013 \mu\text{g mL}^{-1}$ and a linear range of $0.05\text{--}10 \mu\text{g mL}^{-1}$ in PBS. Furthermore, it was tested with real samples (including lake water and urine) and showed good recoverability of spiked concentrations of the drug. This methodology also utilised aptamers to increase binding affinity to the polymer layer and click chemistry to provide a more simplified chemical route for polymer attachment to the QDs compared with conventional methods. Zhang *et al.* integrated ZnS QDs into a mesoporous silica network containing an imprinted polymer for tetracycline [179]. Quenching of the fluorescence was seen upon addition of tetracycline to the MIPs only, which they propose is due to an electron transfer between the target and the QDs. The particles showed high selectivity for tetracycline compared with similarly structured compounds, and an LoD of 15.0 ng mL^{-1} was obtained. Similar quenching probes for antibiotics have been produced using graphene [180], ZnS [181], and CdTe QDs [178], yielding comparable LODs and selectivity. Integrated fluorophores offer a unique alternative to QDs, where the interactions between the fluorescent moiety and the target can be more specifically tailored [182], [183]. In addition, the use of heavy metal atoms can be avoided and integration into the polymer backbone significantly reduces leaching. However, these molecules often require a multistep synthesis and extensive optimisation of the polymer composition as quantifying the fluorescence change requires one-to-one interactions. Niu *et al.* introduced an anthracene-based monomer into MIP nanoparticles for the detection of tetracycline [184]. The fluorescence of the RAFT-polymerised nanoparticles would be quenched in the presence of the target, with the imprinted particles exhibiting a stronger change than the nonimprinted ones. The polymers were able to detect tetracycline at an LoD of $0.26 \mu\text{M}$ and were able to perform in a more complex medium (bovine serum). UV vis analysis demonstrated that the underlying mechanism for quenching was based on electron transfer rather than energy transfer. Sunayama *et al.* used attached fluorophores to explore the binding activities of a cephalexin imprinted polymer [172]. The template was functionalised and crosslinked into the polymer network and then removed using two different chemical reactions. This method is unconventional compared with common imprinting techniques but allows for direct functionalisation of the imprinting

sites; in this case, two fluorophores were introduced via Schiff base and disulfide reactions. Ampicillin was used to monitor rebinding due to solvent constraints, and an increase in fluorescence intensity was observed with corresponding concentrations. An LoD of 5.0 μM was observed and the fluorescence change was highly specific due to the nature of the interaction, regarding to the presence of two differing fluorescent moieties. Ashley *et al.* were able to produce fluorescent doxycycline-imprinted microparticles using an acrylated fluorescein derivative [185]. The moiety was introduced into a thin polymer layer surrounding FeOx nanoparticles and exhibited quenching upon rebinding of the target. Although the interaction between fluorophore and target appears less specific, the polymer demonstrated strong selectivity toward doxycycline compared with similarly structured antibiotics based on fluorescence readings. Recently, work has explored the use of a fluorescein-based MIP as an optical detection platform for beta lactam antibiotics [186].

1.4.3 Using Redox Probes to Monitor MIP/Target Binding Phenomena

If the target analyte is not electrochemically active, a redox-active probe can suffice for the detection. A redox reaction involves the transfer of electrons, which is facilitated through the working of an auxiliary (counter) electrode, whereby if an oxidation process occurs at the working electrode, the corresponding reduction process will take place at the auxiliary electrode. In electrochemistry, redox probes can be used to follow interfacial changes in a system, such as adsorption, electrode modification, and binding phenomena. There is a vast array of redox probes and care must be taken when choosing one for use in characterisation of a system or for use as an indicator for sensing applications. All these systems are classified under two main categories, outer-sphere and inner-sphere redox probes, summarised by McCreery *et al.* (see Figure 1.7) [187]. Outer-sphere probes come close to the electrode surface, but do not directly contact it, to allow the electrons to tunnel/hop across the solvent monolayer, and as such are only influenced by the electronic structure of the electrode surface. Ruthenium hexamine (RuHex) is the best example of a near-ideal outer sphere redox probe; it does not exhibit any variation in electron transfer

rate for any changes other than the electronic structure of the electrode (density of states and the Fermi level).

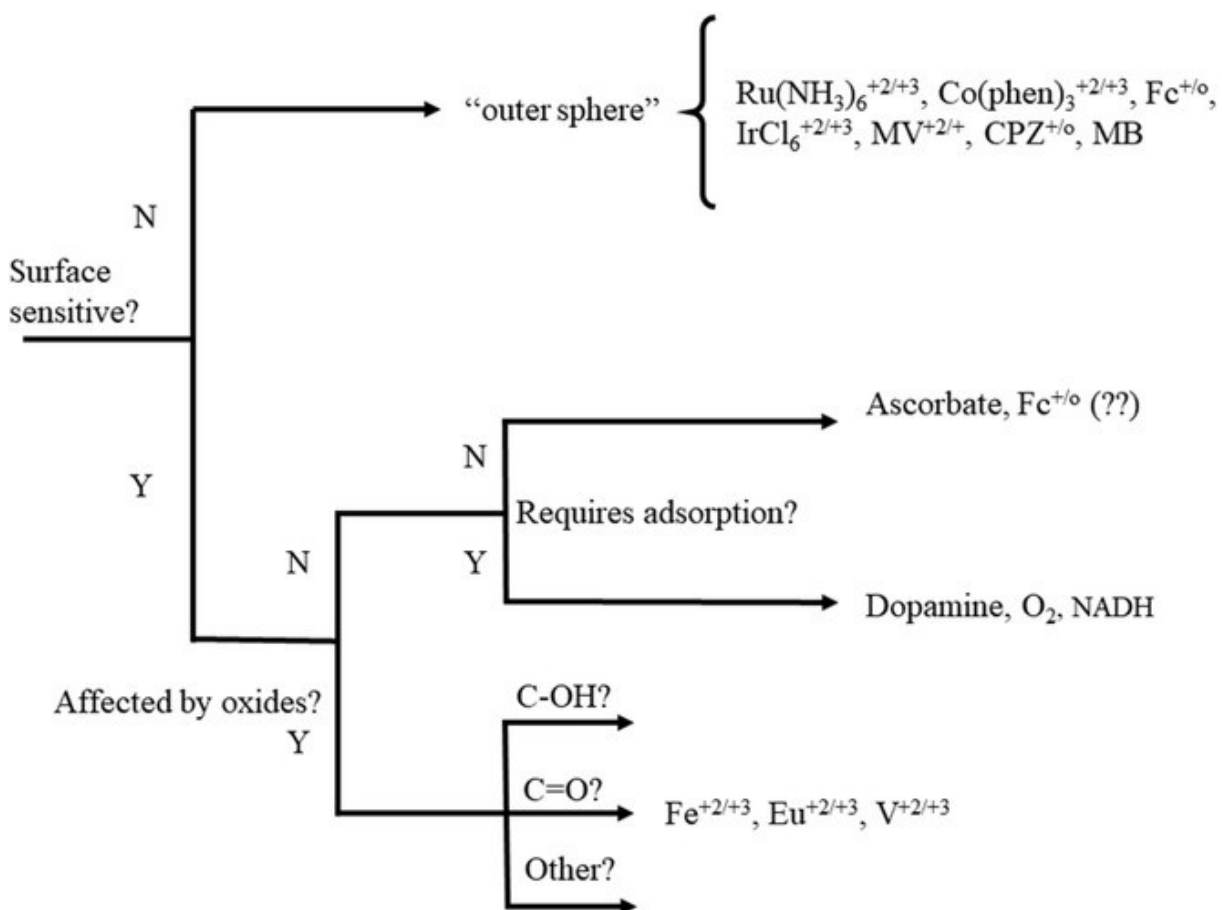


Figure 1.7. Flow diagram showing classification of outer- and inner-sphere probes. Reproduced with permission [187].

Alternatively, inner-sphere redox probes require contact with the electrode surface to facilitate the electron transfer; as such, they are affected by both the electronic structure of the electrode surface and the surface chemistry at play (i.e., surface functional groups and adsorption sites) [188]. When using MIPs as recognition elements, the desire is typically to record and track changes in binding phenomena between the imprinted polymers (typically on the surface of an electrode) and a target analyte (in solution that diffuses to the electrode surface and binds to the MIP). Most papers in literature combine MIPs and redox probes, where the use of an inner-sphere redox probe in solution is as an indirect detection method, where

the binding of the target to the polymer blocks the access of the redox probe to the electrode surface, producing a reduction in measured response. As such, the most common redox probe in this area of research, as an indirect detection method, is potassium ferri/ferrocyanide ($K_3/K_4[Fe(CN)_6]^{3-/4-}$). This can be done utilising various electro(analytical) techniques such as cyclic voltammetry (CV) [189], electrochemical impedance spectroscopy (EIS) [190], and differential pulse voltammetry (DPV) [191]–[193]. CV typically will not reach the same levels of detection as other electroanalytical techniques; however, the analytical response can be amplified by adding extra components to the system. Lian *et al.* [194], accomplished this for the detection of the antibiotic kanamycin through the addition of horseradish peroxidase and H_2O_2 , where potassium ferricyanide acts as a mediator for the reaction. This reaction mechanism gives a large amplification in the measured current; therefore, when the electrode surface is blocked through the binding between kanamycin and MIP, there is large reduction in current as the reaction can no longer be mediated. These methodologies typically require two-step analysis, consisting of an incubation step in the analysis solution and a subsequent measurement step in the probe solution, which is not ideal for production, reproducibility, and analysis time.

Instead of using a free in-solution redox probe, an alternative strategy is to incorporate the redox probe directly into the polymer matrix. In this process, known as redox tagging, a redox probe such as ferrocene is attached to a moiety capable of taking part in the polymerisation process. Mazzotta *et al.* [195], reported this for the detection of the antibiotic vancomycin through using two ferrocene-derived monomers, vinylferrocene and ferrocenylmethyl methacrylate, in conjunction with the solid-phase synthesis approach [196], for the development of nanoMIPs that produce homogeneous binding sites and pseudo monoclonal binding properties. The direct anchoring of the redox probe into the polymer allows for a reduction in analysis time and a more direct interaction between the probe and target, which does not rely on diffusion of the probe in solution. The main drawback of using ferrocene-derived redox probes covalently attached to the system is a natural reduction in the current signal when cycling for prolonged periods. As seen from the cyclic voltammograms in the manuscript from Mazzotta, over the course of 250 scans, there is a

significant reduction in the measured current; this needs to be taken into account when developing a sensor platform using this methodology and may require significant calibration steps to produce a reliable system.

1.5 Different MIP Production Methods

There are many different production methods for MIPs, depending on the desired function of the polymer. MIPs intended for use in chromatography are usually prepared by free-radical polymerisation, which results in the production of heterogeneous microparticles. Research into other MIPs has elevated their use, such as, their synthesis via solid-phase imprinting to generate homogeneous high-affinity nanoparticles, which have the added benefit of biocompatibility and superior thermal and chemical stability compared to their biological counterparts. MIPs can be stored in dry conditions and ambient temperatures for many years, without loss of recognition capability, whereas antibodies denature rapidly unless they are kept frozen. This provides advantages for manufactured MIPs sensing devices as they can have appropriate shelf life for use outside of lab settings. In addition, MIPs are able to withstand many adverse conditions (heat, cold, changes in pH, etc.), which allow them to be used for a variety of in-field, real-time sensing applications [193]. For the interest of this work, MIPs can easily be implemented into sensors for food and water analysis for antibiotics. One of the biggest stumbling blocks, however, for broad-scale commercial use of MIPs as sensors has been reproducible mass manufacture. The advent and recent development of nanoparticles, and especially coreshell and gel nanoparticles, whose solubility can finely be tuned, is promising for the next generation of sensors [197]. Recently, photolithography has been used to pattern MIPs for the wafer-scale production of biochips. This technique allows for the control of shape and size (1.5 μm) of the patterns and the deposition of different MIPs on the same chip [198]. Some of the advancements to mass manufacture will be discussed later.

1.5.1 Screen-Printing Techniques

Screen printing is a well-established methodology for the mass production of biosensors [199]. The most common commercial example is the glucose sensor, used in the treatment of diabetes, that utilises a screen-

printed electrode (SPE) and is responsible for a billion-dollar market annually [200]. Screen printing offers the ability to mass produce disposable platforms that offer high reproducibility, flexibility, versatility, and high sensitivity at a low production cost. This technique involves the spreading of a thixotropic fluid, containing a mixture of predominantly graphite, solvents, and binder, through a predesigned mesh that will produce a printed pattern of a defined shape and size [201]. As such, a vast array of electrodes has been designed utilising this methodology to produce different shapes such as microbands [202], shallow recessed arrays, and [203] back-to-back sensors [204]–[206] and produce electrodes containing a wide range of constituents for various applications in biosensors [207]. MIPs can be incorporated into and used in conjunction with screen-printed platforms in a variety of ways, such as the direct formation of MIPs on the surface through processes like electropolymerisation [208], incorporation of MIPs into the screen-printing ink [209]–[211], or depositing onto nanomaterials decorated on the surface [212]. Direct formation of MIPs onto the surface of an unmodified SPE was reported by Ayankojo *et al.* [193], who used computational modelling to choose *m*-phenylenediamine as their chosen monomer for the detection of erythromycin. In strategies such as this, where direct electrochemical detection is used, the thickness of the MIP layer is a crucial parameter. The manuscript discusses the signal was enhanced with a thinner MIP layer; however, a thinner layer reduced specificity due to having more non-specific interactions with the surface. Conversely, when the layer was too thick, there was a significant decrease in the electroanalytical signal due to the MIP layer being insulating. Therefore, when using MIP layers on SPEs, each system must be optimised for electrochemical detection. Electropolymerisation (discussed later) is the most obvious route for MIP formation on SPE surfaces; however, this methodology can struggle from a limited selection of suitable monomers and poor scalability. Jamieson *et al.* [213], reported a sensor for amoxicillin through the direct formation of MIPs onto the SPE surface through UV polymerisation. This offers better prospects in terms of mass production; however, more work has to be done to increase the synergy between the transducer, MIP, and detection methodology. The enhancement of electroanalytical output for SPE platforms is typically done through the incorporation of nanomaterials. These materials are either incorporated in the ink, on the surface of the electrode, or on top of the MIP and help to overcome

problems with poor conductivity and electroanalytical response. This can be seen in the work by Devkota *et al.* [214], who reported a sensor platform for the detection of tetracycline, in which the formation of the MIP was achieved using the conductive polymer pyrrole. Following MIP formation, the polypyrrole layer was overoxidized, a process that while stabilising also removes the conductivity associated with the polymer layer. Therefore, to increase the efficacy of the sensor, gold nanoparticles (AuNPs) were deposited on the surface of the MIPs. Although this helps to counteract the loss of conductivity, the multiple electrochemical modification steps do not lend the system ability for simple mass production, which is a great advantage when using SPEs. This can be further seen through the work of Moghadam *et al.* [215], using a combination of gold nano-urchins and graphene oxide for the detection of oxacillin. In this case, the nanomaterials were deposited onto the surface of the electrode prior to the MIP. Although the use of drop casting to modify electrodes is standard practice and scalable, using multiple drying conditions followed by electropolymerisation and template removal provides difficult production steps. Instead of multiple electrochemical functionalisation steps, Dechirat *et al.* [192], utilised inkjet printing of a nanocomposite layer, containing AuNPs and poly(3,4-ethylenedioxythiophene)/poly(styrene sulfonate) (PEDOT:PSS), onto the surface of the SPE. This synergetic approach to the incorporation of nanomaterials onto the electrode allowed for the detection of nitrofurantoin at two orders of magnitude lower than the bare sensor platform. This sensor exhibited the advantages of using screen printing and MIPs in combination, producing a sensor platform that is both highly reproducible and stable over a long lifetime.

1.5.2 Electrodeposition of MIP Layers on Transducer Surfaces

Electrodeposition enables the immobilization or formation of MIPs directly onto an electrode surface using an electrochemical methodology [216]. The vast majority of MIPs that fall into this category is electrosynthesised MIPs (eMIPS). A more detailed overview of this subsection of MIPs, including their formation and application to the detection of biologically important molecules, including antibiotics, up to 2019, can be found in a recent past review [208]. Briefly, the formation of eMIPs takes place through

electropolymerisation, where a polymer layer is formed upon an electrode/substrate in the presence of the desired template. This can be achieved through a variety of electrochemical techniques, such as voltammetry [217], potentiometry [218], and galvanostatic techniques [219]. It is vital when using this methodology to define the working material, counter and reference electrodes, monomer composition, solvent, supporting electrolyte, electropolymerisation methodology, and time as these variables will greatly affect the binding affinities, layer sizes, conductivities, and surface morphologies of the polymeric films [220]. Good recent examples, presenting the optimisation required for the production of a sensor array for the detection of β -lactam antibiotics, were reported by Moro *et al.* [221] and Bottari *et al.* [222]. Both explained the rationale behind the design of their eMIP-based sensor platform through computational modelling. Moro *et al.* discussed the importance of utilising a conductive polymer (4-aminobenzoic acid, 4-ABA) to synergize with their chosen square wave voltametric (SWV) detection method and the use of modifiers, in this example multiwalled carbon nanotubes (MWCNTs), to enhance the electroanalytical properties of the device. The overwhelming majority of sensor platforms utilising electrodeposition also use electrochemistry as their chosen detection method. This can be achieved either through indirect detection, such as the redox probes described earlier, or by direct detection of the binding between the target and recognition element. One such way to monitor the interfacial changes at the MIP/electrode surface is through EIS, where a change in the measured charge transfer resistance (R_{CT}) can signify the binding of a target molecule. Roushani *et al.* [223], demonstrated this using a design that utilises a combination of electrosynthesised poly(resorcinol) MIP and a silver nanoparticle (AgNP)/reduced graphene oxide (RGO)/aptamer system. Although this methodology uses a large amount of preparation steps, it was able to detect chloramphenicol (CAP) in milk samples. Resorcinol ($C_6H_6O_2$) offers another effective choice of monomer for antibiotic detection through eMIP layers, due to its ease of polymerisation and favourable structure. This presents an improved chance of advantageous hydrogen bonding occurring between the hydroxyl groups present and the functional groups on the antibiotic molecules. Although electropolymerisation techniques lend themselves toward fast single-sensor production, it does not scale well for mass production due to the often multistep production schemes and varying conditions [224].

Electropolymerisation offers a promising method of fast and varied single-sensor production; however, in its current form, the scalability ready for mass production of sensor platforms is not readily available. In particular, this production methodology does not lend itself to array sensor development for multiple analytes. The use and development of more conductive polymers with an array of functional groups will allow for great improvement on the sensor efficacy of eMIP-based sensor platforms for the detection of antibiotics, allowing for improvements in the sensitivity and selectivity.

1.5.3 Grafting from/to CoreShell Nanoparticles

There has been considerable increase in the use of MIPs based on coreshell nanoparticles that can overcome the drawbacks generally associated with monoliths. The formation of thin imprinted polymer layers on a solid support enhances binding kinetics, mass transfer, and facilitates easy template removal. Among the materials used for MIP functionalisation, Fe₃O₄ magnetic nanoparticles (MNPs) are most often used due to their paramagnetic properties. A comprehensive review on magnetic particles for MIPs in analytical chemistry, including for the extraction of antibiotics from environmental and food samples, is provided by Chen *et al.* [225]. The use of controlled polymerisation techniques allows to devise the molecular architecture of interest. Atom transfer radical emulsion polymerisation (ATREP) was used to functionalise a molecularly imprinted layer for tetracycline onto magnetic particles [226], leading to a material that can extract the antibiotic tetracycline with very high specificity from a food sample. AuNPs have the advantages of excellent optical, electronic, and catalytic properties [227] and are therefore often used for sensor applications. Gold structures combined with silica nanoparticles were used for the specific detection of ENR. The presence of gold core branches [228] acted as intrinsic hot spots that strongly enhance the electric magnetic field, thereby significantly augmenting the Raman scattering and thus leading to a higher specificity. It was shown that the combination of silica and AuNPs increased the signal by a factor of two compared to AuNPs on its own. It is expected that different cores, such as polystyrene microspheres [229] and chitosan microspheres, which possess excellent biocompatibility, will be explored in the future. However, it has to be noted that the use of a thin MIP layer can limit the number of recognition

sites, which will hamper the sensor sensitivity. Therefore, currently, the preferred method of choice is suspension or emulsion polymerisation, which has proven to yield MIPs with high adsorption capacity while maintaining excellent binding kinetics. The key issues with the current methodology include precise controlling of the thickness, as buried templates can limit the extraction process, and a multistep process that is often not scalable, even though examples of one-pot synthesis of MIP particles are present. The group of Niu *et al.* developed a range of MIP particles bearing hydrophilic polymer brushes via controlled polymerisation [184] techniques. A one-pot synthesis method, based on hydrophilic macromolecular chain-transfer agent (macro-CTA)-mediated reversible addition fragmentation chain transfer precipitation polymerisation, was used to prepare fluorescent MIP nanoparticles for tetracycline. The use of hydrophilic polymers ensured that measurements are compatible with biological samples, which enabled direct quantification of tetracycline in complex biological samples [184]. Instead of a solid support, it is possible to use as a sacrificial support matrix. The approach chosen by Tang *et al.* [230], shown in Figure 1.3, demonstrates the preparation of hollow MIPs with fast absorption kinetics (10 min) for ENR. This method was used to determine the levels of this antibiotic in fish samples, with LoDs well below the legally maximum residual level. The sacrificed support matrix, $K_2Ti_4O_9$ was chosen because of its nontoxicity, low cost, and easy removal process. Silica is one of the popular choices as sacrificial support as the polymers can be embedded into the pores of the particles.

1.5.4 Solid-Phase Imprinting: Immobilization of the Template on a Solid Support

NanoMIPs have the potential to become cost-efficient and robust alternatives to natural antibodies in diagnostics. However, intrinsic problems associated with the imprinting technique have limited their adoption at an industry level. In particular, the most evident drawbacks are: 1) the presence of residual template in the MIP; 2) high binding site heterogeneity; and 3) lengthy or labor-intensive methodologies required for MIP production. The solid-phase imprinting approach allows to overcome these drawbacks. In this method, the template is covalently immobilized on the surface of a suitable solid support (such as solid glass beads, magnetic particles, or similar). This support bearing the immobilized template is then

placed in contact with the monomer mixture, and polymerisation is initiated under conditions that promote the formation of polymeric nanoparticles. After the polymerisation, the solid support acts as an affinity medium: by means of a temperature-based affinity step, unreacted monomers, oligomers, and low-affinity particles are eluted. Then, the temperature of the system is increased and this leads to the disruption of the stronger interactions between high-affinity particles and template, allowing to selectively collect high-affinity nanoMIPs only (Figure 1.8). A thermos-responsive monomer is required for MIP syntheses such as these as explained by Chen *et al.* [231]. As previously demonstrated [232], this process can be easily automated and executed in a matter of a few hours. Because of the affinity purification step, nanoMIPs possess high affinity and specificity toward their targets, exhibit a homogeneous distribution of binding site affinities, and do not contain any residual template (as it was covalently attached to the solid-support). However, template leaching may occur if the bond used to immobilize the template onto the solid phase gets cleaved (usually by hydrolysis) during the elution process. It should be noted that high-affinity nanoMIPs can also potentially be collected by means of changes in pH and/or solvent.

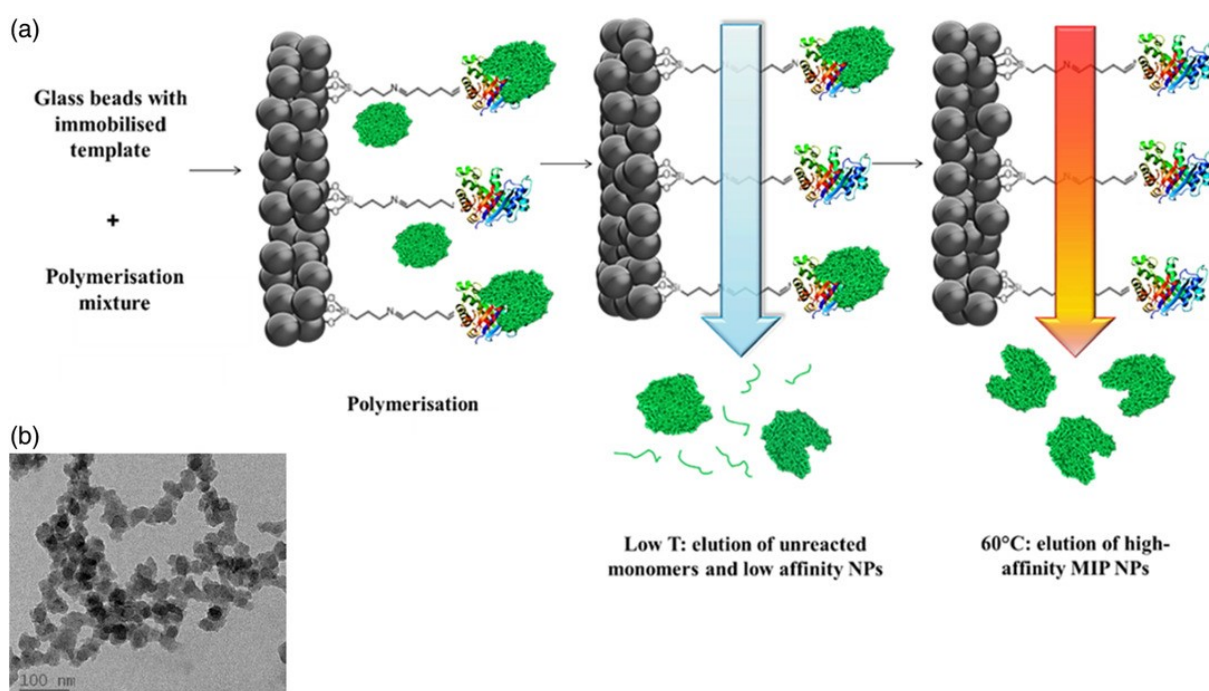


Figure 1.8. a) Solid-phase synthesis of nanoMIPs. In this example, a protein is shown as the template molecule. b) Representative TEM of nanoMIPs. Reproduced with permission [233].

Medina Rangel and co-workers [234] used the transition temperature of NIPAm to collect the high-affinity nanoMIPs, conducting imprinting at 37 °C and the elution at lower temperature (i.e., at 25 °C—which is below the lower critical solution temperature of the MIP polymer). This allows the nanoMIPs to swell, detach from the immobilized template, and be eluted. The proposed approach is generic in nature as virtually any molecule can be imprinted, and it can be conducted both in water and in organic solvents (via a UV-triggered process). However, the template is required to bear at least one functional group for immobilization on the solid phase, and this may be problematic especially for small molecules, which potentially enable real-time detection of biomolecules. In a similar example, nanoMIPs for vancomycin produced by solid-phase synthesis were doped with ferrocene derivatives to make them electroactive [196]. This allowed the indirect electrochemical detection of vancomycin due to the change of redox properties of the ferrocene label upon binding. The authors claimed that the observed behaviour is likely due to hindering of the electron transfer process of ferrocene in the nanoMIPs by their interaction with vancomycin. As mentioned earlier, nanoMIPs have also replaced antibodies in assays. In one such example, antigentamicin-imprinted nanoparticles were used in a pseudo-enzyme-linked immunosorbent assay in spiked milk [235], as a synthetic capture antibody, whereas target detection was achieved in competitive binding tests with a horseradish peroxidase-gentamicin conjugate. The developed polymers showed superior selectivity over other antibiotics (streptomycin and ampicillin) and were capable of detecting gentamicin in milk at clinically relevant concentrations.

1.6 Outlook on the Future of Commercial MIP Sensors for Antibiotics

The straightforward approach, ease of synthesis, and, more importantly, great chemical stability means that MIP integration within sensors is an appealing prospect as they can function in a variety of different environments. In contrast, a natural receptor that might have to be used instead often suffers from poor stability and lower specificity to the target compounds. In this research scenario, where the target/analyte is an antibiotic, an antibody or receptor might not be available [236], and in cases such as this, MIPs have

a clear advantage over naturally occurring ligands. Due to their relative ease of fabrication, researchers have utilised imprinted polymers for separation purposes, in the development of complex matrix pre-treatment strategies [237], [238], and as artificial antibodies [232], [239]–[241]. While the imprinting techniques have improved greatly over the course of the years, it is easy to see how their use in combination with novel smart and nanomaterials greatly benefits the selectivity and the specificity of the sensors as the interest in exploring the integration of MIPs into chemo- [242]–[245] and biosensors [246]–[249] keeps rising. As a multidisciplinary technology, the use of MIPs will greatly benefit from the developments in polymer and material sciences, drug, and environmental research: in contrast, they can be tailored to get maximum advantage from the existing techniques e.g., microfluidic, nanotechnology, biotechnology, and stimuli responsive technology among others [250]. In recent years, the threat of AMR has been gathering much interest as the adverse consequences of such resistance are better understood. The manufacture of cheap, reliable sensors able to monitor antibiotic presence in a variety of environments and conditions will provide an avenue of determining the level of human exposure to antibiotics in our everyday life and what implications and impacts this may present for current and future increasing antibiotic resistance. The intrinsic stability of MIPs would allow for a long shelf life and robustness regardless of the conditions they might be used in. The adaptability of MIPs toward a target of interest and their accessibility makes them great candidates for this very delicate and important task. Despite their unequivocal usefulness and practicability, a few factors limit the commercial use of MIPs, including 1) limited sensitivity of microparticles, which makes them unable to compete with commercial antibodies; 2) integration of MIPs into electrodes that is not an evident task; and 3) mass production of these sensors, which is complicated with standard methods of producing nanoMIPs including electropolymerisation or lithographic techniques, even though several examples have been shown where these problems are partially overcome. Currently, only a few companies are present in the market and the commercialisation of MIPs has mostly been confined to laboratory research, mostly focused on SPE of several environmental contaminants.[83] MIPs are usually prepared in organic solvents (water affects mostly H-bond-driven template-functional monomer equilibrium) but it has been shown that rebinding is usually more efficient when synthesis takes

place in the same solvent used for synthesis [251]. Water and food analysis might thus be a challenge for the obvious presence of water; however, if practices such as taking hydrophilicity of monomers into consideration during monomer selection and conducting controlled radical polymerisation to control surface modification are considered, then, compatibility issues can be reduced. Another issue is the number of functional monomers available that are appropriate for their synthesis, which is a hurdle to overcome. However, this limitation has pushed several researchers to explore alternatives, including the combination of different monomers and the exploitation of amino acids. The issue can also be tackled by the design of new monomers with multiple and varied functional groups, as they can facilitate the ability to offer several interactions with the target, a highly desirable development at the current stage [86]. The exceptional circumstances in which the COVID-19 pandemic has significantly accelerated the recent growing interest in AMR have drawn the attention to the mass production of in-field sensors, whose main features include long shelf life, stability, and ease of use. Despite the increase in academic output recorded in the last 20 years, industrial application has not followed a similar trend mostly due to the limitations mentioned earlier. Nonetheless, the recent breakthroughs in the synthesis are likely to ignite interest in novel MIPs. Mass production of polymers imprinted with antibiotics, especially if produced using the noncovalent method and mild temperatures, can benefit the great advantage of reusing the template and make sustainability a great selling point. The EU has banned animal-derived antibodies [252], which boosts the appeal of MIP usage as their design and production does not require animal exploitation, constituting a significant ethical advantage. Moreover, their low cost and robustness make them a safe bet for the construction of field deployable and in vivo sensors.

1.7 Aim of the study

Through speculation on the severe impact of AMR bacteria detailed in Section 1.1 and the insufficiencies of current sensor platforms to aid the issue mentioned thereafter, exploration and development of a polymer-based sensor platform for antibiotic detection has been carried out. Primary objectives were to-

Chapter 3: Optimise and survey the validity of a dual sensor platform incorporating both a thermal and fluorescent read out.

Chapter 4: Investigate the polymerisation process in terms of possible sensor platform expansion and methodology to maximise the versatility and applications of the sensor produced.

Chapter 5: Extrapolate the use of MIP based sensors from small molecule targets to much larger targets such as full cells (e.g. yeast cells) in a proof-of-concept study to demonstrate future ability for application to direct AMR bacteria detection, further aiding the AMR crisis via an alternative route and cut down identification times in infections to give rise to faster, more specialised treatment.

Chapter 2 explains the general methodologies that were used throughout the thesis whilst a specific parameter selection of aforementioned methodologies will be explained in each chapter and how they were optimised for the work that was being carried out. Chapter 3 will explore the optimisation and development of the dual sensing platform, from the monomer selection process, the polymer optimisation, and the sequential thermal and fluorescent analysis of the polymers. The small sample quantity needed, allows for the conceptualization of this device to be future developed into an on-site sensor. Chapter 4 will explore an electrochemical approach to the polymers and how the polymers can be used to create MIP modified SPEs via two differing polymerisation methods with a following contrasting evaluation of both methods. Chapter 5 will explore the adaption of the target versatility of the polymers and delve into how the imprinted polymers can be used to detect targets ranging from small pharmaceutical molecules up to much larger targets such as full cells (e.g. yeast cells) Finally, Chapter 6 summarises all the work carried out and evaluates what work there is still required in order to produce a commercially viable sensor platform.

Chapter 2. General Methodologies and Chemicals

Hereafter is a discussion and explanation of methodologies used throughout this thesis. The experiments were carried out in the manner disclosed in this chapter unless otherwise stated in an individual chapter.

2.1 General Chemicals

A summary of the chemicals used within this thesis are stated in Table 2.1. Deionised water was used throughout with the resistivity of 18.2 Ω cm.

Table 2.1. General chemicals used throughout the presented thesis.

| Chemical | Source | Chemical | Source |
|--|-----------------------------------|---|---|
| 2-vinylpyridine | Sigma Aldrich (Gillingham, UK) | Hydrochloric acid | Sigma Aldrich (Gillingham, UK) |
| 3-(trimethoxysilyl)propyl methacrylate (MAP TMS) | Sigma Aldrich (Gillingham, UK) | Hydrogen peroxide | Sigma Aldrich (Gillingham, UK) |
| 9-vinyl anthracene | Alfa Aesar (Heysham, UK) | Methacrylic Acid (MAA) | Sigma Aldrich (Gillingham, UK) |
| Acetone | Sigma Aldrich (Gillingham, UK) | Methanol | Sigma Aldrich (Gillingham, UK) |
| Acrylamide (AA) | Sigma Aldrich (Gillingham, UK) | Nafcillin sodium monohydrate | Fisher Scientific (Loughborough, UK) |
| Adenine sulfate | Alfa Aesar (Heysham, UK) | Phosphate buffered saline (PBS) tablets | Oxoid (Hampshire, UK) |
| Ammonium hydroxide | Sigma Aldrich (Gillingham, UK) | Potassium chloride | Sigma Aldrich (Gillingham, UK) |

| | | | |
|----------------------------------|---|---|--|
| Amoxicillin | Sigma Aldrich (Gillingham, UK) | Potassium dihydrogen phosphate | Sigma Aldrich (Gillingham, UK) |
| Azobisisobutyronitrile (AIBN) | Sigma Aldrich (Gillingham, UK) | Pyrrole | Acros Organics (Loughborough, UK) |
| Chloroform | Sigma Aldrich (Gillingham, UK) | Sodium chloride | Sigma Aldrich (Gillingham, UK) |
| D (+)-glucose | Fisher Scientific (Basingstoke, UK) | Tetracycline | Sigma Aldrich (Gillingham, UK) |
| Dimethylsulfoxide (DMSO) | TCL (Oxford, UK) | Tetrahydrofuran (THF) | Sigma Aldrich (Gillingham, UK) |
| Dimethylformamide (DMF) | Sigma Aldrich (Gillingham, UK) | Toluene | Sigma Aldrich (Gillingham, UK) |
| Disodium phosphate | Sigma Aldrich (Gillingham, UK) | Trimethylolpropane trimethacrylate (TRIM) | Sigma Aldrich (Gillingham, UK) |
| Ethanol | Fisher Scientific (Loughborough, UK) | Yeast extract | Fisher Scientific (Basingstoke, UK) |
| Glucose | Fisher Scientific (Basingstoke, UK) | | |

2.2 MIP polymerisation

Conventional MIPs have a composition made up from five categories of reagents: target, functional monomer, crosslinker monomer, solvent (also called porogen) and an initiator. These reagents are individually selected for each unique MIP depending on the platform there are destined to incorporate into

and what the MIP is designed to detect. The template, functional monomer and solvent are traditionally added first to allow a pre-polymerisation complex to form after which the crosslinker is added. With the initiator being added last, oxygen was purged from the reaction mixture via bubbling through nitrogen gas. Polymerisation methods differ depending on the desired polymer form. In this thesis, polymer microparticles and direct polymer film formation onto electrodes via UV and thermal polymerisation were explored.

2.2.1 Production of polymer microparticles using free radical polymerisation

After combining the reactants described in Section 2.2, the solution was degassed, after which a rubber septum was placed over the sample vial. A nitrogen balloon was fitted on top via a syringe needle. The reaction was heated to 65°C for 30 min. During this, the reaction solution changed to a cloudy solid. Once polymerised, the polymer was extracted from the vial and ground via pestle and mortar into a fine powder. The powder was then placed in a 50:50 solution of methanol: water and refluxed. Every 24 hrs, the suspension was taken off reflux and separated via a Büchner funnel. The filtrate was analysed via UV vis spectroscopy which determined template leaching from the microparticles. This extraction step was repeated until no trace of template was observed via the optical analysis.

2.2.2 Film polymer production

After degassing, the polymerisation solution (5 μ L) was placed onto a functionalised glass chip with a microscope slide placed on top this ensured uniform distribution of the solution as well as limiting access of oxygen to the polymerisation. UV polymerisation (1 min) was used to create a thin polymer film on the functionalised glass. The procedure was repeated twice more with each polymerisation given 15 sec less each time. In between each polymerisation, the chip was slid off the microscope slide, allowed to stand for 1 min and then washed with chloroform. After the final polymerisation, a methanol wash was required after the chloroform wash. This afforded 3 layers of polymer film that are still transparent, avoiding thick “crusting” of the polymer which renders that sample defective for fluorescent analysis. The MIP modified

glass chip was then placed in 1:1 methanol: water solution and left on an orbital shaker (100 rpm) until no trace of target could be detected via optical analysis. All NIPs mentioned in this research were produced according to the same protocol for the MIPs apart from addition of a target molecule in the reaction mixture.

2.3 Glass cleaning and functionalisation

Modified glass chips were achieved via cutting microscope slides into 1 cm² glass chips. The chips were then washed separately in the following solutions and sonicated for 8 mins at 65 °C – first wash DI water, second wash with methanol and the final wash with acetone. The chips were then dried completely with nitrogen gas. The chips were then washed separately in the following solutions and sonicated for 15 min each at 65 °C, rinsing with DI water 2 times between the two cleaning solutions. Firstly, with ammonium hydroxide, hydrogen peroxide and water (1:1:5 volume ratio) followed by hydrochloric acid, hydrogen peroxide, water (1:1:5 volume ratio). After this final washing step, the chips were rinsed 3 times with DI water and dried completely with nitrogen gas. Directly after drying the chips were placed in 4% MAP TMS in toluene (15 mL). The tube was turned horizontally, shaken so that no overlapping of chips was present and placed onto an orbital shaker and then left for 24 hr at 100 rpm. Afterwards, the chips were washed in methanol and dried individually with nitrogen. Once the chips were functionalised, polymerisation solution (5 µL) was placed onto the functionalised glass slide with a microscope slide then placed on top.

2.4 Batch rebinding

Batch rebinding experiments provided insight into the specificity and selectivity of the polymer produced. As stated in Chapter 1, specificity is related to the binding capability of a MIP to a target compared to that of a NIP, which can be measured quantitatively by determining the imprint factor. A higher level of binding affinity expressed by a MIP demonstrated that the produced material had cavities for specific binding of the target whereas the reference NIP only possessed non-specific binding to the surface.

Selectivity is related to the MIPs ability to discern between two differing targets. Depending on what sensor is being developed influences what level of selectivity is required i.e., it would be beneficial to detect a family of compounds rather than isolate a single molecule in certain cases.

Batch rebindings were carried out by initially weighing known amounts of polymer into sperate vials. A known volume of solution (target or competitor target solution) was added to a corresponding vial containing the polymer. The suspension was left on an orbital shaker for 30 min after which separation of the suspension was achieved via syringe filters with the filtrate being saved. The filtrate was then analysis via UV vis (before which a calibration curve was derived) and the concentration of the filtrate can be acquired. The batch rebinding experiments are defined by Equation 2.1. (C_i is the initial concentration (mM), C_f is the final concentration (mM) and C_b is the concentration bound to the polymer (mM)).

$$C_b = C_i - C_f \quad [\text{Equation 2.1}]$$

C_f was calculated by division of the gradient parameter from the calibration graph. This was then subtracted from C_i , the known concentration, to give the concentration bound to the polymer. C_b was then multiplied by the volume used (L) and subsequently divided by the amount of polymer used in the vial (g). This affords the substrate bound (S_b , $\mu\text{mol g}^{-1}$) as a quantification to the polymers binding capabilities taking into consideration how much target (g) a certain amount of polymer can bind to. However, this includes both specific binding and non-specific surface binding. The difference between MIP and NIP will yield the specific binding due to interaction of the polymer and target molecule at a given concentration. This is noted as an Imprint factor (IF) which is described in Equation 2.2.

$$IF = \frac{S_b(C_i=x)}{S_b(C_i=x)} \quad [\text{Equation 2.2}]$$

2.5 Fluorescent Analysis

The thesis presented employed two different fluorescent analysis techniques. A plate reader coupled with a fluorometer was utilised for fluorescent analysis of fluorescent polymer suspensions. Filters were chosen with respect to the fluorescent monomer selected, 9-vinyl anthracene, with the excitation at 485 nm and the emission at 520 nm. Results were gathered in triplicate with background readings taken away for each reading taken. During the analysis, suspensions of the fluorescent polymer were introduced to a stated target solution in PBS. Unpolymerised 9-vinyl anthracene was also introduced to target solutions in separate wells. The readings taken from these monomer solutions were subtracted from the suspension sample readings to try to minimise autofluorescence fluctuations of the monomer from interfering with the signal of the polymer suspensions. The use of PBS solution limited the influence of pH on the fluorophore. The readings gathered were in arbitrary units (AU) and were converted to percentages for the purpose of analysis. The procedure was carried out with agitation of the well plate to try to minimise polymer particulate aggregation. Well plates were covered with film to reduce oxidation of the target solutions. In another effort to reduce oxidation, an experiment was set up in which ascorbic acid was incorporated into the PBS solution to act as a radical scavenger however the error percentage of the results were significant and therefore the experimental data was excluded from the chapters analysis, see Appendix A.

A second form of fluorescent analysis was carried out via an inverted fluorescent microscope ($\lambda_{\text{ex}} = 340$ nm and $\lambda_{\text{em}} = 425$ nm). A fluorescent MIP modified glass chip (1cm^2) was inserted into a HTM flow cell and mounted onto an in-house printed flow cell stage holder, see Figure 2.1.

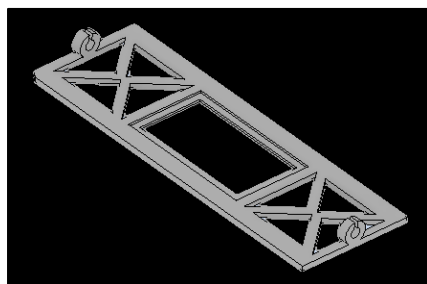


Figure 2.1. In-house designed and printed flow cell stage holder in which inlet and outlet tubes are fastened into position through each clip at either end.

The polymer modified glass chip had a score cut through the polymer layer that acted as a reference point and allowed for a background reading to be taken. The back of chip was painted matte black which avoided any issues associated with light scattering. The sample was white light illuminated and observed under a 4x objective lens. The flow cell was fitted with an inlet and outlet tube to allow for target solution injections. Once the flow cell was sealed, PBS solution was injected in to fill the flow chamber (volume = 110 μL). A section of the chip was selected to observe under the microscope that was covered in polymer but also displayed a section of uncovered glass (a section of the score that was cut through the polymer). Captures of the selected section were taken every 2 mins for 10 min. At 1 min 45 sec into the experiment, 3 mL of solution (target or PBS blank as stated in Chapter 3) was injected into the flow cell. The captures gathered were then analysed via a bespoke Python script (see Appendix B) which allowed for quantification of the fluorescent intensity. The analysis took three regions (100 000 μm^2 each) of polymer covered glass within the chosen study area and averaged the triplicates. As with the first fluorescent analysis, a background reading was taken from a region of the uncovered glass (100 000 μm^2) and was subtracted and then the data was converted into a percentage of fluorescent intensity.

2.6 HTM analysis

A heat transfer set up designed in-house was coupled with an in-house printed flow cell (see Figure 2.2) which were used for all thermal analysis experiments and had an internal volume of 110 μL .

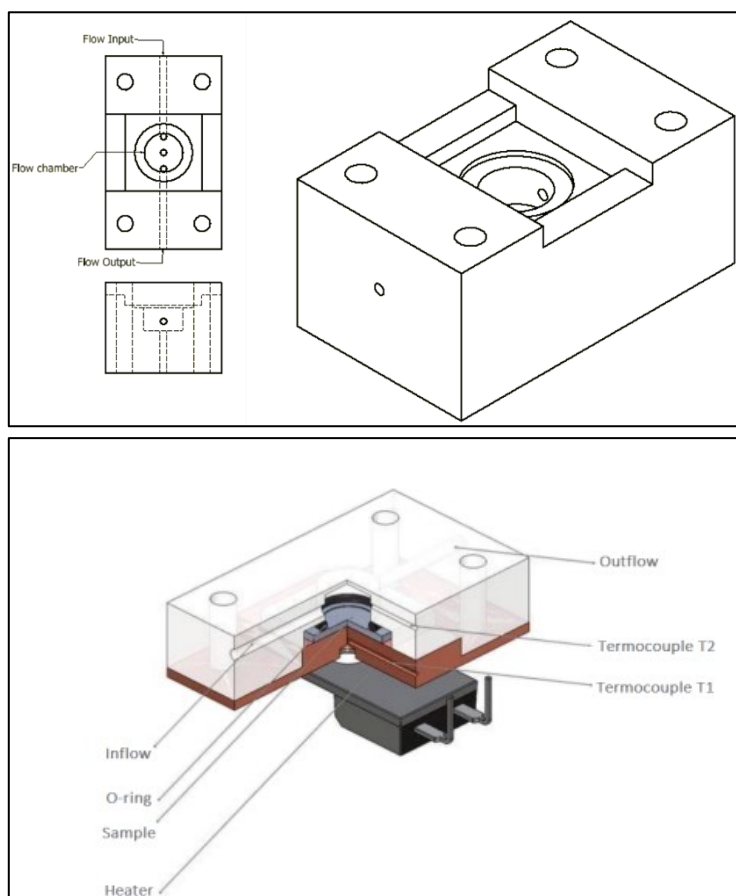


Figure 2.2. Schematic of the flow cell used unless specified (see Chapter 3). An O ring and a copper block is placed on top of the flow cell to create a seal.

The flow cell was placed in an in-house printed flow cell platform as shown in Figure 2.3, this ensured a secure position of the flow cell throughout the experiment as minor movements would cause the thermocouples to move which would have led to leakages of various injection solutions.

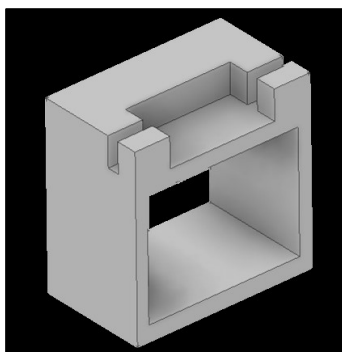


Figure 2.3. In-house designed and printed platform to hold the HTM flow cell secure in which the inlet and outlet tubes are fed through the channels at either end.

Once mounted on the printed holder the inlet and outlet tubes are attached as shown in Figure 2.4. A copper block was attached to the flow cell and acts as a heat sink. The copper block was heated by sending out a voltage to a 22 Ω thick film 20 W power resistor (Conrad Electronic, Germany).

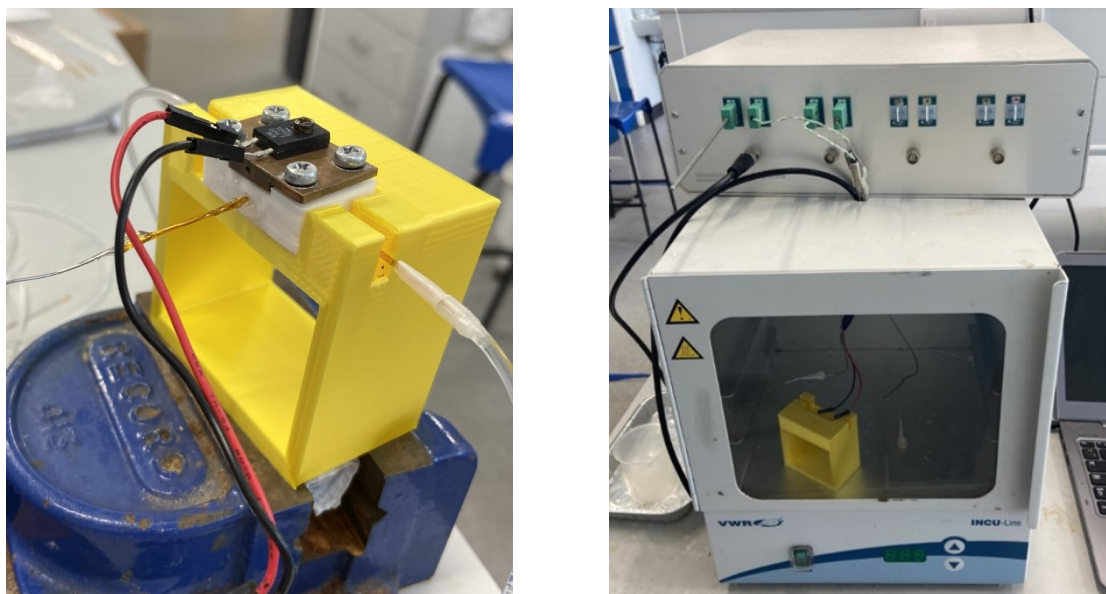


Figure 2.4. HTM flow cell mounted onto printed holder and placed in the HTM set up coupled with an incubator.

A Proportional-Integral-Derivative (PID) controller heats this copper block to 37 °C (T_1). PID parameters were set to the optimized values determined for this environment and heat source of $P = 1$, $I = 14$, $D = 0.3$ [253]. The temperature inside the flow chamber (T_2) is recorded via a type-K thermocouple (RS Components, UK) 1.7 mm above the electrode surface. By subtracting T_2 from T_1 the thermal resistance at the solid-liquid interface can be found, this is then divided by the power input (P) to give the thermal resistance R_{th} (see Equation 2.3 (Thermal resistance (R_{th}) calculated by dividing the thermal resistance at the solid liquid interface (T_1-T_2) by the input power (P)).)

$$R_{th} = \frac{(T_1 - T_2)}{P} \quad \text{[Equation 2.3]}$$

PBS solution was injected through the flow cell in order to flood the flow chamber. The copper block was heated to $37 \text{ °C} \pm 0.02 \text{ °C}$ and allowed to stabilise. A blank injection of PBS solution (3 mL) was passed through after which increasing concentrations of solution (3 mL) were injected at 30 min intervals at a flow rate of $250 \text{ } \mu\text{L} \cdot \text{min}^{-1}$ by an automated NE500 programmable syringe pump (Prosense, Oosterhout, the Netherlands). A final injection of PBs was issued to ensure no loosely bound target remained which would have affected the response measured. The LoD was calculated through Equation 2.4 (SD_{blank} = standard deviation of the PBS blank). This approximate LoD was compared to the SD of the target solution injections to ensure it as symbolic of all injections.

$$LoD = 3 \times SD_{\text{blank}} \quad \text{[Equation 2.4]}$$

Chapter 3. Development of a dual detection polymer-based sensor for antibiotics in aqueous samples.

3.1 Abstract

A polymer-based dual detection platform for sensing of antibiotic traces was developed, which will improve the reliability and accuracy compared to existing sensor platforms. The Heat-Transfer Method as a thermal sensing technique has been extensively investigated previously by the group and has shown added benefits in terms of fast analysis, low-cost and straightforward operation compared to current state-of-the-art. Fluorescent sensing is another widely used technique in commercial sensing; however, incorporating a fluorescent moiety into polymers is complex as the fluorophores are sensitive to changes in signal and as result, not as widely used upon as the use of carbon/ quantum dots. A polymer that can emit a fluorescent signal was developed, enabling the use of both fluorescent and HTM analysis. The HTM analysis afforded an LoD of 0.1 ± 0.3 mM. MIP T (MIP tetracycline) exhibited a ten times greater response to the target tetracycline compared to the response saw with amoxicillin, a different antibiotic. A response such as this dictated that the polymer possessed significant levels of selectivity. MIP T also exhibited an additional $34 \pm 1.1\%$ fluorescent quenching over that of NIP T, which highlights it also possessed crucial level of specificity. Described through the work was a polymer recognition element that was easily used for detection of antibiotic targets which lead to the output of a sensor that can be applicable to both thermal and fluorescent detection, lending to a new avenue for imprinted polymer sensing.

3.2 Introduction

Tetracyclines are broad spectrum antibiotics that are widely used for treatment of bacterial infections in patients and animals. It was also a common food additive in the food industry, but its blanket use has led to a significant rise in AMR [254] whilst its bioaccumulation in humans has led to severe health impacts such as hepatotoxicity and exacerbation of renal failure symptoms [255], [256]. With Hamscher *et al.* conveying the persistent nature of tetracycline and new tetracyclines developed with additional heavy

metal groups attached to increase their bactericidal effect, there is now more need than ever to revolutionise the detection of this class of antibiotics [257].

A dual detection system has been developed for tetracycline by Han *et al.* which exploits europium-doped CdTe quantum dots for visual and colorimetric detection of tetracycline [258]. The work undertaken gives insight as to the advantages of a dual detection system; however, it applied one analysis technique for two read-out systems whereas the work presented in this chapter is the combination of thermal and fluorescent as two separate techniques. This poses advantageous as environmental sensitivity in CdTe quantum dots could affect both the read outs whereas the separation of analysis techniques avoids this potential issue.

Most fluorescent studies seen on antibiotic selection employed either carbon or quantum dots which have benefits associated with accuracy; however, a more simplistic approach is the incorporation of a fluorescent moiety into the polymer structure rather than adding on fluorescent probes as this provides an ease of use and production advantage whilst still maintaining high levels of reliability [186]. Hudson *et al.* has shown how both fluorescent and thermal analysis can be used to detect antibiotics (nafcillin) but the sensitivity of the fluorescent monomer used served as a limitation as to the appropriateness for the future use in environmental samples. The work will be improved upon by optimisation of the polymer composition primarily on the fluorescent moiety used to avoid pH sensitivity of the fluorescent moiety.

The use of 9-vinyl anthracene as a fluorescent monomer in MIPs is relatively unreported on. However, an environmentally friendly recognition element was developed by Zhang *et al.* saw 9-vinyl anthracene being employed in with a MIP to detect Theophylline, a respiratory disease treatment drug [259]. Here the 9-vinyl anthracene was used to functionalise the carbon nanotubes and the sensors binding capabilities were measured via a UV vis batch rebinding methodology rather than the monitoring of the fluorescent signal of the polymer on introduction to the intended target. The work here was not intended as an analysis system based on the fluorescent intensity of the polymer.

MIPs have been utilised for tetracycline detection previously such as the work carried out by Pizan-Aquino *et al.* who synthesised magnetic MIPs that were analysed via an electrochemical and HPLC-UV methodology. The work afforded MIPs with an imprint factor of 3.5 which shows significant specificity,

which can be attributed to the use of a combination of functional monomers. The sensor was also applied to commercial milk samples, providing proof-of-application. The synthesis of the MIPs however, was complex and time consuming which is one of the critical issues facing MIP use [260].

Jamieson *et al.* showed in 2019 that through HTM analysis, LoD as low 0.54 ± 0.10 nM could be achieved for the antibiotic amoxicillin. From this work, it was clearly demonstrated how HTM analysis can be employed for specific and selective detection of antibiotics [213]. Jamieson *et al.* have demonstrated the HTM analysis can also be used to determine concentrations of yeast, a much larger target than an antibiotic [261]. With the ability to detect large, whole cells, the detection scope could be extended to AMR bacteria, a much more direct approach at battling the rise in AMR. However, preliminary foundation work such as the current project was needed to pave the way for such future generations of sensor platform.

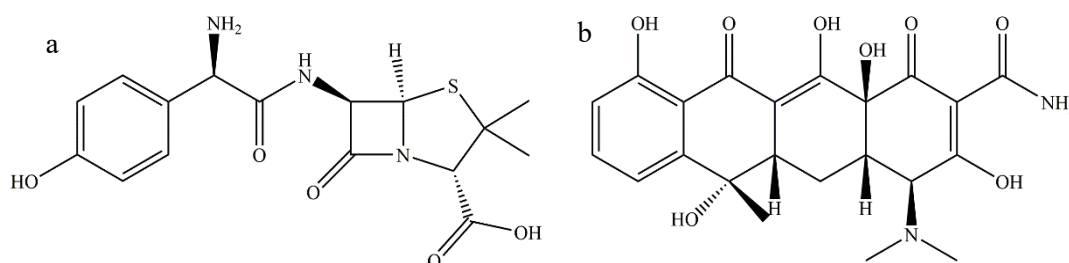


Figure 3.1. Structure of a) amoxicillin and b) tetracycline

The study hereafter will predominantly focus primarily on tetracycline but will also touch on other commonly found antibiotics (such as amoxicillin) to further display the versatility of MIPs. From Figure 3.1, the structures of tetracycline and amoxicillin can be observed. It was prevalent that many of the functional groups, hydroxyl groups, benzene rings and amine groups, are present in both structures. Therefore, monomer selection was carefully considered as any of these groups in either antibiotic molecule could interact with the monomers chosen. Another aspect of a MIPs selectivity comes from the shape of the pore created. This meant that even though both antibiotic molecules could interact with similar functional groups, the shape of the pore will also affect whether or not a molecule binds within an imprinted cavity. A dual detection platform combining fluorescent analysis with thermal detection will

produce a novel sensor that will exhibit the commercially desirable attributes of both detection systems. This will be the first step in a new generation of sensors with applications far beyond traditional detection platforms.

3.3 Experimental

3.3.1 Equipment and Reagents

A UV-VIS spectrophotometer (BMG LabTech, FLUOstar Omega, BMG Labtech, Aylesbury, UK) was used for initial fluorescence studies. A Nikon Eclipse Ti-E, Nikon (Surbiton, UK) inverted microscope was subsequently used for fluorescent analysis. A Stuart mini orbital shaker SSM1 (Staffordshire, UK) was throughout the study. All experiments were carried out at $21\pm 1^\circ\text{C}$ unless otherwise stated. 9-vinyl anthracene was sourced from Alfa Aesar (Heysham, UK), DMSO was procured from TCL (Oxford, UK) while all other chemicals were purchased from Sigma Aldrich (Gillingham, UK). PBS tablets were acquired from Oxoid (Hampshire, UK) and were used to ensure a constant ionic strength of solutions experimented on whilst maintaining a constant pH level (7.4). UV polymerisation was induced by a Polytec UV LC-5 light source ($\lambda_{\text{max}} = 365 \text{ nm}$, Karlsbad, Germany). Ambient temperature was achieved via a VWR INCU-Line Digital Mini Incubator (Lutterworth, UK) during HTM analysis.

3.3.2 Synthesis of Polymers

Consultation with Prof Rurack's team at BAM Bundesanstalt für Materialforschung und -prüfung, saw the formulation of the polymer composition. This composition saw a high amount of crosslinker added, which led production of a more robust polymer [174]. A 20:1 ratio of MAA functional monomer to the target was in effort to drive forward higher levels of specificity in the cavities synthesised while the relative quantity of the fluorescent functional monomer stayed at a 1:1 ratio with the target. This was primarily due to the fluorescent monomer not being used for an increase in specificity but primarily utilised for fluorescence intensity change inducing interactions between cavity and target.

MIP synthesis was carried out in a similar manner as described in Chapter 2 (compositions can be seen in Table 3.1 and Table 3.2) by dissolving the functional monomer (s), target in the solvent. Once dissolved, the crosslinker was added, followed by the initiator, AIBN. This solution was then degassed with nitrogen gas and then sealed in the vial with a nitrogen balloon adorning the vial. This reaction solution was left at 65 °C for 1 hr until the reaction solution had become solid, indicating polymer formation.

| | Target | | Fluorescent Monomer | | Functional monomer | | Crosslinker | | Solvent | Initiator | |
|-------|---------------|----|----------------------------|------|---------------------------|-----|--------------------|-----|----------------|------------------|----------|
| MIP A | Amoxicillin | | 9-VA | | MAA | | TRIM | | DMSO/ DMF | AIBN | |
| | mM | mg | mM | mg | mM | μL | mM | μL | mL | mM | mg |
| | 1.368 | 50 | 1.368 | 27.9 | 2.737 | 232 | 13.68 | 175 | 3 | 0.1368 | 22. 4 |
| MIP T | Tetracycline | | 9-VA | | MAA | | TRIM | | THF | AIBN | |
| | mM | mg | mM | Mg | mM | μL | mM | μL | mL | mM | mg |
| | 0.1125 | 50 | 0.1125 | 23 | 2.25 | 191 | 11.25 | 359 | 3 | 0.1125 | 18 |
| Ratio | 1 | | 1 | | 20 | | 100 | | - | 1 | |

Table 3.1. Compositions of bulk polymers synthesised in this work

The polymer was then added to 200 mL solution methanol: water (1:1) and left at reflux to enable extraction of the target molecule. The suspension was filtered through a Büchner funnel to separate the polymer from the solution. The dried polymer was then ground into a fine dust via a pestle and mortar. The filtrate was analysed via UV-vis to determine the levels of target it contained. The extraction was then continued until negligible traces of target was present in the filtrate thus indicating maximum extraction.

Polymer films were synthesised in a similar manner to the aforementioned method however lower quantities of the reactants were implemented given the nature of the smaller scale synthesis. These smaller quantities are shown in Table 3.2. This reaction solution was degassed with nitrogen and then sealed completely for later polymerisation.

| | Target | | Fluorescent Monomer | | Functional monomer | | Crosslinker | | Solvent | | Initiator | |
|-------|---------------|-----|---------------------|------|--------------------|---------------|-------------|---------------|---------------|---------------|-----------|--|
| | μM | mg | μM | mg | mM | μL | mM | μL | μL | μM | mg | |
| MIP A | Amoxicillin | | 9-VA | | MAA | | TRIM | | DMSO/ DMF | | AIBN | |
| | μM | mg | μM | mg | mM | μL | mM | μL | μL | μM | mg | |
| | 5.473 | 2 | 5.473 | 1.12 | 0.1094 | 9.2 8 | 0.5473 | 175 | 150 | 5.473 | 0.9 | |
| MIP T | Tetracycline | | 9-VA | | MAA | | TRIM | | THF | | AIBN | |
| | μM | mg | μM | mg | μM | μL | mM | μL | μL | μM | mg | |
| | 4.95 | 2.2 | 4.95 | 1.01 | 0.099 | 8.4 | 4.95 | 158 | 150 | 4.95 | 0.8 | |
| Ratio | 1 | | 1 | | 20 | | 100 | | - | 1 | | |

Table 3.2. Compositions for polymers synthesised as thin films.

Modified glass chips were achieved as described in 2.3 Glass cleaning and functionalisation. Once the chips were functionalised, 5 μL of the polymerisation solution was placed onto the functionalised glass slide with a microscope slide then placed on top. The chip was polymerised three times for 2 min, 1 min 30 secs and 1 min 15 secs respectively. In between each polymerisation, the chip was slid off the microscope slide, allowed to stand for 1 min and then washed with chloroform. After the final polymerisation, a methanol wash was required after the chloroform wash. All NIPs mentioned in this

research were produced according to the same protocol for the respective MIPs apart from addition of a target molecule in the reaction mixture.

3.3.3 Batch rebinding

A calibration graph was produced from 5 different tetracycline concentrations (10 μM , 25 μM , 40 μM , 55 μM , 70 μM). 5 mg of polymer was then placed into 5 separate vials. Each vial was then administered with 7 mL of one of each of the TC concentrations. The vials were then placed onto an orbital shaker for 1 hr at 100 rpm. Afterwards the suspensions were filtered with the filtrate being collected. The filtrate was then analysed by UV-vis spectrometry and then processed via the calibration graph. The batch rebinding experiments are defined by $C_b = C_i - C_f$, where C_i is the initial concentration (μM), C_f is the final concentration (μM) and C_b is the concentration bound to the polymer (μM). C_f is calculated by division of the gradient parameter from the calibration graph. This was then subtracted from C_i , the known concentration, to give the concentration bound to the polymer. C_b is then multiplied by the volume used (L) and subsequently divided by the amount of polymer used in the vial (g). This affords the substrate bound (S_b , $\mu\text{mol/g}$) as a quantification as to the polymers binding capabilities taking into consideration how much target a certain amount of polymer can binding to. However, this includes both specific binding and non-specific surface binding. The difference between MIP and NIP will yield the specific binding due to interaction of the polymer and target molecule.

3.3.4 HTM analysis

A heat transfer set up designed in-house was utilised as described in Chapter 2. The HTM was coupled with an in-house printed flow cells (see Figure 3.3) which were used for all thermal analysis experiments and had an internal volume of 110 μL . A copper block is attached to the flow cell and acts as a heat sink. A Proportional-Integral-Derivative (PID) controller heats this copper block to 37 $^{\circ}\text{C}$ (T_1). PID parameters were set to the optimized values determined for this heat source of $P = 1$, $I = 14$, $D = 0.3$ [253]. By subtracting T_2 (the temperature inside the flow chamber) from T_1 (37 $^{\circ}\text{C}$) the thermal resistance at the solid-

liquid interface can be found, this is then divided by the power input (P) to give the thermal resistance R_{th} ($^{\circ}\text{C}/\text{W}$), see Equation 3.1.

$$R_{th} = \frac{(T_1 - T_2)}{P} \quad [\text{Equation 3.1}]$$

PBS solution was injected through the flow cell in order to flood the flow chamber. A blank injection of PBS solution was passed through after which increasing concentrations of solution were injected at 30 min intervals at a flow rate of $250 \mu\text{L} \cdot \text{min}^{-1}$ via an automated NE500 programmable syringe pump (Prosense, Oosterhout, the Netherlands).

3.3.5 Fluorescent Analysis

Fluorescent analysis was initially carried out via a UV-VIS spectrophotometer (BMG LabTech, FLUOstar Omega, BMG Labtech, Aylesbury, UK). 20 mg of polymer was suspended in 5 mL of PBS. The suspension was added to each well ($100 \mu\text{L}$) and then the plate was inserted into the plate reader. The plate reader was programmed to initiate with an agitation step for 2 min, then a background reading was taken. Then, $100 \mu\text{L}$ of solution (variable e.g., PBS solution, amoxicillin solution, tetracycline solution) was injected into corresponding wells and another agitation step was initiated. A reading was then taken every 2 min for 10 min (unless stated otherwise) with plate agitation happening in-between times to avoid particulate settlement as much as possible. All results were carried out in triplicate and had a reference blank of polymer with PBS injections instead of antibiotic solutions. The fluorescent intensity recorded of these blank wells were subtracted at each point of the experiment to rule out any fluorescent intensity change seen by the interaction of the polymer in PBS, be it the salts interacting with fluorophores or fluorophores interacting with other fluorophores. The fluorescent intensity was plotted over time after triplicate results were averaged to produce timed fluorescent intensity plots.

A secondary fluorescent analysis was carried out using an inverted fluorescent microscope and flow cell set up (Figure 3.2) that allowed for the fluorescent polymer to be analysed at surface level.

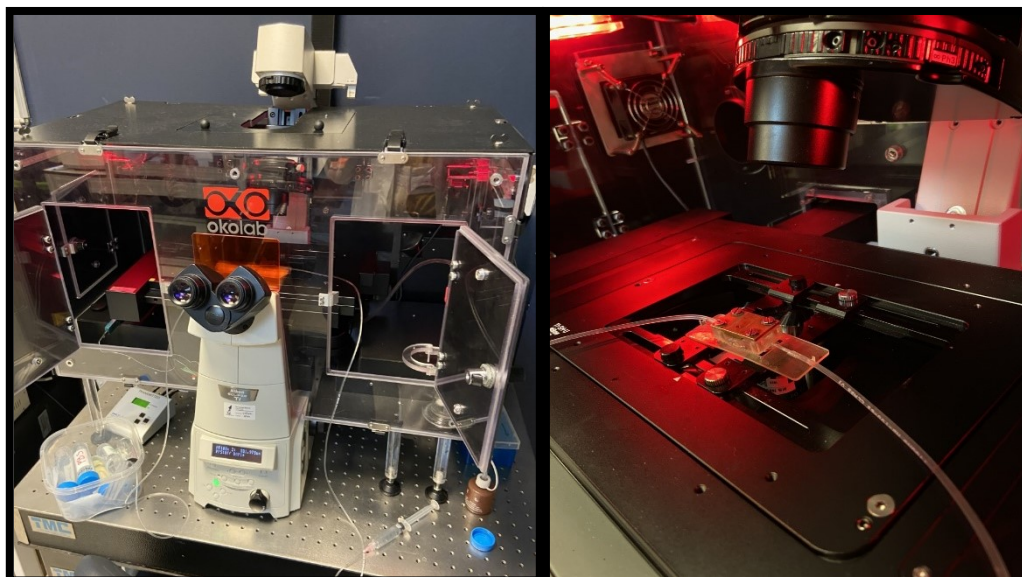


Figure 3.2. image of the individual fluorescent microscope set up.

A MIP chip modified glass chip had a score cut through the polymer layer to produce a blank region of glass on the sample chip. The chip was then mounted into the flow cell atop an O-ring. The flow cell was sealed with a copper block. The set up was kept as close as possible to the set up required for HTM analysis to gauge how well fluorescent analysis could be carried out with the similar set up before attempting a simultaneous thermal and fluorescent analysis.

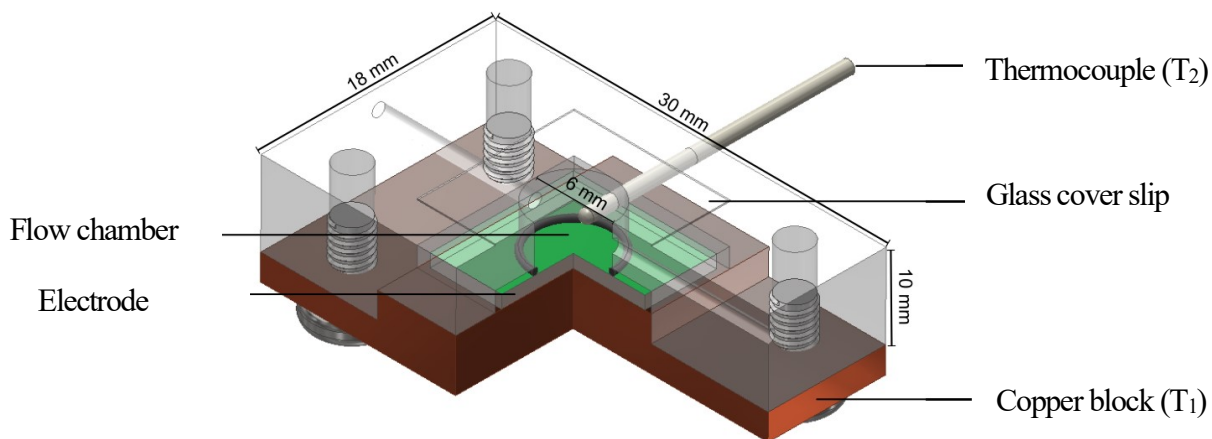


Figure 3.3. depiction of the flow cell set up, demonstrating the glass cover slip over the flow chamber to allow for fluorescent analysis.

Inlet and outlet tubing was attached at either end of the flow cell and then the apparatus was placed onto a 3D printed stage which was then mounted inside the microscope set up. Once positioned on top of the microscope the score acted as a landmark reference point while observing the image through the microscope. A region of the chip was selected to have both polymer and blank glass present as this blank region is needed as a reference. An example region is shown below in Figure 3.4. Initially, the cell was filled with PBS solution and an absence of air bubbles was ensured. The analysis was set up for 10 min allowing for an initial reading to be taken at 0 min and then an image capture every 2 min. Just before the 2 min image capture (time = 1 min 45 sec) the flow cell had tetracycline solution in PBS, 0.1 mM, (unless otherwise stated for a reference or selectivity study) pumped through. Then the experiment carried out with no further additions. This allowed for 4 image captures of the same section of polymer after the injection with an initial blank acting as a baseline. A Python script was created to quantify the fluorescent intensity of the region (see Appendix B). Three areas of polymer were chosen (shown by the white boxes in Figure 3.4) in each electrode region to gain triplicate results. The Python script followed each area over each image capture allowing the formulation of timed fluorescent intensity plots.

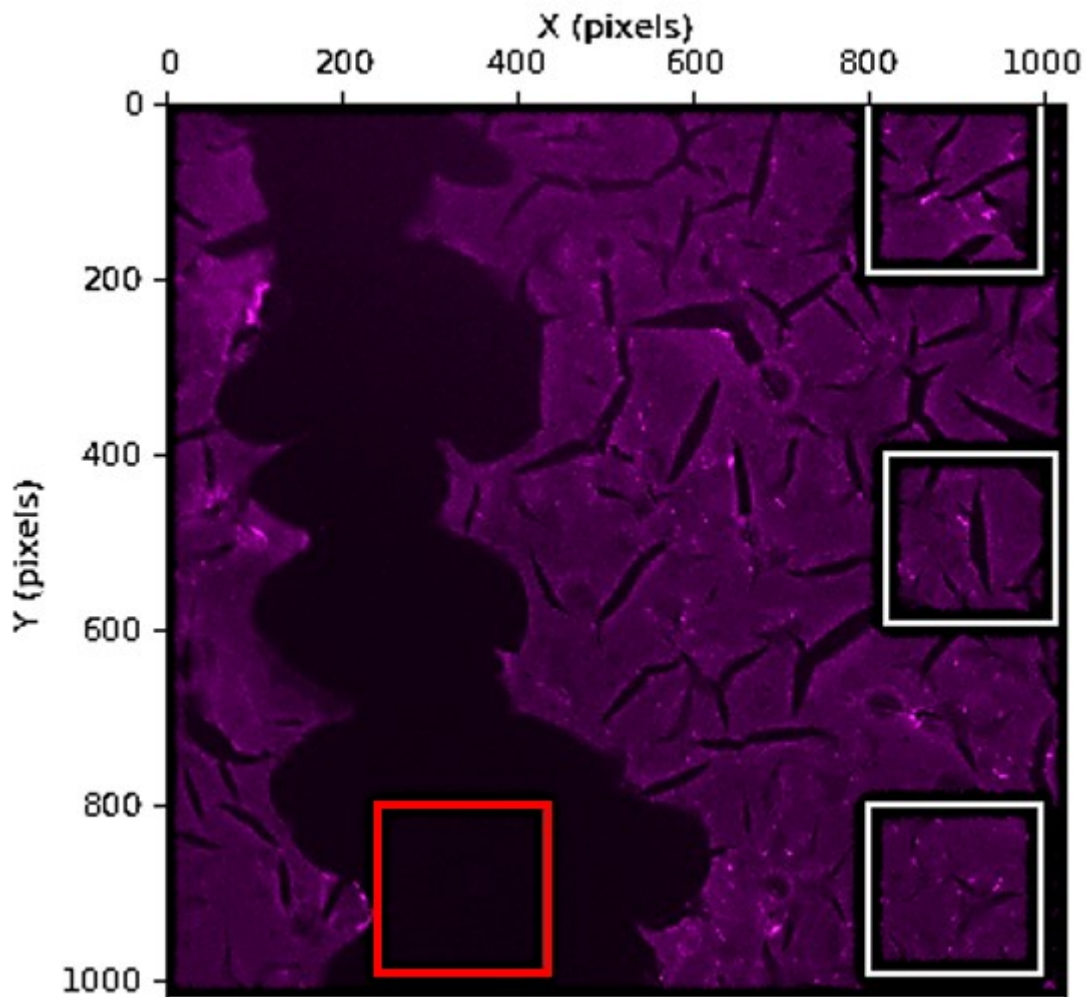


Figure 3.4. Example region of polymer modified glass electrode showing both polymer covered (shown by the white boxes) and uncovered regions (shown by the red box).

3.4 Results and Discussion

3.4.1 *Synthesis of MIPs*

Bulk and film polymerisations were carried out as specified in Chapter 2. Oxygen was purged from the reaction mixtures via bubbling through nitrogen gas. This is because oxygen is a radical scavenger and therefore could scavenge radicals during the propagation stage of polymerisation, leading to early termination and therefore giving rise to the production of short chain polymers. This would inherently be

problematic in polymer production as this could lead to incomplete polymer formation around the target and therefore negatively impact cavity production. During the functionalisation process, the chips were separated, ensuring no overlap, due to overlapping of glass electrodes during functionalisation leading to issues with incomplete functionalisation of the whole surface area of the glass chip.

A microscope slide was placed onto of the monomer solution covered glass slide ensures uniform distribution of the solution as well as limiting access of oxygen to the polymerisation. The final two polymerisations made the films flaky, crusty and opaque. It was observed that when polymer film of this 'flaky' type was extracted, the films fragmented and fell off the chip, this led to non-uniformity of the polymer layer and only partial polymer coverage. Washing procedure was optimised from an existing protocol from the group [186].

3.4.2 Batch rebinding via UV-vis absorption spectroscopy

Specificity studies were carried out on MIP A and MIP T, differing by only the template they were imprinted with used. MIP A was used for the initial fluorescent analysis with the fluorometer coupled to a plate reader while MIP T was used in the second fluorescent analysis and in the HTM analysis. This was due primarily as tetracycline has a lower quantum yield (see Section 3.4.4) and therefore posed less as an interferant in fluorescent analysis. MIP A, imprinted with amoxicillin, was subjected to a specificity study and a selectivity study in which saw its binding affinity to amoxicillin compared with its reference NIP and to two other antibiotics: cephalexin and tetracycline. Figure 3.5a shows that MIP A had a much higher binding affinity to amoxicillin, the target it was imprinted with, over that of the other two targets. Through the batch rebinding experiment, it was shown that at 0.14 mM, MIP A had binding capabilities almost 4x that of the reference NIP A. This portrayed that the bespoke pores synthesised in MIP A elevated the polymers ability to bind to amoxicillin. MIP T was subjected to a specificity study and possessed an IF of 1.8 at 70 mM. Although this IF was lower than MIP A, it was still necessary to change the template to help aid in the development of the fluorescent analysis, due to the higher quantum yield of amoxicillin as discussed in Section 3.3.4.

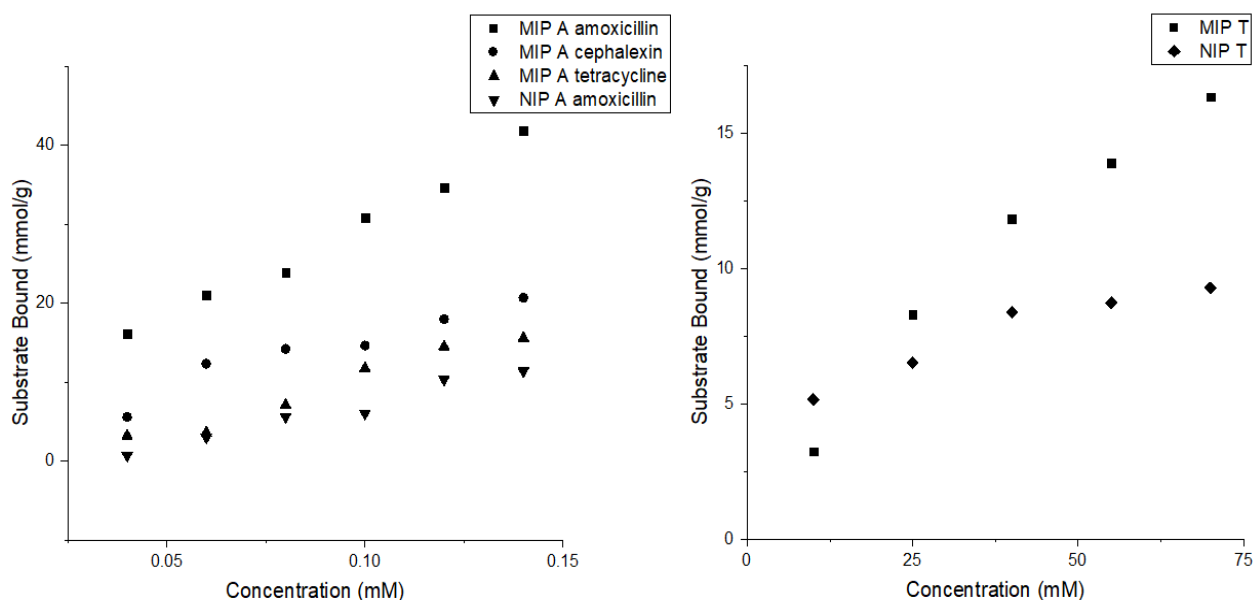


Figure 3.5. a) specificity and selectivity study of MIP A, showing its binding capabilities compared to that of NIP A and also to other targets and b) the specificity study of MIP T (using 10 mM, 25 mM, 40 mM, 55 mM and 70 mM tetracycline solutions).

Although the studies were carried out using a bulk-produced powder polymer and the dual detection system will utilise a polymer film, the composition being the same, means that whatever imprint factor was determined would be applicable to the polymer film also.

3.4.3 HTM Analysis

MIP modified glass electrodes were placed inside the flow cell described in Figure 3.3 and coupled to the HTM set up. PBS solution was flowed through the cell and stabilisation was allowed to occur.

An initial injection of PBS was injected through after stabilisation, this acts as a reference base level. The starting R_{th} of the MIP was slightly higher than that of the NIP. This would be caused by 2 main reasons. Firstly, the position of the thermocouple within the flow chamber is crucial to the R_{th} received, therefore any slight differences between the position of this thermocouple when recording for the separate experiments would have resulted in the difference seen. Secondly, differences in surface structures would lead to a difference in initial R_{th} . The initial R_{th} of the signal would not have affected the results seen as the

results were interpreted with respect to the initial R_{th} signal of the singular polymer in question, not between the responses received for both the polymers. Figure 3.6b displayed the change in R_{th} , to aid the analysis. 30 mins was allowed for stabilisation before increasing concentrations of tetracycline solutions were injected through the flow cell (0.01, 0.1, 1, 10, 100 mM). 30 mins was allowed between each of the solution injections to allow time for stabilisation. Slight drift was experienced; however, it was clear that after each injection, a higher thermal resistance was experienced. After the first PBS injection a stabilisation was seen at was $5.2^{\circ}\text{C}/\text{W}$ (based on a 100 sec average), with weaker initial concentrations only very slight increases were witnessed however at 1 mM we can see a definitive increase at $5.6987^{\circ}\text{C}/\text{W}$. After the final PBS injection, a stabilised signal shows a R_{th} of $5.9975^{\circ}\text{C}/\text{W}$, a $0.0688^{\circ}\text{C}/\text{W}$ increase in the R_{th} from the initial PBS injection. This final PBS injection is a crucial step in HTM analysis. It washed away any loosely bound target which allowed for the conclusion that any rise in R_{th} was due to strongly bound target molecules to the custom-made pores.

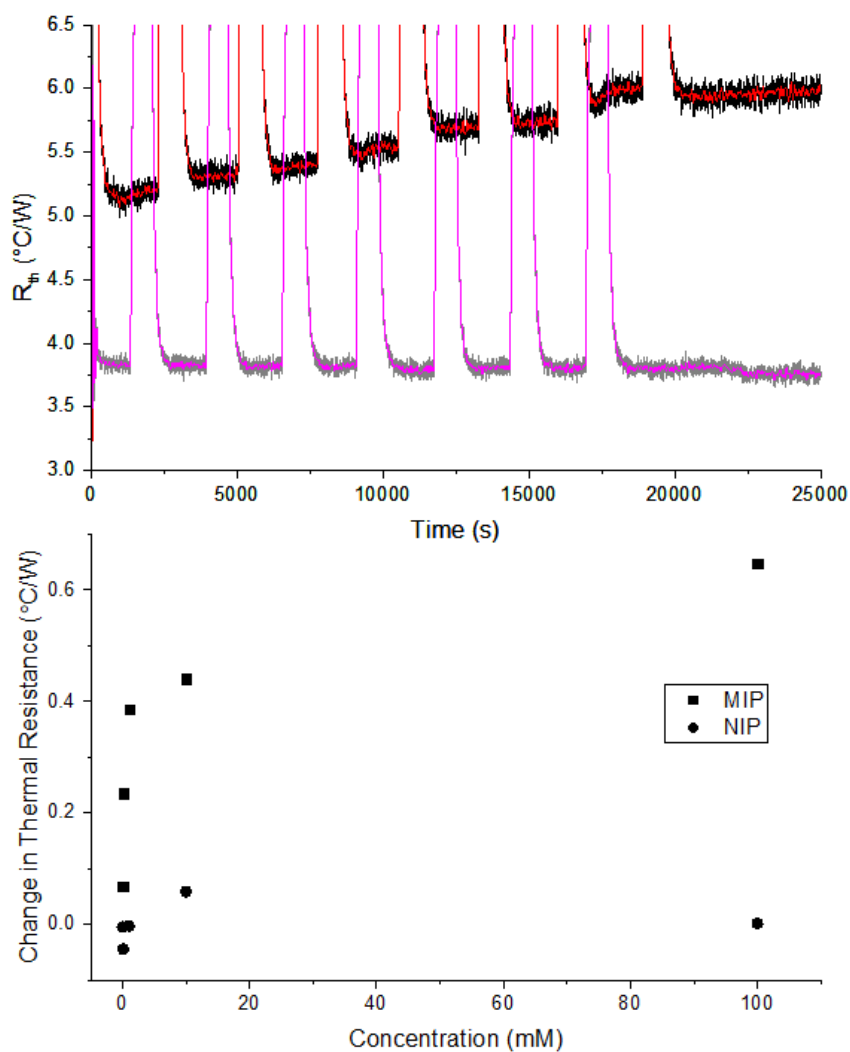


Figure 3.6. a) Comparison of the thermal resistance of MIP T (black and red) and NIP T (grey and magenta) upon injections of increasing tetracycline solution and b) displaying the dose response curve for MIP T.

It was clear from the dose response curve, Figure 3.6b, and repeat data in Appendix C, that at all concentrations of tetracycline solution, the MIP displayed a higher change in thermal resistance upon binding than the NIP, confirming the hypothesised theory of specific binding occurring. The HTM displayed an approximate LoD of 0.101 ± 0.3 mM. The standard deviation at the highest tetracycline concentration used ($SD=0.03197$) was lower than that of the blank PBS sample ($SD=0.03381$) which affirms that the LoD would be very similar if not lower.

3.4.4 Fluorescent Analysis

An exploration of two methods for fluorescent analysis were carried out. Initially a well plate reader coupled with a fluorometer was used. Polymer suspensions were added to the wells and the fluorescent signals were monitored over time after an injection of either target solution or PBS solution.

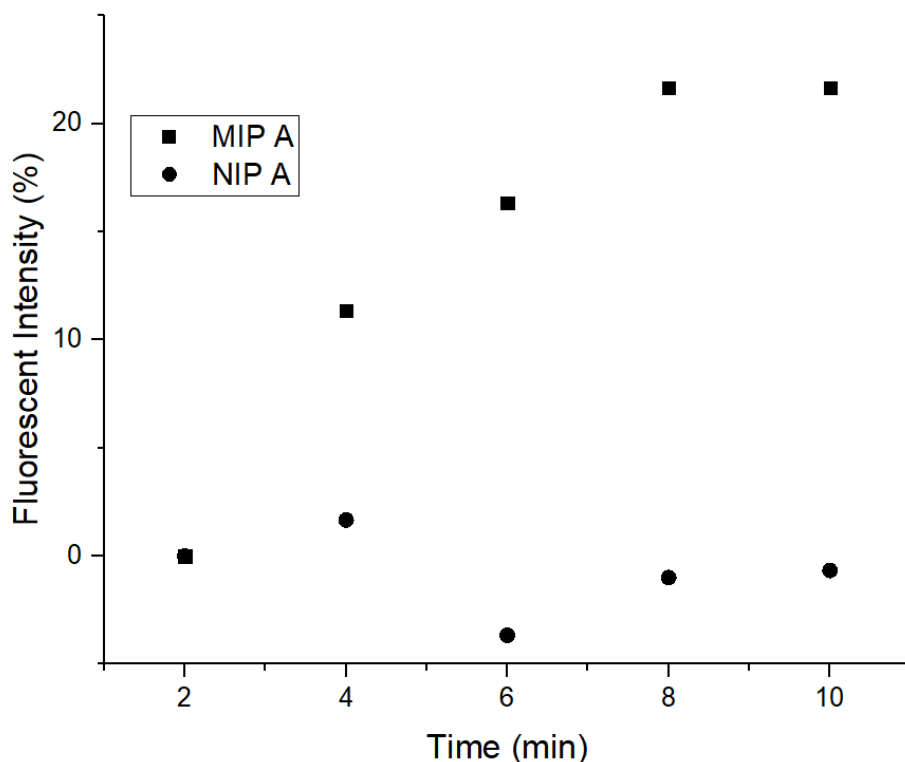


Figure 3.7. Specificity study of MIP A via fluorescent analysis during the introduction of amoxicillin (0.01 mM).

An initial specificity study was carried out on MIP A via UV vis analysis in 3.3.2. MIP A was subjected to another specificity study via fluorescent analysis as portrayed in Figure 3.7. It was evident from this that when MIP A was exposed to amoxicillin solution it had an elevation in fluorescent intensity of $22 \pm 0.6\%$ after 10 min compared to that of NIP A which showed a minor decrease in fluorescent intensity of $0.6 \pm 0.6\%$ after 10 min. This proved that the specific binding of the template to the imprinted pores on the polymer spurred a change in the fluorescent intensity and not the nonspecific binding associated with NIP binding capabilities.

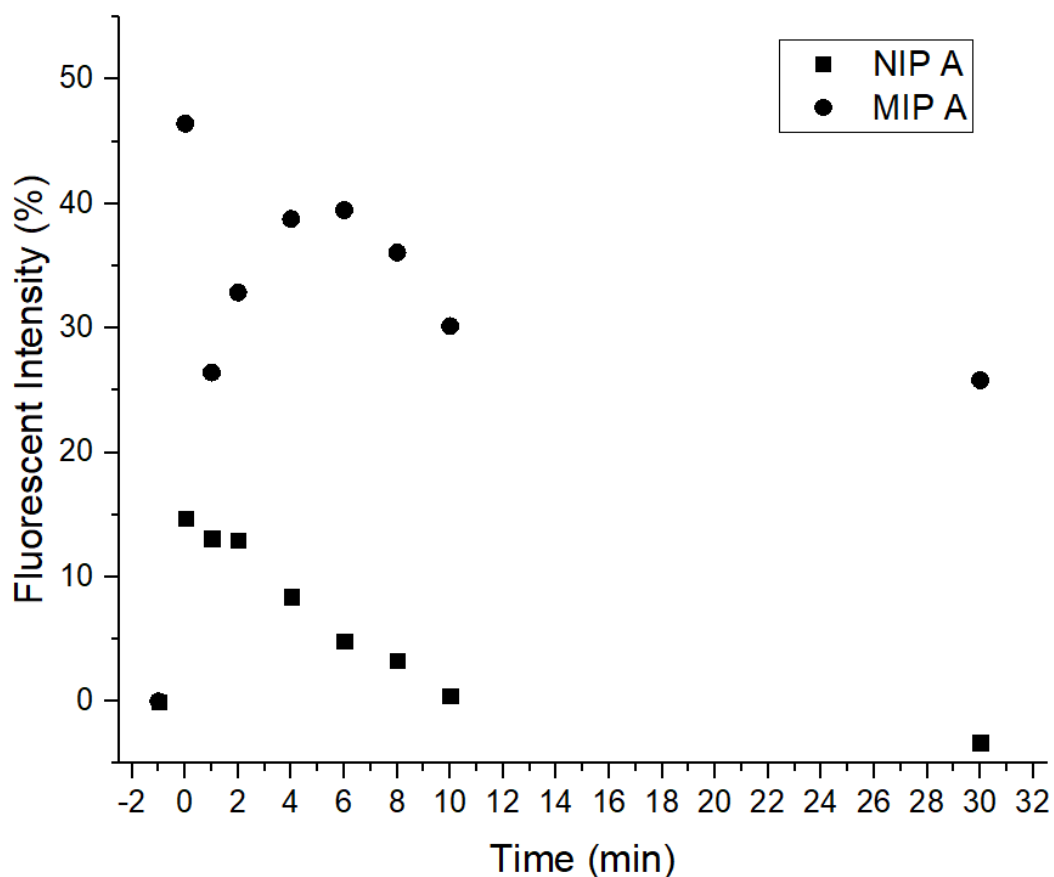


Figure 3.8. Specificity of MIP A with 0.03 mM amoxicillin in PBS, displaying the difference in fluorescent intensity exhibition between that of the MIP and the NIP.

Figure 3.8 shows another specificity study via measuring the fluorescent intensity on amoxicillin introduction to MIP and NIP A over 30 min to gauge a clearer insight as to the fluorescent analysis for the specificity of MIP A. It was clear a different trend was observed in the first 10 min from that observed in Figure 3.7 which, as the analyse was the same apart from the duration of the experiment, called into question the reliability of this form of analysis for the desired observation. A clear difference was seen again between the MIP and NIP in regard to the fluorescent intensity measured throughout the experiment. It is plausible to account the significant increase due to specific binding of the target (amoxicillin) to the specific cavities, the interactions formed in these cavities could induce a higher number of cyclical electron

transmissions (from S_0 to S_1 to S_1 to S_0 energy states) in the fluorophore, causing increased fluorescence [156]. The increase shown by the NIP could be explained by non-specific surface binding that led to a similar increase in fluorescence but due to the lack of specific cavities, this increase was a much more limited exhibition. The general decrease over time of the fluorescence showed a different trend to that analysed in Figure 3.8 which could be due to the target-cavity complex having time to stabilise into a lower energy conformation and therefore reducing the amount of these cyclical electron transmissions. The polymers, where possible, were kept in darkness however absolute darkness cannot be guaranteed in the plate reader, therefore photobleaching may have been a contributing phenomenon in the quenching fluorescent signal over time.

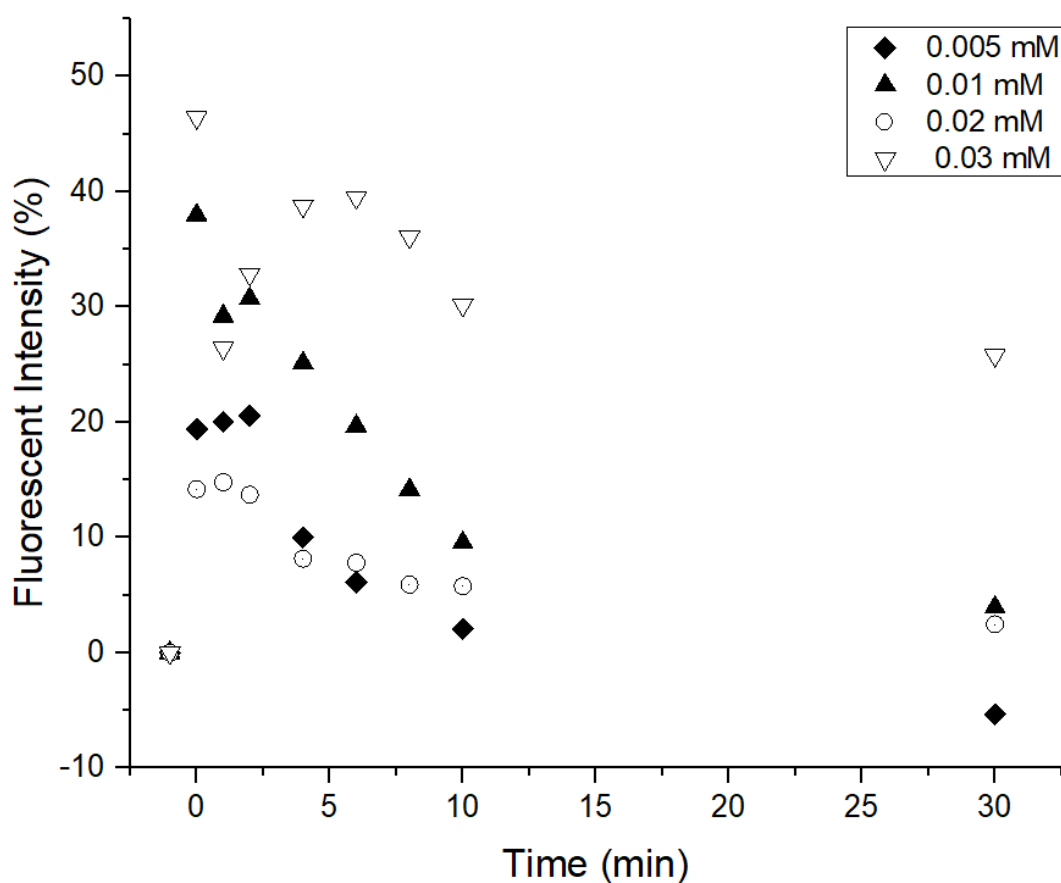


Figure 3.9. Comparison of target concentration effect on fluorescent intensity produced by MIP A.

Varying the target concentration is an important factor when considering developing a sensor platform. A sensor that can only detect the presence of a target is a much more qualitative approach and therefore less favourable for the current sensor under development. Figure 3.9 shows the fluorescence intensity recorded at intervals of MIP A when exposed to a series of amoxicillin solutions (0.005-0.03 mM). At the end of the experiment (time = 30 min), a general trend can be described; the lower the concentration, the lower the percentage fluorescent intensity will be displayed as the end, a chronological order of fluorescent intensity with each higher concentration at 30 min. However, upon closer inspection of the intermediate results, this trend was not prevailing throughout the whole experiment. This could be for a number of reasons. With higher concentrations there will be high levels of non-specific surface binding, depending on this and the position this occurred, the target molecules exhibiting this may have acted as non-competitor inhibitors of the specific cavity i.e. although the molecule itself was not bound into the specific cavity, its position on the surface caused steric hinderance, which disabled another molecule to bind specifically. Another reason is sub-surface binding, which was present due to the heterogenous nature of the polymer particles through manual pestle and mortar grinding. The binding in instances such as these is more appropriately described by a Freundlich adsorption isotherm than a Langmuir isotherm as described by Umpleby *et al.* [262], who demonstrated the appropriateness of applying the Freundlich adsorption isotherm for polymers where high affinity and low affinity binding sites are present. It is plausible to assume that even at the lower concentrations, the majority of surface cavities are interacting in the intended manner with the template. However, progressing through the experiment, the target has time to infiltrate the polymer and access cavities which were below the surface, meaning that the later recorded data may be a truer representation of what was occurring. Though due to the many modes of fluorescent quenching mentioned in Chapter 1, the steady quenching throughout the experiment could be explained via other mechanisms than target-pore interactions. Due to the conflicted results gathered in Figure 3.7 and Figure 3.8 which have displayed an increase and decrease respectively in the fluorescent intensity another experiment was carried out, which ran for 6 hrs, as shown in Figure 3.10. This experiment utilised MIP T, a polymer similar in composition to MIP A but imprinted with tetracycline instead. From Figure 3.10,

much lower fluorescent intensities were observed, this could be to with the change in target as amoxicillin and tetracycline have critically different quantum yields (0.571 and 3.4×10^{-4} respectively at similar pH levels) [263]. The lower quantum yield of the tetracycline target allows for less concern to be donated to the autofluorescence of the target itself, meaning that the focus of the change can be attributed more to the target-pore interactions. Figure 3.10 demonstrated that after 6 hrs MIP T when introduced to 0.25 mM solution of tetracycline, exhibited a decrease of 26.4%. Figure 3.10 also displayed a noticeable drop for all samples at 180 min. The ongoing rise of the fluorescent intensity noticed after this for three of the samples calls into question a defect with the instrumentation in terms of an environmental disturbance.

The lack of clarity on what is happening at a surface level on MIP T when it interacts with targets and controls gave cause for concern. A major consideration in hindsight was particle size. Although all polymers synthesised were ground with a pestle and mortar, the exact polymer particle size is crude and nonuniform due to the nature of the grinding method employed. This could exacerbate the aforementioned explanation of subterranean cavities- target binding but also has negative repercussions on the reliability of the experiments with the plate reader. Diffusion is known to be an issue [264]. A sample of polymer, of known weight, at a smaller particle size would inherently have more readily available specific cavities for rapid target interactions and therefore seem to exhibit more proficient specific binding capabilities. Another drawback of this methodology was its incompatibility with the HTM method. There was no obvious manner in which to combine both methodologies, particularly due unchangeable features of the fluorometer coupled plate reader such as the shaking step and lack of access for thermocouples while the plate reader is operating.

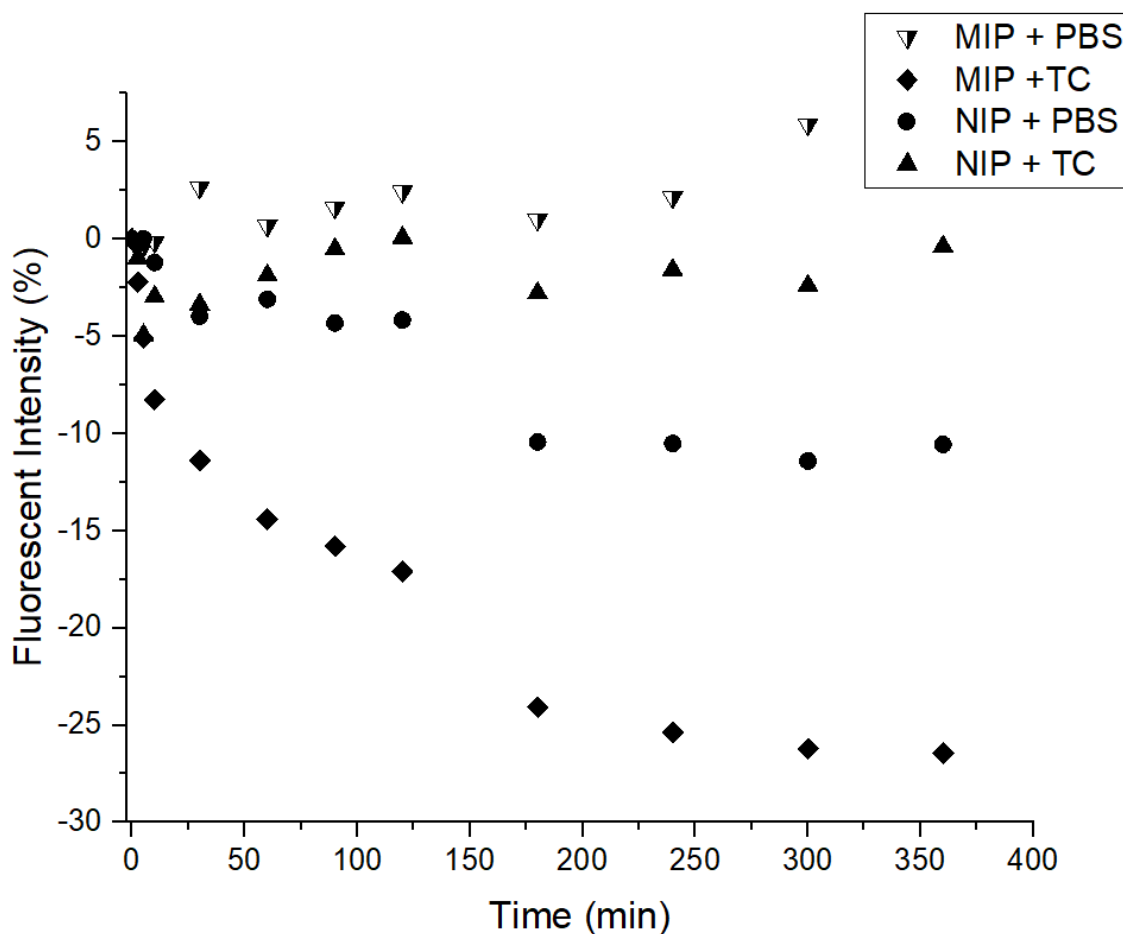


Figure 3.10. Fluorescent intensity of MIP T and NIP T on introduction of PBS and TC (0.25 mM).

Progressive particle congregation is another cause for concern in such experiments as these due to the suspension nature of the sample. Particle settlement at the bottom of each well could critically affect the analysis despite the method being carried out under agitation to minimise this affect as much as possible. Due to the serious concern of particle settlement, a new analysis technique was devised. Fluorescent analysis through an inverted microscope gave many advantages for the desired analysis. Overcoming particle settlement issues aside, it allowed for a significantly higher level of understanding of what was happening on the surface of the polymer. The polymer was successfully mounted onto a functionalised glass electrode in thin layers as seen in Figure 3.11.

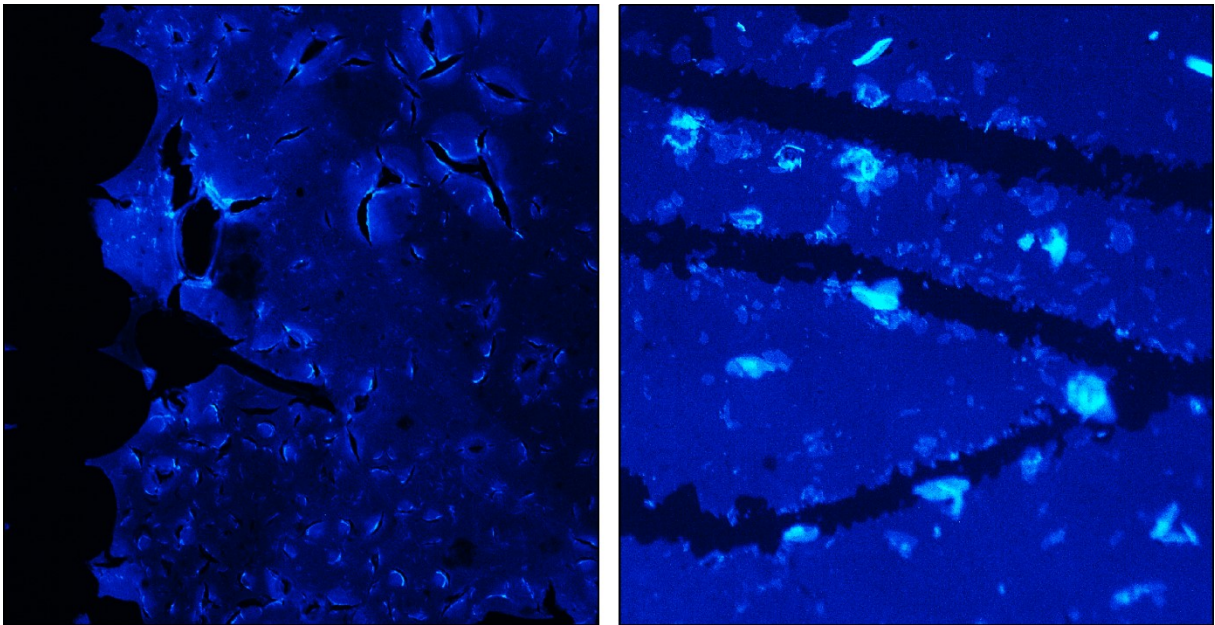


Figure 3.11. Capture of MIP films polymerised onto functionalised glass. Scores have been cut through the polymer to act as reference points.

These polymer chips were enclosed in a flow cell (see Figure 3.3) which was then mounted onto the microscope stage under a 4x objective lens (Plan Apochromat, Lambda, 0.2NA, Nikon, Surbiton, UK), the sample was white light illuminated, with the excitation set at 340 and the emission recorded at 425 nm. During the experiment, specific areas were chosen within each individual frames being captured by a sCMOS camera (Andor Zyla 4.2, Andor, Belfast, UK) and an exposure time of 0.5 sec ensured. Three regions of polymer covered glass and a single region of blank glass. These 4 regions were monitored while varying solutions were introduced into the flow chamber for a known stated of time.

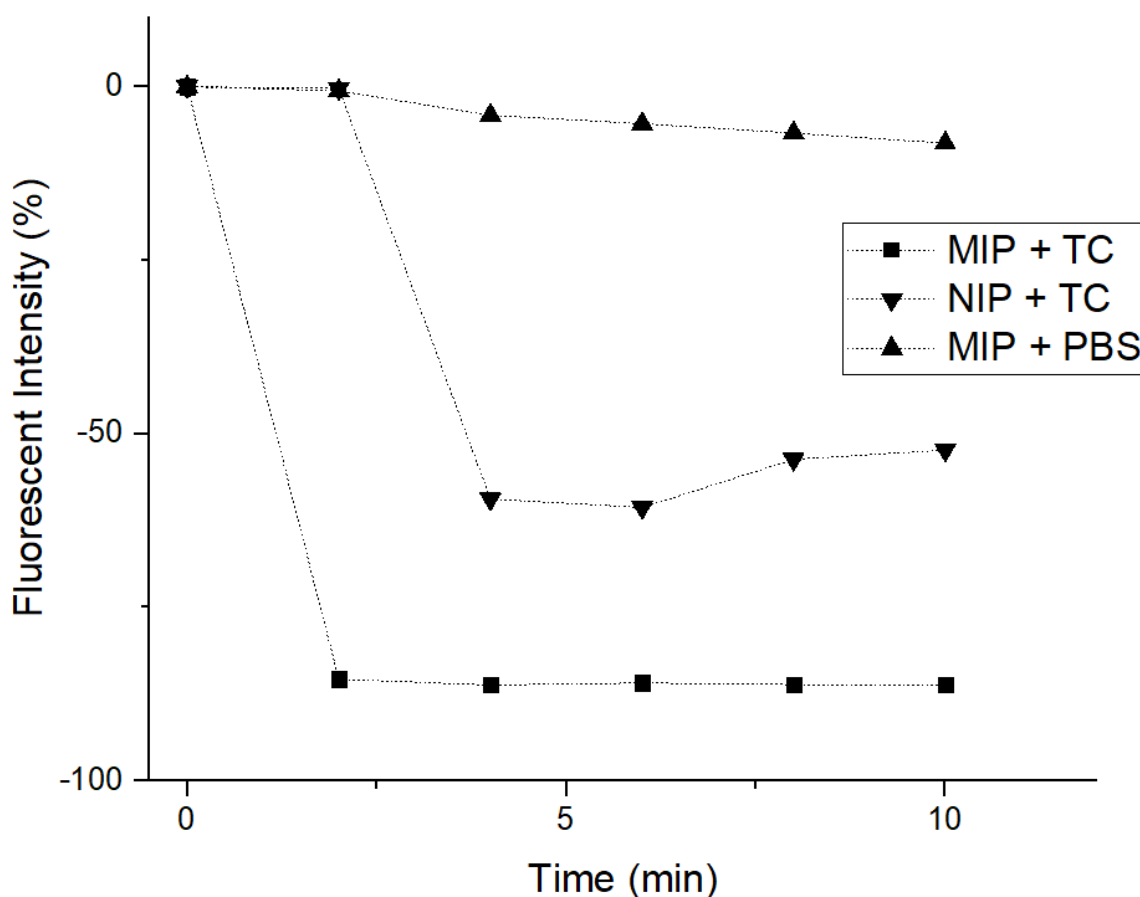


Figure 3.12. monitoring of fluorescent intensity between MIP and NIP with tetracycline and a PBS control, with guideline for readers eye to follow.

As was detailed in 3.2.5, the capture at 2 min was 15 sec after the influx of solution injected through the flow cell, whether that be target solution or PBS. An immediate quenching was observed for the MIP with the tetracycline solution, the fluorescent intensity immediately dropped by $85.4 \pm 1.1\%$. The NIP also exhibited a quenching of $59.4 \pm 1.1\%$ but this was after 135 sec. After the initial influx of tetracycline solution into the flow cell, the quenching was -0.3% at 15 sec. This negligible decrease suggested that the non-specific binding of the target to the surface was not instantaneous like the specific binding was with the MIP. Furthermore, the fluorescent quenching recorded was much less stable in the NIP than the MIP, suggesting that the non-specific interactions are much more reversible than those experienced by the MIPs specific pores to the target. The MIP which had PBS solution pushed through, displayed much less quenching than the other two experiments, this can be accounted to the lack of tetracycline present, there

for it cannot interact with the fluorophore to cause any change in the intensity. A potential mechanism for the observed quenching was described by Ooyama *et al.*, 2011, in which the mechanism of quenching proposed was photoinduced electron transfer (PET) [265]. Ooyama *et al.*, 2011, proposed the electron transfer was intramolecular whereas in the presented work in this chapter, the electron transfer would be hypothesised to be intermolecular. An electron from a functional group (e.g. the nitrogen of the amine group) on the target (tetracycline) was exchanged to the fluorophore, thus inhibiting the excited electron from returning to its lower energy state, thus quenching the fluorescence. When the target bound inside the imprinted cavity, the fluorophore and antibiotic were close enough for the electron transfer to take place intermolecularly.

The specificity of the fluorescent system can be observed from Figure 3.12. There was a significantly decreased fluorescent intensity when the MIP was exposed to the tetracycline solution (the intended target), than when the NIP was exposed to it, a $33.8 \pm 1.1\%$ difference. As stated during the batch rebinding experiments, any difference in exhibited binding between that of a MIP and NIP was due to the presence of the specific pores present on the MIP. This means that when the target interacts with the functional groups present in the custom pores; electronegative double bound oxygen, conjugated systems and methyl groups, the electron exchange that occurred between the target and polymer surface functional groups in the specific cavities generated higher levels of fluorescent quenching than experienced in the non-specific interactions which can be accounted to the closer proximity the target can achieve when specifically bound into the imprints.

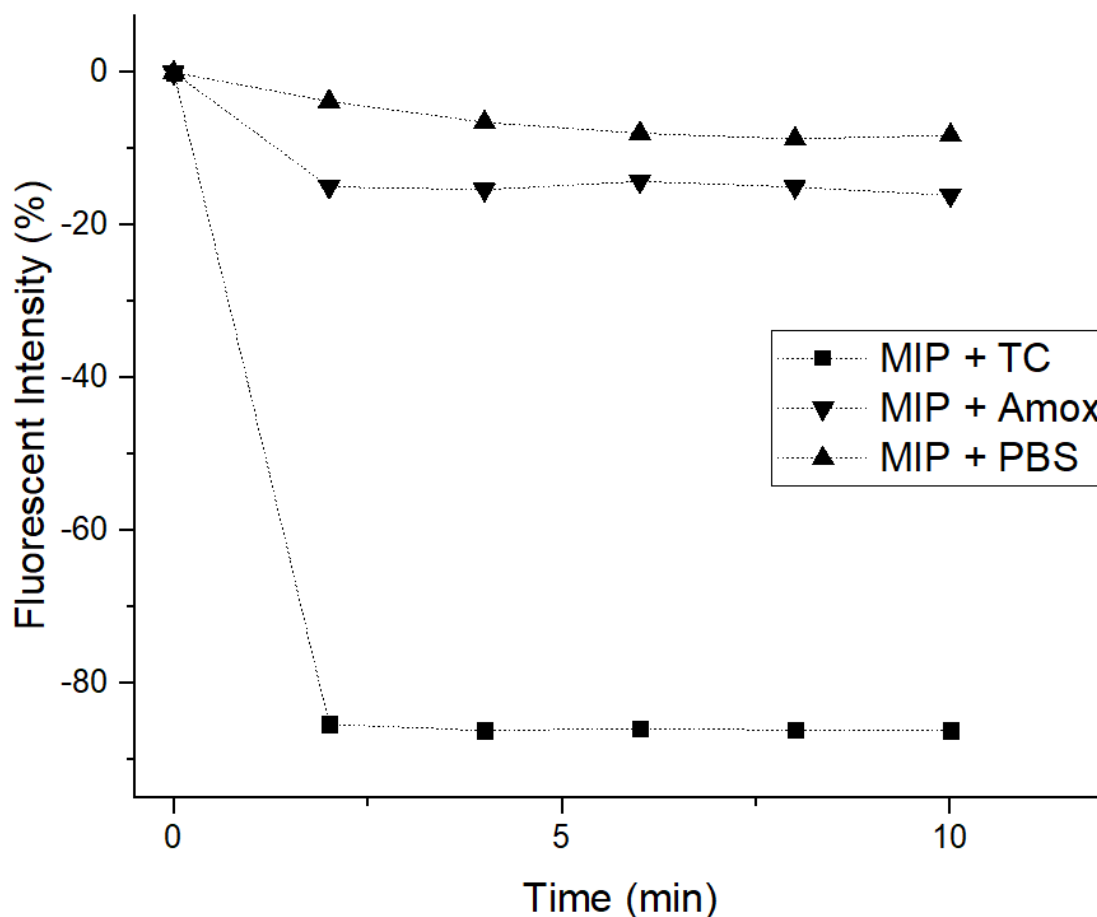


Figure 3.13. Selectivity study via fluorescent microscopy of MIP T, comparing the effects of three different solutions on the fluorescent intensity emitted by the polymer, with guideline for readers eye to follow

The selectivity test of MIP T presented in Figure 3.13 exposed a much higher degree of fluorescent quenching when it was introduced to the target it was imprinted for over than of another antibiotic. The fluorescent intensity of the MIP introduced to tetracycline dropped by $86.2 \pm 1.1\%$ just 15 sec after the introduction the target solution. Unlike in Figure 3.12, all fluorescent intensities were stable, with no significant change observed after the initial capture at 2 min. The MIP introduced to amoxicillin in Figure 3.13 saw a drop of $15.4 \pm 1.1\%$ after 135 sec of the introduction of the amoxicillin solution, compared to the $59.4 \pm 1.1\%$ drop the NIP experienced when interacting with tetracycline, displaying that the monomer selection for tetracycline sensing was appropriate, as even without cavities, the NIP exhibited a stronger

response. This further highlights the importance of the cavity shape and that it is almost as crucial as the monomers used. Amoxicillin has potential to interact with the functional groups present via hydrogen bonding and π - π stacking but still exhibited a relatively minor response in regard to the NIP and tetracycline. Another consideration was the lack of syringe pump used; 3 mL was injected by hand which would lead to discrepancies in the exact amount of solution added. The purpose was to flood the flow cell as quickly as possible with solution and therefore minor volume differences would not have affected the fact that the flow cell was completely flooded. As mentioned previously, the higher quantum yield of amoxicillin may have shadowed the decrease in the fluorescent intensity.

In future work, it would be opportune to test the selectivity with another tetracycline analogue. This would give a truer representation of the calibre of the selectivity the polymer exhibits however as the aim of the work is to tackle antibiotic resistance from all antibiotics, hence the use of varying targets throughout this chapter, a sensor platform that can detect a family of antibiotics gives rise to broad spectrum sensing capabilities.

3.5 Conclusions

This chapter composed of an investigation into a new sensor platform, seeing MIP being developed for 2 different analysis techniques. The imprinted polymers produced have been proven to have a significant level of specificity. The MIP developed has demonstrated the ability to discriminate between two targets which both can form the same inter molecular forces portrayed that the shape of the cavity plays a critical role in imprinting selectivity. Several optimisation alterations were employed, primarily to the polymer composition and analysis technique. The composition of the polymer was altered to dramatically increase the amount of cross linker than was being used before to the incorporation of a second non-fluorescent functional monomer- MAA, whilst also increasing the amount of fluorescent monomer by 4 times the amount than was first proposed. The HTM data shows a considerable change in the thermal resistance between that of MIP and NIP T when introduced to tetracycline solutions. The MIP had an increase of

0.65 °C/W compared to that of 0.0015 °C/W which the NIP exhibited when introduced to 100 mM tetracycline solution in PBS. The LoD was 0.1 ± 0.3 mM. The initial fluorescent analysis technique of a fluorometer coupled to a plate reader gave partial insight but proved to lack appropriateness to the desired fluorescent analysis. An inverted fluorescent microscope was then utilised as it eliminated most of the issues encountered. Fluorescent analysis gathered from the inverted fluorescent microscope showed a significant level of specificity in the imprinted polymers produced with MIP T exhibiting a fluorescent quenching over a third of that experienced by the NIP. When the selectivity of the MIP was investigated, a fluorescent quenching of ~8 times higher was experienced in the MIP than the controls. A difference such as this is a significant indicator of the MIP composition being appropriate for the detection of tetracycline. Future work could see a non-fluorescent MIP being analysed in the same way to see if any autofluorescence is influencing the data obtained in this chapter, this would completely eliminate any effect the experiment. Furthering from just MIP T, this chapter has seen the detection of other targets, displaying the poignant versatility of imprinted polymers and their applicability in sensing a vast array of targets, not only antibiotics as Chapters 4 and 5 will demonstrate. the capabilities of imprinted polymers have been demonstrated throughout this thesis and has exhibited the capabilities of polymers such as these for dual detection and with minor optimisation of both analysis set ups, it is more than plausible to suggest that simultaneous real time detection which could lend to gaining insight to bacterial growth in infections, an area in need of enlightenment.

Chapter 4. Functionalisation of Molecularly Imprinted Polymers onto Screen Printed Electrode for the Detection of the Antibiotic Amoxicillin in Aqueous Samples.

(Published as O. Jamieson *et al*, *Chemosensors* (2020) 8(1)) [213]

4.1 Abstract

Within this chapter, I will move from functionalising glass chips with MIPs towards use of Screen-Printed Electrodes (SPEs), which are disposable electrodes with high commercial potential. The optimisation of the solid-phase functionalisation is discussed along with the main objective of selective detection of amoxicillin in aqueous samples. Different functional monomers were tested to determine the optimal composition *via* optical batch rebinding experiments. Two different sensor platforms were tested using the same MIP composition; one being bulk synthesized and surface modified SPEs *via* drop casting the microparticles onto the electrode surface and the other being UV polymerized directly onto the SPE surface in the form of a thin film. The sensors were used to measure amoxicillin in conjunction with the Heat-Transfer Method (HTM), a low-cost and simple thermal detection method that is based on differences in the thermal resistance at the solid-liquid interface. It was demonstrated that both sensor platforms could detect amoxicillin in the relevant concentration range with Limits Of Detection (LOD) of 1.89 nM and 0.54 ± 0.10 nM for the drop cast and direct polymerisation methods respectively. The sensor platform utilising direct UV polymerisation exhibited an enhanced response for amoxicillin detection, a reduced sensor preparation time and the selectivity of the platform was proven through the addition of nafcillin, a pharmacophore of similar shape and size.

The use of MIP-modified SPEs combined with thermal detection provides sensors that can be used for fast and low-cost detection of analytes on-site, which holds great potential for contaminants in environmental aqueous samples.

4.2 Introduction

It has been explained previously that veterinary and clinical use of antibiotics exerts selective pressure to bacteria, which accelerates the emergence of bacteria with AMR properties due to the accumulation of pharmaceuticals in the food chain and water systems. Pharmaceutical products are considered point source pollution due to a significantly high level quantities of pharmaceuticals being disposed of through factory effluent. Watkinson *et al.* have shown that even in a first world country such as Australia with modern waste water treatment plant infrastructure, beta lactam antibiotics have a undeniable presence in the water system [24]. Recent studies from India, one of the world's leading pharmaceutical producers, has revealed excessively high concentrations of antibiotic compounds in drinking water that exceed the maximum regulatory limits (MRLs). The ramifications of this has been seen in vulnerable populations living near manufacturing facilities, with an estimate of 58,000 new-borns dying in India in these regions from multi-drug resistant infection [266]–[268]. Developing countries are at a critically higher risk of negative health impacts from antibiotics leaching into water systems, which has been attributed to the lack of optimal wastewater treatment facilities and high costs associated with vigilant monitoring of pharmaceutical waste [269]. In Europe, the MRL of pharmaceuticals in food products of animal origin are strictly monitored however waste and surface water concentrations of micro pollutants is much less stringently monitored, allowing for negative effects of their presence in water ways to be exacerbated [270]. Beta-lactams, fluoroquinolones, macrolides, sulfonamides, and tetracyclines make up the majority of antibiotic residues that are most often found in aquatic environment [271]. Current commercial screening tests for antibiotics in food and environmental samples either require a long response time (several hours), or are not able to selectively detect antibiotic compounds and solely provide semi-quantitative information. From the limitations of current sensors for antibiotics listed in Chapter 1, there is a strong need for low-cost, robust, and easy to use sensors that can be used on site to determine trace levels of antibiotics in aquatic systems without the need of highly specialised training to use the device. Many electrochemical sensors display promise in this respect [272]–[274]. Pellegrini *et al.* [275], gave insight as

to the usability of electrochemical sensors for the determination of antibiotics and promote their use for on-site testing due to their efficient analysis time (~2 hrs) and small sample volume (~100 μ L). A lack of any pre-treatment steps while still maintaining a high level of precision motivates a strong indication of the appropriateness of this type of analysis for the desired purpose. Previous reports in literature have shown the ability of synthetic polymeric recognition elements, namely MIPs, to improve the affinity and selectivity of electrochemical sensors. Yang *et al.* [276], have demonstrated limits of detection in the nanomolar regime in buffered solutions and in spiked food samples, which can be achieved with MIP layers grown onto multiwalled carbon nanotubes. Zeinali *et al.* [277], used magnetic MIPs modified onto carbon paste electrodes combined with cyclic voltammetry to detect amoxicillin with a LoD of 0.26 nM. Betlem *et al.* [211], have shown the effective use for the Heat-Transfer Method (HTM) as an appropriate analysis technique for small molecules such as caffeine. The current study was built on from this work and tailored the detection system to a beta lactam antibiotic.

The work carried out in Chapter 2 demonstrated the novel capabilities of MIPs when polymerised onto modified glass. This chapter will explore alternative polymerisation strategies that could be used to further improve the commercial potential for MIP-based sensors. Amoxicillin was used in this chapter as a case study and compared the sensors characteristics of microparticle modified screen-printed electrodes (SPEs) to those functionalised with a thin film. Amoxicillin, like tetracycline, is a heavily used and relied upon antibiotic, therefore warranting the monitoring of its presence in water systems. Amoxicillin is a major cause for concern in relation to AMR bacteria as 40%-80% is excreted in an un-metabolised state from humans and has a half-life of 9 days [10]. This will lead to high levels of amoxicillin present at various stages of the water system, allowing resistant bacteria to survive in conditions that non-resistant bacteria cannot will therefore inherently lead to a significant rise in the growth of AMR. The structures of amoxicillin and nafcillin, another beta lactam antibiotic used in this study to test the selectivity of the sensors, are shown in Figure 4.1. The inherent versatility of MIPs makes them ideal candidates as recognition elements for antibiotics as the issue of AMR growth is not limited to one family of antibiotics.

An easily modified sensor, such as a MIP based sensor would afford, could be tailored to a host of different targets exponentially increasing its usefulness in aiding this issue

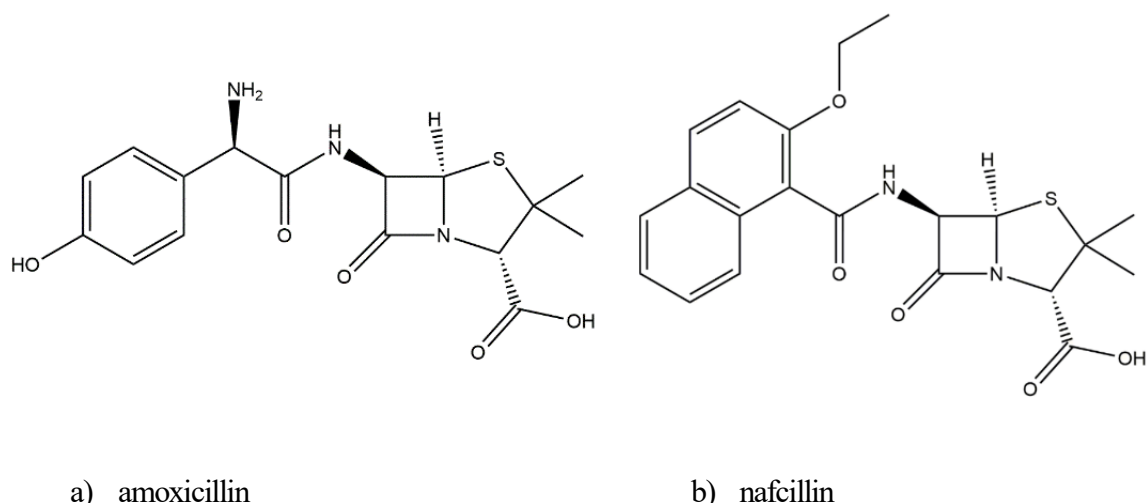


Figure 4.1. Structures of a) amoxicillin and b) nafcillin showing matching β -lactam ring pharmacophores.

SPEs, due to their high reproducibility, low-cost, and inherent suitability for mass-production, are often used in commercial sensor [278]. However, integration of polymer structures into SPEs is complicated due to their low resistance to traditional organic solvents such as chloroform and toluene [279].

In this work, two different electrode modification strategies and compare and contrast towards the analytical detection of amoxicillin are explored. The SPEs are modified with MIPs in two manners:

- i) surface modification *via* dropcasting of MIP microparticles suspended into ethanol directly onto the sensor surface along with a thin layer of polypyrrole to hold the MIPs in place;
- ii) Directly deposition of MIP thin films onto SPEs using UV polymerization.

The disadvantage of working with MIP microparticles is the two-step (indirect) functionalisation process and the fact that the resulting electrodes are insulating and not compatible with traditional electrochemical detection. Recent work has demonstrated that thermal analysis, in particular the Heat-Transfer Method (HTM), can provide an interesting alternative analysis technique that is easy to employ and provides rapid detection [253].

4.3 Experimental

4.3.1. *Equipment and reagents*

Dimethyl Sulfoxide (DMSO) was sourced from TCI (Oxford, United Kingdom). Pyrrole, amoxicillin, nafcillin, azobisisobutyronitrile (AIBN), trimethylolpropane trimethacrylate (TRIM), methacrylic acid (MAA), acrylamide (AA) and 2-vinylpyridine were sourced from Sigma Aldrich (Gillingham, United Kingdom). Ethanol was sourced from Fisher Scientific (Loughborough, UK). The orbital shaker used was a Stuart mini orbital shaker SSM1 (Staffordshire, United Kingdom). Experiments were carried out at 20 ± 1 °C unless otherwise noted. UV/Vis analysis was carried out on an Agilent 8453 UV-Vis spectrophotometer (United States). Phosphate Buffered Saline (PBS) tablets were purchased from Sigma (Gillingham, United Kingdom) and used to maintain pH level (7.4 ± 0.2) and the ionic strength of solutions used throughout the experimental portion of the study.

4.3.2. *MIP and NIP microparticle syntheses*

MIPs for amoxicillin were synthesised with varying compositions, which are listed in Table 4.1. The general functionalization procedure includes mixing of the template (0.35 mmol) with the monomer (1.4 mmol) in 3.3 mL of DMSO. Subsequently, the crosslinker monomer TRIM (2.8 mmol) was added followed by the initiator AIBN (0.22 mmol). The mixture was sonicated and degassed with N₂. Polymerization was initiated by exposing the samples to a UV lamp (200 mW, Polytec UV LC-S, Karlsbad, Germany) for 10-15 min. The obtained polymer block was washed with water and subsequently ground to obtain a fine powder. The template was removed by continuous Soxhlet extraction with a mixture of methanol and water (50/50) until UV-vis analysis no longer showed traces of amoxicillin in the extract. The powders were washed with water and dried overnight under vacuum. Non-Imprinted Polymers (NIPs) were synthesized in the same manner but without the addition of the template.

Table 4.1. The composition of the different MIPs, listing the amount of template, functional monomer, crosslinker monomers, initiator, and porogen used.

| | MIP-1 | MIP-2 | MIP-3 |
|---------------------------|-------|-------|-------|
| Amoxicillin (mmol) | 0.35 | 0.35 | 0.35 |
| MAA (mmol) | 1.4 | - | - |
| Acrylamide (mmol) | - | 1.4 | - |
| 2-vinylpyridine (mmol) | - | - | 1.4 |
| TRIM (mmol) | 2.8 | 2.8 | 2.8 |
| Initiator (mmol) | 0.22 | 0.22 | 0.22 |
| DMSO (mL) | 3.3 | 3.3 | 3.3 |

4.3.3. Batch rebinding experiments evaluated with optical detection

Batch rebinding experiments were performed and optical detection was used to evaluate the binding of amoxicillin to the MIP and NIP powders. The antibiotic concentration was determined by measuring the absorbance at $\lambda=272$ nm. In each experiment, 10 mg of MIP or NIP powder was added to 5.0 mL of PBS

solutions with amoxicillin concentrations between 0.5-1.0 mM. The resulting suspensions were placed on a rocking table (110 rpm) for 60 min and subsequently filtered. The free concentration of amoxicillin (C_f) in the filtrate was determined by comparing the absorbance to that of a pre-determined calibration curve. Subsequently, the amount of bound template (C_b) was calculated by subtracting the initial concentration added to the solution (C_i) by the free template concentration (C_f)- $C_b = C_i - C_f$. The molecule of template bound per gram (S_b) were obtained by multiplying C_b by the volume in litres and then dividing this by the amount of polymer used in the experiment (10 mg). The Imprint Factor (IF) was determined by dividing S_b for a given MIP by the S_b for the corresponding NIP at a C_f value of 0.5 mM [280].

4.3.4. Thin film polymerization

A pre-polymerization mixture of MIP 2 was produced as described in Section 4.3.2. The solution (0.3 μ L) was applied onto the working electrode of the SPE and subsequently exposed to UV light (365 nm) for 1 min. A cover slip was placed over the droplet and it was exposed to UV light for a further 1 min to complete the polymerization. The functionalized SPE was then washed in methanol and the template extracted in deionized water (40 mL) using an orbital shaker (160 rpm) overnight. A NIP was produced using an identical protocol without the presence of the target amoxicillin.

4.3.5. Electrochemical deposition of polypyrrole

Electrochemical experiments were performed using a standard three electrode set up. Graphite Screen-Printed macroelectrodes (SPE, Manchester Metropolitan University, UK) [209], [281] were utilised as the working electrode alongside a nickel/chromium wire auxiliary electrode and silver|silver chloride (Ag|AgCl) reference electrode (BASi, USA). These were controlled by an Ivium Compactstat (Eindhoven, the Netherlands) connected to a Desktop PC (Dell, UK). The SPEs were fabricated in-house using a stencil design to achieve a 3.1 mm diameter working electrode using a graphite ink (Product Ink: C2000802P2; Gwent Electronic Materials Ltd., Pontypool, UK) and were printed using a DEK 248 screen printer machine (DEK, Weymouth, UK) onto a polyester flexible film (Autostat, Milan, Italy, 250 micron

thickness). The layer was cured in a fan oven at 60 °C for 30 min and finally, a dielectric paste (Product Code: D2070423D5; Gwent Electronic Materials Ltd., Pontypool, UK) was then printed onto the polyester substrate to cover the connections. The SPEs were then cured for an additional 30 min at 60 °C before used [282], [283].

All electrochemical measurements were carried out at 20 ± 1 °C and using deionised water of resistivity ≥ 18.2 M Ω cm. Prior to all electrochemical measurements the solutions were thoroughly degassed with highly pure nitrogen for 15 min.

MIP microparticles were dispersed in ethanol (1 mg/mL), dropcast (30 μ L) onto the SPE surface and allowed to dry. Following this, a thin layer of polypyrrole was applied to the SPE surface to hold the MIPs in place. A droplet (30 μ L) of pyrrole (0.1 M) in PBS was applied to the electrode surface. Electropolymerisation was performed through chronoamperometry, using the three-electrode system described above and applying a potential of + 0.8 V for 30 s. The electrodes were thoroughly rinsed with deionised water and the presence of MIPs on the surface confirmed by Scanning Electron Microscopy (SEM) (Appendix D)

4.3.6. Scanning electron microscopy (SEM)

SEM measurements were recorded on a Supra 40VP Field Emission from Carl Zeiss Ltd (Cambridge, UK) with an average chamber vacuum of 1.3×10^{-5} mbar and average gun vacuum of 1×10^{-9} mbar. To enhance the contrast of these images, a thin layer of Au/Pd ((8 V, 30 s) was sputtered onto the electrodes with a SCP7640 from Polaron (Hertfordshire, UK).

4.3.7. HTM measurements with MIP-modified SPEs

HTM analysis was carried out in a similar manner as to that described in Chapter 2. The functionalized SPE's were cut into 1x1 cm squares, inserted into an additively manufactured/3D-printed flow cell [210] and sealed with an O-ring (RS Components, United Kingdom). Thermal measurements were carried out using the flow cell (Chapter 2, Figure 2.2) of volume 110 μ L in conjunction with the heat-transfer set-up

which was designed in-house [233], [284]. The flow cell is connected to a copper block which acts as a heat sink. The temperature of this block (T_1) is controlled *via* a Proportional-Integral-Derivative (PID) controller. As such, the PID parameters were set to the optimized values determined for this heat source of $P=1$, $I=14$, $D=0.3$ [253].

For all experiments, the flow cell was filled with PBS solution and the copper block was heated to a pre-set temperature of 37.00 ± 0.02 °C. The cell was left to stabilise for 15 min before a first injection of PBS was added to act as the blank measurement. Sequential amounts of amoxicillin (1-500 nM) were injected into the flow cell using an automated NE500 programmable syringe pump (Prosense, Oosterhout, the Netherlands) at a flow rate of $250 \mu\text{l min}^{-1}$. Following each injection, the temperature was allowed to stabilise for 30 min, of which the last 10 min (600 data points) were averaged out and used to calculate the R_{th} . The calculated R_{th} values were used to produce dose-response curves and calculate the LoD using the three-sigma method. Specificity tests were carried out by injecting the same concentrations of amoxicillin to an electrode modified with a NIP. Selectivity studies were carried out by injecting the same concentration of nafcillin, an antibiotic with a similar chemical structure.

4.4 Results

4.4.1. Batch rebinding results

First, batch rebinding experiments with MIP1-3, that have similar compositions, but differ in the functional monomer, were performed. The time of the experiments was fixed at 1 hr since after this time no increase in the binding to the MIP particles was observed. In each experiment, 5 mL of amoxicillin solutions in PBS ($C_i = 0.5 - 1.0$ mM) were added to 10 mg of the MIP particles.

Table 4.2. The amount of binding for MIP and NIP at $C_f = 0.5$ mM.

| Polymers | S_b [μmol/g] | Imprint factor C_f = 0.5 mM |
|-----------------|-------------------------------|--|
| MIP1 | 43.86 | 1.3 |
| NIP1 | 35.09 | |
| MIP 2 | 63.38 | 6.5 |
| NIP 2 | 9.8 | |
| MIP 3 | 2.48 | 0.3 |
| NIP 3 | 8.47 | |

The results obtained from the batch rebinding experiments are presented in Figure 4.2. It was observed that MIP 2, made of acrylamide (AA) as the functional monomer, exhibited a significantly higher binding affinity for the amoxicillin target compared to MIP 1 (based on methacrylic acid) and MIP 3 (based on 2-vinyl pyridine). In addition to this, at a C_f value of 0.5 mM the calculated Imprint Factor (IF) for MIP 2 was significantly higher than either of the other MIPs at 6.47, exhibiting the MIPs affinity efficiency compared to the corresponding NIP. The highest affinity MIP using AA as a functional monomer was most likely due to the nature of the functional groups on the monomer when compared to the structure of the target. These functional groups would allow self-assembling of monomers around the target to form the non-covalent forces necessary to hold them together [251]. On the other hand, 2-vinylpyridine lacks these functional groups required for binding [285]. This further portrayed the vital nature of optimisation for each target, showing that each MIP synthesised for a unique purpose intrinsically needs unique optimisation even though the template-target interactions present in the binding may be the same as that of another MIP sensor developed for a different target. It was noted however that MIP 3 had a very low imprint factor of 0.3 at a C_f value of 0.5 mM. This raised concern as imprinted would not lower binding capabilities of a polymer and therefore it was assumed that target leaching had a significant effect here.

The use of a MIP imprinted with a different target could have provided more insight as the impact of imprints could have been discounted. This highlights the issues raised around target leaching brought up in Chapter 1.

Time dependent experiments were performed to determine the optimal time for rebinding. Readings were taken at 30 min, 2 hr, and 24 hr after mixing MIP with target solution, which resulted in absorbance values of 1.52, 1.51 and 1.47, respectively. This shows that there was no significant change over time and that 30 min was sufficient to gain an accurate representation of batch rebinding data. Insight was also gained from this in respect to the equilibrium of the binding and in this case, showed that even after 24 hrs no significant leaching of the template from the MIP had occurred.

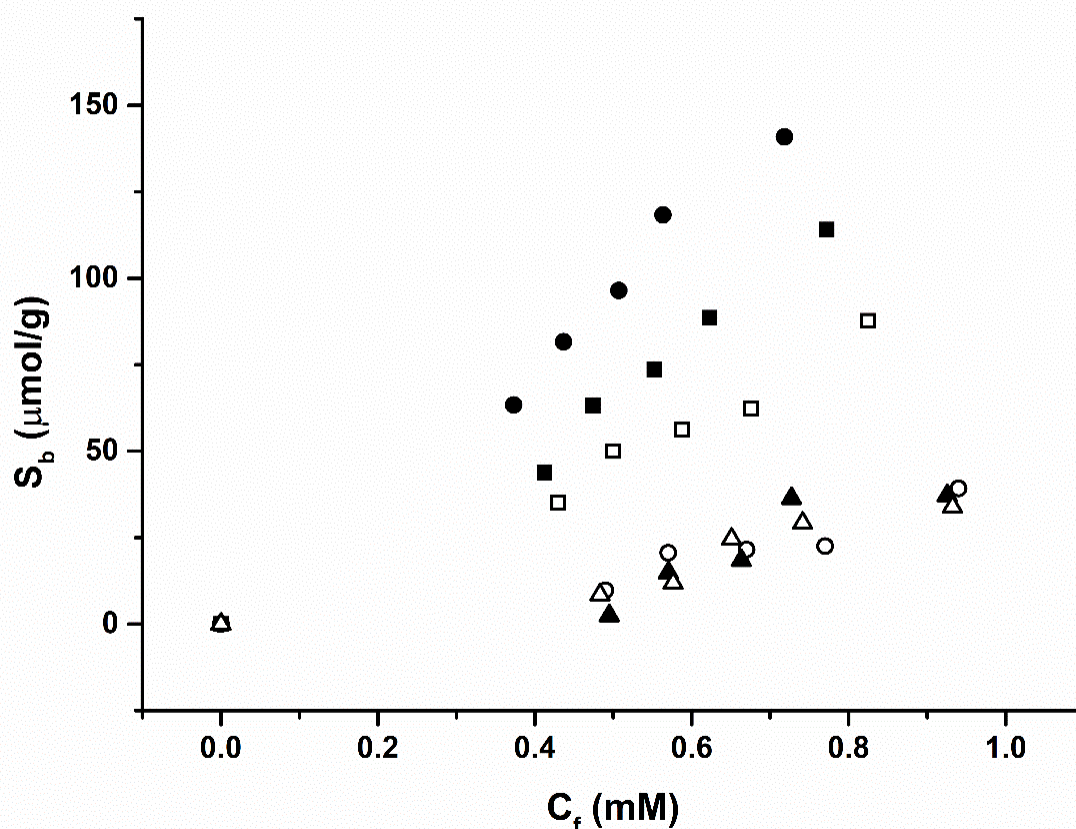


Figure 4.2. Binding isotherms of the polymerised MIP/NIPs upon exposure to Amoxicillin solutions in PBS. MIP 1 (filled squares) and NIP 1 (hollow squares), MIP 2 (filled circles) and NIP 2 (hollow circles), and MIP 3 (filled triangles) and NIP 3 (hollow triangles).

Figure 4.3 displays the selectivity presented by MIP 2, which exhibits a higher binding affinity towards amoxicillin than towards nafcillin. This shows that the binding cavities in the imprinted polymer have a higher affinity towards their intended target even if a very similar pharmacophore is used, thus confirming the polymers ability to recognise the target. The NIPs have no significant difference in binding affinity as expected, since they do not possess the stereoselective cavities present in the MIP.

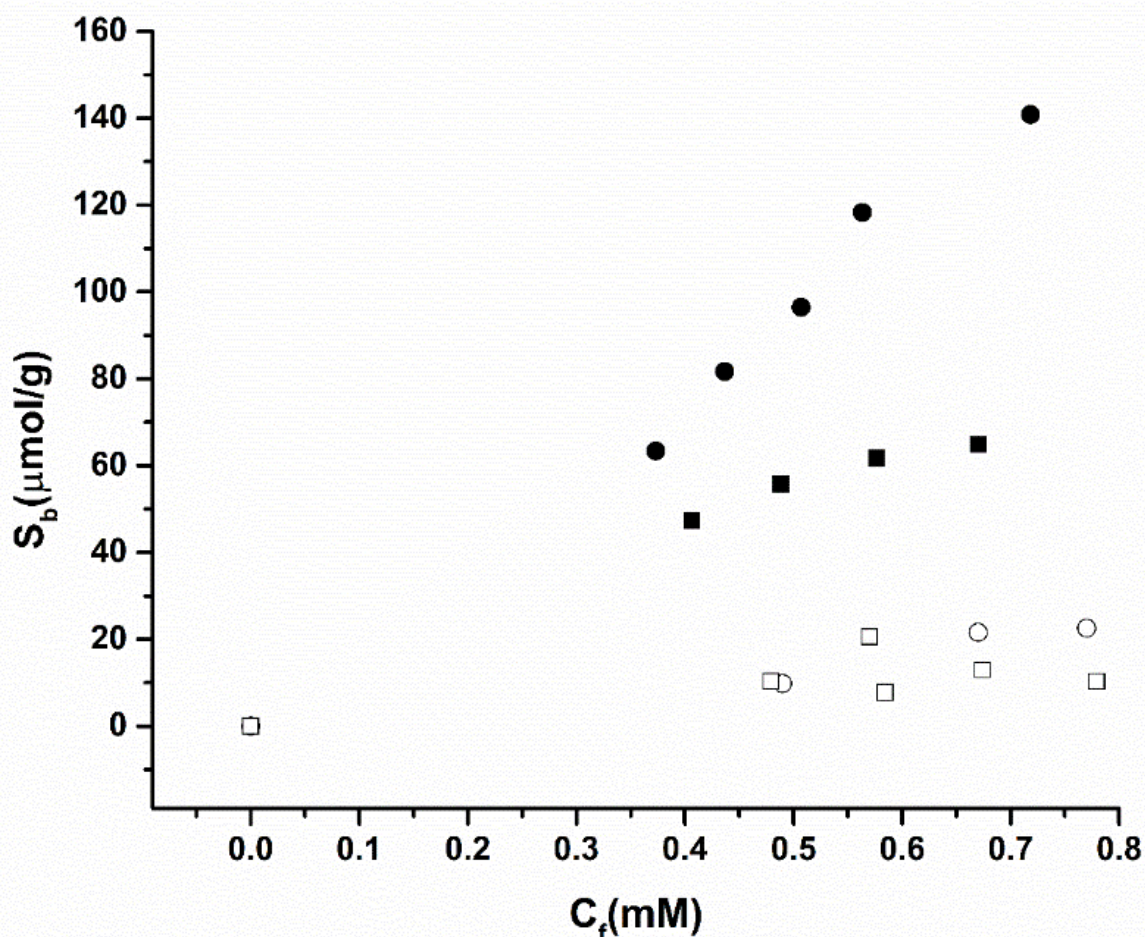


Figure 4.3. Selectivity batch rebinding of MIP 2 (filled symbols) and NIP 2 (hollow symbols) with amoxicillin (circles) and nafcillin (squares) in PBS.

The relevant concentration range of amoxicillin in water samples is in the low nanomolar range [286]. Therefore, it was decided to evaluate the performance of the sensor to discriminate amoxicillin from its

competitor molecule in the nanomolar concentration, for which it is required to use a more sensitive read-out strategy such as HTM.

4.4.2. Detection of amoxicillin using MIP microparticles

Bulk polymerized MIPs (MIP 2) were functionalized onto SPEs (Appendix D) as explained in section 4.2.5, fitted inside the flow cell (Chapter 2, Figure 2.2) and connected to the HTM equipment. The flow cell was filled with PBS and allowed to stabilise for 45 min. Then, sequential injections of the target analyte amoxicillin (1 – 500 nM) in PBS were started, allowing the system to equilibrate for 30 min after each injection. The raw data output obtained for these additions is presented in Figure 4.4 A. Specific values for the R_{th} values for each concentration of amoxicillin were calculated using the last 10 min of each stabilisation period. This resulted in a value and standard deviation being calculated over 600 data points. In PBS, the R_{th} of the MIP functionalized system stabilized at a value of 5.91 ± 0.05 °C/W. Upon the addition of 1 nM of amoxicillin the R_{th} increased from this baseline value to 6.06 ± 0.05 °C/W. The R_{th} value increased further until the addition of 500 nM of amoxicillin where it stabilised at a value of 6.42 ± 0.06 °C/W. An identical experiment was performed using an SPE modified with the NIP. In this case, R_{th} of the NIP functionalized system stabilized at a value of 5.51 ± 0.06 °C/W. After the addition of 1 nM of amoxicillin the R_{th} exhibited no statistically significant deviation from the baseline value to 5.55 ± 0.06 °C/W. The R_{th} value for the addition of 500 nM of amoxicillin showed a small increase due to non-specific binding, where it stabilised at a value of 5.61 ± 0.06 °C/W.

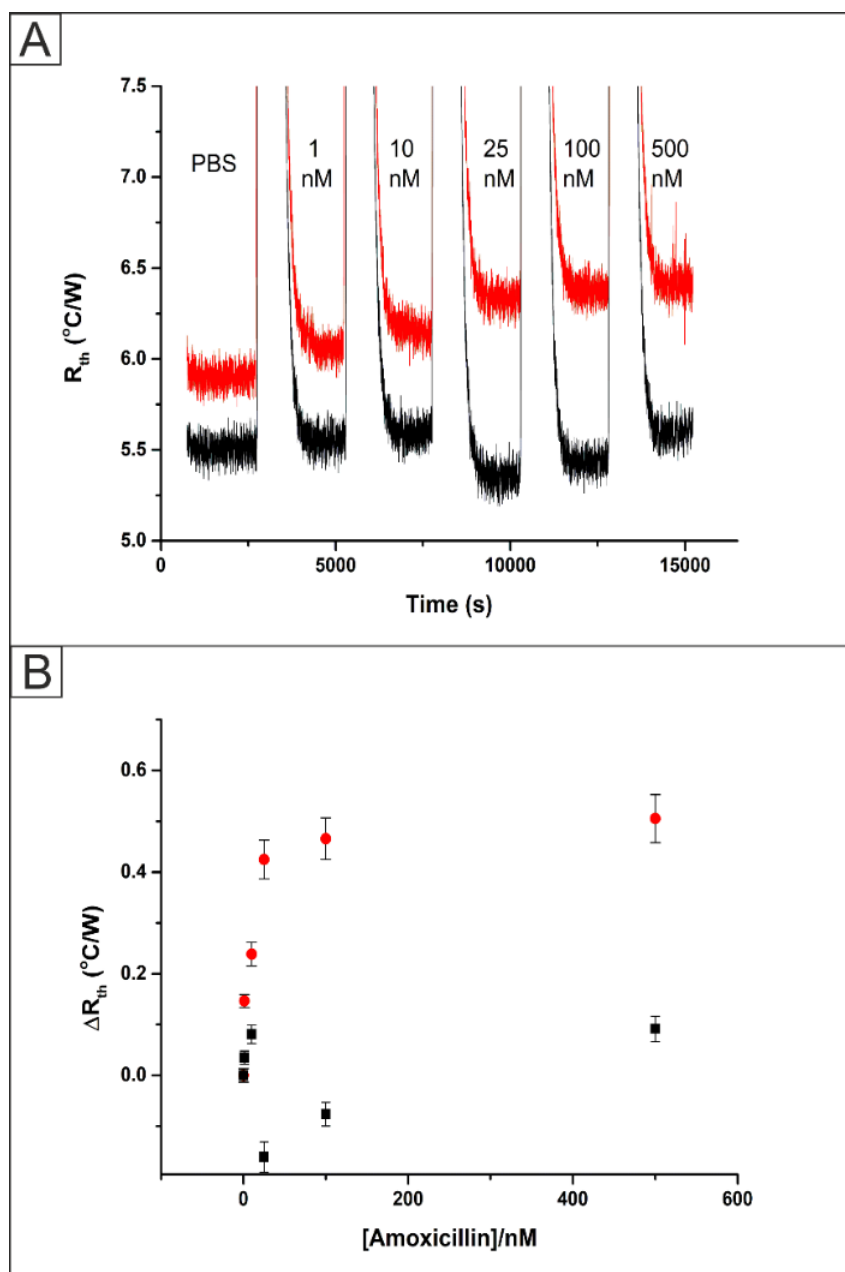


Figure 4.4. **A**) The raw HTM data plot of R_{th} versus time for the addition of amoxicillin (1 – 500 nM) in PBS to an SPE functionalized with bulk UV polymerized MIP (red) and NIP (black). **B**) Comparison between the absolute R_{th} values obtained from the HTM for a MIP functionalized SPE (red circles) and NIP functionalized SPE (black).

These R_{th} values were plotted against the concentration of amoxicillin injected into the system to produce a dose-response curve, Figure 4.4B. This was used to calculate a LoD for the bulk UV polymer system of 1.90 nM. These results were found to exhibit a lower LoD and wider detection range than that observed in previous work on caffeine detection[211]. This was expected due to the limited loading of MIP when incorporated directly into the SPE ink in comparison to drop casting. Additionally, template bleeding is a problem in the use of MIP microparticles. Up to 99 % of the template is removed during the extraction step; however, the remaining template can cause issues when ‘leeching’ out of the polymer matrix during measurements giving erroneous quantification [45]. The removal of MIP over time is of considerable concern when using a drop casting method, therefore the direct formation of the MIP onto the electrode surface using UV polymerisation was investigated.

4.4.3. Detection of amoxicillin using MIP thin films

Screen-Printed Electrodes (SPE's) were functionalized with amoxicillin MIPs *via* UV-Vis polymerization (Appendix D) as described in section 4.2.4. These MIP-modified SPEs were inserted into a flow cell (Chapter 2, Figure 2.2) and exposed to PBS solutions containing sequential amounts of the target analyte amoxicillin. The HTM raw data obtained for the addition of amoxicillin (1 – 500 nM) are presented in Figure 4.5 A. In PBS, the R_{th} of the MIP functionalized system stabilized at a value of 7.58 ± 0.05 °C/W. The increase in the R_{th} value compared to previous work [211], [253] was expected due to the presence of a thicker layer of polymer present on the electrode surface, which in turn will increase the resistance to heat flow through the interface. Upon the addition of 1 nM of amoxicillin an increase in the absolute R_{th} value was observed from its baseline of 7.58 ± 0.05 °C/W to 7.67 ± 0.06 °C/W. The R_{th} increased until the last addition of 500 nM amoxicillin where it reached a value of 8.16 ± 0.06 °C/W and an additional injection of PBS produced no significant change in the R_{th} . This final PBS injection was vital to show that no loosely bound target on the surface on the polymer was affecting the observed change thermal resistance. An identical experiment was performed using a NIP functionalized SPE where the R_{th} stabilized

at a value of 7.59 ± 0.06 °C/W. Upon the addition of 1 nM of amoxicillin to the system there was no significant change to the R_{th} value with it remaining at 7.59 ± 0.06 °C/W. Once 500 nM of amoxicillin was added to the NIP modified SPE there was an increase in the R_{th} to 7.68 ± 0.07 °C/W. The increase in the R_{th} can be explained by some non-specific binding of the target molecule to the polymer on the surface of the SPE however, the increase is significantly less than observed for the MIP modified SPE. Both of these results were used to produce a dose-response curve (Figure 4.5 B) which shows the improved response of the MIP based platform and was used to calculate the LoD of 0.54 ± 0.10 nM.

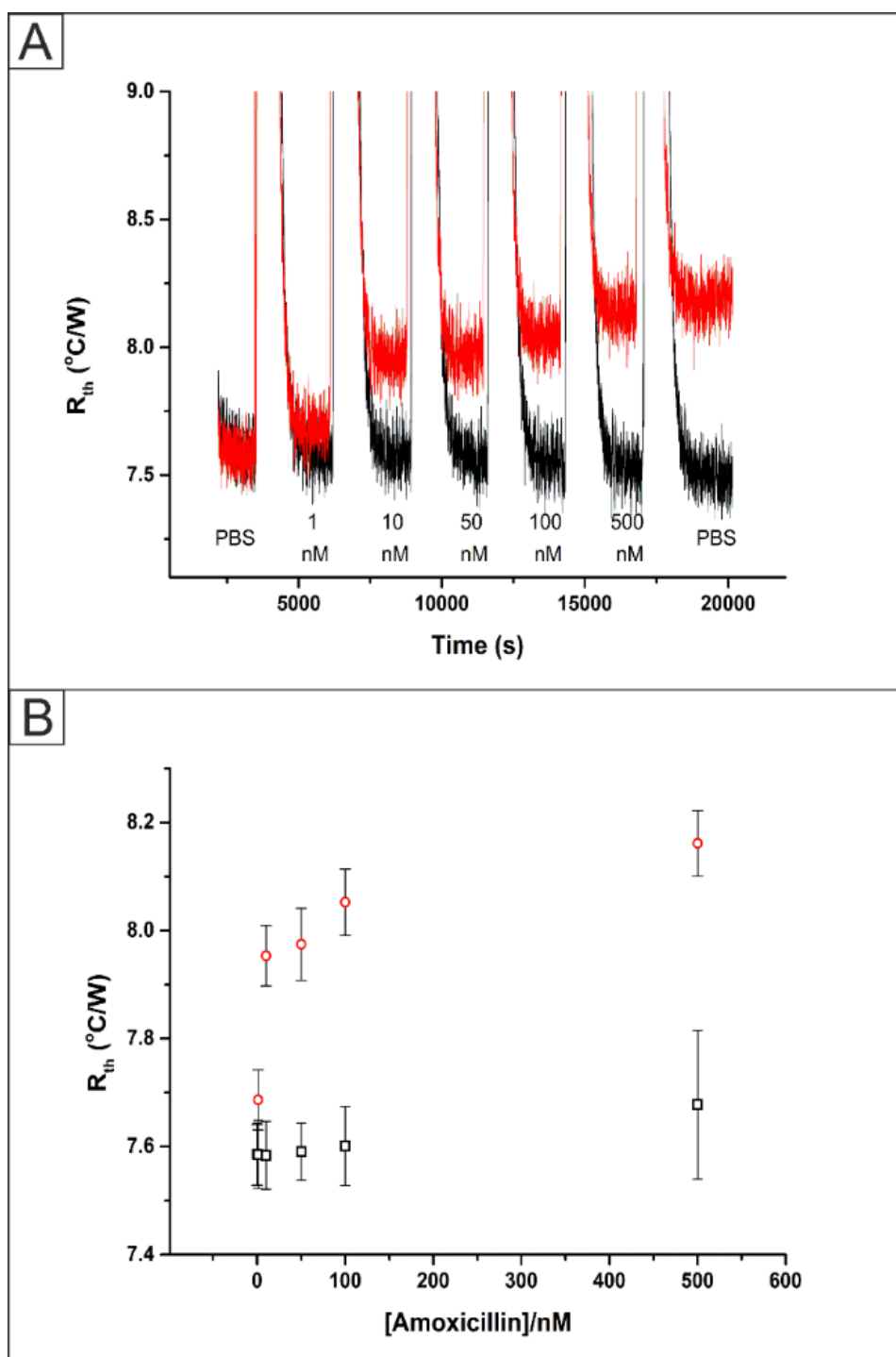


Figure 4.5. **A**) The raw HTM data plot of R_{th} versus time for the addition of amoxicillin (1 – 500 nM) in PBS to an SPE functionalized with a direct UV polymerized MIP (red) and NIP (black). **B**) Comparison between the absolute R_{th} values obtained from the HTM for a MIP functionalized SPE (red circles) and NIP functionalized SPE (black).

The selectivity of the MIP was assessed through repeating the experiment with additions of a molecule with the same pharmacophore and similar size, nafcillin (1 – 500 nM). An SPE functionalized with a MIP *via* UV polymerization directly onto the surface was placed inside the flow cell (Appendix D) and attached to the HTM equipment. The data collected from the addition of the competitor (black) was plotted alongside the previous results for the addition of the target molecules (red) to MIP functionalized SPE's.

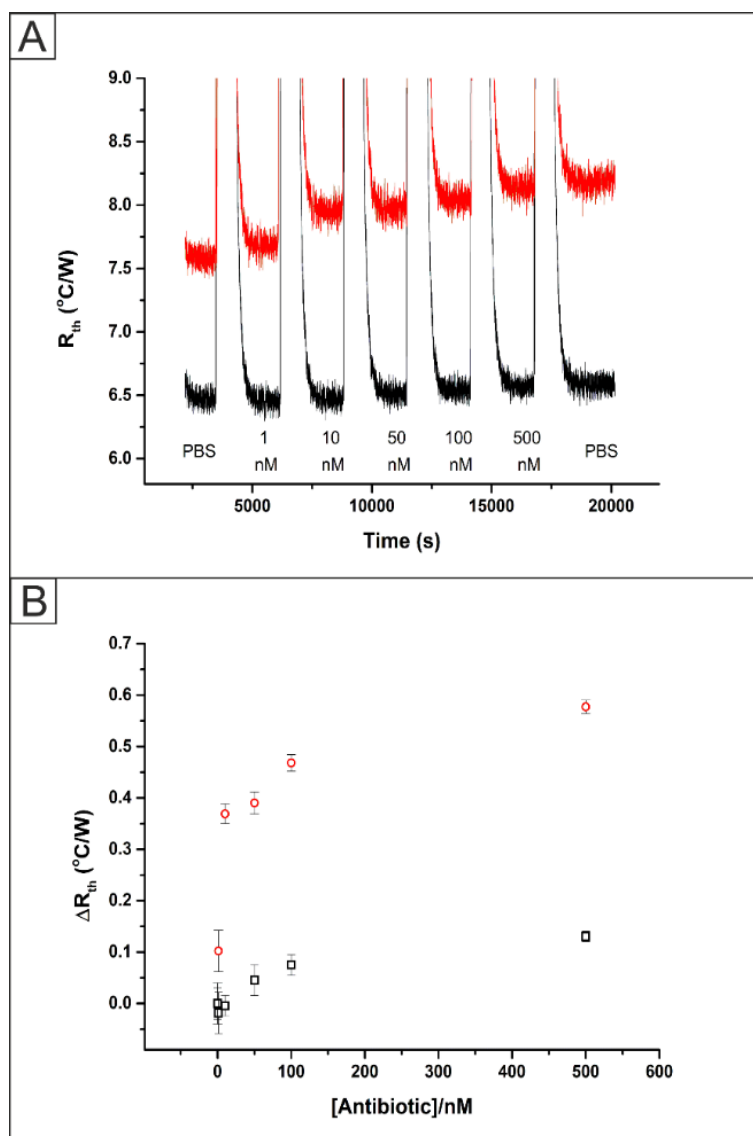


Figure 4.6. A) The raw HTM data plot of R_{th} versus time for the addition of amoxicillin (1 – 500 nM, red) and nafcillin (1 – 500 nM, black) in PBS to an SPE functionalized with a direct UV polymerized MIP. B) Comparison between the absolute R_{th} values obtained from the HTM for a MIP functionalized SPE with additions of amoxicillin (red circles) and nafcillin (black).

The raw data plot that was obtained is presented in Figure 4.6A (black) where there was a clear difference between the stabilized R_{th} values. This can be explained as the Type K thermocouples used in the experiment have a temperature error of up to 2%. The R_{th} value of the system in PBS stabilized at a value of 6.47 ± 0.05 °C/W. Upon the addition of 1 nM of nafcillin, there was no observed statistically significant change in the stabilized R_{th} value at 6.46 ± 0.05 °C/W. Once 500 nM of nafcillin had been injected into the flow cell an increase in the R_{th} was observed from the baseline level of 6.47 ± 0.05 °C/W up to 6.60 ± 0.05 °C/W. These values, along with those obtained for the addition of the target molecule were used to produce dose-response curves, Figure 4.6B, showing the increase in the R_{th} from the baseline stabilized levels for both the target (red circles) and competitor (black squares). This indicated that there was some non-specific binding of the competitor antibiotic to the surface of the polymer. However, the increase was significantly lower than that observed for the injections of the target antibiotic, showing the high selectivity of the sensing platform.

4.5 Conclusions

MIPs for the detection of amoxicillin were synthesized using bulk UV polymerisation with the functional monomers methacrylic acid, acrylamide (AA) and 2-vinylpyridine. Batch rebinding experiments evaluated *via* spectroscopic methods determined that the MIPs using AA (MIP 2) as the functional monomer exhibited the highest recognition capability (IF=6.5) for amoxicillin. MIP 2 was successfully functionalized onto SPEs via two routes with each method being evaluated independently. Firstly, MIP 2 was drop cast onto a SPE, fitted to the HTM and subjected to injections of increasing concentrations of amoxicillin (1 – 500 nM). An increase in the measured R_{th} was observed from the baseline of 5.91 ± 0.05 °C/W to 6.42 ± 0.06 °C/W after the addition of 500 nM amoxicillin for the MIP functionalised SPE; whereas, the NIP functionalised exhibited an R_{th} of 5.52 ± 0.05 °C/W and 5.61 ± 0.06 °C/W for the baseline and 500 nM amoxicillin respectively. These results were used to construct a dose-response curve and calculate a LoD of 1.89 ± 1.03 nM. Secondly, MIP 2 was formed directly onto the SPE surface through UV polymerisation and analysis was carried out in the same manner. This methodology significantly

reduced the preparation time and increased the reliability of the sensor through the attachment of the polymer to the electrode surface. An increase in the measured R_{th} was observed for the addition of amoxicillin (1 -500 nM) to the MIP functionalised SPE from the baseline value of 7.58 ± 0.06 °C/W to 8.16 ± 0.06 °C/W at 500 nM amoxicillin. The NIP produced a significantly smaller increase in the R_{th} from 7.59 ± 0.06 °C/W to 7.68 ± 0.07 °C/W after 500 nM amoxicillin. The dose-response curve for the MIP allowed for the determination of the LoD of 0.54 ± 0.1 nM which is a big improvement over the drop cast method. The direct UV polymerized SPE was also tested for interference from a competitive pharmacophore, nafcillin. This exhibited a rise in the measured R_{th} from of 6.47 ± 0.05 °C/W in PBS to of 6.60 ± 0.05 °C/W after 500 nM nafcillin, showing the excellent specificity the MIP sensing platform has for amoxicillin.

A full procedure of a MIP based sensor has been explained from the initial optimisation of MIP composition to comparison of mounting methods evaluated by thermal analysis. The developed sensor platform has shown the ability to detect amoxicillin at relevant concentration ranges for environmentally contaminated aqueous samples. Considering concentrations such as 128 µg/L have been found in hospital effluent [287], the sensor proposed currently could easily be used for many effluents from different sources. Other sensors described as having “low” LoD values in 2020, reported values of 50 nM, showing that the sensor developed in the current work outcompetes recent advances to a significant degree [288]. Molecular imprinting is versatile and by adapting the MIP, other antibiotics and pollutants can be targeted. The polymerisation methodology was significantly shortened in comparison to the bulk synthesis method and in conjunction with the thermal set-up, offers a portable, relatively fast and low-cost sensing platform suitable for on-site measurements. This work further demonstrates the vast range of sensing capabilities that MIPs are appropriate for, not only in regards to target versatility but also different sensor platforms they can be incorporated into.

Chapter 5. Electropolymerised Molecularly Imprinted Polymers for the Heat-Transfer Based Detection of Microorganisms: A Proof-of-Concept Study using Yeast

(Published as O. Jamieson *et. al.*, *Thermal Science and Engineering Progress* (2021) 24 100956) [261]

5.1 Abstract

In this chapter, MIPs were electropolymerised onto screen-printed carbon electrodes (SPCEs) to develop specific sensors for the thermal detection of yeast (*Saccharomyces cerevisiae*). A laboratory yeast strain free of interferences was used to optimise the polymerisation procedure, whereas yeast in a complex mixture (yeast for baking) was employed to produce the final sensors and demonstrated proof-of-application. Two different electropolymerisation methods were employed and compared, cyclic voltammetry and chronoamperometry respectively; the electrochemical methodology allowed for controlled deposition and the ability to tailor the polymer surface to the required application. Infrared spectroscopy and scanning electron microscopy confirmed that the methods led to different structures; with cyclic voltammetry a high surface area was achieved, whereas for chronoamperometry a dense film was formed. Subsequently, these functionalised electrodes were inserted into a home-made thermal device that can measure the selective binding of yeast cells to the MIP layer via monitoring the thermal resistance (R_{th}) at the solid–liquid interface.

This study demonstrated that MIP-functionalised electrodes produced, according to both methods, a significant response in thermal signal for the MIP-functionalised electrode, which was not the case for the reference Non-Imprinted Polymer (NIP)-functionalised electrode. This demonstrated that thermal analysis can be employed for the detection of yeast, even in a complex sample such as food or during the brewing

of beer. To the best knowledge, this is the first report of MIPs electropolymerised onto screen-printed electrodes for the thermal detection of fungi.

The proposed approach enables the fast production of low-cost electrodes using a simple manufacturing procedure compatible with a portable device, implying high commercial potential. In the future, this could be adapted to a broad range of microorganisms including bacteria. This would allow for direct monitoring of AMR bacteria and aid the AMR crisis and give rise to faster, more specialised treatment of infection.

5.2 Introduction

Previously, the detection of small molecules has been discussed. Here an example of MIPs employed as recognition elements for the detection of cells (yeast cells) is explored. A proof-of-concept study showing scope for the detection of cells with this technology would open the future possibility that the platform could be used for in situ detection of AMR pathogens, a much more direct route to reducing the accelerated rise in AMR. Microbiological contamination presents huge concerns in a wide variety of sectors throughout the world, such as in food and drink [289], [290], sports [291], medicine [292] and even the construction industry [293]. Contamination of food and drink products specifically presents significant concerns for both health and economic reason [294]. Even in developed economies foodborne illness is commonplace, with an estimated one third of populations suffering from a type of foodborne illness annually[295]. The quality and safety of food is best preserved by delaying the growth of specific bacteria or by reducing contamination by bacterial pathogens; therefore, rapid detection and removal of infected foodstuff is vital [296]. Microbiological techniques, analytical antibody assays and nucleic acid-based assays (such as the polymerise chain reaction (PCR) assays) make up the majority of current detection methods for microorganism [297]. All these methodologies require time-consuming preparation, procedures and/or measurement protocols, thus, development of a fast, reliable, on-site sensor platform for the recognition of microorganisms is of high interest to the analytical community. Antibodies are commonly used as a recognition element in sensor development due to the specific recognition between the antibody and the target antigen, which can be released by, (e.g. virulence factors) or is present on the

surface of the microorganism [298], [299]. However, antibody-based sensors have associated issues such as high cost, high batch-to-batch variation, limited stability, and the fact that some antibodies still require animals for production leading to concerns about the ethicalness of their use [300]–[302].

An alternative recognition element that could be used to overcome these issues whilst maintaining satisfactory detection limits would be beneficial to future sensor development. MIPs, which can easily be integrated into a portable sensor platform, have gained significant interest as biomimetic recognition elements capable of replacing antibodies due to their high affinity, low production cost and superior chemical and thermal stability [303]–[305]. They can be produced using a wide range of monomers and synthetic methodologies, leading to a vast array of sensitive and selective recognition elements [306], [307]. They have been shown to produce highly specific sensing platforms in conjunction with optical [308], electrochemical [212] and thermal [309] detection methodologies. Due to their synthetic production, these polymers also provide an ethical solution that can be applied to a wider range of targets than antibodies due to their intrinsically high level of versatility. Thermal detection strategies have been relatively unexplored; when simply measuring the temperature such as with thermistors, it is difficult to require the level of specificity required for biomarker sensing. However, there has been promise in using the Heat-Transfer Method (HTM) which detection principle is based on measuring changes in heat transfer at the solid-liquid interface due to its low-cost, fast analysis, and ability to measure different markers by changing the functionalised interface. MIPs can be combined with the HTM as a read-out technique and have been shown to produce sensor platforms suitable for the detection of small molecules [211] and proteins [233], [253], as well as for the monitoring of the growth of microorganisms such as yeast and *Staphylococcus aureus* in various media [310]. The selective detection of the presence of yeast cells has been reported previously using surface imprinted polymers (SIPs) combined with HTM [311], [312]. In this chapter, the use of electropolymerisation was explored which significantly reduces the manufacturing process of the biosensor, in addition to forming the MIP layer directly onto the surface of the transducer [208]. There have been multiple reports on conductive and non-conductive MIPs for various transducers including glassy carbon electrodes (GCE) [313]–[315], gold [316]–[318] and screen-printed

carbon electrodes (SPCE).[319]–[321]. The latter are attractive options due to the ability to mass produce such sensors, in addition to their reliability, flexibility and low-cost [281], [322]. Previously, it has been shown that SPCEs can be used as substrates for the deposition of MIP particles for the detection of antibiotics [213] or have the MIP microparticles directly incorporated into the screen-printing ink [210]. As such, in this chapter, a proof-of-concept study is presented that displays MIPs generated directly onto SPCE substrates using electropolymerisation for the detection of microorganisms, in this case yeast, using the HTM. Due to the low-cost and reproducible nature of the SPCEs, there is scope to use them as disposable sensors in the future for screening of contaminants in the food and water industry.

5.3 Experimental

5.3.1 Reagents

To optimise the synthesis procedure, I worked with *Saccharomyces cerevisiae* laboratory strain DLY640 originating from the Rothstein lab [323], [324] which has the advantages of not containing interferents such as sorbitan monostereate and ascorbic acid that are present in commercial baker's yeast. These compounds significantly interfere with analysis and mask the yeast and/or polymer signal. Therefore, a “pure” laboratory strain was used to optimise the synthesis procedure and enabling analysis with infrared (IR) spectroscopy and scanning electron microscopy (SEM). For each experiment, a fresh yeast colony was grown from a yeast extract peptone dextrose (YEPD) agar plate in 250 mL of YEPD broth until an optical density (OD) of at least 1.4 at 660 nm was reached. The optical density for cell concentration was determined by UV-vis analysis which was carried out on a Jenway 7205 UV-visible 72 Series Diode Array Scanning Spectrophotometer (UK). Allinson's Easy Bake Yeast (UK), containing *Saccharomyces cerevisiae* (7 g per sachet), sorbitan monostearate as emulsifier, and ascorbic acid as flour treatment agent, was used for all thermal analysis experiments to evaluate yeast detection in a complex sample such as food. Suspensions of yeast were prepared in sterile deionised water solutions, where the concentration was estimated using the optical density at 660 nm [325].

An optimal profilometer (Omniscan, UK) which uses a MicroXAM (phase shift) surface mapping microscope with an ADE phase shift (XYZ 4400 mL system) and an AD phase shift controller (Omniscan, UK) was used to determine layer thickness. This system was coupled to image analysis software Mapview AE (Omniscan, UK).

SPCEs were produced according to a well-known procedure described in [281]. Carbon-graphite ink formulation (Product Code: C2000802P2; Gwent Electronic Materials Ltd, UK) was printed onto a standard polyester substrate and cured at 60 °C for 30 min, followed by a dielectric layer (Product Code: D2070423D5; Gwent Electronic Materials Ltd., Pontypool, United Kingdom) to cover the connections, which was also cured at 60 °C for 30 min. The pyrrole was sourced from Acros Organics (Loughborough, UK), the yeast extract, peptone bacteriological agar bacteriological (AgarNO.1), D (+)-glucose and glycerol were all obtained from Fisher Scientific (Basingstoke, UK), while the adenine sulfate was purchased from Alfa Aesar (Heysham, United Kingdom). All other chemicals mentioned were acquired from Sigma Aldrich (Gillingham, UK). All experiments were carried out at 21 ± 1 °C (ambient temperature) unless noted differently. For polymerisation, a modified PBS solution (pH=2) was used to ensure a constant ionic strength was maintained for all experiments. All other experiments were carried out in deionised water.

5.3.2 MIP and NIP syntheses

MIPs and NIPs were produced by electrodeposition. A solution of pyrrole (1 mM) in a phosphate buffered saline solution at pH = 2 was prepared as follows: 4 g of NaCl, 0.1225 g of KCl, 0.72 g of Na₂HPO₄ and 0.12 g of KH₂PO₄ were dissolved in 25 mL of deionised water (resistivity 18.2 MΩ cm). The solution was then acidified to pH 2 via the addition of dilute HCl.

Yeast cells were re-suspended in 2 mL of this solution to the density of approximately 5.0×10^6 colony forming units (CFU) / mL [326]. For the “real” yeast sample, powder from Allinson’s Easy Bake Yeast was suspended into deionised water solutions and the suspension density was determined spectrophotometrically as described in chapter 5.2.1. As the yeast was specialised for use in the culinary

sector, it had other additives to enhance its performance. The inclusion of these additives complicates determination of the yeast cell concentration. Prior to using the *Saccharomyces cerevisiae* laboratory strain DLY640, it was recovered from cryo-storage on a YEPD plate. Then a single colony was re-suspended in 250 mL of YEPD broth and grown at 23.00 ± 0.05 °C (for approx. 48 h) to an optical density of at least 1.4 at 660 nm. After growth, the yeast cells were washed 3 times with fresh YEPD, aliquoted into 2 mL samples containing 20% of glycerol which serves as a cryo-protector and stored at -80 °C.

All electrochemical experiments were performed using a three-electrode set up controlled by a PalmSens4 Potentiostat (Netherlands), where the working electrode was an SPCE (diameter = 3.1 mm), counter electrode was a nickel wire and the reference was an external Ag|AgCl reference electrode. The procedures were all performed at 21 ± 1 °C in solutions made with deionised water (resistivity no less than 18 M Ω cm). The SPCE was placed in the acidified pyrrole PBS solution and polymerised according to two electrochemical methods. The first method was cyclic voltammetry, where the electrodes were placed in solution and cycled from - 0.2 V to + 1.2 V at 0.1 V s⁻¹ for 10 scans. The second method was chronoamperometry, where the potential was set to + 0.98 V and maintained for 100 sec for polymerisation.

The polymerised SPCEs were placed under running hot water to remove yeast cells from the polymer complex, SEM analysis was carried out to confirm this method of extraction was sufficient (see Appendix E). SEM measurements were recorded on a Supra 40VP Field Emission from Carl Zeiss Ltd. (Cambridge, UK) with an average vacuum chamber of 1.3×10^{-5} mbar and average gun vacuum of 1×10^{-9} mbar. To enhance the contrast of these images, a thin layer of Au/Pd (8 V, 30 s) was sputtered onto the electrodes with a SCP7640 from Polaron (Hertfordshire, UK). Furthermore, references (Non-Imprinted Polymers) were prepared in a similar manner except there was no addition of yeast to the pyrrole solution in PBS. Diffuse reflectance Fourier transform infrared spectroscopy (DRIFTS) was conducted to monitor polymerisation over time; the high roughness and dark colour of the electrode surfaces made them suitable for DRIFTS. A Thermo-Nicolet Nexus FTIR (DTGS detector), fitted with a Spectra-Tech DRIFTS cell (equivalent to the current Thermo-Fisher Scientific Collector™ II Diffuse Reflectance Accessory) was

used for this analysis. Spectra were made up of 164 scans with resolution set to 4 cm^{-1} . The thickness of the polymerised film (a measure of the extent of pyrrole polymerisation) on the electrode was proportional to the absorbance of the N-H stretching band at 1600 cm^{-1} .

5.3.3 HTM measurements of yeast with MIP-modified SPEs

The MIPs polymerised onto SPEs (MIP-modified SPEs) were cut into squares (1 cm^2) around the working electrode. These were pressed onto a copper block and mounted into a 3D printed flow cell with an inner volume of $110\text{ }\mu\text{L}$ that was designed in house, where a glass slide of the same size was used to create a seal. HTM analysis was carried out to a similar manner stated in Chapter 2. The flow cell was sealed off with an O-ring and connected to the HTM set up that is described by van Grinsven *et al.* [284]. The copper block, which serves as a heat sink, is actively steered with a Proportional-Integral-Derivative (PID) controller. PID parameters can significantly affect the response recorded and therefore were kept at constant, optimised values of $P=1$, $I=14$, $D=0.3$ [253].

Previous research has shown that changes at the solid-liquid interface result in a change in R_{th} . In the case of MIPs, the “pore blocking model” [327] demonstrates how binding of the target to the cavities in the polymer leads to an increase in R_{th} . All experiments were conducted at $37 \pm 0.02\text{ }^\circ\text{C}$, except for one experiment carried out at $50.00 \pm 0.02\text{ }^\circ\text{C}$ to determine if higher temperatures increase binding to the surface (Appendix F). However, no significant change in the measured R_{th} was found which could be due to disintegration of the yeast at elevated temperatures [326].

The MIP-modified SPE were stabilised in PBS for at least 45 min after which a second injection of PBS was performed to establish a stable baseline. Subsequently, at 30 min intervals, suspensions of increasing yeast concentrations (1.0×10^2 , 1.0×10^3 , 1.0×10^4 , 1.0×10^5 , 1.0×10^6 and 1.0×10^7 CFU/mL) in deionised water were added into the flow cell with an automated NE500 programmable syringe pump (Prosense, Oosterhout, the Netherlands). The solutions were injected at intervals of 30 min, with an injection volume

of 3 mL being injected with a flow rate of 1.975 mm/min. The thermal resistance was monitored over time and determined at each concentration. This was used to construct dose-response curves, where the limit of detection was calculated using the three-sigma method in the linear range of the sensor. To establish the specificity of the sensor platform, identical measurements were performed with NIP-modified SPEs.

5.4 Results

5.4.1 IR and SEM analyses to determine surface structure of MIP-modified SPEs

Firstly, the formation and deposition of polypyrrole (PPy) on the surface of the electrode material was investigated. The substrate of choice for the final sensor platform was a SPCE; however, this substrate is notoriously difficult to analyse due to its large, rough surface area and high absorbance. Therefore, to analyse the initial deposition technique, it was first performed using a gold substrate. PPy layers were formed on this substrate using chronoamperometry for different periods of time (0, 30, 60 and 120 s) to monitor the growth of the polymer layer. This was achieved by placing the electrode in the solution specified above and held at + 0.98 V vs. Ag|AgCl for the specified amount of time. The FTIR spectra for the different polymerisation times is presented in Figure 5.1 A, where the increase in the peak at 1600 cm⁻¹, corresponding to N-H stretching, confirmed an increase in the amount of PPy on the surface of the electrode. The IR absorption bands of the electrode composition (e.g. the ester carbonyl stretch of the binder at ca. 1730 cm⁻¹) were unaffected by the PPy [327]. As expected, the longer the system was subjected to the potential, the thicker the layer of PPy formed on the surface as seen by the increase in absorbance of the peak.

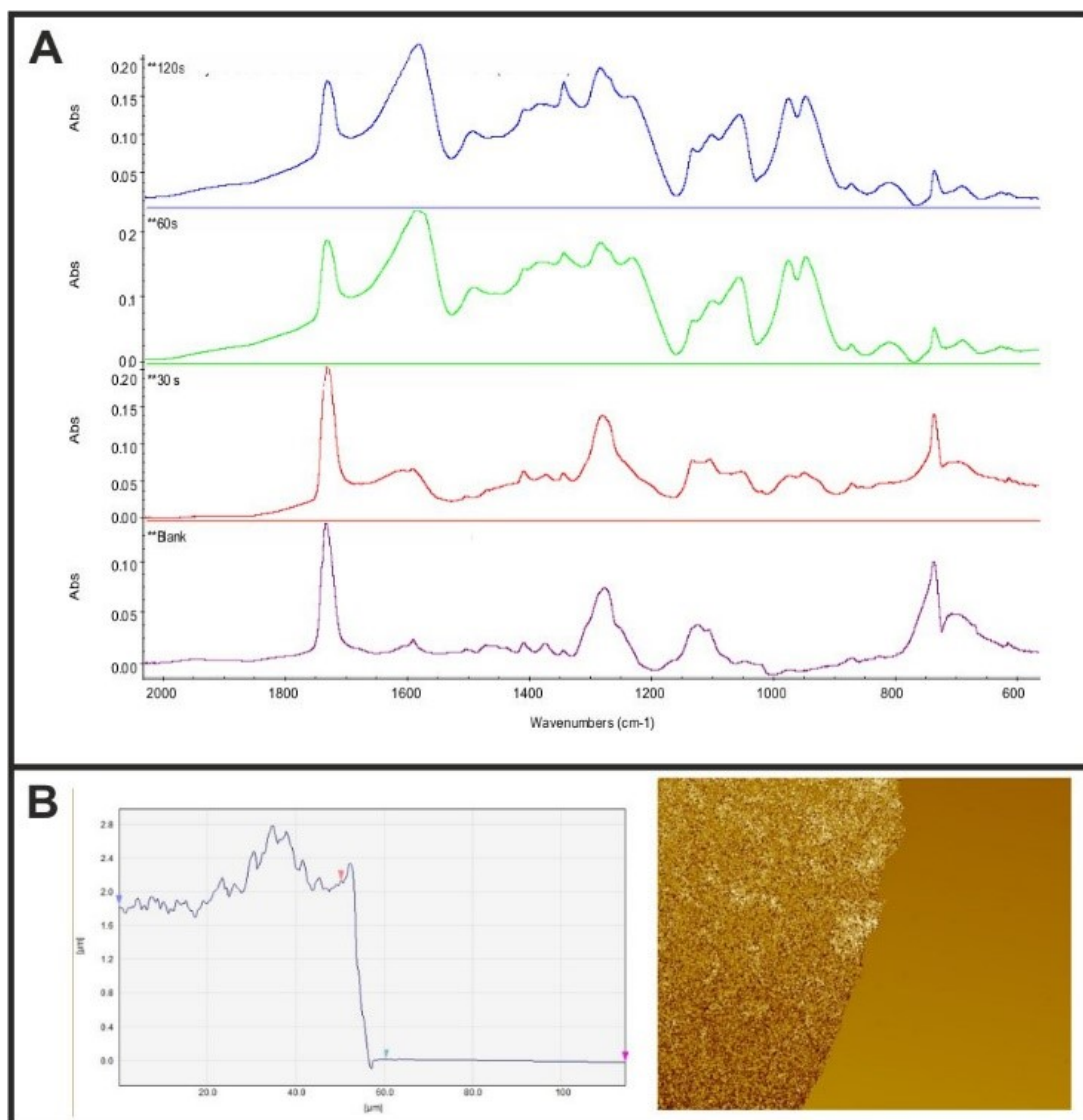


Figure 5.1. A) FTIR result showing the generation of PPy on the surface of the electrode. B) White light profilometry of the PPy layer generated on the surface of the electrode.

To obtain an estimate for the thickness of the layer of PPy, an Au electrode was coated with PPy and placed under a White Light Profilometer (Figure 5.1B). While the binding kinetics for Au electrodes and SPCEs are different, this provided an indication of the layer thickness which is needed to bind the microbial cells but not too high, so it hampers mass transfer.

As can be seen, the layer was non-uniform, manifesting a rough texture and an estimated thickness between 1.5 – 3 μm . It is reasonable to assume that the thickness of the layer deposited on an SPE would be thinner than this due to the slower electrode kinetics [328]. Yeast cells typically range from 5 – 10 microns in size [329], therefore a slightly longer deposition time of 100 s was chosen for sensing

experiments. This would allow for the formation of cavities roughly 50 % of the size of the yeast cells, suggesting that they would not be fully covered by polymer. It was important to keep the polymer layer as thin as possible, whilst still offering binding sites for yeast that were deep enough for the yeast to bind to through both size, shape and functionality. Therefore, both cyclic voltametric and chronoamperometric deposition methodologies were performed and compared, Figure 5.2.

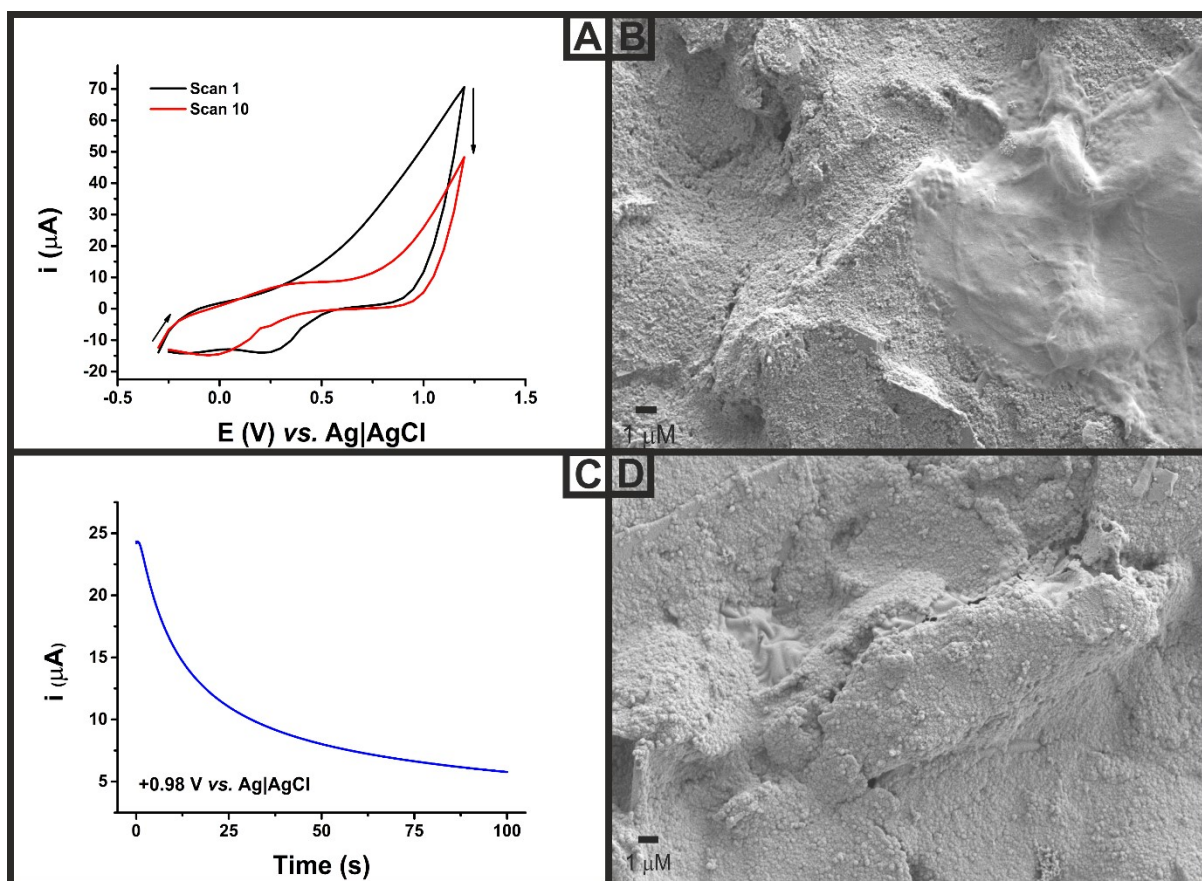


Figure 5.2. A) Cyclic voltammograms for the formation of PPy on the surface of the SPCE performed at 100 mV s⁻¹. B) SEM image for the formation of PPy patches on the surface of the SPCE using cyclic voltammetry. C) Chronoamperogram for the formation of a PPy layer on the surface of an SPCE at +0.98 V vs Ag|AgCl for 100 s. D) SEM image for the formation of a PPy layer on the surface of an SPCE using chronoamperometry.

As can be seen in Figure 5.2, both exhibit the typical rough surface of SPEs, due to the graphite flakes. However, there were significant differences observed in the polymeric coverage when using cyclic voltammetry (CV) and chronoamperometry (CA). When using CV, Figure 5.2 A, the formation of PPy on the surface begins following the oxidation of the pyrrole monomer on the first scan. The formation of PPy can be tracked by following the decrease in the current on the oxidation scan due to the polymerisation of monomeric pyrrole into polypyrrole. This was confirmed via SEM, Figure 5.2 B, where patches of polymer can be seen although there is not a uniform coverage across the SPE surface. In comparison, when using CA, Figure 5.2 C, a greater coverage of polymer was observed on the surface, Figure 5.2 D. This was expected as while CA is run, polymer was continuously formed since it is at the oxidation potential; however, when CV was used the polymer was only formed when the potential was raised above the required oxidation potential of the monomer [330]. Both of these polymer systems were subsequently used for the detection of yeast cells.

5.4.2 Thermal resistance measurements for yeast using MIP-modified SPCEs

HTM allows for the monitoring of changes occurring at the solid-liquid interface through the change in measured thermal resistance. As such, PPy formed via both CV and CA imprinted with yeast cells was electrochemically deposited on the surface of SPCEs as described above; after which, the yeast cells were removed leaving specific associated cavities. SPCEs were chosen as the substrate for these sensing experiments as they offer ease of preparation for the MIPs due to the inclusion of counter and reference electrode in addition to a significant reduction in cost compared to other commonly used electrodes such as gold and glassy carbon. The functionalised SPCEs were then inserted into the flow cell presented in Figure 5.3 A and sealed with a rubber O-ring and copper block. The copper block temperature was set to 37 ± 0.02 °C, in line with previous studies on proteins and real-time monitoring of organisms [253], [310]. To demonstrate proof-of-concept, a MIP-modified electrode produced with *Saccharomyces cerevisiae* laboratory strain DLY640 was measured (Figure 5.4). The electrode was stabilised in a buffered solution after which a suspension of *Saccharomyces cerevisiae* in PBS (1.0×10^7 CFU/mL) was added. A sharp

increase in the thermal resistance was observed, which was due to binding of the yeast cells on the surface. Washing with the buffered solution did not change the signal, indicating that the yeast cells were firmly bound into cavities.

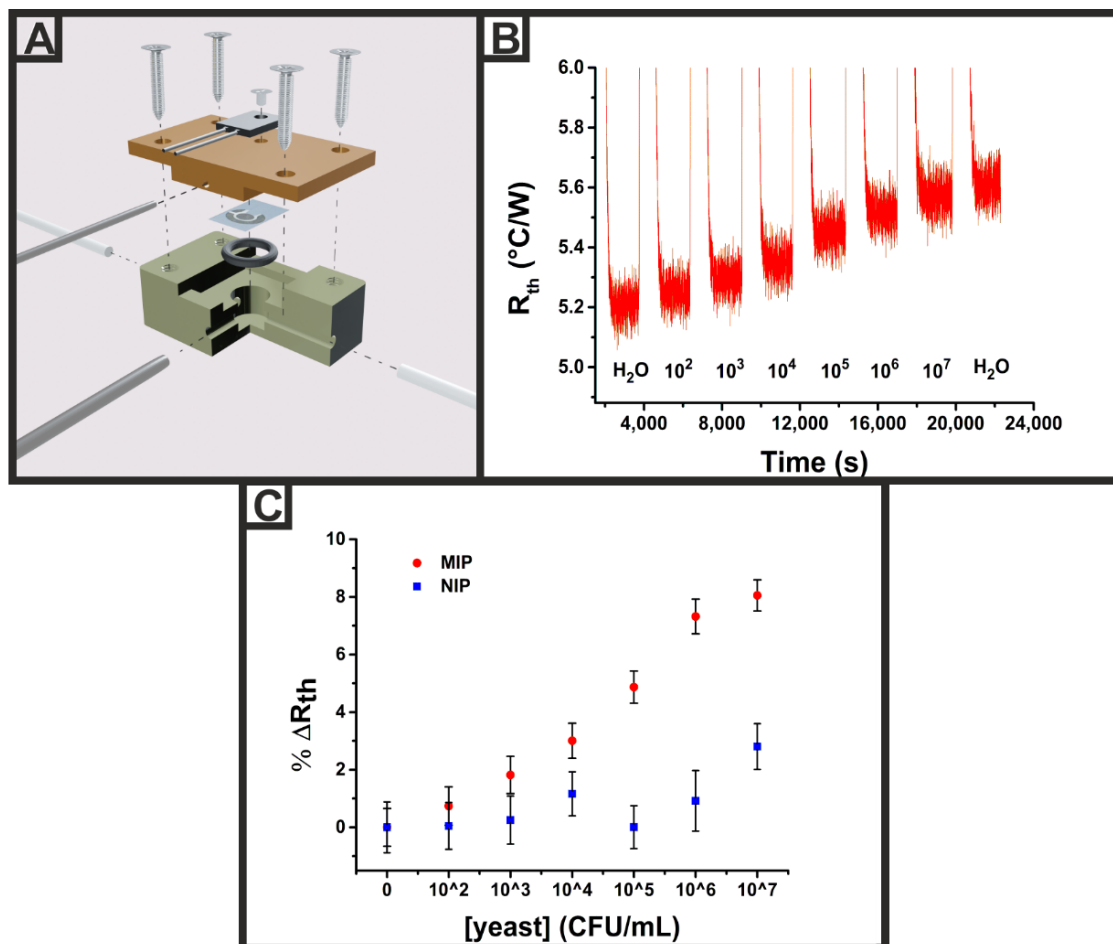
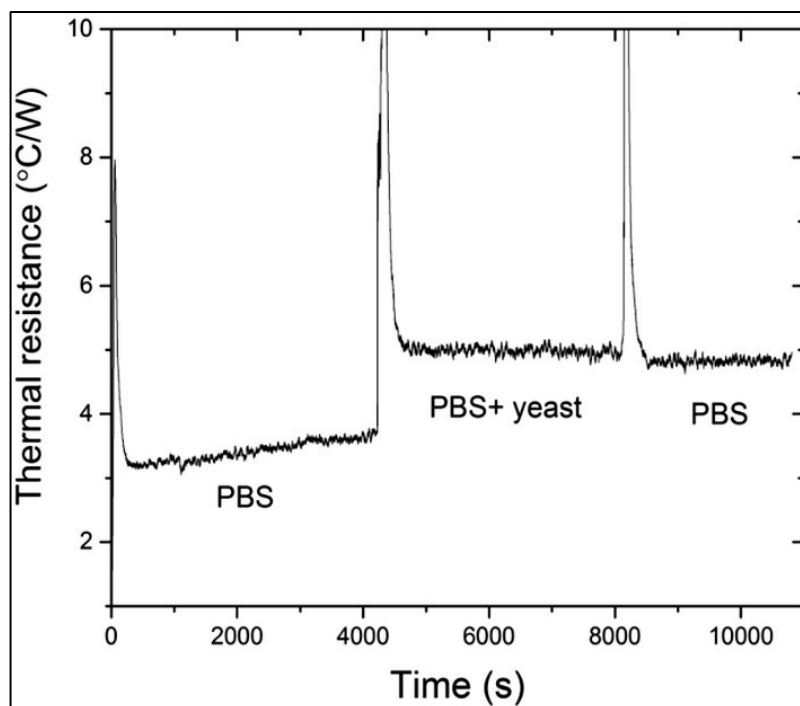


Figure 5.3. A) Schematic diagram of the flow cell used throughout the thermal measurements in this work, comprising of a single thermocouple inserted into a main chamber with a flow inlet and outlet. B) HTM raw data plot of the measured R_{th} versus the time for sequential additions of yeast cells to a MIP-coated SPCE produced using CV. C) Plot of the change in measured R_{th} against the concentration of added yeast cells to a HTM set-up with both a MIP and NIP coated SPE.

Subsequently, I moved towards the yeast in a complex sample to further evaluate the specificity of the sensor platform. Initially, comparisons in the sensing proficiency for both the CV and CA MIPs were explored. The same procedure was used for both systems. A blank solution of deionised water was injected

to fill the flow cell, and the system allowed to reach a stable temperature for 45 min. The baseline Rth value was calculated from the average of the final 600 data points (10 min) prior to the injection of the first concentration of yeast cells. Following this 3 mL of the lowest concentration of yeast cells (10^2 CFU/mL)



was injected into the flow cell, indicated by the sharp vertical line in the raw data plots in Figure 5.3. This sharp increase in the Rth was due to the injection of room temperature liquid (~ 20 °C) into the system at 37 °C. After the injection was completed, the Rth was left to stabilise for 30 min before the next injection of analyte, thus facilitating calculation of the Rth from the last 600 data points of each stabilisation period.

Figure 5.4. A MIP-modified electrode (prepared with laboratory strain of yeast) was mounted into the HTM set up and stabilised in a standard PBS solution (pH=7.4). While there is some minor drift in the signal, addition of a suspension of yeast (1.0×10^7 CFU/mL) in PBS led to a significant increase in the thermal resistance due to binding of yeast in the activities on the surface. This provided proof-of-concept and in following experiments, yeast from a complex mixture was considered.

For the CV based MIP the baseline stabilised at a value of calculated to be 5.20 ± 0.03 °C/W. After the addition of yeast cells (10^2 CFU/mL) the measured Rth increased to 5.24 ± 0.03 °C/W. It continued to rise

after further additions of yeast cells in higher concentrations, which was attributed to the binding of yeast cells to the MIP layer on the SPE surface, making transfer of heat across the interface polymer/solution more difficult. For the final addition of yeast to the system, the R_{th} reached $5.61 \pm 0.03 \text{ } ^\circ\text{C/W}$ which represented an overall increase of $8 \pm 1 \%$. Then, the system was injected with a blank solution of DI water and no significant increase was found in the measured R_{th} ($5.62 \pm 0.03 \text{ } ^\circ\text{C/W}$). This indicated that the change in the R_{th} was due to the presence of yeast cells binding to the MIP layer on the SPE and that washing with water did not cause a significant amount of yeast cells to be removed. An image obtained with the white light profilometer is shown in Figure 5.5, demonstrating the presence of yeast on the surface after HTM measurements with a MIP-modified electrode.

In contrast to this, the NIP-modified electrode showed little changes in the measured R_{th} for any injection of yeast into the flow cell, Figure 5.3C, up to 10^6 CFU/mL . This indicated that the binding of yeast cells to the electrode surface was specific for the MIP platform and did not rely on non-specific adsorption to the polymer surface.

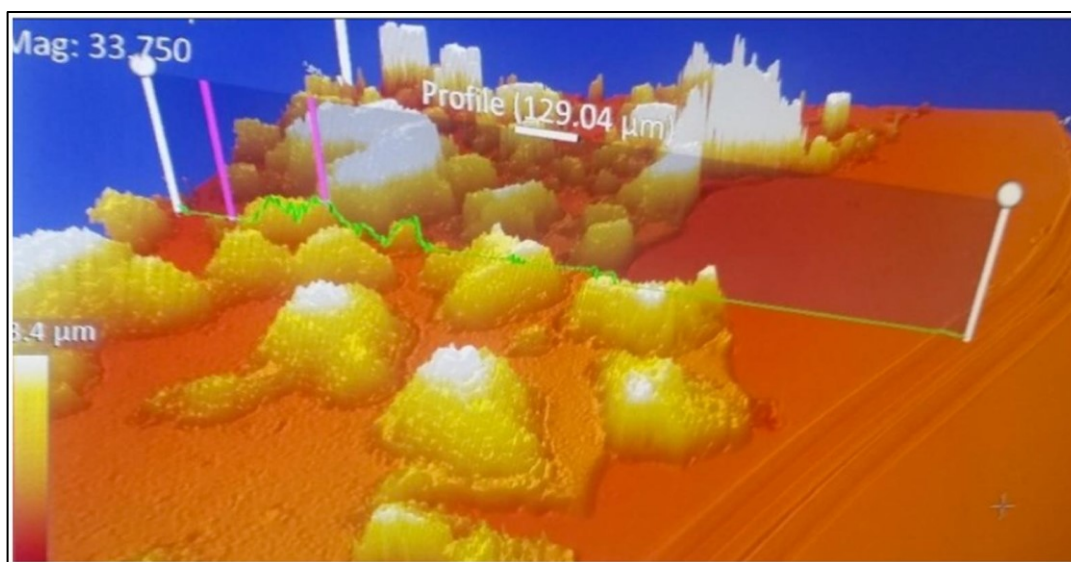


Figure 5.5. Measurements with the white light profilometer of a MIP-modified electrode after HTM measurements confirmed the presence of yeast on the surface.

In comparison to the CV prepared platform, when CA was used the baseline stabilised at a value of 6.49 ± 0.03 °C/W, which was a higher value than was observed for CV based MIPs. This was expected due to the thicker, more uniform coverage of polymer across the SPCE surface increasing the resistance to heat-transfer across the system. For the MIP, there was an increase in the R_{th} for every addition of increased concentration of yeast until the final addition of 10^7 CFU/mL where the R_{th} stabilised at a value of 6.87 ± 0.04 °C/W. In the case of the NIP, there was an initial rise in the measured R_{th} ; however, this then reduced back to the baseline level.

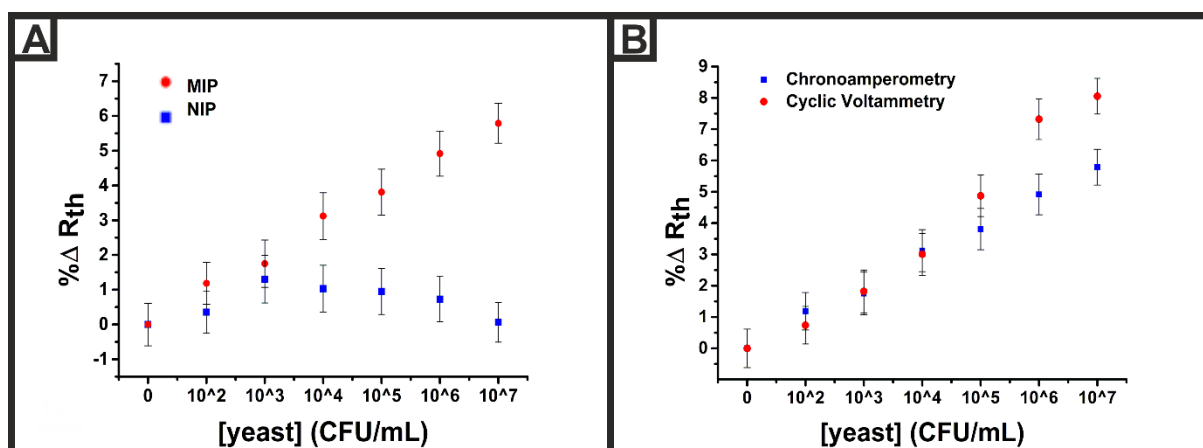


Figure 5.6. A) Plot of the percentage change in the measured R_{th} against the concentration of added yeast cells to a HTM set-up with both a MIP and NIP coated SPCE using chronoamperometry. B) Plot comparing the percentage change in R_{th} for the MIP platforms produced by chronoamperometry and cyclic voltammetry. Error bars relate to the standard deviation of the experiment.

Both the CV and CA production methods produced a system capable of detecting the presence of yeast in the system when the MIP was present and showed minimal or no response when the NIP was present. The CV produced system exhibited a higher specificity between MIP and NIP, where the LoD was determined at the three-sigma method. For the system with CV, a LoD was determined of $10^{1.25} \pm 0.09$ CFU/mL, whereas this compared to a LoD of $10^{1.12} \pm 0.07$ CFU/mL for CA, which are well below the concentrations found in the brewing process of $\sim 10^4$ - 10^6 CFU/mL [331]. The data in Figure 5.6B confirm that at low concentrations the response is similar whereas the polymers produced using CV have higher

response at higher concentration, suggesting a higher binding capacity. This could be due to higher surface area of the electrodes produced in this manner, although for detection of macromolecules it would normally be preferred to have a dense layer covering the surface to minimise non-specific binding by similar microorganisms or interferents from the matrix structure. In the future, more work on understanding the surface structure of electropolymerised MIPs is needed to understand how it impacts on the specificity and selectivity of binding of macromolecules.

5.4 Conclusions

This chapter has demonstrated the extrapolation of the knowledge acquired and developed throughout this thesis on imprinted polymers to the detection of yeast cells at a commercially accurate standard. MIPs, along with reference NIPs, for the detection of yeast were deposited onto SPCEs using cyclic voltammetry and chronoamperometry. To optimise the synthesis procedure, MIPs were prepared using a *Saccharomyces cerevisiae* laboratory strain DLY640 which is free from interferents, allowing to study the layer thickness and surface structure by using IR and SEM analysis. It was shown that with cyclic voltammetry a “patch-type” structure was formed, with polymer mainly forming around the ridges of the SPCEs. In contrast, if CA was used, a thick homogeneous coating was formed with an estimated layer thickness of several microns, which is sufficient to incorporate the yeast cells. SPCEs coated with both methods were mounted into a home-made thermal device, where the response of the thermal signal was used to monitor binding of yeast from a commercial baker’s yeast sample (Allinson’s Easy Bake) to demonstrate proof-of-concept. A significant response in the thermal resistance was observed from the MIP, contrary to reference NIP electrodes, demonstrating the change in signal was due to selective binding of yeast in the imprinted cavities. Electrodeposition of MIPs onto the SPCEs led to sensors with similar levels of detection attained; however, the polymers produced using CA had a higher binding capacity. These levels of detection are within the relevant range in the brewing industry, suitable for in-situ monitoring in fermenters, or to determine the yeast presence in food samples [332]. The advantage of the

method proposed in this project is that it is fast, low-cost, and portable, providing it with high commercial potential, and demonstrating that analysis of heat-transfer analysis can play a vital role in the biosensor community. Due to the versatility of the molecular imprinting technology, in the future this can be expanded to other relevant objects such as macromolecules, bacteria and eukaryotic cells which will open many other applications beyond the food industry. This chapter shows a second example of a possible extension to the detection platform developed in Chapter 3. If the dual detection platform could be extended from small molecules to a target such as yeast, a target which is much more complex and larger in size (as this chapter shows can be achieved), then full cells could be detected simultaneously via HTM and optical detection. This work provides the first step into specialised cell detection which could be applied to AMR bacterial cells through further optimisation and development. This would provide another pathway to aid the AMR crisis; not only detecting small molecules to combat antibiotic pressure but directly detecting resistant bacteria cells which could have significant implications in the healthcare service.

Chapter 6. General Conclusions and Outlook

Contained within this chapter is a summary of the work carried out and the results contained in this thesis with the aim to provide and explain future workings and the expected scope of the work detailed within. Conclusions and comments will be made with respect to the five primary objectives of the work detailed in Chapter 1.

1. Optimise a MIP composition that is appropriate for Fluorescent and thermal analysis utilising a fluorescent monomer that is less sensitive to pH changes than has been previously reported.
2. Devise an appropriate means of fluorescent analysis that is compatible with thermal analysis
3. Survey the validity of a dual sensor platform incorporating both a thermal and fluorescent read out.
4. Investigate the polymerisation process in terms of possible sensor platform expansion and methodology to maximise the versatility and applications of the sensor produced.
5. Extrapolate the use of MIP based sensors from small molecule targets to much larger targets such as full cells (e.g. yeast cells) in a proof of concept study to demonstrate future ability for application to direct AMR bacteria detection.

The work detailed within this thesis has been aid significantly by academic collaborations detailed in Table 6.1. the work produced has resulted in the conference contributions and contribution to scientific journals as listed below.

6.1 Conference contributions-

Oral (in person)- “Development of a polymer based optical identification system for the detection of pharmaceuticals in water systems”, Water Treatment Symposium, Manchester, 2019

Oral (in person)- “Development of a polymer based optical identification system for the detection of antibiotics in water systems”, Graduate Student Symposium on Molecular Imprinting, Berlin, 2019

Oral (in person)- “Antibiotic detection platform utilising fluorescent Molecularly Imprinted Polymers”, UK-Russia Bioinspired Materials Conference, Lancaster, 2020

Oral (virtual)- “Development of a polymer-based detection platform for antibiotics in water system”, Newcastle University PGR annual symposium, Newcastle, 2020

Oral (virtual)- “Development of a polymer-based detection platform for antibiotics in water system”, Macro 2020+, Korea, 2021

Oral (virtual)- “Development of a polymer-based detection platform for antibiotics in water system”, Antimicrobial and Biosensing Nanotechnologies, Kazakhstan, 2021

Oral- “Development of a polymer-based detection platform for antibiotics in water system”, Newcastle University PGR annual symposium, Newcastle, 2021

6.2 Scientific journal contribution-

1. A. Hudson, R. Sola Mestres, J. T. Ueta, W. Battell, **O. Jamieson: Investigation**, T. Dunbar, B. Macia, M. Peeters, accepted in Biomimetics, 2019, **article 420507**

2. **O. Jamieson: Conceptualisation, Methodology, Investigation, writing- original draft, writing-review and editing, Visualisation, Formal analysis, reagents, Data curation, Project administration,**

T. C. C. Soares, B. A. de Faria, A. Hudson, F. Mecozzi, S. J. Rowley-Neale, C. E. Banks, J. Gruber, K. Novakovic, M. Peeters and R. D. Crapnell, accepted in Chemosensors, 2020, <https://doi.org/10.3390/chemosensors8010005>

3. **O. Jamieson: Conceptualisation, Methodology, Investigation, writing- original draft, writing-review and editing, Visualisation, Formal analysis, reagents, Data curation, Project administration,**

K. Betlem, N. Mansouri, R. D. Crapnell, F. S. Vieira, A. Hudson, C. E. Banks, C. M. Liauw, J. Gruber, M. Zubko, K. A. Whitehead and M. Peeters, accepted in Physica Status Solidi a, 2021, DOI: 10.1002/pssa.202100021

4. **O. Jamieson: Conceptualisation, Investigation, writing- original draft, writing- review and editing, Visualisation**, et. al, accepted in Thermal Science and Engineering Progress, 2021, <https://doi.org/10.1016/j.tsep.2021.100956>
5. A. Hudson, **O. Jamieson: Methodology, Investigation, Writing- Original draft, Writing- review and editing**, R. Crapnell, K. Rurack, T. Soares, F. Mecozzi, A. Laude, J. Gruber, K. Novakovic, M. Peeters, Materials Advances, DOI: 10.1039/D1MA00192B
6. P. Singla, S. Garg, J. McClements, **O. Jamieson: writing- review and editing**, M. Peeters, R. Kumar Mahajan, accepted in Advances in Colloid and Interface Science, 2022, <https://doi.org/10.1016/j.cis.2021.102563>
7. L.F. Figueiredo, F. S. Vieira, **O. Jamieson: Conceptualization, Methodology, writing- review and editing**, J. Reeder, T. McLean, J. Olsen, R. D. Crapnell, M. J. Whittingham, C. E. Banks, R. Law, J. Gruber, M. Peeters, accepted in Microchimica Acta, 2022,
8. *Planned paper currently in writing-* **O. Jamieson: Conceptualisation, Methodology, Investigation, writing- original draft, writing- review and editing, Visualisation, Formal analysis, reagents, Data curation, Project administration**, A. Hudson, K. Rurak, J. Saczek, K. Novakovic, M. Davies, E. Foster, M. Peeter, planned journal- Materials Advances 2022,
9. *Planned paper currently in writing-* **O. Jamieson: Conceptualisation, Methodology, Investigation, writing- original draft, writing- review and editing, Visualisation, Formal analysis, reagents, Data curation, Project administration**, W. Battell, M. Schmidt Silva, J. McClements, K. Novakovic, M. Peeters, Analytical and Bioanalytical Chemistry, 2022

Table 6. 1 Listed research exchanges

| Period | University | Description |
|-----------------|--|---|
| 08/2019-01/2022 | BAM Bundesanstalt für Materialforschung und -prüfung (Germany) | Collaboration on fluorescent MIP composition aiding in publication no. 5 and Chapter 3. |

| | | |
|-----------------|---|--|
| 10/2018-08/2021 | Manchester Metropolitan University (UK) | Collaboration on MIP analysis and knowledge transfer aiding in publication no. 1,2,3,4,5,7 |
| 08/2019-01/2022 | University of Bath (UK) | Collaboration for computer modelling for template-monomer interactions and knowledge transfer resulting in publication no. 1,3 |
| 11/2019-01/2022 | Universidade de São Paulo (Brazil) | Continuous knowledge transfer and supervision of several student contributing to publication no. 1,2,4,5,7 |

6.3 Overview of contribution to knowledge

To explore the versatility of MIPs, MIP modified SPEs for the detection of amoxicillin were developed. Careful monomer selection was carried out and solvent choice was evaluated to be compatible with the SPEs. A MIP was produced with an IF of 6.5, which demonstrated high levels of specificity. This was hypothesised to be due to the acrylamide and the template forming more significant of interactions such as hydrogen bonds, than the other two monomers tested: 2-vinylpyridine and methacrylic acid . Two production methods were carried out, firstly by the bulk polymerisation of a MIP which was then deposited on top of the SPE by drop casting. Secondly, direct polymerisation on SPE electrode was carried out via electrochemical means in the presence of pyrrole, with both versions of MIP modified SPE analysed via thermal analysis while introducing increasing concentrations of amoxicillin and nafcillin. Both systems showed significant response (5.91 ± 0.05 °C/W to 6.42 ± 0.06 °C/W against that of the NIP- 5.52 ± 0.05 °C/W and 5.61 ± 0.06 °C/ 5.52 ± 0.05 °C/W and 5.61 ± 0.06 °C/W for the baseline for the baseline when exposed to 500 nM amoxicillin solution in PBS) with each increasing concentration of both solutions.

Although there was binding of both compounds to the MIP, there was an elevated response when binding to amoxicillin. Both molecules have a very similar structure, both sharing the same pharmacophore. Due to the elevated response to the desired target, amoxicillin, it was deduced that the MIP produced, for both production methodologies, have a significant level of selectivity. It was evident from the results gathered that the MIP modified SPE that was produced via the direct polymerisation method had elevated binding capabilities over that of the first method, in terms of both specificity and selectivity. Through this work it was explained how MIP versatility is not limited to the targets it can detect but also to the various types of platforms in which it can be incarnated into.

A significant reason for embracing MIP use is their target versatility. The work carried out in Chapters 3&4 have given insight into how MIPs can detect small molecules at commercially relevant concentrations to combat the rise of AMR bacteria via pinpointing sources of contamination. Another route for aiding combatting AMR is by the direct detection of resistant pathogens. To highlight the capabilities of MIPs and how they can alleviate the issue of AMR growth, Chapter 5 focused on a proof-of-concept study on detection of yeast cells. MIP modified SPEs were produced utilising pyrrole, an electroactive monomer. The polymerisation was carried out via electrodeposition, similar to procedures described in Chapter 4. Thermal analysis was performed on the SPEs with increasing concentrations of yeast solution. The yeast solution used was from a baker's yeast product which contained additives, therefore allowing to draw conclusions about the sensor capabilities in complex media. The MIP modified SPE showed elevated response with each increasing concentration of yeast containing solution showing clear indication of its ability to detect cells as targets, not just small molecules. To the best knowledge, this is the first report of MIPs electropolymerised onto screen-printed electrodes for the thermal detection of fungi. Although there are dramatic differences between yeast and AMR cells, one being prokaryotic and the other eukaryotic, it was still an advancement in the versatility of the sensor away from primary use in small molecule detection. This work allowed speculation towards detecting AMR bacterial cells and with

slight adaptations and optimisation it is plausible to suggest the system developed could be extrapolated to sensing such cells in the near future.

Thermal analysis was utilised for the majority of the work in this thesis. A crucial aspect of the work undertaken was for the development of a MIP composition that could be used for fluorescent analysis as well as thermal. MIP compositions were devised incorporating a fluorescent moiety which were then evaluated via optical batch rebinding experiments. MIP A and MIP T saw IF of 3.8 and 1.8 respectively. Although MIP A had a higher IF value, MIP T was used for later fluorescent analysis due to the lower quantum yield of tetracycline which would cause less interference with the analysis. Initial fluorescent assays were carried out to examine fluorescent MIP suspensions in PBS via a UV-VIS spectrophotometer BMG LABTECH, FLUOstar Omega Microplate Reader. After this initial analysis, it was concluded that, due to particulate settlement within the suspension and a lack of a scrupulous view on what was happening on the polymer surface in regard to fluorescent signal, this means of monitoring the MIPs fluorescence was not completely appropriate. This prompted a change to the MIP production and analytic device to MIP modified glass electrode analysed via an inverted fluorescent microscope. Examination of the fluorescent intensity before, during and after the addition of various solutions (target, competitor target and reference solutions) showed a significantly higher response (a 85.4% quenching of fluorescent intensity) of the fluorescence response when the MIP was exposed to solution containing the intended target (tetracycline, 0.1 mM), 10 times higher when compared with the MIP exposed to PBS and amoxicillin (quenching of 8% and 7% respectively). A future experiment would be the introduction of multiple target solution injections instead of a singular injection, to observe whether or not the fluorescent quenching would be experienced further with each injection. This was validated by data gathered from the employed thermal analysis technique (HTM). The combination of both techniques demonstrates the ability to produce a multi-purpose MIP as a recognition element. Future work would see the MIP given solutions responses by combining both analysis techniques in a simultaneous manner. This would require minimum optimisation primarily focused on alternations to the thermocouple used.

Further exploration of the binding affinities of all polymers synthesised throughout this thesis, in terms of specificity and selectivity would ideally be carried out an aspect to be considered is the breadth of targets used in selectivity experiments. In most selectivity experiments, targets of different drug families were compared. Furthering from this, experiments could be carried out using a range of antibiotics within the same family of antibiotics and therefore sharing the same pharmacophore. Differential between closely related target molecules would give a more significant insight as the level of specificity of the MIP synthesised. However, as mentioned throughout, with such sensors as the sensor under development in the work, selectivity is a subjective measurement as certain sensors would have a higher level of usefulness if they can detect a pharmacophore rather than an isolated molecule as would be the case with many water quality monitoring applied sensors. As mentioned throughout this thesis, template leaching is of significant consideration when analysing the binding affinity of MIPs. Further specificity studies could be carried out using MIPs imprinted with a different target. This would afford the assumption that target leaching could not affect the resulting filtrate concentration after a batch rebinding experiment. Furthermore, throughout the work carried out, there was significant ambiguity in the particle size due to no access to a ball mill and no sieves being used. To consolidate the results gathered, repeats could be carried out using a sieve on the MIP particles so that a more definite particle size range could be quantified. This would lead to a more concrete estimation of the surface area of the particles within each suspension sample and rule out any anomalies that vast differences in surface areas would lead to.

6.4 Final remarks and future scope

MIPs offer substantial versatility in terms of their composition. With little optimisation, vastly different polymer capabilities have been shown, even with only changing a functional monomer as demonstrated in this thesis. The development of fluorescent MIPs detailed in Chapter 3 opens a conversation on the future applicability of their use. A study into a wider range of fluorescent monomers would be beneficial in terms of exploring the benefits or limited capabilities of various fluorescent monomers. As detailed in

Chapter 3, fluorescence can be influenced by a plethora of different aggravators including pH, ionic strength and contaminants that would be evidently present in real samples. By creating a library of fluorescent monomers and their characteristics when incorporated into a MIP, a better understanding of fluorescent monomer selection could be gathered, aiding to fluorescent MIP optimisation.

A dual detection system was developed that possess significant future scope. At the end of the study however both analysis techniques are individual and not simultaneous as was planned. This is due primarily to time restraints from the period of the work carried out in the pandemic. As mentioned, a different thermocouple can be employed to combine both systems. Another elevation would be the employment of a resin flow cell to completely eliminate any fluorescence experienced from the glue used that may interfere with the analysis. Combination of both analysis techniques, in a simultaneous manner, would afford a detection system with a higher degree of usefulness whilst validating and promoting MIP use as recognition elements in future sensor platforms. Furthermore, the miniaturization of the thermal analysis system would allow for significantly promoted applicability to an onsite sensor. Secondly, further exploration into other means of fluorescence analysis could bestow a compact and transportable fluorescent analysis system, allowing for promising applications into producing an onsite, simultaneous dual sensor platform, the final aim for the research. Another venture would be the combination of the work reported in Chapter 3 and 5. The potential to produce a dual detection system for AMR bacteria directly has momentous implications for healthcare and would be a further contribution to scientific knowledge. This would lead to real-time monitoring of bacterial development which is an area in need of enlightenment. As a finalised sensor platform, this would produce faster diagnosis time (~15 min against that of 2 hr analysis which are then only possible with expensive infrastructure that is not widely affordable) for infections which would lend to specialised treatment over the use of broad-spectrum antibiotics and faster treatment times, reducing hospitalisation times for patients resulting in more efficient treatment, higher patient turnover and reduction of costs. The use of MIPs in this area would be beneficial due to their inherent robustness as explained in Chapter 1. A universal sensor which is applicable to

multiple sample media (blood, urine, saliva etc) would increase useability and commercial aspects significantly.

Chapter 4 gave insight into the compatibility of MIPs with other electrodes, as SPEs base material is polyester, issues had to be overcome in terms of solvent compatibility. Given that a sensor was successfully produced utilising an electrode with somewhat complicated compatibility, the desirable adaptability of MIPs was demonstrated, promoting their use over that of antibodies as recognition elements.

In summary, demonstrated in this thesis is an alternative recognition element to traditional antibody use. Lengthy MIP monomer selection and optimisation remains an obstacle in furthering MIP use to commercial products. MIP sensing capabilities have been shown to be comparable to that of antibodies when employed as recognition elements; further work is needed in this area to consolidate this to combat commercial scepticism around their abilities. With the advancements in computational modelling as highlighted in Chapter 1, both issues should soon be overcome. This thesis has shown the versatility, adaptability and capability of MIPs, showing their path from a predominately academic-based standpoint to their future application and role in commercial sensors.

Chapter 8. References

- [1] O. Jamieson *et al.*, “Approaches to the Rational Design of Molecularly Imprinted Polymers Developed for the Selective Extraction or Detection of Antibiotics in Environmental and Food Samples,” *Physica Status Solidi (A) Applications and Materials Science*, vol. 218, no. 13, Jul. 2021, doi: 10.1002/PSSA.202100021.
- [2] J. Clardy, M. A. Fischbach, and C. R. Currie, “The natural history of antibiotics,” *Current Biology*, vol. 19, no. 11, pp. R437–R441, Jun. 2009, doi: 10.1016/J.CUB.2009.04.001.
- [3] F. Bambeke, J.-M. Pages, and V. Lee, “Inhibitors of Bacterial Efflux Pumps as Adjuvants in Antibiotic Treatments and Diagnostic Tools for Detection of Resistance by Efflux,” *Recent Patents on Anti-Infective Drug Discovery*, vol. 1, no. 2, pp. 157–175, Jun. 2006, doi: 10.2174/157489106777452692.
- [4] J. Rubí, M. Díaz, J. A. Guevara-Salazar, R. I. Cuevas Hernández, J. Guadalupe, and T. Ferrara, “Expert Opinion on Drug Discovery ISSN: (Print) (Online) Journal homepage: <https://www.tandfonline.com/loi/iedc20> A more specific concept of a pharmacophore to better rationalize drug design, tailor patient therapy, and tackle bacterial resistance to antibiotics,” 2021, doi: 10.1080/17460441.2022.1985459.
- [5] M. A. Kohanski, D. J. Dwyer, and J. J. Collins, “How antibiotics kill bacteria: from targets to networks,” *Nature Publishing Group*, 2010, doi: 10.1038/nrmicro2333.
- [6] R. S. Singer, “Antibiotic resistance—the interplay between antibiotic use in animals and human beings,” *The Lancet Infectious Diseases*, vol. 3, no. 1, pp. 47–51, Jan. 2003, doi: 10.1016/S1473-3099(03)00490-0.
- [7] X.-M. Wang, X.-D. Zhou, and T. Hesketh, “Massive misuse of antibiotics by university students in China: a cross-sectional survey,” *The Lancet*, vol. 388, p. S94, Oct. 2016, doi: 10.1016/S0140-6736(16)32021-9.

- [8] “Perspectives Misuse of Antibiotics by Physicians in Clinical Practice.”
- [9] C. J. Murray *et al.*, “Global burden of bacterial antimicrobial resistance in 2019: a systematic analysis,” *The Lancet*, vol. 399, no. 10325, pp. 629–655, Feb. 2022, doi: 10.1016/S0140-6736(21)02724-0.
- [10] V. D. Litskas, · X N Karamanlis, · S P Prousalis, and · D S Koveos, “Effects of the Antibiotic Amoxicillin on Key Species of the Terrestrial Environment,” vol. 100, pp. 509–515, 2018, doi: 10.1007/s00128-018-2302-z.
- [11] M. Kolář, K. Urbánek, and T. Látal, “Antibiotic selective pressure and development of bacterial resistance,” *International Journal of Antimicrobial Agents*, vol. 17, no. 5, pp. 357–363, May 2001, doi: 10.1016/S0924-8579(01)00317-X.
- [12] M. de Kraker, A. J. Stewardson, and S. Harbarth, “Will 10 Million People Die a Year due to Antimicrobial Resistance by 2050?,” *PLoS Med*, vol. 13, no. 11, p. 1002184, 2016, doi: 10.1371/journal.pmed.1002184.
- [13] A. Cassini *et al.*, “Attributable deaths and disability-adjusted life-years caused by infections with antibiotic-resistant bacteria in the EU and the European Economic Area in 2015: a population-level modelling analysis,” *The Lancet Infectious Diseases*, vol. 19, no. 1, pp. 56–66, Jan. 2019, doi: 10.1016/S1473-3099(18)30605-4.
- [14] C. L. Ventola, “The Antibiotic Resistance Crisis: Part 1: Causes and Threats,” *Pharmacy and Therapeutics*, vol. 40, no. 4, p. 277, 2015, Accessed: Sep. 20, 2020. [Online]. Available: <https://www.ncbi.nlm.nih.gov/pmc/articles/PMC4378521/>
- [15] A. Misurski, D Lipson, D Changolkar, “Inappropriate antibiotic prescribing in managed care subjects with influenza,” *The American Journal of Managed Care*, vol. 17, no. 9, pp. 601–608, 2011.
- [16] T. M. Rawson *et al.*, “COVID-19 and the potential long-term impact on antimicrobial resistance,” *Journal of Antimicrobial Chemotherapy*, vol. 75, no. 7, pp. 1681–1684, Jul. 2020, doi: 10.1093/jac/dkaa194.

- [17] F. Zhou *et al.*, “Clinical course and risk factors for mortality of adult inpatients with COVID-19 in Wuhan, China: a retrospective cohort study,” *The Lancet*, vol. 395, no. 10229, pp. 1054–1062, Mar. 2020, doi: 10.1016/S0140-6736(20)30566-3.
- [18] M. P. Stevens, P. K. Patel, and P. Nori, “Involving antimicrobial stewardship programs in COVID-19 response efforts: All hands on deck,” *Infection Control & Hospital Epidemiology*, vol. 41, no. 6, pp. 744–745, Jun. 2020, doi: 10.1017/ice.2020.69.
- [19] S. K. Behera, H. W. Kim, J. E. Oh, and H. S. Park, “Occurrence and removal of antibiotics, hormones and several other pharmaceuticals in wastewater treatment plants of the largest industrial city of Korea,” *Science of the Total Environment*, vol. 409, no. 20, pp. 4351–4360, Sep. 2011, doi: 10.1016/j.scitotenv.2011.07.015.
- [20] P. Paíga and C. Delerue-Matos, “Anthropogenic contamination of Portuguese coastal waters during the bathing season: Assessment using caffeine as a chemical marker,” *Marine Pollution Bulletin*, vol. 120, no. 1, pp. 355–363, 2017, doi: <https://doi.org/10.1016/j.marpolbul.2017.05.030>.
- [21] N. Watanabe, T. H. Harter, and B. A. Bergamaschi, “Environmental Occurrence and Shallow Ground Water Detection of the Antibiotic Monensin from Dairy Farms,” *Journal of Environmental Quality*, vol. 37, no. S5, p. S-78-S-85, Sep. 2008, doi: 10.2134/jeq2007.0371.
- [22] R. P. Tasho and J. Y. Cho, “Veterinary antibiotics in animal waste, its distribution in soil and uptake by plants: A review,” *Science of The Total Environment*, vol. 563–564, pp. 366–376, 2016, doi: <https://doi.org/10.1016/j.scitotenv.2016.04.140>.
- [23] H. Willer, M. Yussefi-Menzler, and N. Sorensen, *THE WORLD OF ORGANIC AGRICULTURE STATISTICS AND EMERGING TRENDS 2008*. Frick, Switzerland, 2011.
- [24] A. J. Watkinson, E. J. Murby, D. W. Kolpin, and S. D. Costanzo, “The occurrence of antibiotics in an urban watershed: From wastewater to drinking water,” *Science of the Total Environment, The*, vol. 407, pp. 2711–2723, 2009, doi: 10.1016/j.scitotenv.2008.11.059.

- [25] T. Lin, Y. Q. Chen, and W. Chen, "Impact of toxicological properties of sulfonamides on the growth of zebrafish embryos in the water," *Environmental Toxicology and Pharmacology*, vol. 36, no. 3, pp. 1068–1076, Nov. 2013, doi: 10.1016/J.ETAP.2013.09.009.
- [26] S. Rodriguez-Mozaz *et al.*, "Occurrence of antibiotics and antibiotic resistance genes in hospital and urban wastewaters and their impact on the receiving river," 2014, doi: 10.1016/j.watres.2014.11.021.
- [27] P. Carsten Von Der Ohe *et al.*, "A new risk assessment approach for the prioritization of 500 classical and emerging organic microcontaminants as potential river basin specific pollutants under the European Water Framework Directive," 2011, doi: 10.1016/j.scitotenv.2011.01.054.
- [28] I. T. Carvalho and L. Santos, "Antibiotics in the aquatic environments: A review of the European scenario," *Environment International*, vol. 94, pp. 736–757, 2016, doi: 10.1016/j.envint.2016.06.025.
- [29] S. Ranallo, A. Rossetti, K. W. Plaxco, A. Valløe-Bøllis, and F. Ricci, "A Modular, DNA-Based Beacon for Single-Step Fluorescence Detection of Antibodies and Other Proteins", doi: 10.1002/anie.201505179.
- [30] A. Verdian, E. Fooladi, and Z. Rouhbakhsh, "Recent progress in the development of recognition bioelements for polychlorinated biphenyls detection: Antibodies and aptamers," *Talanta*, vol. 202, pp. 123–135, Sep. 2019, doi: 10.1016/J.TALANTA.2019.04.059.
- [31] D. E. Koshland, "The Key-Lock Theory and the Induced Fit Theory".
- [32] N. Mungroo and S. Neethirajan, "Biosensors for the Detection of Antibiotics in Poultry Industry—A Review," *Biosensors (Basel)*, vol. 4, no. 4, pp. 472–493, Nov. 2014, doi: 10.3390/bios4040472.
- [33] D. Debayle, G. Dessalces, and M. Florence Grenier-Loustalot, "Multi-residue analysis of traces of pesticides and antibiotics in honey by HPLC-MS-MS", doi: 10.1007/s00216-008-2003-2.

- [34] P. Nag, K. Sadani, S. Mukherji, and S. Mukherji, "Beta-lactam antibiotics induced bacteriolysis on LSPR sensors for assessment of antimicrobial resistance and quantification of antibiotics," *Sensors and Actuators B: Chemical*, vol. 311, p. 127945, May 2020, doi: 10.1016/J.SNB.2020.127945.
- [35] A. A. Weaver *et al.*, "Paper Analytical Devices for Fast Field Screening of Beta Lactam Antibiotics and Antituberculosis Pharmaceuticals," 2013, doi: 10.1021/ac400989p.
- [36] H. I. A. S. Gomes and M. G. F. Sales, "Development of paper-based color test-strip for drug detection in aquatic environment: Application to oxytetracycline," *Biosensors and Bioelectronics*, vol. 65, pp. 54–61, Mar. 2015, doi: 10.1016/J.BIOS.2014.10.006.
- [37] M. Khaskheli, R. S. Malik, M. A. Arain, A. H. Soomro, and H. H. Arain, "Detection of β -Lactam Antibiotic Residues in Market Milk," *Pakistan Journal of Nutrition*, vol. 7, no. 5, pp. 682–685, 2008.
- [38] B. G. Knecht, A. Strasser, R. Dietrich, E. Ma, R. Niessner, and M. G. Weller, "Automated Microarray System for the Simultaneous Detection of Antibiotics in Milk," *Analytical Chemistry*, vol. 76, no. 3, pp. 646–654, 2004, doi: 10.1021/ac035028i.
- [39] H. Wang *et al.*, "Antibiotic residues in meat, milk and aquatic products in Shanghai and human exposure assessment," vol. 80, pp. 217–225, 2017, doi: 10.1016/j.foodcont.2017.04.034.
- [40] M. G. Pikkemaat, "Microbial screening methods for detection of antibiotic residues in slaughter animals," *Analytical and Bioanalytical Chemistry*, vol. 395, no. 4, pp. 893–905, Oct. 2009, doi: 10.1007/s00216-009-2841-6.
- [41] F. Baquero, J.-L. Martínez, and R. Cantón, "Antibiotics and antibiotic resistance in water environments," *Current Opinion in Biotechnology*, vol. 19, no. 3, pp. 260–265, Jun. 2008, doi: 10.1016/j.copbio.2008.05.006.
- [42] A. J. Smith, J. L. Balaam, and A. Ward, "The development of a rapid screening technique to measure antibiotic activity in effluents and surface water samples," *Marine Pollution Bulletin*, vol. 54, no. 12, pp. 1940–1946, Dec. 2007, doi: 10.1016/j.marpolbul.2007.08.019.

- [43] D. Bitas and V. Samanidou, "Molecularly imprinted polymers as extracting media for the chromatographic determination of antibiotics in milk," *Molecules*, vol. 23, no. 2. MDPI AG, 2018. doi: 10.3390/molecules23020316.
- [44] F. Horemans *et al.*, "MIP-based sensor platforms for the detection of histamine in the nano- and micromolar range in aqueous media," *Sensors and Actuators B: Chemical*, vol. 148, no. 2, pp. 392–398, 2010, doi: <https://doi.org/10.1016/j.snb.2010.05.003>.
- [45] B. Tse Sum Bui and K. Haupt, "Molecularly imprinted polymers: synthetic receptors in bioanalysis," *Analytical and Bioanalytical Chemistry*, vol. 398, no. 6, pp. 2481–2492, Nov. 2010, doi: 10.1007/s00216-010-4158-x.
- [46] P. A. G. Cormack and A. Z. Elorza, "Molecularly imprinted polymers: synthesis and characterisation," *Journal of Chromatography B*, vol. 804, no. 1, pp. 173–182, May 2004, doi: 10.1016/j.jchromb.2004.02.013.
- [47] A. G. Mayes and K. Mosbach, "Molecularly imprinted polymers: Useful materials for analytical chemistry?," *TrAC - Trends in Analytical Chemistry*, vol. 16, no. 6, pp. 321–332, Jun. 1997, doi: 10.1016/S0165-9936(97)00037-X.
- [48] L. Ye and K. Haupt, "Molecularly imprinted polymers as antibody and receptor mimics for assays, sensors and drug discovery," *Analytical and Bioanalytical Chemistry*, vol. 378, no. 8, pp. 1887–1897, Apr. 2004, doi: 10.1007/s00216-003-2450-8.
- [49] A. Bossi, F. Bonini, A. P. F. Turner, and S. A. Piletsky, "Molecularly imprinted polymers for the recognition of proteins: The state of the art," *Biosensors and Bioelectronics*, vol. 22, no. 6, pp. 1131–1137, Jan. 2007, doi: 10.1016/j.bios.2006.06.023.
- [50] D. M. Hawkins, D. Stevenson, and S. M. Reddy, "Investigation of protein imprinting in hydrogel-based molecularly imprinted polymers (HydroMIPs)," *Analytica Chimica Acta*, vol. 542, no. 1, pp. 61–65, Jun. 2005, doi: 10.1016/j.aca.2005.01.052.
- [51] J. U. Klein, M. J. Whitcombe, F. Mulholland, and E. N. Vulfson, "Template-mediated synthesis of a polymeric receptor specific to amino acid sequences," *Angewandte Chemie -*

International Edition, vol. 38, no. 13–14, pp. 2057–2060, Jul. 1999, doi: 10.1002/(sici)1521-3773(19990712)38:13/14<2057::aid-anie2057>3.0.co;2-g.

[52] S. Wei and B. Mizaikoff, “Recent advances on noncovalent molecular imprints for affinity separations,” *Journal of Separation Science*, vol. 30, no. 11, pp. 1794–1805, Jul. 2007, doi: 10.1002/jssc.200700166.

[53] W.-C. Lee, C.-H. Cheng, H.-H. Pan, T.-H. Chung, and C.-C. Hwang, “Chromatographic characterization of molecularly imprinted polymers,” *Analytical and Bioanalytical Chemistry*, vol. 390, no. 4, pp. 1101–1109, 2008, doi: 10.1007/s00216-007-1765-2.

[54] E. Turiel and A. Martin-Esteban, “Molecular imprinting technology in capillary electrochromatography,” *Journal of Separation Science*, vol. 28, no. 8, pp. 719–728, May 2005, doi: 10.1002/jssc.200400076.

[55] M. Kempe and K. Mosbach, “Separation of amino acids, peptides and proteins on molecularly imprinted stationary phases,” *Journal of Chromatography A*, vol. 691, no. 1, pp. 317–323, 1995, doi: [https://doi.org/10.1016/0021-9673\(94\)00820-Y](https://doi.org/10.1016/0021-9673(94)00820-Y).

[56] V. Remcho and Z. Tan, “MIPs As Chromatographic Stationary,” Oregon, 1999.

[57] U. Curti, R. Colombo, “Active sites in stereoselective adsorbents as models of drug receptors and enzyme active sites.,” *Chemistry and Industry*, vol. 23, p. 103, 1951.

[58] A. Tiwari and U. Lokman, *Advanced Molecularly Imprinting Materials*. John Wiley & Sons, Inc., 2016. [Online]. Available: <https://blackwells.co.uk/bookshop/product/Advanced-Molecularly-Imprinting-Materials-by-Ashutosh-Tiwari-editor-Lokman-Uzun-editor/9781119336297>

[59] C. C. Villa, L. T. Sánchez, G. A. Valencia, S. Ahmed, and T. J. Gutiérrez, “Molecularly imprinted polymers for food applications: A review,” *Trends in Food Science & Technology*, vol. 111, pp. 642–669, May 2021, doi: 10.1016/J.TIFS.2021.03.003.

- [60] R. Arshady and K. Mosbach, "Synthesis of substrate-selective polymers by host-guest polymerization," *Die Makromolekulare Chemie*, vol. 182, no. 2, pp. 687–692, Jan. 1981, doi: 10.1002/macp.1981.021820240.
- [61] C. Alexander *et al.*, "Molecular imprinting science and technology: a survey of the literature for the years up to and including 2003," *Journal of Molecular Recognition*, vol. 19, no. 2, pp. 106–180, Mar. 2006, doi: 10.1002/jmr.760.
- [62] J. Haginaka, "Monodispersed, molecularly imprinted polymers as affinity-based chromatography media," *Journal of Chromatography B*, vol. 866, no. 1, pp. 3–13, 2008, doi: <https://doi.org/10.1016/j.jchromb.2007.07.019>.
- [63] J. Yin, G. Yang, and Y. Chen, "Rapid and efficient chiral separation of nateglinide and its l-enantiomer on monolithic molecularly imprinted polymers," *Journal of Chromatography A*, vol. 1090, no. 1, pp. 68–75, 2005, doi: <https://doi.org/10.1016/j.chroma.2005.06.078>.
- [64] J. Matsui *et al.*, "Molecular Recognition in Continuous Polymer Rods Prepared by a Molecular Imprinting Technique," *Analytical Chemistry*, vol. 65, pp. 2223–2224, 1993.
- [65] B. Sellergren, "Imprinted chiral stationary phases in high-performance liquid chromatography," *Journal of Chromatography A*, vol. 906, no. 1, pp. 227–252, 2001, doi: [https://doi.org/10.1016/S0021-9673\(00\)00929-8](https://doi.org/10.1016/S0021-9673(00)00929-8).
- [66] M. Monier and A. M. A. El-Sokkary, "Preparation of molecularly imprinted cross-linked chitosan/glutaraldehyde resin for enantioselective separation of l-glutamic acid," *International Journal of Biological Macromolecules*, vol. 47, no. 2, pp. 207–213, 2010, doi: <https://doi.org/10.1016/j.ijbiomac.2010.04.020>.
- [67] Z. J. Tan and V. T. Remcho, "Molecular imprint polymers as highly selective stationary phases for open tubular liquid chromatography and capillary electrochromatography," *ELECTROPHORESIS*, vol. 19, no. 12, pp. 2055–2060, Sep. 1998, doi: 10.1002/elps.1150191203.

- [68] M. Kempe and K. Mosbach, "Direct resolution of naproxen on a non-covalently molecularly imprinted chiral stationary phase," *Journal of Chromatography A*, vol. 664, no. 2, pp. 276–279, 1994, doi: [https://doi.org/10.1016/0021-9673\(94\)87016-0](https://doi.org/10.1016/0021-9673(94)87016-0).
- [69] R. J. Ansell, "Molecularly imprinted polymers for the enantioseparation of chiral drugs," *Advanced Drug Delivery Reviews*, vol. 57, no. 12, pp. 1809–1835, 2005, doi: <https://doi.org/10.1016/j.addr.2005.07.014>.
- [70] C. He, Y. Long, J. Pan, K. Li, and F. Liu, "Application of molecularly imprinted polymers to solid-phase extraction of analytes from real samples," *Journal of Biochemical and Biophysical Methods*, vol. 70, no. 2, pp. 133–150, 2007, doi: <https://doi.org/10.1016/j.jbbm.2006.07.005>.
- [71] F. G. Tamayo, E. Turiel, and A. Martín-Esteban, "Molecularly imprinted polymers for solid-phase extraction and solid-phase microextraction: Recent developments and future trends," *Journal of Chromatography A*, vol. 1152, no. 1, pp. 32–40, 2007, doi: <https://doi.org/10.1016/j.chroma.2006.08.095>.
- [72] M. Lasáková and P. Jandera, "Molecularly imprinted polymers and their application in solid phase extraction," *Journal of Separation Science*, vol. 32, no. 5-6, pp. 799–812, Mar. 2009, doi: [10.1002/jssc.200800506](https://doi.org/10.1002/jssc.200800506).
- [73] V. Pichon, "Selective sample treatment using molecularly imprinted polymers," *Journal of Chromatography A*, vol. 1152, no. 1, pp. 41–53, 2007, doi: <https://doi.org/10.1016/j.chroma.2007.02.109>.
- [74] E. Caro, R. M. Marcé, F. Borrull, P. A. G. Cormack, and D. C. Sherrington, "Application of molecularly imprinted polymers to solid-phase extraction of compounds from environmental and biological samples," *TrAC Trends in Analytical Chemistry*, vol. 25, no. 2, pp. 143–154, 2006, doi: <https://doi.org/10.1016/j.trac.2005.05.008>.

- [75] E. Turiel and A. Martín-Esteban, “Molecularly imprinted polymers for sample preparation: A review,” *Analytica Chimica Acta*, vol. 668, no. 2, pp. 87–99, 2010, doi: <https://doi.org/10.1016/j.aca.2010.04.019>.
- [76] M. Baker, “Antibody anarchy: A call to order,” *Nature*, vol. 527, no. 7579, pp. 545–551, 2015, doi: 10.1038/527545a.
- [77] W. Kusnezow and J. D. Hoheisel, “Antibody Microarrays: Promises and Problems,” *Biotechniques*, vol. 33, no. 6S, pp. S14–S23, Dec. 2002, doi: 10.2144/dec02kusnezow.
- [78] S. Nestora *et al.*, “Plastic Antibodies for Cosmetics: Molecularly Imprinted Polymers Scavenge Precursors of Malodors,” *Angewandte Chemie.*, vol. 128, no. 21. Weinheim , pp. 6360–6364, 2016. doi: 10.1002/ange.201602076.
- [79] B. B. Prasad, A. Srivastava, and M. P. Tiwari, “Highly selective and sensitive analysis of dopamine by molecularly imprinted stir bar sorptive extraction technique coupled with complementary molecularly imprinted polymer sensor,” *Journal of Colloid and Interface Science*, vol. 396, pp. 234–241, 2013, doi: <https://doi.org/10.1016/j.jcis.2012.12.073>.
- [80] W. Wan, M. Biyikal, R. Wagner, B. Sellergren, and K. Rurack, “Fluorescent Sensory Microparticles that ‘Light-up’ Consisting of a Silica Core and a Molecularly Imprinted Polymer (MIP) Shell,” *Angewandte Chemie International Edition*, vol. 52, no. 27, pp. 7023–7027, Jul. 2013, doi: 10.1002/anie.201300322.
- [81] G. Guan, R. Liu, Q. Mei, and Z. Zhang, “Molecularly Imprinted Shells from Polymer and Xerogel Matrices on Polystyrene Colloidal Spheres,” *Chemistry – A European Journal*, vol. 18, no. 15, pp. 4692–4698, Apr. 2012, doi: 10.1002/chem.201102576.
- [82] F. Lu *et al.*, “Flow injection chemiluminescence sensor based on core–shell magnetic molecularly imprinted nanoparticles for determination of sulfadiazine,” *Analytica Chimica Acta*, vol. 718, pp. 84–91, 2012, doi: <https://doi.org/10.1016/j.aca.2011.12.054>.
- [83] M.-C. Savoy, P. M. Woo, P. Ulrich, A. Tarres, P. Mottier, and A. Desmarchelier, “Determination of 14 aminoglycosides by LC-MS/MS using molecularly imprinted polymer

solid phase extraction for clean-up,” *Food Additives & Contaminants: Part A*, vol. 35, no. 4, pp. 675–686, Apr. 2018, doi: 10.1080/19440049.2018.1433332.

[84] N. W. Turner, C. W. Jeans, K. R. Brain, C. J. Allender, V. Hlady, and D. W. Britt, “From 3D to 2D: A Review of the Molecular Imprinting of Proteins,” *Biotechnology Progress*, vol. 22, no. 6, pp. 1474–1489, Jan. 2006, doi: 10.1021/bp060122g.

[85] R. Li, Y. Feng, G. Pan, and L. Liu, “Advances in Molecularly Imprinting Technology for Bioanalytical Applications,” *Sensors*, vol. 19, no. 1. 2019. doi: 10.3390/s19010177.

[86] L. Chen, X. Wang, W. Lu, X. Wu, and J. Li, “Molecular imprinting: perspectives and applications,” *Chemical Society Reviews*, vol. 45, no. 8, pp. 2137–2211, Apr. 2016, doi: 10.1039/C6CS00061D.

[87] D. SPIVAK, “Optimization, evaluation, and characterization of molecularly imprinted polymers,” *Advanced Drug Delivery Reviews*, vol. 57, no. 12, pp. 1779–1794, Dec. 2005, doi: 10.1016/j.addr.2005.07.012.

[88] D. S. Janiak and P. Kofinas, “Molecular imprinting of peptides and proteins in aqueous media,” *Analytical and Bioanalytical Chemistry*, vol. 389, no. 2, pp. 399–404, Aug. 2007, doi: 10.1007/s00216-007-1327-7.

[89] B. Schweiger, J. Kim, Y. J. Kim, and M. Ulbricht, “Electropolymerized Molecularly Imprinted Polypyrrole Film for Sensing of Clofibric Acid,” *Sensors*, vol. 15, pp. 4870–4889, 2015, doi: 10.3390/s150304870.

[90] L. I. Andersson, “Molecular imprinting for drug bioanalysis: A review on the application of imprinted polymers to solid-phase extraction and binding assay,” *Journal of Chromatography B: Biomedical Sciences and Applications*, vol. 739, no. 1, pp. 163–173, 2000, doi: [https://doi.org/10.1016/S0378-4347\(99\)00432-6](https://doi.org/10.1016/S0378-4347(99)00432-6).

[91] K. Smolinska-Kempisty, A. Guerreiro, F. Canfarotta, C. Cáceres, M. J. Whitcombe, and S. Piletsky, “A comparison of the performance of molecularly imprinted polymer nanoparticles

for small molecule targets and antibodies in the ELISA format,” *Scientific Reports*, vol. 6, no. 1, p. 37638, 2016, doi: 10.1038/srep37638.

[92] S. A. Piletsky, E. v Piletska, A. Bossi, K. Karim, P. Lowe, and A. P. F. Turner, “Substitution of antibodies and receptors with molecularly imprinted polymers in enzyme-linked and fluorescent assays,” *Biosensors and Bioelectronics*, vol. 16, no. 9, pp. 701–707, 2001, doi: [https://doi.org/10.1016/S0956-5663\(01\)00234-2](https://doi.org/10.1016/S0956-5663(01)00234-2).

[93] X. Hu, Y. Hu, and G. Li, “Development of novel molecularly imprinted solid-phase microextraction fiber and its application for the determination of triazines in complicated samples coupled with high-performance liquid chromatography,” *Journal of Chromatography A*, vol. 1147, no. 1, pp. 1–9, Apr. 2007, doi: 10.1016/j.chroma.2007.02.037.

[94] A. N. Baeza, J. L. Urraca, R. Chamorro, G. Orellana, M. Castellari, and M. C. Moreno-Bondi, “Multiresidue analysis of cephalosporin antibiotics in bovine milk based on molecularly imprinted polymer extraction followed by liquid chromatography-tandem mass spectrometry,” *Journal of Chromatography A*, vol. 1474, pp. 121–129, 2016, doi: <https://doi.org/10.1016/j.chroma.2016.10.069>.

[95] E. Yilmaz, O. Ramström, P. Möller, D. Sanchez, and K. Mosbach, “A facile method for preparing molecularly imprinted polymer spheres using spherical silica templates,” *Journal of Materials Chemistry*, vol. 12, no. 5, pp. 1577–1581, Apr. 2002, doi: 10.1039/b109262f.

[96] G. Vlatakis, L. Andersson, R. Muller, and K. Mosbach, “Drug assay using antibody mimics made by molecular imprinting,” *Nature*, vol. 361, pp. 645–647, 1993.

[97] U. Athikomrattanakul, N. Gajovic-Eichelmann, and F. W. Scheller, “Thermometric Sensing of Nitrofurantoin by Noncovalently Imprinted Polymers Containing Two Complementary Functional Monomers,” *Analytical Chemistry*, vol. 83, no. 20, pp. 7704–7711, Oct. 2011, doi: 10.1021/ac201099h.

- [98] M. Haruki, Y. Konnai, A. Shimada, and H. Takeuchi, "Molecularly Imprinted Polymer-Assisted Refolding of Lysozyme," *Biotechnology Progress*, vol. 0, no. 0, pp. 0–0, Aug. 2007, doi: 10.1021/bp070130c.
- [99] N. T. Hoai, D.-K. Yoo, and D. Kim, "Batch and column separation characteristics of copper-imprinted porous polymer micro-beads synthesized by a direct imprinting method," *Journal of Hazardous Materials*, vol. 173, no. 1–3, pp. 462–467, Jan. 2010, doi: 10.1016/j.jhazmat.2009.08.107.
- [100] X. Chen *et al.*, "Novel molecularly imprinted polymers based on multiwalled carbon nanotubes with bifunctional monomers for solid-phase extraction of rhein from the root of kiwi fruit," *Journal of Separation Science*, vol. 35, no. 18, pp. 2414–2421, Sep. 2012, doi: 10.1002/jssc.201101000.
- [101] X. Cai, J. Li, Z. Zhang, F. Yang, R. Dong, and L. Chen, "Novel Pb²⁺ Ion Imprinted Polymers Based on Ionic Interaction via Synergy of Dual Functional Monomers for Selective Solid-Phase Extraction of Pb²⁺ in Water Samples," *ACS Applied Materials & Interfaces*, vol. 6, no. 1, pp. 305–313, Jan. 2014, doi: 10.1021/am4042405.
- [102] L. Guo *et al.*, "Preparation of dual-dummy-template molecularly imprinted polymers coated magnetic graphene oxide for separation and enrichment of phthalate esters in water," *Chemical Engineering Journal*, vol. 361, pp. 245–255, 2019, doi: <https://doi.org/10.1016/j.cej.2018.12.076>.
- [103] Y. Liu *et al.*, "Dummy-template molecularly imprinted micro-solid-phase extraction coupled with high-performance liquid chromatography for bisphenol A determination in environmental water samples," *Microchemical Journal*, vol. 145, pp. 337–344, 2019, doi: <https://doi.org/10.1016/j.microc.2018.10.054>.
- [104] A. Rachkov and N. Minoura, "Recognition of oxytocin and oxytocin-related peptides in aqueous media using a molecularly imprinted polymer synthesized by the epitope approach,"

Journal of Chromatography A, vol. 889, no. 1, pp. 111–118, 2000, doi:

[https://doi.org/10.1016/S0021-9673\(00\)00568-9](https://doi.org/10.1016/S0021-9673(00)00568-9).

[105] A. Rachkov and N. Minoura, “Towards molecularly imprinted polymers selective to peptides and proteins. The epitope approach,” *Biochimica et Biophysica Acta (BBA) - Protein Structure and Molecular Enzymology*, vol. 1544, no. 1, pp. 255–266, 2001, doi:

[https://doi.org/10.1016/S0167-4838\(00\)00226-0](https://doi.org/10.1016/S0167-4838(00)00226-0).

[106] M. J. Abdin, Z. Altintas, and I. E. Tothill, “In silico designed nanoMIP based optical sensor for endotoxins monitoring,” *Biosensors and Bioelectronics*, vol. 67, pp. 177–183, 2015, doi: <https://doi.org/10.1016/j.bios.2014.08.009>.

[107] Z. Altintas, B. France, J. O. Ortiz, and I. E. Tothill, “Computationally modelled receptors for drug monitoring using an optical based biomimetic SPR sensor,” *Sensors and Actuators B: Chemical*, vol. 224, pp. 726–737, 2016, doi:

<https://doi.org/10.1016/j.snb.2015.10.075>.

[108] Y. Lv, T. Tan, and F. Svec, “Molecular imprinting of proteins in polymers attached to the surface of nanomaterials for selective recognition of biomacromolecules,” *Biotechnology Advances*, vol. 31, no. 8, pp. 1172–1186, 2013, doi:

<https://doi.org/10.1016/j.biotechadv.2013.02.005>.

[109] L. I. Andersson, A. Paprica, and T. Arvidsson, “A highly selective solid phase extraction sorbent for pre-concentration of sameridine made by molecular imprinting,” *Chromatographia*, vol. 46, no. 1, pp. 57–62, 1997, doi: 10.1007/BF02490930.

[110] K. Karim, T. Cowen, A. Guerreiro, E. Piletska, M. J. Whitcombe, and S. A. Piletsky, “A Protocol for the Computational Design of High Affinity Molecularly Imprinted Polymer Synthetic Receptors,” *Global Journal of Biotechnology and Biomaterial Science*, 2017, [Online]. Available:

https://leicester.figshare.com/articles/journal_contribution/A_Protocol_for_the_Computational_Design_of_High_Affinity_Molecularly_Imprinted_Polymer_Synthetic_Receptors/10199942

- [111] I. A. Nicholls *et al.*, “Theoretical and computational strategies for rational molecularly imprinted polymer design,” *Biosensors and Bioelectronics*, vol. 25, no. 3, pp. 543–552, 2009, doi: <https://doi.org/10.1016/j.bios.2009.03.038>.
- [112] E. B. B. Castro, G. Ramirez, M. F. Rubio, M. J. Whitcombe, E. N. Vulfson, R. Vazquez-Duhalt, “No Title,” *American Institute of Chemical Engineers Journal*, pp. 329–336, 1998.
- [113] S. A. Piletsky *et al.*, “Recognition of ephedrine enantiomers by molecularly imprinted polymers designed using a computational approach,” *Analyst*, vol. 126, no. 10, pp. 1826–1830, Oct. 2001, doi: 10.1039/b102426b.
- [114] L. Zhang, L. Chen, H. Zhang, Y. Yang, and X. Liu, “Recognition of 5-fluorouracil by thermosensitive magnetic surface molecularly imprinted microspheres designed using a computational approach,” *Journal of Applied Polymer Science*, vol. 134, no. 43, p. 45468, Nov. 2017, doi: 10.1002/app.45468.
- [115] Y. Kong *et al.*, “Molecular dynamics simulations of molecularly imprinted polymer approaches to the preparation of selective materials to remove norfloxacin,” *Journal of Applied Polymer Science*, vol. 133, no. 1, Jan. 2016, doi: 10.1002/app.42817.
- [116] B. Gao, X.-P. He, Y. Jiang, J.-T. Wei, H. Suo, and C. Zhao, “Computational simulation and preparation of fluorescent magnetic molecularly imprinted silica nanospheres for ciprofloxacin or norfloxacin sensing,” *Journal of Separation Science*, vol. 37, no. 24, pp. 3753–3759, Dec. 2014, doi: 10.1002/jssc.201401014.
- [117] L. D. Marestoni *et al.*, “Semi-Empirical Quantum Chemistry Method for Pre-Polymerization Rational Design of Ciprofloxacin Imprinted Polymer and Adsorption Studies,” *J Braz Chem Soc*, vol. 27, no. 1, pp. 109–118, 2015, doi: 10.5935/0103-5053.20150256.
- [118] Z. Dai, J. Liu, S. Tang, Y. Wang, Y. Wang, and R. Jin, “Optimization of enrofloxacin-imprinted polymers by computer-aided design,” *Journal of Molecular Modeling*, vol. 21, no. 11, p. 290, 2015, doi: 10.1007/s00894-015-2836-5.

- [119] S. J. Pace, E. Nguyen, M. P. Baria, and E.-R. E. Mojica, "Use of computational modeling in preparation and evaluation of surface imprinted xerogels for binding tetracycline," *Microchimica Acta*, vol. 182, no. 1, pp. 69–76, 2015, doi: 10.1007/s00604-014-1305-7.
- [120] Boerje. Sellergren, Matti. Lepistöe, and Klaus. Mosbach, "Highly enantioselective and substrate-selective polymers obtained by molecular imprinting utilizing noncovalent interactions. NMR and chromatographic studies on the nature of recognition," *J Am Chem Soc*, vol. 110, no. 17, pp. 5853–5860, Aug. 1988, doi: 10.1021/ja00225a041.
- [121] L. Wang, W. Fu, Y. Shen, H. Tan, and H. Xu, "Molecularly Imprinted Polymers for Selective Extraction of Oblongifolin C from *Garcinia yunnanensis* Hu," *Molecules*, vol. 22, no. 4. 2017. doi: 10.3390/molecules22040508.
- [122] P. Mattos dos Santos, A. J. Hall, and P. Manesiotis, "Stoichiometric molecularly imprinted polymers for the recognition of anti-cancer pro-drug tegafur," *Journal of Chromatography B*, vol. 1021, pp. 197–203, 2016, doi: <https://doi.org/10.1016/j.jchromb.2015.12.015>.
- [123] L. Fielding, "Determination of Association Constants (K_a) from Solution NMR Data," *Tetrahedron*, vol. 56, no. 34, pp. 6151–6170, 2000, doi: [https://doi.org/10.1016/S0040-4020\(00\)00492-0](https://doi.org/10.1016/S0040-4020(00)00492-0).
- [124] J. O'Mahony, A. Molinelli, K. Nolan, M. R. Smyth, and B. Mizaikoff, "Towards the rational development of molecularly imprinted polymers: ^1H NMR studies on hydrophobicity and ion-pair interactions as driving forces for selectivity," *Biosensors and Bioelectronics*, vol. 20, no. 9, pp. 1884–1893, Mar. 2005, doi: 10.1016/J.BIOS.2004.07.036.
- [125] J. Sánchez-González, Á. Peña-Gallego, J. Sanmartín, A. M. Bermejo, P. Bermejo-Barrera, and A. Moreda-Piñeiro, "NMR spectroscopy for assessing cocaine-functional monomer interactions when preparing molecularly imprinted polymers," *Microchemical Journal*, vol. 147, pp. 813–817, 2019, doi: <https://doi.org/10.1016/j.microc.2019.03.088>.

- [126] S. Akatani, R. Takemoto, T. Kitade, A. Konishi, and S. Takegami, "Potentiometric and ¹H NMR Spectroscopic Studies of Functional Monomer Influence on Histamine-Imprinted Polymer-Modified Potentiometric Sensor Performance," *Journal of Analytical & Bioanalytical Techniques*, vol. 08, no. 05, pp. 1–8, Oct. 2017, doi: 10.4172/2155-9872.1000378.
- [127] H. S. Andersson and I. A. Nicholls, "Spectroscopic Evaluation of Molecular Imprinting Polymerization Systems," *Bioorganic Chemistry*, vol. 25, no. 3, pp. 203–211, 1997, doi: <https://doi.org/10.1006/bioo.1997.1067>.
- [128] Y. Zhang *et al.*, "¹³C NMR aided design of molecularly imprinted adsorbents for selectively preparative separation of erythromycin," *J. Mater. Chem. B*, vol. 2, no. 10, pp. 1390–1399, Feb. 2014, doi: 10.1039/C3TB21636E.
- [129] K. M. Annamma and B. Mathew, "Design of 2,4-Dichlorophenoxyacetic Acid Imprinted Polymer with High Specificity and Selectivity," *Materials Sciences and Applications*, vol. 2, pp. 131–140, 2011.
- [130] V. K. Srivastava and R. Yadav, "Chapter 9 - Isothermal titration calorimetry," G. B. T.-D. P. H. for C. B. D. S. Misra, Ed. Academic Press, 2019, pp. 125–137. doi: <https://doi.org/10.1016/B978-0-12-816548-5.00009-5>.
- [131] M. W. Freyer and E. A. B. T.-M. in C. B. Lewis, "Isothermal Titration Calorimetry: Experimental Design, Data Analysis, and Probing Macromolecule/Ligand Binding and Kinetic Interactions," in *Biophysical Tools for Biologists, Volume One: In Vitro Techniques*, vol. 84, Academic Press, 2008, pp. 79–113. doi: [https://doi.org/10.1016/S0091-679X\(07\)84004-0](https://doi.org/10.1016/S0091-679X(07)84004-0).
- [132] S. Wei, M. Jakusch, and B. Mizaikoff, "Capturing molecules with templated materials—Analysis and rational design of molecularly imprinted polymers," *Analytica Chimica Acta*, vol. 578, no. 1, pp. 50–58, 2006, doi: <https://doi.org/10.1016/j.aca.2006.06.077>.
- [133] J. K. Awino and Y. Zhao, "Molecularly imprinted nanoparticles as tailor-made sensors for small fluorescent molecules," *Chemical Communications*, vol. 50, no. 43, p. 5752, May 2014, doi: 10.1039/c4cc01516a.

- [134] S. Striegler, "Discrimination of epimeric disaccharides by templated polymers," *Analytica Chimica Acta*, vol. 539, no. 1, pp. 91–95, 2005, doi: <https://doi.org/10.1016/j.aca.2005.03.014>.
- [135] W. P. Fish, J. Ferreira, R. D. Sheardy, N. H. Snow, and T. P. O'Brien, "Rational Design of an Imprinted Polymer: Maximizing Selectivity by Optimizing the Monomer–Template Ratio for a Cinchonidine MIP, Prior to Polymerization, Using Microcalorimetry," *Journal of Liquid Chromatography & Related Technologies*, vol. 28, no. 1, pp. 1–15, Jan. 2005, doi: 10.1081/JLC-200038551.
- [136] R. J. Ansell, "Characterization of the Binding Properties of Molecularly Imprinted Polymers BT - Molecularly Imprinted Polymers in Biotechnology," B. Mattiasson and L. Ye, Eds. Cham: Springer International Publishing, 2015, pp. 51–93. doi: 10.1007/10_2015_316.
- [137] Z. Zhang and J. Liu, "Improving molecularly imprinted nanogels by pH modulation," *RSC Advances*, vol. 5, no. 110, pp. 91018–91025, Oct. 2015, doi: 10.1039/C5RA16777A.
- [138] W.-Y. Chen, C.-S. Chen, and F.-Y. Lin, "Molecular recognition in imprinted polymers: thermodynamic investigation of analyte binding using microcalorimetry," *Journal of Chromatography A*, vol. 923, no. 1, pp. 1–6, 2001, doi: [https://doi.org/10.1016/S0021-9673\(01\)00971-2](https://doi.org/10.1016/S0021-9673(01)00971-2).
- [139] L. Chen *et al.*, "Preparation of magnetic molecularly imprinted polymer for the separation of tetracycline antibiotics from egg and tissue samples," *Journal of Chromatography A*, vol. 1216, no. 18, pp. 3710–3719, 2009, doi: <https://doi.org/10.1016/j.chroma.2009.02.044>.
- [140] T. Hasegawa, S. Tatsuta, and Y. Katsumoto, "Infrared spectroscopic study of molecular interaction of tacticity-controlled poly(N-isopropylacrylamide) in a cast film deposited on a solid substrate," *Analytical and Bioanalytical Chemistry*, vol. 398, no. 5, pp. 2203–2209, 2010, doi: 10.1007/s00216-010-4113-x.
- [141] S. Wei, J. Li, Y. Liu, and J. Ma, "Development of magnetic molecularly imprinted polymers with double templates for the rapid and selective determination of amphenicol

- antibiotics in water, blood, and egg samples,” *Journal of Chromatography A*, vol. 1473, pp. 19–27, 2016, doi: <https://doi.org/10.1016/j.chroma.2016.10.067>.
- [142] N. Karaseva, T. Ermolaeva, and B. Mizaikoff, “Piezoelectric sensors using molecularly imprinted nanospheres for the detection of antibiotics,” *Sensors and Actuators B: Chemical*, vol. 225, pp. 199–208, 2016, doi: <https://doi.org/10.1016/j.snb.2015.11.045>.
- [143] Z. Zhang *et al.*, “Synthesis of dummy-template molecularly imprinted polymer adsorbents for solid phase extraction of aminoglycosides antibiotics from environmental water samples,” *Talanta*, vol. 208, p. 120385, 2020, doi: <https://doi.org/10.1016/j.talanta.2019.120385>.
- [144] Y. Liu *et al.*, “Sensitive analysis of trace macrolide antibiotics in complex food samples by ambient mass spectrometry with molecularly imprinted polymer-coated wooden tips,” *Talanta*, vol. 204, pp. 238–247, 2019, doi: <https://doi.org/10.1016/j.talanta.2019.05.102>.
- [145] Y. Fuchs, O. Soppera, and K. Haupt, “Photopolymerization and photostructuring of molecularly imprinted polymers for sensor applications—A review,” *Analytica Chimica Acta*, vol. 717, pp. 7–20, 2012, doi: <https://doi.org/10.1016/j.aca.2011.12.026>.
- [146] X. Xie, X. Liu, X. Pan, L. Chen, and S. Wang, “No TitleSurface-imprinted magnetic particles for highly selective sulfonamides recognition prepared by reversible addition fragmentation chain transfer polymerization,” *Analytical and Bioanalytical Chemistry*, vol. 408, pp. 963–970, 2016.
- [147] F. Chen, J. Zhang, M. Wang, and J. Kong, “Magnetic molecularly imprinted polymers synthesized by surface-initiated reversible addition-fragmentation chain transfer polymerization for the enrichment and determination of synthetic estrogens in aqueous solution,” *Journal of Separation Science*, vol. 38, no. 15, pp. 2670–2676, Aug. 2015, doi: [10.1002/jssc.201500407](https://doi.org/10.1002/jssc.201500407).
- [148] X. Wang, L. Chen, X. Xu, and Y. Li, “Synthesis of molecularly imprinted polymers via ring-opening metathesis polymerization for solid-phase extraction of bisphenol A,” *Analytical and Bioanalytical Chemistry*, vol. 401, no. 4, p. 1423, 2011, doi: [10.1007/s00216-011-5178-x](https://doi.org/10.1007/s00216-011-5178-x).

- [149] X. Li *et al.*, “Surface molecular imprinting onto magnetic yeast composites via atom transfer radical polymerization for selective recognition of cefalexin,” *Chemical Engineering Journal*, vol. 198–199, pp. 503–511, 2012, doi: <https://doi.org/10.1016/j.cej.2012.05.106>.
- [150] F. Liu, S. Zhang, G. Wang, J. Zhao, and Z. Guo, “A novel bifunctional molecularly imprinted polymer for determination of Congo red in food,” *RSC Advances*, vol. 5, no. 29, pp. 22811–22817, Feb. 2015, doi: 10.1039/C4RA14719G.
- [151] P. Wang, S. Chen, X. Zhu, and J. Xie, “Daidzein-imprinted membranes using co-functional monomers,” *Journal of Chromatography A*, vol. 1216, no. 45, pp. 7639–7644, 2009, doi: <https://doi.org/10.1016/j.chroma.2009.08.093>.
- [152] K. Chullasat, P. Nurerk, P. Kanatharana, F. Davis, and O. Bunkoed, “A facile optosensing protocol based on molecularly imprinted polymer coated on CdTe quantum dots for highly sensitive and selective amoxicillin detection,” *Sensors and Actuators B: Chemical*, vol. 254, pp. 255–263, 2018, doi: <https://doi.org/10.1016/j.snb.2017.07.062>.
- [153] Y. Tunc, N. Hasirci, A. Yesilada, and K. Ulubayram, “Comonomer effects on binding performances and morphology of acrylate-based imprinted polymers,” *Polymer (Guildf)*, vol. 47, no. 20, pp. 6931–6940, 2006, doi: <https://doi.org/10.1016/j.polymer.2006.07.043>.
- [154] M. Valtchev, B. S. Palm, M. Schiller, and U. Steinfeld, “Development of sulfamethoxazole-imprinted polymers for the selective extraction from waters,” *Journal of Hazardous Materials*, vol. 170, no. 2, pp. 722–728, 2009, doi: <https://doi.org/10.1016/j.jhazmat.2009.05.007>.
- [155] H. Wang, R. Wang, and Y. Han, “Preparation of molecular imprinted microspheres based on inorganic–organic co-functional monomer for miniaturized solid-phase extraction of fluoroquinolones in milk,” *Journal of Chromatography B*, vol. 949–950, pp. 24–29, 2014, doi: <https://doi.org/10.1016/j.jchromb.2013.10.042>.
- [156] P. Atkins and J. de Paula, *Physical Chemistry*, 10th ed. Oxford, UK: Oxford University Press, 2014.

- [157] A. Fű, M. D. Julliard, T. G. Deligeorgiev, N. I. Gadjev, A. A. Vasilev, and E. Vauthey, "Ultrafast Excited-State Dynamics of DNA Fluorescent Intercalators: New Insight into the Fluorescence Enhancement Mechanism," 2006, doi: 10.1021/ja0609001.
- [158] Y. Hong, J. W. Y. Lam, and B. Z. Tang, "Aggregation-induced emission," *Chem. Soc. Rev*, vol. 40, pp. 5361–5388, 2011, doi: 10.1039/c1cs15113d.
- [159] H. Yang *et al.*, "Aggregation-induced emission monomer-based fluorescent molecularly imprinted poly(ionic liquid) synthesized by a one-pot method for sensitively detecting 4-nitrophenol," 2022, doi: 10.1039/d1ay02132j.
- [160] by Yuwei Wu *et al.*, "Cite this," *J. Mater. Chem. C*, vol. 8, p. 13574, doi: 10.1039/d0tc01703e.
- [161] Y. Li, W. He, Q. Peng, L. Hou, J. He, and K. Li, "Aggregation-induced emission luminogen based molecularly imprinted ratiometric fluorescence sensor for the detection of Rhodamine 6G in food samples," *Food Chemistry*, vol. 287, pp. 55–60, Jul. 2019, doi: 10.1016/J.FOODCHEM.2019.02.081.
- [162] B. Song *et al.*, "14769–14778 ACS Nano 2020, 14, 14769–14778 Downloaded via NEWCASTLE UNIV on May 26," *ACS Nano*, vol. 14, p. 48, 2020, doi: 10.1021/acsnano.0c01973.
- [163] "Methods and Applications in Fluorescence Photobleaching of organic fluorophores: quantitative characterization, mechanisms, protection *," 2020, doi: 10.1088/2050-6120/ab7365.
- [164] G. E. Dobretsov, T. I. Syrejschikova, and N. v Smolina, "On mechanisms of fluorescence quenching by water," *Biophysics (Oxf)*, vol. 59, no. 2, pp. 183–188, 2014, doi: 10.1134/S0006350914020079.
- [165] R. M. Clegg, "Fluorescence resonance energy transfer," *Current Opinion in Biotechnology*, vol. 6, no. 1, pp. 103–110, Jan. 1995, doi: 10.1016/0958-1669(95)80016-6.
- [166] D. Feng *et al.*, "Dual selective sensor for exosomes in serum using magnetic imprinted polymer isolation sandwiched with aptamer/graphene oxide based FRET fluorescent ignition,"

Biosensors and Bioelectronics, vol. 207, p. 114112, Jul. 2022, doi:

10.1016/J.BIOS.2022.114112.

[167] C. Liang *et al.*, “A virus-MIPs fluorescent sensor based on FRET for highly sensitive detection of JEV,” *Talanta*, vol. 160, pp. 360–366, Nov. 2016, doi:

10.1016/J.TALANTA.2016.06.010.

[168] Z. Xu, P. Deng, J. Li, L. Xu, and S. Tang, “Molecularly imprinted fluorescent probe based on FRET for selective and sensitive detection of doxorubicin,” *Materials Science and Engineering: B*, vol. 218, pp. 31–39, Apr. 2017, doi: 10.1016/J.MSEB.2017.02.005.

[169] W. Mao, L. Xia, and H. Xie, “Detection of Carbapenemase-Producing Organisms with a Carbapenem-Based Fluorogenic Probe,” *Angewandte Chemie International Edition*, vol. 56, no. 16, pp. 4468–4472, Apr. 2017, doi: 10.1002/anie.201612495.

[170] R. E. Hargrove, R. J. Lehman, and C. A. Matthews, “Use of Fluorescent Materials for the Indirect Detection of Antibiotics in Milk,” *Journal of Dairy Science*, vol. 41, no. 5, pp. 617–623, 1958, doi: [https://doi.org/10.3168/jds.S0022-0302\(58\)90974-3](https://doi.org/10.3168/jds.S0022-0302(58)90974-3).

[171] H. Nakata, K. Kannan, P. D. Jones, and J. P. Giesy, “Determination of fluoroquinolone antibiotics in wastewater effluents by liquid chromatography–mass spectrometry and fluorescence detection,” *Chemosphere*, vol. 58, no. 6, pp. 759–766, 2005, doi:

<https://doi.org/10.1016/j.chemosphere.2004.08.097>.

[172] H. Sunayama, T. Ohta, A. Kuwahara, and T. Takeuchi, “Fluorescence signaling molecularly imprinted polymers for antibiotics prepared via site-directed post-imprinting introduction of plural fluorescent reporters within the recognition cavity,” *Journal of Materials Chemistry B*, vol. 4, no. 44, pp. 7138–7145, Nov. 2016, doi: 10.1039/C6TB02000C.

[173] E. Benito-Peña, M. C. Moreno-Bondi, S. Aparicio, G. Orellana, J. Cederfur, and M. Kempe, “Molecular Engineering of Fluorescent Penicillins for Molecularly Imprinted Polymer Assays,” *Analytical Chemistry*, vol. 78, no. 6, pp. 2019–2027, Mar. 2006, doi:

10.1021/ac051939b.

- [174] S. Wagner, J. Bell, M. Biyikal, K. Gawlitza, and K. Rurack, "Integrating fluorescent molecularly imprinted polymer (MIP) sensor particles with a modular microfluidic platform for nanomolar small-molecule detection directly in aqueous samples," *Biosensors and Bioelectronics*, vol. 99, pp. 244–250, 2018, doi: <https://doi.org/10.1016/j.bios.2017.07.053>.
- [175] Y. Liu, Y. Wang, L. Liu, Y. He, Q. He, and Y. Ji, "The detection method for small molecules coupled with a molecularly imprinted polymer/quantum dot chip using a home-built optical system," *Analytical and Bioanalytical Chemistry*, vol. 408, no. 19, pp. 5261–5268, Jul. 2016, doi: [10.1007/s00216-016-9620-y](https://doi.org/10.1007/s00216-016-9620-y).
- [176] M.-R. Chao, C.-W. Hu, and J.-L. Chen, "Comparative syntheses of tetracycline-imprinted polymeric silicate and acrylate on CdTe quantum dots as fluorescent sensors," *Biosensors and Bioelectronics*, vol. 61, pp. 471–477, 2014, doi: <https://doi.org/10.1016/j.bios.2014.05.058>.
- [177] Y. Geng *et al.*, "A fluorescent molecularly imprinted polymer using aptamer as a functional monomer for sensing of kanamycin," *Sensors and Actuators B: Chemical*, vol. 268, pp. 47–54, 2018, doi: <https://doi.org/10.1016/j.snb.2018.04.065>.
- [178] T. Shi, L. Tan, H. Fu, and J. Wang, "Application of molecular imprinting polymer anchored on CdTe quantum dots for the detection of sulfadiazine in seawater," *Marine Pollution Bulletin*, vol. 146, pp. 591–597, 2019, doi: <https://doi.org/10.1016/j.marpolbul.2019.07.010>.
- [179] L. Zhang and L. Chen, "Fluorescence Probe Based on Hybrid Mesoporous Silica/Quantum Dot/Molecularly Imprinted Polymer for Detection of Tetracycline," *ACS Applied Materials & Interfaces*, vol. 8, no. 25, pp. 16248–16256, Jun. 2016, doi: [10.1021/acsami.6b04381](https://doi.org/10.1021/acsami.6b04381).
- [180] T. Zhou, A. Halder, and Y. Sun, "Fluorescent Nanosensor Based on Molecularly Imprinted Polymers Coated on Graphene Quantum Dots for Fast Detection of Antibiotics," *Biosensors (Basel)*, vol. 8, no. 3, p. 82, Sep. 2018, doi: [10.3390/bios8030082](https://doi.org/10.3390/bios8030082).

- [181] K. Chen *et al.*, “A fluorescent glycosyl-imprinted polymer for pH and temperature regulated sensing of target glycopeptide antibiotic,” *Biosensors and Bioelectronics*, vol. 94, pp. 609–615, 2017, doi: <https://doi.org/10.1016/j.bios.2017.03.059>.
- [182] Q. Yang, J. Li, X. Wang, H. Peng, H. Xiong, and L. Chen, “Strategies of molecular imprinting-based fluorescence sensors for chemical and biological analysis,” *Biosensors and Bioelectronics*, vol. 112, pp. 54–71, 2018, doi: <https://doi.org/10.1016/j.bios.2018.04.028>.
- [183] O. Y. F. Henry, D. C. Cullen, and S. A. Piletsky, “Optical interrogation of molecularly imprinted polymers and development of MIP sensors: a review,” *Analytical and Bioanalytical Chemistry*, vol. 382, no. 4, pp. 947–956, 2005, doi: 10.1007/s00216-005-3255-8.
- [184] H. Niu, Y. Yang, and H. Zhang, “Efficient one-pot synthesis of hydrophilic and fluorescent molecularly imprinted polymer nanoparticles for direct drug quantification in real biological samples,” *Biosensors and Bioelectronics*, vol. 74, pp. 440–446, 2015, doi: <https://doi.org/10.1016/j.bios.2015.06.071>.
- [185] J. Ashley, X. Feng, and Y. Sun, “A multifunctional molecularly imprinted polymer-based biosensor for direct detection of doxycycline in food samples,” *Talanta*, vol. 182, pp. 49–54, 2018, doi: <https://doi.org/10.1016/j.talanta.2018.01.056>.
- [186] A. D. Hudson *et al.*, “Dual detection of nafcillin using a molecularly imprinted polymer-based platform coupled to thermal and fluorescence read-out †,” vol. 2, p. 5105, 2021, doi: 10.1039/d1ma00192b.
- [187] R. L. McCreery, “Advanced Carbon Electrode Materials for Molecular Electrochemistry,” *Chemical Reviews*, vol. 108, no. 7, pp. 2646–2687, Jul. 2008, doi: 10.1021/cr068076m.
- [188] A. García-Miranda Ferrari, C. W. Foster, P. J. Kelly, D. A. C. Brownson, and C. E. Banks, “Determination of the Electrochemical Area of Screen-Printed Electrochemical Sensing Platforms,” *Biosensors*, vol. 8, no. 2. 2018. doi: 10.3390/bios8020053.

- [189] I.-A. Stoian *et al.*, “Biomimetic electrochemical sensor for the highly selective detection of azithromycin in biological samples,” *Biosensors and Bioelectronics*, vol. 155, p. 112098, 2020, doi: <https://doi.org/10.1016/j.bios.2020.112098>.
- [190] A. R. Cardoso *et al.*, “Molecularly-imprinted chloramphenicol sensor with laser-induced graphene electrodes,” *Biosensors and Bioelectronics*, vol. 124–125, pp. 167–175, 2019, doi: <https://doi.org/10.1016/j.bios.2018.10.015>.
- [191] B. Feier, A. Blidar, A. Pusta, P. Carciuc, and C. Cristea, “Electrochemical Sensor Based on Molecularly Imprinted Polymer for the Detection of Cefalexin,” *Biosensors (Basel)*, vol. 9, no. 1, p. 31, Feb. 2019, doi: [10.3390/bios9010031](https://doi.org/10.3390/bios9010031).
- [192] D. Dechtrirat *et al.*, “A screen-printed carbon electrode modified with gold nanoparticles, poly(3,4-ethylenedioxythiophene), poly(styrene sulfonate) and a molecular imprint for voltammetric determination of nitrofurantoin,” *Microchimica Acta*, vol. 185, no. 5, p. 261, 2018, doi: [10.1007/s00604-018-2797-3](https://doi.org/10.1007/s00604-018-2797-3).
- [193] A. G. Ayankojo, J. Reut, V. Ciocan, A. Öpik, and V. Syritski, “Molecularly imprinted polymer-based sensor for electrochemical detection of erythromycin,” *Talanta*, vol. 209, p. 120502, 2020, doi: <https://doi.org/10.1016/j.talanta.2019.120502>.
- [194] W. Lian, S. Liu, L. Wang, and H. Liu, “A novel strategy to improve the sensitivity of antibiotics determination based on bioelectrocatalysis at molecularly imprinted polymer film electrodes,” *Biosensors and Bioelectronics*, vol. 73, pp. 214–220, 2015, doi: <https://doi.org/10.1016/j.bios.2015.06.006>.
- [195] E. Mazzotta, A. Turco, I. Chianella, A. Guerreiro, S. A. Piletsky, and C. Malitesta, “Solid-phase synthesis of electroactive nanoparticles of molecularly imprinted polymers. A novel platform for indirect electrochemical sensing applications,” *Sensors and Actuators B: Chemical*, vol. 229, pp. 174–180, 2016, doi: <https://doi.org/10.1016/j.snb.2016.01.126>.

- [196] F. Canfarotta, A. Poma, A. Guerreiro, and S. Piletsky, "Solid-phase synthesis of molecularly imprinted nanoparticles," *Nature Protocols*, vol. 11, no. 3, pp. 443–455, 2016, doi: 10.1038/nprot.2016.030.
- [197] A. Poma, A. P. F. Turner, and S. A. Piletsky, "Advances in the manufacture of MIP nanoparticles," *Trends in Biotechnology*, vol. 28, no. 12, pp. 629–637, 2010, doi: <https://doi.org/10.1016/j.tibtech.2010.08.006>.
- [198] S. Guillon, R. Lemaire, A. V. Linares, K. Haupt, and C. Ayela, "Single step patterning of molecularly imprinted polymers for large scale fabrication of microbiochips," *Lab on a Chip*, vol. 9, no. 20, p. 2987, Oct. 2009, doi: 10.1039/b905608d.
- [199] J. P. Metters, R. O. Kadara, and C. E. Banks, "New directions in screen printed electroanalytical sensors: an overview of recent developments," *Analyst*, vol. 136, no. 6, p. 1067, 2011, doi: 10.1039/c0an00894j.
- [200] A. Heller and B. Feldman, "Electrochemical Glucose Sensors and Their Applications in Diabetes Management," *Chemical Reviews*, vol. 108, no. 7, pp. 2482–2505, Jul. 2008, doi: 10.1021/cr068069y.
- [201] E. P. Randviir, D. A. C. Brownson, J. P. Metters, R. O. Kadara, and C. E. Banks, "The fabrication, characterisation and electrochemical investigation of screen-printed graphene electrodes," *Physical Chemistry Chemical Physics*, vol. 16, no. 10, pp. 4598–4611, 2014, doi: 10.1039/C3CP55435J.
- [202] J. P. Metters, R. O. Kadara, and C. E. Banks, "Fabrication of co-planar screen printed microband electrodes," *Analyst*, vol. 138, no. 9, p. 2516, 2013, doi: 10.1039/c3an00268c.
- [203] J. P. Metters, R. O. Kadara, and C. E. Banks, "Electroanalytical properties of screen printed graphite microband electrodes," *Sensors and Actuators B: Chemical*, vol. 169, pp. 136–143, 2012, doi: <https://doi.org/10.1016/j.snb.2012.04.045>.
- [204] A. P. Ruas de Souza, M. Bertotti, C. W. Foster, and C. E. Banks, "Back-to-Back Screen-Printed Electroanalytical Sensors: Extending the Potential Applications of the Simplistic

- Design,” *Electroanalysis*, vol. 27, no. 10, pp. 2295–2301, Oct. 2015, doi: 10.1002/elan.201500155.
- [205] J. P. Metters, E. P. Randviir, and C. E. Banks, “Screen-printed back-to-back electroanalytical sensors,” *Analyst*, vol. 139, no. 21, pp. 5339–5349, Sep. 2014, doi: 10.1039/C4AN01501K.
- [206] A. P. Ruas de Souza, C. W. Foster, A. v. Kollipoulos, M. Bertotti, and C. E. Banks, “Screen-printed back-to-back electroanalytical sensors: heavy metal ion sensing,” *Analyst*, vol. 140, no. 12, pp. 4130–4136, Jun. 2015, doi: 10.1039/C5AN00381D.
- [207] Z. Taleat, A. Khoshroo, and M. Mazloun-Ardakani, “Screen-printed electrodes for biosensing: a review (2008–2013),” *Microchimica Acta*, vol. 181, no. 9, pp. 865–891, 2014, doi: 10.1007/s00604-014-1181-1.
- [208] R. Crapnell *et al.*, “Recent Advances in Electrosynthesized Molecularly Imprinted Polymer Sensing Platforms for Bioanalyte Detection,” *Sensors*, vol. 19, no. 5, p. 1204, Mar. 2019, doi: 10.3390/s19051204.
- [209] M. Peeters, B. van Grinsven, C. Foster, T. Cleij, and C. Banks, “Introducing Thermal Wave Transport Analysis (TWTA): A Thermal Technique for Dopamine Detection by Screen-Printed Electrodes Functionalized with Molecularly Imprinted Polymer (MIP) Particles,” *Molecules*, vol. 21, no. 5, p. 552, Apr. 2016, doi: 10.3390/molecules21050552.
- [210] S. Casadio *et al.*, “Development of a novel flexible polymer-based biosensor platform for the thermal detection of noradrenaline in aqueous solutions,” *Chemical Engineering Journal*, vol. 315, pp. 459–468, 2017, doi: <https://doi.org/10.1016/j.cej.2017.01.050>.
- [211] K. Betlem *et al.*, “Evaluating the temperature dependence of heat-transfer based detection: A case study with caffeine and Molecularly Imprinted Polymers as synthetic receptors,” *Chemical Engineering Journal*, vol. 359, pp. 505–517, Mar. 2019, doi: 10.1016/j.cej.2018.11.114.

- [212] R. Gui, H. Jin, H. Guo, and Z. Wang, "Recent advances and future prospects in molecularly imprinted polymers-based electrochemical biosensors," *Biosensors and Bioelectronics*, vol. 100, pp. 56–70, 2018, doi: <https://doi.org/10.1016/j.bios.2017.08.058>.
- [213] O. Jamieson *et al.*, "Screen printed electrode based detection systems for the antibiotic amoxicillin in aqueous samples utilising molecularly imprinted polymers as synthetic receptors," *Chemosensors*, vol. 8, no. 1, 2020, doi: 10.3390/chemosensors8010005.
- [214] L. Devkota, Loc. T. Nguyen, T. T. Vu, and B. Piro, "Electrochemical determination of tetracycline using AuNP-coated molecularly imprinted overoxidized polypyrrole sensing interface," *Electrochimica Acta*, vol. 270, pp. 535–542, 2018, doi: <https://doi.org/10.1016/j.electacta.2018.03.104>.
- [215] M. Rohani Moghadam, L. Salehi, S. Jafari, N. Nasirizadeh, and J. Ghasemi, "Voltammetric sensing of oxacillin by using a screen-printed electrode modified with molecularly imprinted polyaniline, gold nanourchins and graphene oxide," *Microchimica Acta*, vol. 186, no. 12, p. 798, 2019, doi: 10.1007/s00604-019-3981-9.
- [216] A. Florea, B. Feier, and C. Cristea, "In situ analysis based on molecularly imprinted polymer electrochemical sensors," in *MIP Synthesis, Characteristics and Analytical Application*, M. Marc, Ed. Elsevier, 2019.
- [217] I. Losito, F. Palmisano, and P. G. Zambonin, "o-Phenylenediamine Electropolymerization by Cyclic Voltammetry Combined with Electrospray Ionization-Ion Trap Mass Spectrometry," *Analytical Chemistry*, vol. 75, no. 19, pp. 4988–4995, Oct. 2003, doi: 10.1021/ac0342424.
- [218] S. Komaba, M. Seyama, T. Momma, and T. Osaka, "Potentiometric biosensor for urea based on electropolymerized electroinactive polypyrrole," *Electrochimica Acta*, vol. 42, no. 3, pp. 383–388, 1997, doi: [https://doi.org/10.1016/S0013-4686\(96\)00226-5](https://doi.org/10.1016/S0013-4686(96)00226-5).

- [219] Y.-M. Uang and T.-C. Chou, "Criteria for Designing a Polypyrrole Glucose Biosensor by Galvanostatic Electropolymerization," *Electroanalysis*, vol. 14, no. 22, pp. 1564–1570, Nov. 2002, doi: 10.1002/1521-4109(200211)14:22<1564::AID-ELAN1564>3.0.CO;2-H.
- [220] A. Tiwari, J. Rawlins, and L. Hihara, Eds., *Intelligent Coatings for Corrosive*. Elsevier, 2015.
- [221] G. Moro *et al.*, "Conductive imprinted polymers for the direct electrochemical detection of β -lactam antibiotics: The case of cefquinome," *Sensors and Actuators B: Chemical*, vol. 297, p. 126786, 2019, doi: <https://doi.org/10.1016/j.snb.2019.126786>.
- [222] F. Bottari *et al.*, "Electropolymerized o-Phenylenediamine on Graphite Promoting the Electrochemical Detection of Nafcillin," *Electroanalysis*, vol. 32, no. 1, pp. 135–141, Jan. 2020, doi: 10.1002/elan.201900397.
- [223] M. Roushani, Z. Rahmati, S. J. Hoseini, and R. Hashemi Fath, "Impedimetric ultrasensitive detection of chloramphenicol based on aptamer MIP using a glassy carbon electrode modified by 3-ampy-RGO and silver nanoparticle," *Colloids and Surfaces B: Biointerfaces*, vol. 183, p. 110451, 2019, doi: <https://doi.org/10.1016/j.colsurfb.2019.110451>.
- [224] A. Kumar Prusty and S. Bhand, "Molecularly Imprinted Polyresorcinol Based Capacitive Sensor for Sulphanilamide Detection," *Electroanalysis*, vol. 31, no. 9, pp. 1797–1808, Sep. 2019, doi: 10.1002/elan.201900099.
- [225] L. Chen and B. Li, "Application of magnetic molecularly imprinted polymers in analytical chemistry," *Analytical Methods*, vol. 4, no. 9, pp. 2613–2621, 2012, doi: 10.1039/C2AY25354B.
- [226] J. Dai *et al.*, "Preparation of molecularly imprinted nanoparticles with superparamagnetic susceptibility through atom transfer radical emulsion polymerization for the selective recognition of tetracycline from aqueous medium," *Journal of Hazardous Materials*, vol. 205–206, pp. 179–188, 2012, doi: <https://doi.org/10.1016/j.jhazmat.2011.12.056>.

- [227] R. Ahmad, N. Griffete, A. Lamouri, N. Felidj, M. M. Chehimi, and C. Mangeney, “Nanocomposites of Gold Nanoparticles@Molecularly Imprinted Polymers: Chemistry, Processing, and Applications in Sensors,” *Chemistry of Materials*, vol. 27, no. 16, pp. 5464–5478, Aug. 2015, doi: 10.1021/acs.chemmater.5b00138.
- [228] S. Carrasco *et al.*, “Multibranched Gold–Mesoporous Silica Nanoparticles Coated with a Molecularly Imprinted Polymer for Label-Free Antibiotic Surface-Enhanced Raman Scattering Analysis,” *Chemistry of Materials*, vol. 28, no. 21, pp. 7947–7954, Nov. 2016, doi: 10.1021/acs.chemmater.6b03613.
- [229] M. Niu, C. Pham-Huy, and H. He, “Core-shell nanoparticles coated with molecularly imprinted polymers: a review,” *Microchimica Acta*, vol. 183, no. 10, pp. 2677–2695, 2016, doi: 10.1007/s00604-016-1930-4.
- [230] Y. Tang *et al.*, “Preconcentration of the antibiotic enrofloxacin using a hollow molecularly imprinted polymer, and its quantitation by HPLC,” *Microchimica Acta*, vol. 183, no. 2, pp. 589–596, 2016, doi: 10.1007/s00604-015-1681-7.
- [231] W. Chen, Y. Ma, J. Pan, Z. Meng, G. Pan, and B. Sellergren, “Molecularly Imprinted Polymers with Stimuli-Responsive Affinity: Progress and Perspectives,” *Polymers (Basel)*, vol. 7, pp. 1689–1715, 2015, doi: 10.3390/polym7091478.
- [232] A. Poma, A. Guerreiro, M. J. Whitcombe, E. v Piletska, A. P. F. Turner, and S. A. Piletsky, “Solid-Phase Synthesis of Molecularly Imprinted Polymer Nanoparticles with a Reusable Template–‘Plastic Antibodies,’” *Advanced Functional Materials*, vol. 23, no. 22, pp. 2821–2827, Jun. 2013, doi: 10.1002/adfm.201202397.
- [233] F. Canfarotta *et al.*, “A novel thermal detection method based on molecularly imprinted nanoparticles as recognition elements,” *Nanoscale*, vol. 10, no. 4, pp. 2081–2089, Jan. 2018, doi: 10.1039/C7NR07785H.

- [234] P. X. Medina Rangel *et al.*, “Solid-phase synthesis of molecularly imprinted polymer nanolabels: Affinity tools for cellular bioimaging of glycans,” *Scientific Reports*, vol. 9, no. 1, p. 3923, 2019, doi: 10.1038/s41598-019-40348-5.
- [235] S.-P. Tang, F. Canfarotta, K. Smolinska-Kempisty, E. Piletska, A. Guerreiro, and S. Piletsky, “A pseudo-ELISA based on molecularly imprinted nanoparticles for detection of gentamicin in real samples,” *Analytical Methods*, vol. 9, no. 19, pp. 2853–2858, May 2017, doi: 10.1039/C7AY00398F.
- [236] C. Chen *et al.*, “Molecularly Imprinted Polymer as an Antibody Substitution in Pseudo-immunoassays for Chemical Contaminants in Food and Environmental Samples,” *Journal of Agricultural and Food Chemistry*, vol. 66, no. 11, pp. 2561–2571, Mar. 2018, doi: 10.1021/acs.jafc.7b05577.
- [237] W. Zhang and Z. Chen, “Preparation of micropipette tip-based molecularly imprinted monolith for selective micro-solid phase extraction of berberine in plasma and urine samples,” *Talanta*, vol. 103, pp. 103–109, 2013, doi: <https://doi.org/10.1016/j.talanta.2012.10.014>.
- [238] M. Bompart, K. Haupt, and C. Ayela, “Micro and Nanofabrication of Molecularly Imprinted Polymers,” Springer, Berlin, Heidelberg, 2011, pp. 83–110. doi: 10.1007/128_2011_308.
- [239] Z. Altintas, J. Pocock, K.-A. Thompson, and I. E. Tohill, “Comparative investigations for adenovirus recognition and quantification: Plastic or natural antibodies?,” *Biosensors and Bioelectronics*, vol. 74, pp. 996–1004, 2015, doi: <https://doi.org/10.1016/j.bios.2015.07.076>.
- [240] M. J. Whitcombe *et al.*, “The rational development of molecularly imprinted polymer-based sensors for protein detection,” *Chem. Soc. Rev.*, vol. 40, no. 3, pp. 1547–1571, Feb. 2011, doi: 10.1039/C0CS00049C.
- [241] I. Chianella *et al.*, “Direct Replacement of Antibodies with Molecularly Imprinted Polymer Nanoparticles in ELISA—Development of a Novel Assay for Vancomycin,” *Analytical Chemistry*, vol. 85, no. 17, pp. 8462–8468, Sep. 2013, doi: 10.1021/ac402102j.

- [242] G. Guan, B. Liu, Z. Wang, and Z. Zhang, “Imprinting of Molecular Recognition Sites on Nanostructures and Its Applications in Chemosensors,” *Sensors*, vol. 8, no. 12, 2008. doi: 10.3390/s8128291.
- [243] Y. Wu *et al.*, “Monitoring bisphenol A and its biodegradation in water using a fluorescent molecularly imprinted chemosensor,” *Chemosphere*, vol. 119, pp. 515–523, 2015, doi: <https://doi.org/10.1016/j.chemosphere.2014.07.017>.
- [244] P. Turkewitsch, B. Wandelt, G. D. Darling, and W. S. Powell, “Fluorescent Functional Recognition Sites through Molecular Imprinting. A Polymer-Based Fluorescent Chemosensor for Aqueous cAMP,” *Analytical Chemistry*, vol. 70, no. 10, pp. 2025–2030, May 1998, doi: 10.1021/ac980003i.
- [245] O. Güney and F. Ç. Cebeci, “Molecularly imprinted fluorescent polymers as chemosensors for the detection of mercury ions in aqueous media,” *Journal of Applied Polymer Science*, vol. 117, no. 4, pp. 2373–2379, Aug. 2010, doi: 10.1002/app.32077.
- [246] Z. Uygun, H. Uygun, N. Ermise, and E. Canbay, “Biosensors: Micro and Nanoscale Application,” T. Rincken, Ed. Rijeka: InTech, 2015.
- [247] V. Tsouti, C. Boutopoulos, I. Zergioti, and S. Chatzandroulis, “Capacitive microsystems for biological sensing,” *Biosensors and Bioelectronics*, vol. 27, no. 1, pp. 1–11, 2011, doi: <https://doi.org/10.1016/j.bios.2011.05.047>.
- [248] L. Lebogang, M. Hedström, and B. Mattiasson, “Development of a real-time capacitive biosensor for cyclic cyanotoxic peptides based on Adda-specific antibodies,” *Analytica Chimica Acta*, vol. 826, pp. 69–76, 2014, doi: <https://doi.org/10.1016/j.aca.2014.03.028>.
- [249] W. Limbut, M. Hedström, P. Thavarungkul, P. Kanatharana, and B. Mattiasson, “Capacitive biosensor for detection of endotoxin,” *Analytical and Bioanalytical Chemistry*, vol. 389, no. 2, pp. 517–525, 2007, doi: 10.1007/s00216-007-1443-4.
- [250] R. Suedee, C. Songkram, A. Petmoreekul, S. Sangkunakup, S. Sankasa, and N. Kongyart, “Direct enantioseparation of adrenergic drugs via thin-layer chromatography using

- molecularly imprinted polymers,” *Journal of Pharmaceutical and Biomedical Analysis*, vol. 19, no. 3, pp. 519–527, 1999, doi: [https://doi.org/10.1016/S0731-7085\(98\)00248-9](https://doi.org/10.1016/S0731-7085(98)00248-9).
- [251] G. Vasapollo *et al.*, “Molecularly Imprinted Polymers: Present and Future Prospective,” *OPEN ACCESS Int. J. Mol. Sci.*, vol. 12, p. 12, 2011, doi: 10.3390/ijms12095908.
- [252] A. C. Gray, A. R. M. Bradbury, A. Knappik, A. Plückthun, C. A. K. Borrebaeck, and S. Dübel, “Animal-derived-antibody generation faces strict reform in accordance with European Union policy on animal use,” *Nature Methods*, vol. 17, no. 8, pp. 755–756, 2020, doi: 10.1038/s41592-020-0906-9.
- [253] R. D. Crapnell *et al.*, “Thermal Detection of Cardiac Biomarkers Heart-Fatty Acid Binding Protein and ST2 Using a Molecularly Imprinted Nanoparticle-Based Multiplex Sensor Platform,” *ACS Sensors*, vol. 4, no. 10, pp. 2838–2845, Oct. 2019, doi: 10.1021/acssensors.9b01666.
- [254] X. Liu *et al.*, “Recent advances in sensors for tetracycline antibiotics and their applications,” *TrAC Trends in Analytical Chemistry*, vol. 109, pp. 260–274, Dec. 2018, doi: 10.1016/J.TRAC.2018.10.011.
- [255] J. F. Westphal, D. Vetter, and J. M. Brogard, “Hepatic side-effects of antibiotics,” *Journal of Antimicrobial Chemotherapy*, vol. 33, no. 3, pp. 387–401, Mar. 1994, doi: 10.1093/jac/33.3.387.
- [256] M. E. Phillips, J. B. Eastwood, J. R. Curtis, P. E. Gower, and H. E. de Wardener, “Tetracycline Poisoning in Renal Failure,” *British Medical Journal*, vol. 2, no. 5911, p. 149, Apr. 1974, doi: 10.1136/bmj.2.5911.149.
- [257] A. A. Borghi and M. S. A. Palma, “Tetracycline: production, waste treatment and environmental impact assessment,” *Brazilian Journal of Pharmaceutical Sciences*, vol. 50, no. 1, pp. 25–40, Mar. 2014, doi: 10.1590/S1984-82502011000100003.

- [258] S. Han *et al.*, “A dual-response ratiometric fluorescent sensor by europium-doped CdTe quantum dots for visual and colorimetric detection of tetracycline,” *Journal of Hazardous Materials*, vol. 398, p. 122894, Nov. 2020, doi: 10.1016/J.JHAZMAT.2020.122894.
- [259] X. L. Zhang, Y. Zhang, X. F. Yin, B. B. Du, C. Zheng, and H. H. Yang, “A facile approach for preparation of molecularly imprinted polymers layer on the surface of carbon nanotubes,” *Talanta*, vol. 105, pp. 403–408, Feb. 2013, doi: 10.1016/J.TALANTA.2012.10.062.
- [260] C. Pizan-Aquino, A. Wong, L. Avilés-Félix, S. Khan, G. Picasso, and M. D. P. T. Sotomayor, “Evaluation of the performance of selective M-MIP to tetracycline using electrochemical and HPLC-UV method,” *Materials Chemistry and Physics*, vol. 245, p. 122777, Apr. 2020, doi: 10.1016/J.MATCHEMPHYS.2020.122777.
- [261] O. Jamieson *et al.*, “Electropolymerised molecularly imprinted polymers for the heat-transfer based detection of microorganisms: A proof-of-concept study using yeast,” *Thermal Science and Engineering Progress*, vol. 24, p. 100956, Aug. 2021, doi: 10.1016/J.TSEP.2021.100956.
- [262] R. J. Umpleby, S. C. Baxter, M. Bode, J. K. Berch, R. N. Shah, and K. D. Shimizu, “Application of the Freundlich adsorption isotherm in the characterization of molecularly imprinted polymers,” *Analytica Chimica Acta*, vol. 435, no. 1, pp. 35–42, May 2001, doi: 10.1016/S0003-2670(00)01211-3.
- [263] S. Yan and W. Song, “Photo-transformation of pharmaceutically active compounds in the aqueous environment: a review,” 2014, doi: 10.1039/c3em00502j.
- [264] M. C. Cela-Pérez, M. M. Castro-López, A. Lasagabáster-Latorre, J. M. López-Vilariño, M. v. González-Rodríguez, and L. F. Barral-Losada, “Synthesis and characterization of bisphenol-A imprinted polymer as a selective recognition receptor,” *Analytica Chimica Acta*, vol. 706, no. 2, pp. 275–284, Nov. 2011, doi: 10.1016/J.ACA.2011.09.002.

- [265] Y. Ooyama *et al.*, “Fluorescence PET (photo-induced electron transfer) sensor for water based on anthracene-amino acid,” *Journal of Photochemistry and Photobiology A: Chemistry*, vol. 222, no. 1, pp. 52–55, Jul. 2011, doi: 10.1016/J.JPHOTOCHEM.2011.04.035.
- [266] W. Hall, *Superbugs: An arms race against bacteria*. Harvard University Press, 2018.
- [267] P. K. Mutiyar and A. K. Mittal, “Risk assessment of antibiotic residues in different water matrices in India: key issues and challenges”, doi: 10.1007/s11356-014-2702-5.
- [268] J. Fick *et al.*, “Pharmaceuticals and Personal Care Products in the Environment CONTAMINATION OF SURFACE, GROUND, AND DRINKING WATER FROM PHARMACEUTICAL PRODUCTION,” *Society of Environmental Toxicology and Chemistry*, vol. 28, no. 12, pp. 2522–2527, 2010, doi: 10.1897/09-073.S1.
- [269] N. J. Ashbolt, “Microbial contamination of drinking water and disease outcomes in developing regions,” *Toxicology*, vol. 198, no. 1–3, pp. 229–238, May 2004, doi: 10.1016/J.TOX.2004.01.030.
- [270] Pottering, “environmental quality standards in the field of water policy, amending and subsequently repealing Council Directives 82/176/EEC, 83/513/EEC, 84/156/EEC, 84/491/EEC, 86/280/EEC and amending Directive 2000/60/EC of the European Parliament and of the Council,” 2008.
- [271] N. Kemper, “Veterinary antibiotics in the aquatic and terrestrial environment,” *Ecological Indicators*, vol. 8, no. 1, pp. 1–13, Jan. 2008, doi: 10.1016/J.ECOLIND.2007.06.002.
- [272] B. Rezaei and S. Damiri, “Electrochemistry and Adsorptive Stripping Voltammetric Determination of Amoxicillin on a Multiwalled Carbon Nanotubes Modified Glassy Carbon Electrode”, doi: 10.1002/elan.200804571.
- [273] T. M. Prado, F. H. Cincotto, F. C. Moraes, and S. A. S. Machado, “Electrochemical Sensor-Based Ruthenium Nanoparticles on Reduced Graphene Oxide for the Simultaneous Determination of Ethinylestradiol and Amoxicillin”, doi: 10.1002/elan.201700014.

- [274] A. Muhammad, N. A. Yusof, R. Hajian, J. Abdullah, W. R. Seitz, and J. A. My, “Construction of an Electrochemical Sensor Based on Carbon Nanotubes/Gold Nanoparticles for Trace Determination of Amoxicillin in Bovine Milk,” 2016, doi: 10.3390/s16010056.
- [275] G. E. Pellegrini, G. Carpico, and E. Coni, “Electrochemical sensor for the detection and presumptive identification of quinolone and tetracycline residues in milk,” *Analytica Chimica Acta*, vol. 520, no. 1–2, pp. 13–18, Aug. 2004, doi: 10.1016/J.ACA.2004.04.052.
- [276] G. Yang and F. Zhao, “Molecularly imprinted polymer grown on multiwalled carbon nanotube surface for the sensitive electrochemical determination of amoxicillin,” *Electrochimica Acta*, vol. 174, no. 1, pp. 33–40, Aug. 2015, doi: 10.1016/J.ELECTACTA.2015.05.156.
- [277] S. Zeinali, H. Khoshshafar, M. Rezaei, and H. Bagheri, “Fabrication of a Selective and Sensitive Electrochemical Sensor Modified with Magnetic Molecularly Imprinted Polymer for Amoxicillin,” *ANALYTICAL AND BIOANALYTICAL CHEMISTRY RESEARCH*, vol. 5, no. 2, pp. 194–204, Dec. 2018.
- [278] M. Li, Y. T. Li, D. W. Li, and Y. T. Long, “Recent developments and applications of screen-printed electrodes in environmental assays—A review,” *Analytica Chimica Acta*, vol. 734, pp. 31–44, Jul. 2012, doi: 10.1016/J.ACA.2012.05.018.
- [279] E. S. Almeida *et al.*, “Organic-resistant screen-printed graphitic electrodes: Application to on-site monitoring of liquid fuels,” *Analytica Chimica Acta*, vol. 934, pp. 1–8, Aug. 2016, doi: 10.1016/J.ACA.2016.05.055.
- [280] A. D. Hudson *et al.*, “Synthesis of Optimized Molecularly Imprinted Polymers for the Isolation and Detection of Antidepressants via HPLC †,” 2019, doi: 10.3390/biomimetics4010018.
- [281] C. W. Foster, J. P. Metters, D. K. Kampouris, and C. E. Banks, “Ultraflexible Screen-Printed Graphitic Electroanalytical Sensing Platforms”, doi: 10.1002/elan.201300563.

- [282] L. R. Cumba *et al.*, “Can the mechanical activation (polishing) of screen-printed electrodes enhance their electroanalytical response? †,” *Analyst*, vol. 141, p. 2791, 2016, doi: 10.1039/c6an00167j.
- [283] E. Blanco, C. W. Foster, L. R. Cumba, D. R. do Carmo, and C. E. Banks, “Can solvent induced surface modifications applied to screen-printed platforms enhance their electroanalytical performance? †,” *Cite this: Analyst*, vol. 141, p. 2783, 2016, doi: 10.1039/c6an00440g.
- [284] B. van Grinsven *et al.*, “Heat-Transfer Resistance at Solid-Liquid Interfaces: A Tool for the Detection of Single-Nucleotide Polymorphisms in DNA,” 2012, doi: 10.1021/nm300147e.
- [285] E. v. Piletska, A. R. Guerreiro, M. Romero-Guerra, I. Chianella, A. P. F. Turner, and S. A. Piletsky, “Design of molecular imprinted polymers compatible with aqueous environment,” *Analytica Chimica Acta*, vol. 607, no. 1, pp. 54–60, Jan. 2008, doi: 10.1016/J.ACA.2007.11.019.
- [286] M. Jesús *et al.*, “International Journal of Environmental and Analytical Chemistry Pilot survey of chemical contaminants from industrial and human activities in river waters of Spain Pilot survey of chemical contaminants from industrial and human activities in river waters of Spain,” *International Journal of Environmental and Analytical Chemistry*, vol. 90, no. 6, pp. 321–343, doi: 10.1080/03067310903045463.
- [287] A. Längin, R. Alexy, A. König, and K. Kümmerer, “Deactivation and transformation products in biodegradability testing of β -lactams amoxicillin and piperacillin,” *Chemosphere*, vol. 75, no. 3, pp. 347–354, Apr. 2009, doi: 10.1016/J.CHEMOSPHERE.2008.12.032.
- [288] A. Wong, A. M. Santos, F. H. Cincotto, F. C. Moraes, O. Fatibello-Filho, and M. D. P. T. Sotomayor, “A new electrochemical platform based on low cost nanomaterials for sensitive detection of the amoxicillin antibiotic in different matrices,” *Talanta*, vol. 206, p. 120252, Jan. 2020, doi: 10.1016/J.TALANTA.2019.120252.
- [289] S. Pedley and G. Howard, “The public health implications of microbiological contamination of groundwater,” *Quarterly Journal of Engineering Geology and Hydrogeology*, vol. 30, no. 2, pp. 179–188, May 1997, doi: 10.1144/GSL.QJEGH.1997.030.P2.10.

- [290] Y. Wadamori, R. Gooneratne, and M. A. Hussain, "Outbreaks and factors influencing microbiological contamination of fresh produce," 2016, doi: 10.1002/jsfa.8125.
- [291] C. Dacarro, A. M. Picco, P. Grisoli, and M. Rodolfi, "Determination of aerial microbiological contamination in scholastic sports environments", doi: 10.1046/j.1365-2672.2003.02044.x.
- [292] L. O. Kallings, O. Ringertz, and L. Silverstolpe, "Microbiological contamination of medical preparations," *Acta Pharm Suec*, vol. 3, no. 3, pp. 219–228, 1966, [Online]. Available: <http://europepmc.org/abstract/MED/5967307>
- [293] N. S. I. Geweely, "Evaluation of ozone for preventing fungal influenced corrosion of reinforced concrete bridges over the River Nile, Egypt", doi: 10.1007/s10532-010-9391-7.
- [294] S. H. Magnússon *et al.*, "State of the art in benefit–risk analysis: Food microbiology," *Food and Chemical Toxicology*, vol. 50, no. 1, pp. 33–39, Jan. 2012, doi: 10.1016/J.FCT.2011.06.005.
- [295] S. Akhtar, M. R. Sarker, and A. Hossain, "Critical Reviews in Microbiology Microbiological food safety: a dilemma of developing societies," 2012, doi: 10.3109/1040841X.2012.742036.
- [296] J. Gruber *et al.*, "A conductive polymer based electronic nose for early detection of *Penicillium digitatum* in post-harvest oranges," *Materials Science and Engineering: C*, vol. 33, no. 5, pp. 2766–2769, Jul. 2013, doi: 10.1016/J.MSEC.2013.02.043.
- [297] P. D. Skottrup, M. Nicolaisen, and A. F. Justesen, "Towards on-site pathogen detection using antibody-based sensors," *Biosensors and Bioelectronics*, vol. 24, no. 3, pp. 339–348, Nov. 2008, doi: 10.1016/J.BIOS.2008.06.045.
- [298] F. S. Felix and L. Angnes, "Electrochemical immunosensors – A powerful tool for analytical applications," *Biosensors and Bioelectronics*, vol. 102, pp. 470–478, Apr. 2018, doi: 10.1016/J.BIOS.2017.11.029.

- [299] O. A. Sadik and J. M. van Emon, “Applications of electrochemical immunosensors to environmental monitoring,” *Biosensors and Bioelectronics*, vol. 11, no. 8, pp. i–x, Jan. 1996, doi: 10.1016/0956-5663(96)85936-7.
- [300] S. Banta, K. Dooley, and O. Shur, “Replacing Antibodies: Engineering New Binding Proteins,” 2013, doi: 10.1146/annurev-bioeng-071812-152412.
- [301] A. C. Gray, A. R. M Bradbury, A. Knappik, A. Plückthun, C. A. K Borrebaeck, and S. Dübel, “Animal-derived-antibody generation faces strict reform in accordance with European Union policy on animal use,” *Nature Methods*, doi: 10.1038/s41592-020-0906-9.
- [302] J. Wackerlig and P. A. Lieberzeit, “Molecularly imprinted polymer nanoparticles in chemical sensing – Synthesis, characterisation and application,” *Sensors and Actuators B: Chemical*, vol. 207, no. Part A, pp. 144–157, Feb. 2015, doi: 10.1016/J.SNB.2014.09.094.
- [303] M. Jia, Z. Zhang, J. Li, X. Ma, L. Chen, and X. Yang, “Molecular imprinting technology for microorganism analysis,” *TrAC Trends in Analytical Chemistry*, vol. 106, pp. 190–201, Sep. 2018, doi: 10.1016/J.TRAC.2018.07.011.
- [304] J. W. Lowdon *et al.*, “MIPs for commercial application in low-cost sensors and assays – An overview of the current status quo,” *Sensors and Actuators B: Chemical*, vol. 325, p. 128973, Dec. 2020, doi: 10.1016/J.SNB.2020.128973.
- [305] K. Haupt and K. Mosbach, “Molecularly Imprinted Polymers and Their Use in Biomimetic Sensors,” *Chemical Reviews*, vol. 100, no. 7, pp. 2495–2504, Jul. 2000, doi: 10.1021/cr990099w.
- [306] J. J. Belbruno, “Molecularly Imprinted Polymers,” 2018, doi: 10.1021/acs.chemrev.8b00171.
- [307] B. Sellergren and A. J. Hall, *In Supramolecular Chemistry: from Molecules to Nanomaterials*. 2012.
- [308] A. Rico-Yuste and S. Carrasco, “polymers Molecularly Imprinted Polymer-Based Hybrid Materials for the Development of Optical Sensors,” 2019, doi: 10.3390/polym11071173.

- [309] H. Dilië *et al.*, “Label-Free Detection of Small Organic Molecules by Molecularly Imprinted Polymer Functionalized Thermocouples: Toward In Vivo Applications,” 2017, doi: 10.1021/acssensors.7b00104.
- [310] K. Betlem *et al.*, “Heat-Transfer Method: A Thermal Analysis Technique for the Real-Time Monitoring of Staphylococcus aureus Growth in Buffered Solutions and Digestate Samples,” 2019, doi: 10.1021/acsabm.9b00409.
- [311] D. Yongabi *et al.*, “Cell detection by surface imprinted polymers SIPs: A study to unravel the recognition mechanisms,” *Sensors and Actuators B: Chemical*, vol. 255, pp. 907–917, Feb. 2018, doi: 10.1016/J.SNB.2017.08.122.
- [312] M. Philips *et al.*, “Selective Microorganism Detection with Cell Surface Imprinted Polymers,” Wiley, 1996.
- [313] V. K. Gupta, M. L. Yola, N. Özaltın, N. Atar, Z. Üstündağ, and L. Uzun, “Molecular imprinted polypyrrole modified glassy carbon electrode for the determination of tobramycin,” *Electrochimica Acta*, vol. 112, pp. 37–43, Dec. 2013, doi: 10.1016/J.ELECTACTA.2013.08.132.
- [314] E. Mathieu-Scheers *et al.*, “Trace anthracene electrochemical detection based on electropolymerized-molecularly imprinted polypyrrole modified glassy carbon electrode,” *Journal of Electroanalytical Chemistry*, vol. 848, p. 113253, Sep. 2019, doi: 10.1016/J.JELECHEMA.2019.113253.
- [315] Y. Wu *et al.*, “Rapid recognition and determination of tryptophan by carbon nanotubes and molecularly imprinted polymer-modified glassy carbon electrode,” *Bioelectrochemistry*, vol. 131, p. 107393, Feb. 2020, doi: 10.1016/J.BIOELECHEMA.2019.107393.
- [316] X. Kan *et al.*, “Molecularly imprinted polymers based electrochemical sensor for bovine hemoglobin recognition,” *Sensors and Actuators B: Chemical*, vol. 168, pp. 395–401, Jun. 2012, doi: 10.1016/J.SNB.2012.04.043.

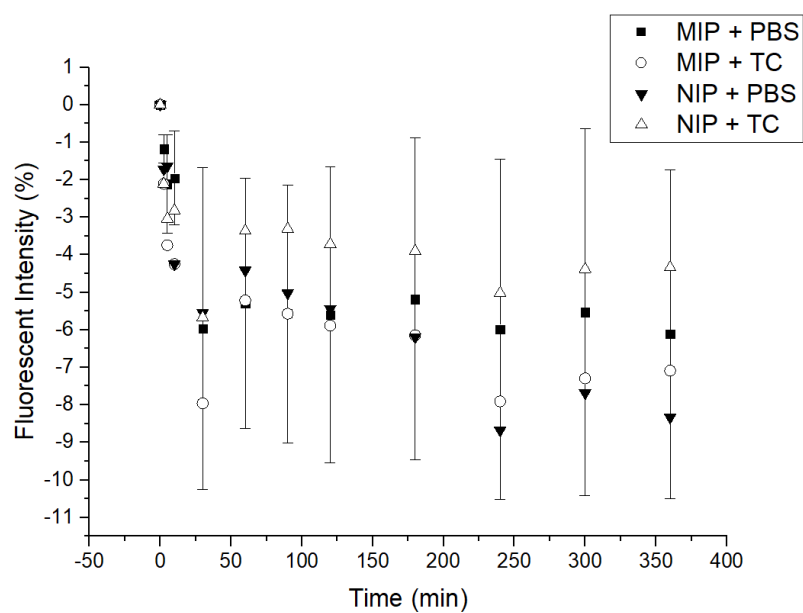
- [317] S. Menon, S. Jesny, and K. Girish Kumar, "A voltammetric sensor for acetaminophen based on electropolymerized-molecularly imprinted poly(o-aminophenol) modified gold electrode," *Talanta*, vol. 179, pp. 668–675, Mar. 2018, doi: 10.1016/J.TALANTA.2017.11.074.
- [318] T. Wang and C. Shannon, "Electrochemical sensors based on molecularly imprinted polymers grafted onto gold electrodes using click chemistry," *Analytica Chimica Acta*, vol. 708, no. 1–2, pp. 37–43, Dec. 2011, doi: 10.1016/J.ACA.2011.09.030.
- [319] R. A. S. Couto *et al.*, "Electrochemical sensing of ecstasy with electropolymerized molecularly imprinted poly(o-phenylenediamine) polymer on the surface of disposable screen-printed carbon electrodes," *Sensors and Actuators B: Chemical*, vol. 290, pp. 378–386, Jul. 2019, doi: 10.1016/J.SNB.2019.03.138.
- [320] V. M. Ekomo *et al.*, "Detection of Bisphenol A in aqueous medium by screen printed carbon electrodes incorporating electrochemical molecularly imprinted polymers," *Biosensors and Bioelectronics*, vol. 112, pp. 156–161, Jul. 2018, doi: 10.1016/J.BIOS.2018.04.022.
- [321] H. Zhang, G. Liu, and C. Chai, "A novel amperometric sensor based on screen-printed electrode modified with multi-walled carbon nanotubes and molecularly imprinted membrane for rapid determination of ractopamine in pig urine," *Sensors and Actuators B: Chemical*, vol. 168, pp. 103–110, Jun. 2012, doi: 10.1016/J.SNB.2012.03.032.
- [322] R. O. Kadara, N. Jenkinson, and C. E. Banks, "Characterization and fabrication of disposable screen printed microelectrodes," *Electrochemistry Communications*, vol. 11, no. 7, pp. 1377–1380, Jul. 2009, doi: 10.1016/J.ELECOM.2009.05.010.
- [323] J. S. Wood and L. H. Hartwell, "A dependent pathway of gene functions leading to chromosome segregation in *Saccharomyces cerevisiae*," *Journal of Cell Biology*, vol. 94, no. 3, pp. 718–726, Sep. 1982, doi: 10.1083/jcb.94.3.718.
- [324] L. Maringele and D. Lydall, "*EXO1* -dependent single-stranded DNA at telomeres activates subsets of DNA damage and spindle checkpoint pathways in budding yeast *yku70* Δ

- mutants,” *Genes & Development*, vol. 16, no. 15, pp. 1919–1933, Aug. 2002, doi: 10.1101/gad.225102.
- [325] D. Burke, D. Dawson, and T. Stearns, *Methods in Yeast Genetics: A Cold Spring Harbor Laboratory Course Manua*. 2000.
- [326] K. Betlem *et al.*, “Real-time analysis of microbial growth by means of the Heat-Transfer Method (HTM) using *Saccharomyces cerevisiae* as model organism,” *Physics in Medicine*, vol. 6, pp. 1–8, Dec. 2018, doi: 10.1016/J.PHMED.2018.05.001.
- [327] A. Yussuf, M. Al-Saleh, S. Al-Enezi, and G. Abraham, “Synthesis and Characterization of Conductive Polypyrrole: The Influence of the Oxidants and Monomer on the Electrical, Thermal, and Morphological Properties,” 2018, doi: 10.1155/2018/4191747.
- [328] E. P. Randviir, “A cross examination of electron transfer rate constants for carbon screen-printed electrodes using Electrochemical Impedance Spectroscopy and cyclic voltammetry,” *Electrochimica Acta*, vol. 286, pp. 179–186, Oct. 2018, doi: 10.1016/J.ELECTACTA.2018.08.021.
- [329] M. Zakhartsev and M. Reuss, “Cell size and morphological properties of yeast *Saccharomyces cerevisiae* in relation to growth temperature,” *FEMS Yeast Research*, vol. 18, p. 52, 2018, doi: 10.1093/femsyr/foy052.
- [330] P. K. Sharma *et al.*, “Synthesis and characterization of polypyrrole by cyclic voltammetry at different scan rate and its use in electrochemical reduction of the simulant of nerve agents,” *Synthetic Metals*, vol. 160, no. 23–24, pp. 2631–2637, Dec. 2010, doi: 10.1016/J.SYNTHMET.2010.10.016.
- [331] F. B. Piló *et al.*, “*Saccharomyces cerevisiae* populations and other yeasts associated with indigenous beers (chicha) of Ecuador,” *Brazilian Journal of Microbiology*, vol. 49, no. 4, pp. 808–815, Oct. 2018, doi: 10.1016/j.bjm.2018.01.002.

[332] L. R. Beuchat, "Media for detecting and enumerating yeasts and moulds," *International Journal of Food Microbiology*, vol. 17, no. 2, pp. 145–158, Oct. 1992, doi: 10.1016/0168-1605(92)90112-G.

Chapter 8- Appendix

Appendix A. MIP A fluorescent intensity study with ascorbic acid to act as a radical scavenger, showing significant percentage error



**Appendix B. Custom Python script for fluorescent analysis for quantification of Microscope data
(created by Matt Davies, PhD candidate, Newcastle University)**

```

## set the size (in pixels) of the analysis rectangle
box_size = (194,194) # (x_size, y_size)

## set the top left rectangle coordinate
background_coordinate = (000,000)

area_coordinates = [(300,800),(400,200),(400,400)]

## set the scale bar size in microns
scalebar = 500

## set the file to analyse
file = 'C:\Users\55131731\Desktop\Ollie Yr
3\Fluorescent
data\TiE\MIP3_3Layer_PBS.nd2'

## time between images in minutes
timestep = 2

#-----#

def main():
    nd2 = nd2reader.Nd2(file)
    plot_image(nd2, scalebar, area_coordinates,
box_size)

    region_vals = calculate_intensity(nd2,
area_coordinates, background_coordinate,
box_size)
    plot_timeseries(nd2, region_vals, timestep)
    titles = [' X ', *[f' Region {i} ' for i, _ in
enumerate(region_vals)], 'Average']
    print(*titles)
    for i, val in enumerate(region_vals):
        print(i, *val, val.mean())

def plot_timeseries(nd2, region_vals, timestep):
    intensity = region_vals.mean(axis=1)
    intensity_error= region_vals.std(axis=1)
    fig = plt.figure(figsize=(7,5), dpi=80)
    ax = fig.add_subplot(111)
    time =
np.arange(0,len(nd2)*timestep,timestep)
    for region in region_vals.T:
        ax.plot(time,region,
marker='o', c='grey', ls='none')
    ax.errorbar(time,intensity,yerr=intensity_error,
color='black', marker='o',

```

```

        ls='none',    capsizer=1,    label='All
regions')

    ax.set_xlabel('Time (min)')

    ax.set_ylabel('Summed Intensity (AU)')

    ax.spines['right'].set_visible(False)

    ax.spines['top'].set_visible(False)

    legend_elements = [mpl.lines.Line2D([0], [0],
marker='o', color='k', label='Averaged',
                                ls='none'),
                      mpl.lines.Line2D([0], [0],
marker='o', color='grey', label='Individual
Region',
                                ls='none')]

    ax.legend(handles=legend_elements)

    pass

def plot_image(nd2, scalebar, area_coordinates,
box_size):
    ## draw image

    img = nd2[0]

    fig = plt.figure(figsize=(7,5), dpi=80)

    ax = fig.add_subplot(111)

    fluor_cmap = LinearSegmentedColormap.from_list('my
cmap',['black','purple'])

    ax.imshow(img,cmap=fluor_cmap,vmin=0)

    ## Set boxes to draw on image

    rect = patches.Rectangle(background_coordinate,
*box_size,
linewidth=2,edgecolor='r',facecolor='none')

    bboxes = [rect]

    for corner in area_coordinates:
        rect = patches.Rectangle(corner,*box_size,
linewidth=2,edgecolor='w',facecolor='none')

        bboxes.append(rect)

    bboxes = mpl.collections.PatchCollection(bboxes,
match_original=True)

    ax.add_collection(bboxes)

    ax.xaxis.tick_top()

    ax.xaxis.set_label_position('top')

    ax.set_xlabel('X (pixels)')

    ax.set_ylabel('Y (pixels)')

    pass

def calculate_intensity(nd2, area_coordinates,
background_coordinate, box_size):
    region_vals = np.zeros((len(nd2),
len(area_coordinates)))

```

```

for i, image in enumerate(nd2):

    bg_x, bg_y = background_coordinate

    ## image is transposed so y axis is first
dimension

    bg_region =
image[bg_y:bg_y+box_size[1],
bg_x:bg_x+box_size[0]]

    for j, corner in
enumerate(area_coordinates):

        x, y = corner

        region = image[y:y+box_size[1],
x:x+box_size[0]]

        region_vals[i,j] = region.sum() -
bg_region.sum()

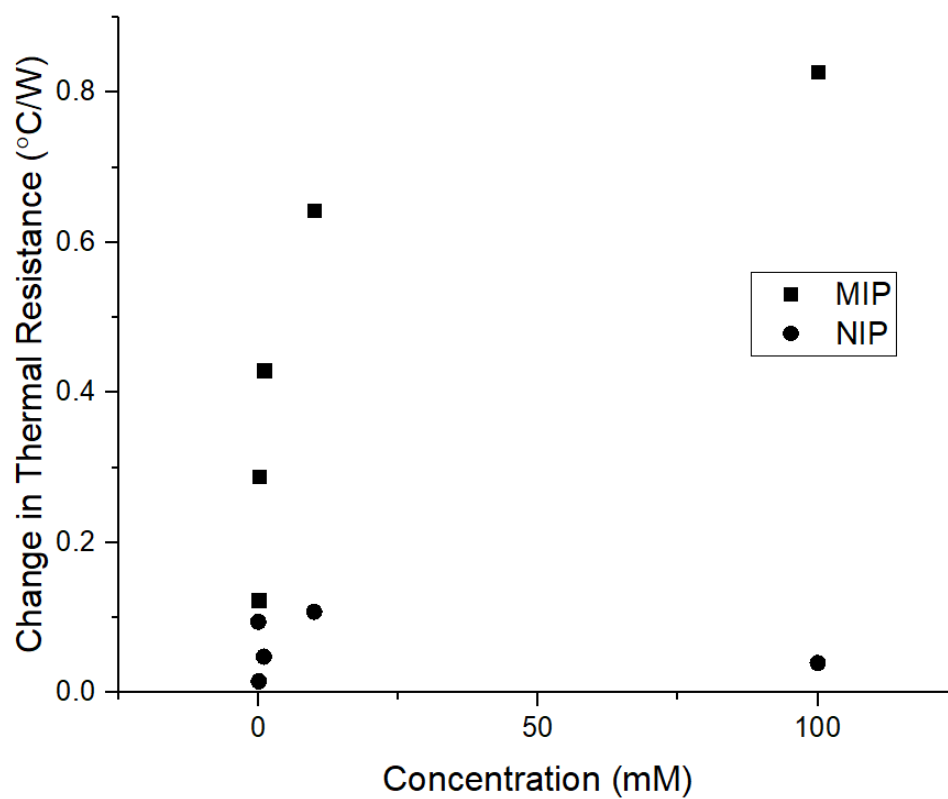
    return region_vals

if __name__ == '__main__':

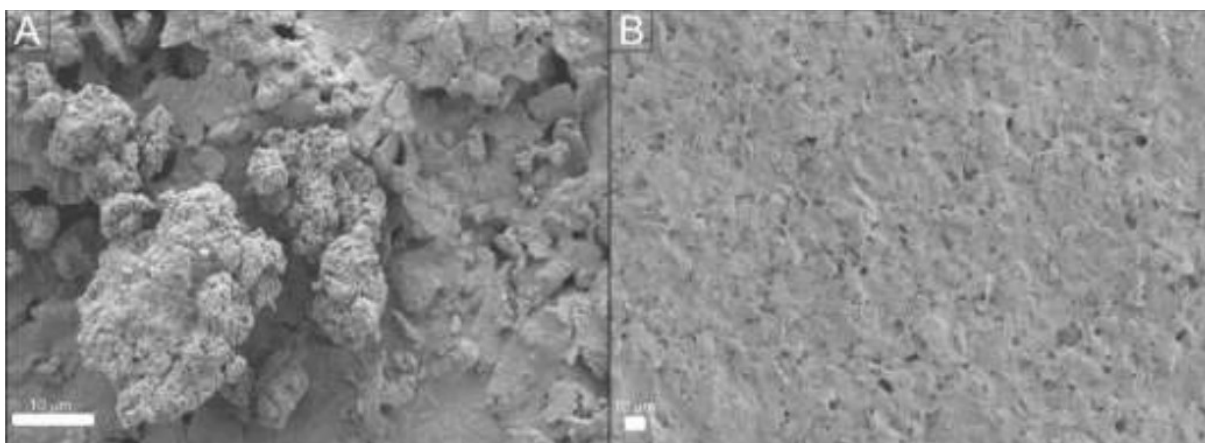
    main()

```

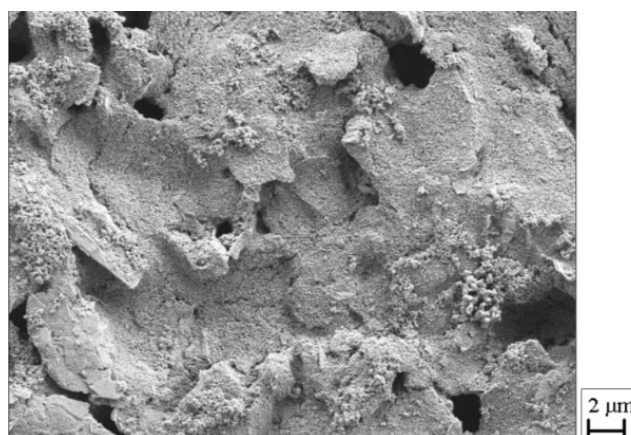
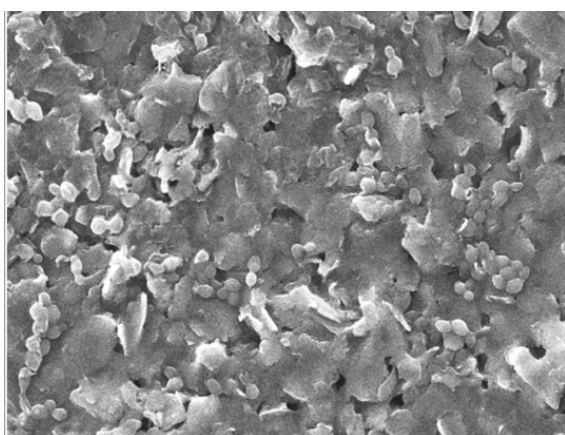
Appendix C. Repeat dose response curve of HTM data for MIP T and NIP T with tetracycline solution injections



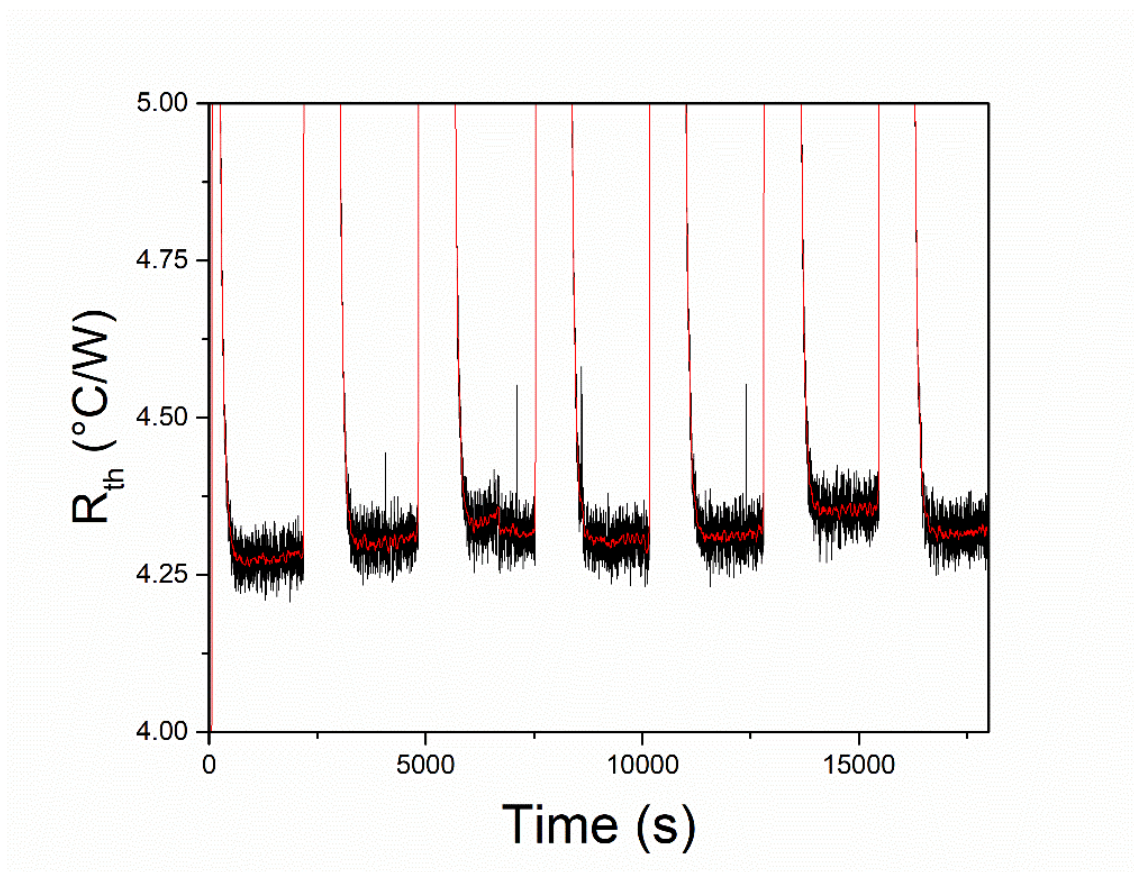
Appendix D. SEM image (2000× magnification) of MIP 2 microparticles immobilized onto an SPE using polypyrrole. (B) SEM image (1000× magnification) of thin film of polymer made directly on an SPE.



Appendix E. After polymerisation (1000x zoom), there was clear presence of the yeast on the SPCEs. Different washing strategies were employed, where washing twice with hot water led to full removal of yeast on the surfaces. Washing once was not sufficient whereas washing with organic solvents, such as methanol, led to damaging the polymer layer.



Appendix F. A MIP-modified electrode was exposed to suspensions with increasing concentrations of yeast (from 10^2 to 10^6 CFU/mL) in water. However, at elevated temperature no significant increases were found.



**Approaches to the Rational Design of Molecularly Imprinted Polymers
Developed for the Selective Extraction or Detection of Antibiotics in
Environmental and Food Samples**

Oliver Jamieson, Francesco Mecozzi, Robert D. Crapnell, William Battell, Alexander Hudson, Katarina Novakovic, Ashwin Sachdeva, Francesco Canfarotta, Carmelo Herdes, Craig E. Banks, Helena Snyder, Marloes Peeters

First published: 25 March 2021

<https://doi.org/10.1002/pssa.202100021>

Abstract

The World Health Organisation (WHO) reported antimicrobial resistance (AMR) as a global threat comparable to terrorism and climate change. The use of antibiotics in veterinary or clinical practice exerts a selective pressure, which accelerates the emergence of antimicrobial resistance. Therefore, there is a clear need to detect antibiotic residues in complex matrices, such as water, food, and environmental samples, in a fast, selective, cost-effective, and quantitative manner. Once problematic areas are identified, can extraction of the antibiotics then be carried out to reduce AMR development. Molecularly imprinted polymer (MIPs) are synthetic recognition elements produced through the biomarker of interest being used as a template in order to manufacture tailor-made ligand selective polymeric recognition sites. They are emerging steadily as a viable alternative to antibiotics, especially given their low-cost,

superior thermal and chemical stability that facilitates on-site detection, simplified manufacturing process, and avoiding the use of animals in the production process. In this paper, the authors critically review literature from primarily 2010–2020 on rational design approaches used to develop MIPs for sensing and extraction of antibiotics, providing an outlook on crucial issues that need to be tackled to bring MIPs for antibiotic sensing to the market.

1 The Need for Detection of Antibiotic Residues

1.1 Antimicrobial Resistance (AMR) and Its Acceleration through Water Contamination

The World Health Organization (WHO) predicts ten million annual deaths, globally, due to antibiotic-resistant infections, by 2050.^[1] The rise in antimicrobial resistance (AMR) bacteria is therefore considered a global threat. Cassini et al.^[2] studied deaths linked to drug-resistant infections in Europe and concluded that $\approx 700\,000$ infections in 2015 were related to resistant bacteria, of which 5% were fatal. Similarly, a study by Ventola^[3] demonstrated that two million patients in the USA developed hospital-acquired infections (HAIs), of which 99 000 cases proved fatal, a significant proportion of which were also caused by resistant bacteria. In addition to their impact on mortality, these resistant bacteria also pose a serious financial burden. Misurski et al.^[4] demonstrated that incorrect antibiotic prescription was estimated to be a \$211 million burden, per year, in the USA alone. These costs are ascribed to prolonged hospitalization, increased morbidity, greater requirement for critical care support, delayed return to the workforce, and consequent economic impact associated with reduced productivity. Moreover, recent events have led to concerns about a new surge in AMR due to the use of antibiotics in patients with COVID-19.^[5] While antibiotics are ineffective against viruses, they can be used in patients with confirmed COVID-19 to prevent or treat secondary bacterial infections: an early study from China showed that secondary infections and HAIs were present in half of all deceased COVID-19 patients.^[6] Surprisingly, no current inclusions of

antimicrobial stewardship programs (ASPs) in disaster planning or emergency response preparedness efforts have been legislated, but there is a strong drive from the medical and scientific community to integrate ASPs into disaster planning and appoint stewards in a more formal role after the COVID-19 outbreak.^[7]

Another concerning issue is the possibility of antibiotics leaching into water systems, via the effluents of the pharmaceutical industry, agriculture, and hospitals (**Figure 1**). However, these routes are all critical to the continuation of modern-day living so a solution is needed that does not impact them. Behera et al.^[8] studied the introduction of pharmaceuticals, including antibiotics, into the environment in an industrial city in South Korea. Among the antibiotics screened, standard water treatments achieved antibiotic removal between only 10 and 70%. Sulfamethazine was found to have a removal efficiency below 30%, suggesting that the majority still entered further waterways. Conversely, caffeine, a common contaminant and a standard indicator molecule, showed a 99% removal efficiency under the same conditions. This



exemplifies how using caffeine as an anthropogenic marker^[9] may therefore yield false confidence in current purification processes.

Figure 1 Routes of entry of antibiotics into the environment. Green arrows displaying antibiotic removal from the environment, red arrows showing the entry routes of antibiotics, and orange arrows explaining that extraction methods are not fully efficient at antibiotic removal.

Effluents from modern-day infrastructure are not the only route of antibiotics into the water systems. Alternative entry routes include livestock feed and excrement. Watanabe et al.^[10] led a study into the waste outputs of two dairy farms in the USA. It was found that monensin, a polyether antibiotic commonly found in animal feeds, leached into ground water assumedly due to relatively high monensin concentrations found in manure. Tasho et al.^[11] highlighted veterinary antibiotic use in livestock and the resulting antibiotic residue in livestock manure, which can be as high as 216 mg L^{-1} . Given that 0.9% of farming worldwide is conducted organically,^[12] which equates to a significant amount of natural fertilizer use, the critical role of agricultural practices in the leaching of antibiotics into the environment is highlighted.

Watkinson et al.^[13] traced the journey of drinking water all the way back to hospital effluent, evaluating the concentration of 28 antibiotics at different stages in Southeast Queensland, Australia. Some antibiotics were detected at concentrations of up to $64.0 \text{ } \mu\text{g L}^{-1}$ in Waste Water Treatment Plant (WWTP) influent, compared with the maximum concentration in the effluent being $3.4 \text{ } \mu\text{g L}^{-1}$. It was shown that rivers having no effluents from WWTPs in their watershed have a significantly lower residual antibiotic concentration, demonstrating the broader impact of hospital pharmaceutical waste. A study based in Ter River, Spain, by Rodriguez-Mozaz et al.,^[14] incorporated a wider range of antibiotics, showing that fluoroquinolones had the highest residual concentration in hospital effluents up to 14.4 mg L^{-1} , which is most likely due to their enhanced stability compared with other common antibiotics. Both studies show significant presence of antibiotics in water systems from developed countries, portraying that even countries

with modern wastewater treatment infrastructure are being impacted by antibiotic presence in water systems.

The European Water Framework Directive is a legislative department set up in 2000, to ensure water safety. Carsten von der Ohe et al.^[15] aimed to improve the existing European Water Framework Directive by classifying chemicals of critical importance in terms of their potential to cause harm. With more in-depth understanding of the harm AMR is causing, improvements to the legislation can lead to more appropriate restrictions on antibiotic presence in the environment. Despite this, Carvalho et al.^[16] subsequently noted the lack of relevant regulations regarding the same issue in the European environmental water quality standards. It is therefore of critical concern that carriers of antibiotics, such as meat or milk, and common water micropollutants are regulated; however, there remains limited scrutiny of antibiotics in water systems; therefore, a system to accurately measure and follow antibiotics from a variety of media, specifically and critically including aqueous media, must be agreed upon.

The current lack of antibiotic regulation and therefore a need for detection within Europe's waterways could have dire consequences and certainly contribute to exacerbating AMR in the future. Hence, there is a need to identify and more closely monitor waste streams that may contain antibiotics and ultimately enforce new regulations for their processing and removal. However, these testing and analyses methods must be cost effective and financially viable if they are to be broadly implemented.

1.2 Limitations of Current Antibiotic Detection Platforms in Different Media

Extensive efforts are required for the research and development of novel detection systems for different families of antibiotics and to be able to do so in different media. In a study, Khaskheli et al.^[17] displayed a procedure for the screening of β -lactam antibiotics in milk using a qualitative field disc assay. Despite encouraging results, the biggest drawbacks of the systems

were 1) the 24 h turnaround time and 2) the extensive sample preparation required. The first issue was originally addressed by Knecht et al.,^[18] with the use of an automated microarray for simultaneous detection of ten antibiotics in milk; however, this system needed the use of costly infrastructure and apparatus. Wang et al.^[19] expanded the scope to meat and aquatic products; after these were minced and extracted, ultraperformance liquid chromatography was used to study residual levels in the range of 0.05 ng g⁻¹ in meat and 0.2–5.0 ng mL⁻¹ in milk. A more detailed review of antibiotics detection was released by Pikkemaat.^[20] From this work, and the studies provided beforehand, it emerges that the most common analysis technique in the first decade of the 2000s involved microbial screening assays: these are cost effective, despite being time-consuming, and do not offer quantitative results.

Baquero et al.^[21] gave an oversight as to the main ways in which antibiotics are detected in water samples. Depending on the analyte of interest, common detection systems include electrophoretic and chromatographic techniques as well as voltammetry and amperometry detection systems. This study shows that several antibiotics can be accurately monitored in a wide range of media and by different detection methods. However, all these techniques required 1) a lab environment, 2) time-consuming procedures, and 3) skilled personnel. Smith et al.^[22] used a commercially available test kit that was modified to enable detection of antibiotics in water systems, trying to optimize the detection. The study provided a qualitative test for antibiotics but lacked the critical quantification. While these in-field testing kits are of promise due to the rapid and on-site detection of antibiotics that will yield more accurate information and simplicity of operation even for nontrained users, further development is still required to enable crucial quantification.

Colorimetric bacterial inhibition approaches and lateral flow immunoassays are common for on-site detection of antibiotics. However, colorimetric bacterial inhibition requires large sample

volumes and is limited by poor sensitivity and complex user protocols, whereas lateral flow immunoassays require user intervention for quantifying results.^[23] All these limitations can be worked around with the use of molecularly imprinted polymers (MIPs).

1.3 Potential of Using MIPs for Antibiotic Detection and Extraction

MIPs are custom-built, synthetic recognition sites, designed for a specific target molecule.^[24] These synthetic receptors can be used in place of antibody–antigen, enzyme–substrate, or ligand–receptor interactions and indeed can be fabricated to have similar, if not better, affinity and selectivity than their naturally occurring counterparts^[25] and crucially when no naturally occurring antibodies exist. The synthesis of MIPs can be accomplished in nonspecialist laboratories, with nondedicated equipment, and is often seen as a relatively simple process, with only little formal training in polymer chemistry required. However, its simplicity might be misleading and can mask the fact that it involves multiple and often interdependent variables. The ways in which these affect and change the properties of the resulting polymers are, in fact, quite complex and require a good understanding of molecular recognition theory, thermodynamics, and polymer chemistry.^[26]

The concept of MIPs and their potential usefulness in multiple fields of scientific research have been gaining significant interest since the early 1990s.^[27-29] Despite their obvious benefits over naturally occurring recognition biomolecules, particularly their increased stability and specificity, as well as their low cost, ease of production, and ability to target molecules for which natural receptors do not exist,^[30, 31] they are yet to garner widespread and commercial success.

MIPs were found to be highly suitable first for application in chromatography,^[32-34] especially liquid chromatography.^[35, 36] Curti et al.^[37] developed the first truly functional silica-derived-imprinted polymer systems, which subsequently became a well-established technique in the

chromatography field. Significant advances in imprinting techniques and new synthetic methodologies, along with their excellent recognition specificity and structural predictability, make them a valuable alternative in the recognition systems landscape. This in turn has opened their potential use to a wide variety of applications.^[38] After the development of a noncovalent fabrication method by Mosbach and coworkers^[39], and modifications thereof, the use of these synthetic ligands has continued to grow. This is evident by the exponential increase in research papers over the past 20 years.

To date the use of MIPs has mostly been limited to academic research. Although MIPs have found their way into several commercial markets (**Table 1**), with further exploration, they could be implemented even further. Whitcombe and coworkers^[40] stated that MIPs could seize 1–3% of the separation techniques market, worth \$1.19 billion, based predominantly in the chromatography column sector alone.

Table 1. Summary of commercial MIPs that have been developed

| MIP | Company | Description |
|--|----------------------|--|
| MIP cartridges for extraction ^[224] | Acros (SupelMIP) | SPE of 14 aminoglycosides (environmental contaminants) in foodstuffs, e.g., meat, milk, and fish |
| Epitope-imprinted MIPs ^[227] | Aspira Biosystems | Specific and selective uptake of micro-organisms |
| MIPs as model drug targets ^[228] | Semorex Inc. | Incorporation into drug discovery, being used to test drug leads by acting as synthetic drug targets |
| Biotage AFFINILUTE MIP columns | Biotage | Incorporation of MIPs into Biotage columns to afford significant sample clean-up |

| | | |
|-----------------------------|-----------------|--|
| High-affinity nanoparticles | MIP diagnostics | High-affinity nanoparticles (nanoMIPs) are produced for extraction and sensing |
|-----------------------------|-----------------|--|

MIPs can be easily synthesized by bulk polymerization, ground, mechanically sieved, and packed in a column.^[41] This method, though crude, is simplistic and versatile. More specifically, monolithic MIP columns have been later prepared directly inside stainless steel columns or capillary columns to solve the problems of nonhomogeneousness of the binding sites and particle size.^[42, 43] High performance liquid chromatography (HPLC) has often seen the use of MIPs as a stationary phase in the racemic resolutions of several species^[44] including amino acid derivatives^[45, 46] and drugs,^[47, 48] though often excessive tailing and peak broadening are the limiting factors for their use and commercialization for this purpose.^[49] Another important area of analytical chemistry, where imprinted polymers have established themselves, is solid-phase extraction (SPE).^[49-54] Sigma-Aldrich and Biotage sell MIPs for the highly selective extraction of trace analytes from complex matrices.^[55-58]

Use in commercialization of MIPs has been limited as their integration into the sensor platforms is not straightforward. In earlier development stages, MIP microparticles prepared by free-radical polymerization were lacking in affinity and the grafting-on and in situ synthesis techniques were not as refined as they are now.^[59-62]

1.3.1 Synthesis of MIPs

A typical MIP synthesis protocol contains a template, one or more functional monomers, a crosslinker monomer, a polymerization initiator, and a solvent.^[63] **Figure 2** shows a simplistic schematic of the molecular imprinting principle.

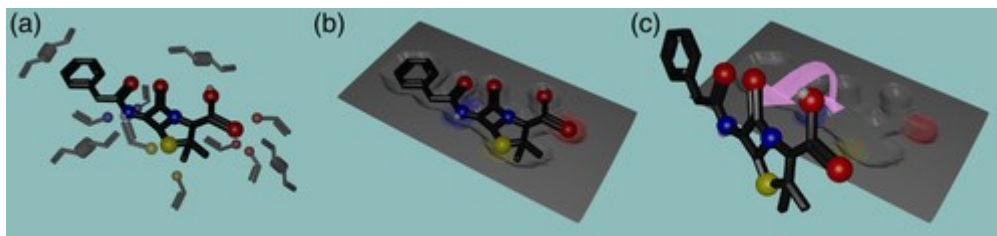


Figure 2 The several steps of molecular imprinting with a) precomplex with the example template of penicillin G surrounded by crosslinker and generic acrylate functional monomers, b) polymerized MIP, and c) amoxicillin molecule extracted, leaving an empty cavity to be used for rebinding.

However, the challenge of designing and synthesizing an MIP involves the selection of each of these variables: 1) monomer(s), 2) crosslinker(s), 3) solvent(s), and 4) initiator and the selection of initiation method along with the duration of the polymerization. Determination of the appropriate monomer(s) and the optimal stoichiometric ratios of each of the components often requires extensive empirical studies and testing to maximize target recognition.^[64] The most common method of fabrication is known as self-assembly or noncovalent imprinting, often chosen for its ease and flexibility. It requires only a small number of synthesis steps, is compatible with a vast majority of target molecules, and template removal is facile post fabrication. The template and the monomers interact through noncovalent interactions and polymerization takes place with the system (interaction between functional monomer and template) at an equilibrium, although it depends on the choice of reagents and the conditions (temperature, solvent) applied. Interactions at interplay involve hydrogen bonding, ionic interactions, Van der Waals forces, and π - π interactions. MIPs are often synthesized (and optimized) in organic solvents, whereas it has been established that binding characteristics are highly dependent on the solvent. In particular, binding in water is complicated as target

molecules can bind in a specific manner to the MIP matrix due to hydrophobic effects.^[65] Another drawback is that generally an excess of functional monomers has to be added to increase the chance of binding, which leads to various configurations and heterogeneous binding site distributions.^[66] The nonhomogeneity of the binding sites in MIPs resulting from noncovalent imprinting is comparable with that of polyclonal antibodies.^[67] This might still be useful when a family of related compounds needs to be analyzed, especially if it is a class of antibiotics. If the MIP would be able to rebind to them, especially when a screening is sufficient and a very precise measure is not required, it would have a sizeable advantage over a biosensor that would have to include different antibodies for each analyte. However, though these types of MIPs can work well within a laboratory research setting, their sensitivity, accuracy, and limits of detection are not suitable for commercial devices.

A solution to the issue earlier is represented by the covalent method: the functional monomers are chosen following the criteria that they are able to form a reversible covalent bond with the template, which will be cleaved after the polymerization process, allowing for the template to be recovered. Covalent fabrication methods yield a homogeneous population of binding sites and minimize nonspecific sites, with selectivity comparable with monoclonal antibodies.^[25, 68, 69] Often, the aforementioned reversible bonding uses boronate esters, ketals/acetals, and Schiff bases. Readily reversible condensation reactions are typically chosen to cleave the covalent bond responsible for the interaction, for its extraction to be successful. However, this type of polymerization introduces an additional step in the fabrication process. Moreover, the covalent strategy poses a major challenge as the covalent bond leads to slow dissociation,^[40] which limits its practical application, particularly in the area of sensing. Dummy templates, which are very similar to the target molecule, in size and shape but, importantly, not present in the system, are a useful workaround for this issue.

Certain hybrid approaches have emerged, one of which is known as semicovalent imprinting.^[70] Semicovalent imprinting exploits covalent interactions to form the prepolymerization complex between functional monomers and template; however, rebinding to the MIP produced will be solely due to noncovalent interactions that, by nature, will occur with faster kinetics. Another similar imprinting technique is hierarchical imprinting, which uses scaffold molecules, which eventually are eliminated, to produce pores that act as microreactors. This approach is hence termed “sacrificial spacer” method and was first introduced by Klein et al.,^[31] but it has since been used in multiple areas of research. This work demonstrates the preparation of MIP shells, an example of the sacrificial support approach, with fast absorption kinetics (≈ 10 min) for detection of the antibiotic enrofloxacin (ENR), as shown in **Figure 3**, in fish samples, with limits of detection well below the legal maximum residual level.

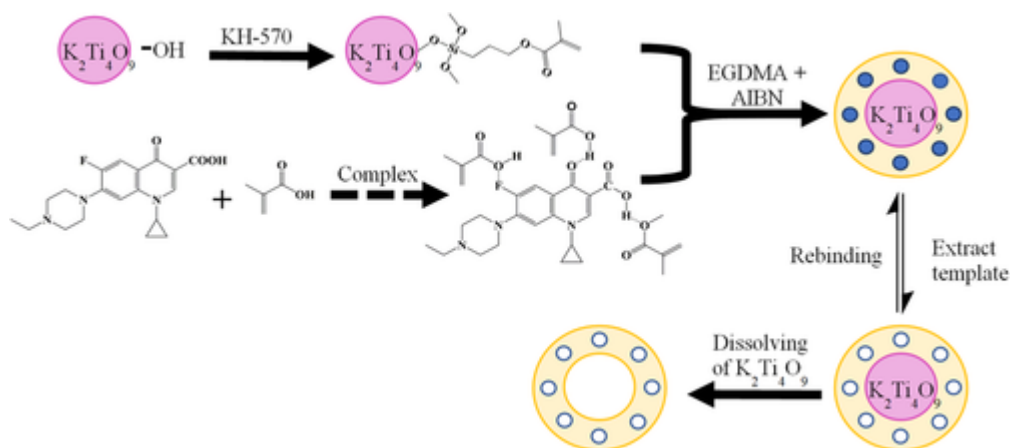


Figure 3 Preparation of hollow MIPs using covalent and noncovalent imprinting for an amino acid sequence, demonstrating the “sacrificial spacer” method using $K_2Ti_4O_9$ as a spacer molecule. Adapted with permission.^{31]} Copyright 1999, Wiley-VCH.

The $K_2Ti_4O_9$ matrix was chosen because of its nontoxicity, low cost, and easy removal. Silica is indeed another popular choice as sacrificial support as the polymers can be embedded into the pores of the particles. The group of Moreno-Bondi developed MIPs that were able to recognize six cephalosporins below the maximum residual levels set for these antibiotics in raw milk.^[71] Silica etching is a more time-consuming process and also involves harsh chemicals, as the particles were treated with an ammonium hydrogen difluoride mixture for 24 h. A similar approach, where silica beads were functionalized with MIPs according to the procedure by Yilmaz et al.,^[72] was used to synthesize selective recognition elements for structurally related penicillins. This antibiotic family base structure, 6-aminopenicillanic acid, acts as a dummy template enabled to detect the entire class of target analytes from milk with high recovery rates.

Another dominant restriction to MIP synthesis is that only a limited number of functional monomers are suited for this task. Methacrylic acid (MAA) was already used by Mosbach et al.^[73] and remains to this date the most common one, given its ability to serve as H-bond donor and acceptor. Lately, several approaches have been attempted where combinations of functional monomers have been used at the same time to enhance binding affinity.^[63, 74-78] Although a wide range of amino acids can be used, several restrictions reduce their availability. While this is certainly interesting, it exposes the fact that only a limited number of functional monomers is still available to this day.

The approach of using a “dummy” template when discussed earlier is advantageous as it would not involve working with target molecules that are expensive, dangerous, unstable, or toxic,^[79, 80] while also allowing to detect classes of compounds which can be of particular

interest in the case of antibiotics. Many successful cases of epitope imprinting have already been reported,^[81, 82] as well as computational simulations that use molecular modelling^[83, 84] to select the epitope that yields the highest specificity.^[85] The recent COVID-19 outbreak has triggered the interest in the epitope approach, considering one could imprint with antigens of the virus or particles with similar size and shape as the virus.

The known difficulties in extracting the template led to a problem known as template leaching, which might interfere with the analysis of a given target. While the extraction of residual template molecule is more exhaustive after every use, it might be possible to avoid it with the use of a dummy template.^[86] However, this leads to less-selective binding cavities as a major drawback.

A common drawback of MIPs is the difference in sensing performance between lab testing, when samples are spiked with the target analyte, and field testing, when a complex matrix is used. Often, even when state-of-the-art biosensors are utilized, the sample is pretreated and concentrated to avoid the interference of several other components. Interestingly, often the separation and removal of unwanted, interfering analytes from a solution is achieved via the use of MIPs in chromatographic methods, as mentioned previously. Therefore, a more complex sensor, first using a variety of MIPs in a separation procedure, prior to MIPs sensing of the analyte, may resolve the aforementioned problem.

Even with the drawbacks mentioned earlier, noncovalent imprinting, given the reduced number of steps and the ease of template extraction, is often the most widely used method of MIPs fabrication during the development of new sensors. Although sometimes less specific than other MIP methods, specificity of the binding sites can be increased via a low-temperature, light-induced polymerization process. The synthetic methodology, in contrast, can be chosen depending on the destination of use of the polymer; whereas monolith synthesis and consecutive

grinding offers a very simplistic approach, and its use is destined to be abandoned in favour of those able to yield more homogeneous binding sites and a better yield. In the future, methods that will also ease scalability such as MIP beads, membranes, in situ-prepared monoliths, surface imprinting, and molecularly imprinted monolayers will likely be preferred, as they ease the rebinding kinetics and offer further improvement in the homogeneity of the binding sites.

2 Rational Design of MIPs for Antibiotics

2.1 Computational Modeling

As mentioned previously, determining the correct functional monomer, crosslinker, and solvent for the chosen template is one of the most important considerations when approaching MIP design and often the most time- and resource-consuming task, which is not eased by the availability of a considerable amount of these components. The experimental optimizations in both type and ratio may require the time-consuming fabrication of many imprinted polymers, whose difference in composition only slightly varies from each other, to obtain the most specific cavities. While this might be a big hindrance in terms of experimental work, such a task lends itself to the use of rational design through computational modeling, offering substantial advantages in both time and cost to the experimental counterpart.^[87] The majority of computational modeling in relation to MIP design is centered around the prepolymerization complex. The nature of these interactions is a key step in obtaining high-affinity binding sites. With the use of varying computational techniques, these interactions can be investigated and optimized.^[88]

While the adoption of simple computational methods toward MIP design was first seen toward the end of the 1990s,^[89] their application toward direct rational design was not fully acknowledged until work by Piletsky et al.^[90] This work utilized monomer screening, similar to experimental combinatorial screening, to predict the correct choice of monomer. This

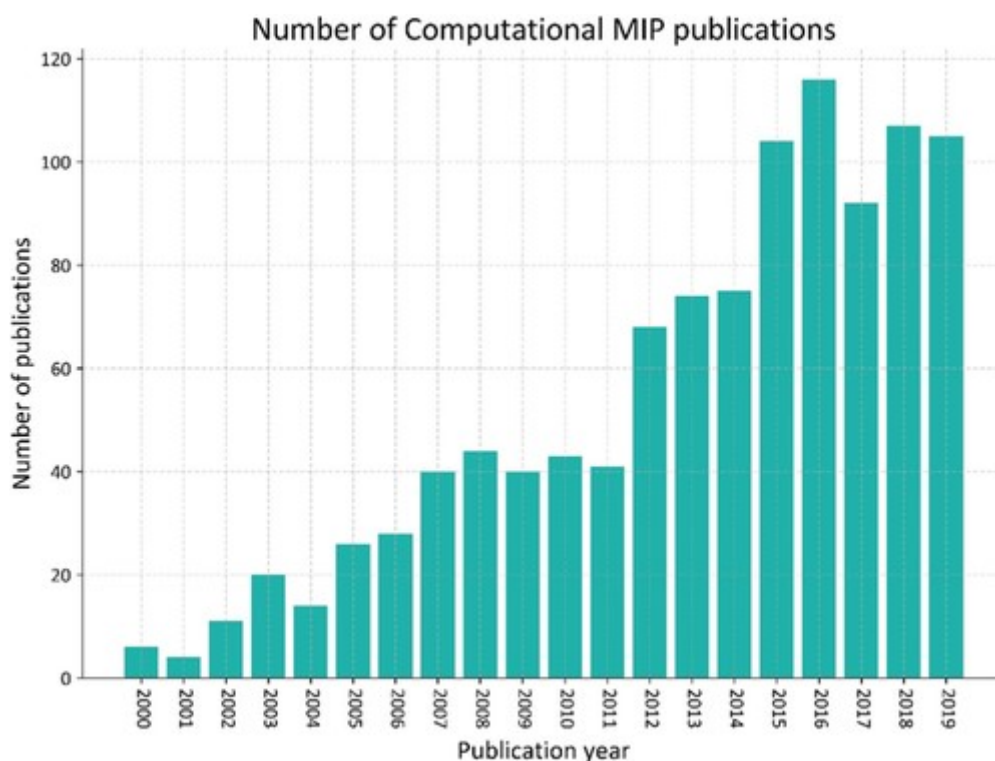
demonstrated the potential power of computational software for monomer selection. This work, besides many others, considers thermodynamic interactions between template and functional monomer. When the computational program shows increased stability of these interactions, the quality of the template-specific cavity being produced experimentally is usually improved.^[91] These energetics-based template-monomer studies are characterized by the determination of binding scores (Equation (1)), comparisons of which identify stronger interactions.

Equation 1: The binding energy/score (ΔH_B) between a template and functional monomer based on heat of formation (ΔH_f).

$$\Delta H_B = \Delta H_f \text{ Final complex} - (\Delta H_f \text{ Monomer} + \Delta H_f \text{ Template})$$

(1)

The energy difference between an independent template and a monomer compared with the final complex, template, and monomer bound by a new bond indicates the strength of this newly formed bond. There has been a considerable decrease in cost and increase in computing power available over the past 20 years. Not only has this increased the number of papers including rational MIP design, but it has also led to the development of more advanced techniques. A search of the available literature (Web of Science) shows a sharp increase in the number of



papers since 2000 (**Figure 4**).

Figure 4 Representation of the increased research in the field via the number of publications including computational methods in MIP design between 2000 and 2019. The data obtained through Web of Science using the keywords “Molecularly Imprinted Polymer,” “MIP,” and “Computational.”

Quantum mechanical (QM) techniques, namely, semiempirical methods such as density functional theory (DFT), have become more widespread. QM-based methods offer a more

advanced approach to predicting molecular energies. Such energies are calculated through the use of electronic structure-based techniques, allowing for determinations of interaction energies as well as structural predictions. For MIP design, QM methods are mainly used in monomer screening approaches and offer a more accurate method for determining energies for use in Equation (1).

While many studies consider only template–monomer interactions, many others have investigated this further with more in-depth structural analysis, considering not only changes in ratios but also interactions of both crosslinker monomers and solvent. Again, QM methods have been used in this area, considering crosslinker interactions to the template; however such techniques are still computationally expensive and limited to only a few molecules. Molecular mechanics (MM) and molecular dynamics (MD) are commonly implemented when a more dynamic system is wanting to be defined, with both solvent and larger systems able to be represented. MD techniques allow these interactions to be investigated over time, analyzing the motion of individual molecules. MM focuses on the observed properties of these molecules, with bond lengths, angles, and dihedrals along with nonbonding interactions considered. Most commonly, these two methods are used in combination.

Specifically, in relation to computational rational design for antibiotics, there have been several papers offering many different techniques outlined previously. A relatively recent paper by Kong et al.^[92] investigated norfloxacin-imprinted polymers using an MD--based approach. They considered changes in the ratio of functional monomer (MAA) and crosslinker (EGDM) while keeping the solvent (acetonitrile) constant. Computational analysis was completed using radial distribution functions (RDF), which allow for two specific atom pairs to be analyzed as a system interacts throughout a simulation. A ratio of 1:8:40 (template: monomer: crosslinker) produced the best pre-polymerization interactions, namely, the carbonyl to alcohol of

norfloxacin to MAA. The experimental rebinding studies also supported this particular polymer composition ratio, with the computationally predicted one offering greater rebinding and specificity than the other MIPs analyzed.

The majority of papers on the subject, however, use the quantum mechanics-based approach, specifically for monomer selection. This is mainly due to the accuracy of the energies predicted, but also the relative speed and ease when determining template-functional monomer bonds in vacuum. Again, they use semiempirical methods, mostly DFT, to determine the energies required for Equation (1). Such work has been completed on the antibiotics norfloxacin,^[93] ciprofloxacin,^[93, 94] ENR,^[95] and tetracycline.^[96] The studies found that the energies derived computationally were consistent with the experimental data produced and that the binding scores generated correlated with the experimental rebinding. The nature of antibiotics, with their relatively small size and presence of multiple, accessible functional groups, makes them a good candidate for computational modeling, as a wide range of techniques can be applied to them, depending on the requirements. Previous work in the area has shown good support for this, with complimentary computational and experimental data.

The rational design of MIPs through computational methods is still a growing area of research, with varying approaches and more advanced techniques being developed since its establishment in the early 2000s. Such methods were applied depending on the research, whether that were simple functional monomer predictions using QM or more in-depth structural analysis utilizing MD. Already, with many papers showing the ability for strong predictions, the application of such aided design looks set to become commonplace in future MIP production.

2.2 NMR Techniques Aiding MIP Production

NMR is an essential technique for structure determination, for a wide range of molecules. The plethora of techniques associated with proton and carbon NMR, which allows investigating

spatial and electronic interactions between different nuclei, can offer very detailed structural information even in the case of complex molecules. MIPs are composed of crosslinked and macroscopic chains, which complicate the characterization due to their intractable and insoluble nature. A pioneering NMR study on MIPs was reported by Sellergren, Lepisto, and Mosbach.^[97] Following a ¹H-NMR study, combined with a chromatographic technique, involving titration of the print molecule (phenylalanine anilide) with carboxylic acid, it was found that the results were consistent with the existence of multimolecular complexes by means of electrostatic and hydrogen-bonding interactions.^[97]

NMR has been mostly used to determine the extent of the template to functional monomer association equilibrium in the prepolymerization stage; the shift of the relative signals, compared with those of the template and monomer alone, can determine the extent of the interaction. Wang et al. used NMR to identify the best template-to-functional monomer ratio,^[98] a procedure that is often very time-consuming, for the preparation of MIPs for the extraction of a valuable compound. The signals of the protons involved in hydrogen bonding and that of the adjacent carbon were used to gauge the strength.

A study by Mattos dos Santos et al. reported on the synthesis of MIPs targeting tegafur (an anticancer 5-fluorouracil prodrug) and used ¹H-NMR titration to study solution association between tegafur and 2,6-bis(acrylamido)pyridine (BAAPy).^[99] This confirmed the formation of a 1:1 complex of template and functional monomer, in MIPs being prepared using stoichiometric imprinting. Interestingly, an affinity constant of $574 \pm 15 \text{ m}^{-1}$ in CDCl_3 was calculated using a previous work by Fielding, who reviewed the topic with a section dedicated to diffusion experiments.^[100] Hydrophobic effects and their contribution to the selectivity of the resulting MIP were investigated with NMR spectroscopy by O'Mahony et al. to identify the interactions occurring in the prepolymerization mixture.^[101]

Sánchez-González et al. used $^1\text{H-NMR}$ and, importantly as it represents a novelty, nuclear overhauser effect (NOE) to study the prepolymerization interaction between the cocaine (COCH) template and the functional monomers MAA and ethylene dimethacrylate; in particular, 1D selective NOE experiments were conducted to assess MAA-COCH and EDMA-COCH hydrogen-bonding interactions, which were contextually confirmed by *in silico* studies.^[102]

Commonly, the other time-consuming step is the quest to identify the most appropriate functional monomer. Konishi and coworkers addressed this using $^1\text{H-NMR}$ to evaluate the influence of several monomers on the potentiometric performance of histamine-imprinted polymer-modified sensors.^[103] Not only was $^1\text{H-NMR}$ able to assess the interaction between histidine and acrylamide (AA) and atropic acid (AT) and MAA, but it was even possible to see the influence of its imidazole ring on the pyridine ring of 4-vinylpyridine (4-VP).

The nature of MIPs makes their characterization usually harder, but solid-state NMR has been shown to evaluate the degree of the binding of the template when the interactions are strong. Less recent works already demonstrated that this technique is useful to provide insights. Andersson et al. used this technique to optimize the template-functional monomer proportion.^[104]

Simple $^{13}\text{C-NMR}$ alone had not been used for the evaluation of the template-functional monomer interaction, until Zhang et al.^[105] reported a study where it was utilized to evaluate the interactions between antibiotic erythromycin (ERY) and a set of functional monomers, with the choice of MAA as the optimal one. The rational binding sites were predicted based on chemical shifts changes in ERY structure. DFT theoretical calculations of Lewis basicity of the O/N atoms located at the sites proposed by a sequence regarding their interaction force confirmed its reliability. Solid-state NMR was used by Annamma et al. to design a 2,4-

dichlorophenoxyacetic (2,4-D) acid-imprinted polymer with 4-vinylpyridine (4-VP) as the functional monomer,^[106] intriguingly showing the effect of increasing concentrations of 4-VP on the equilibrium; see **Figure 5**.

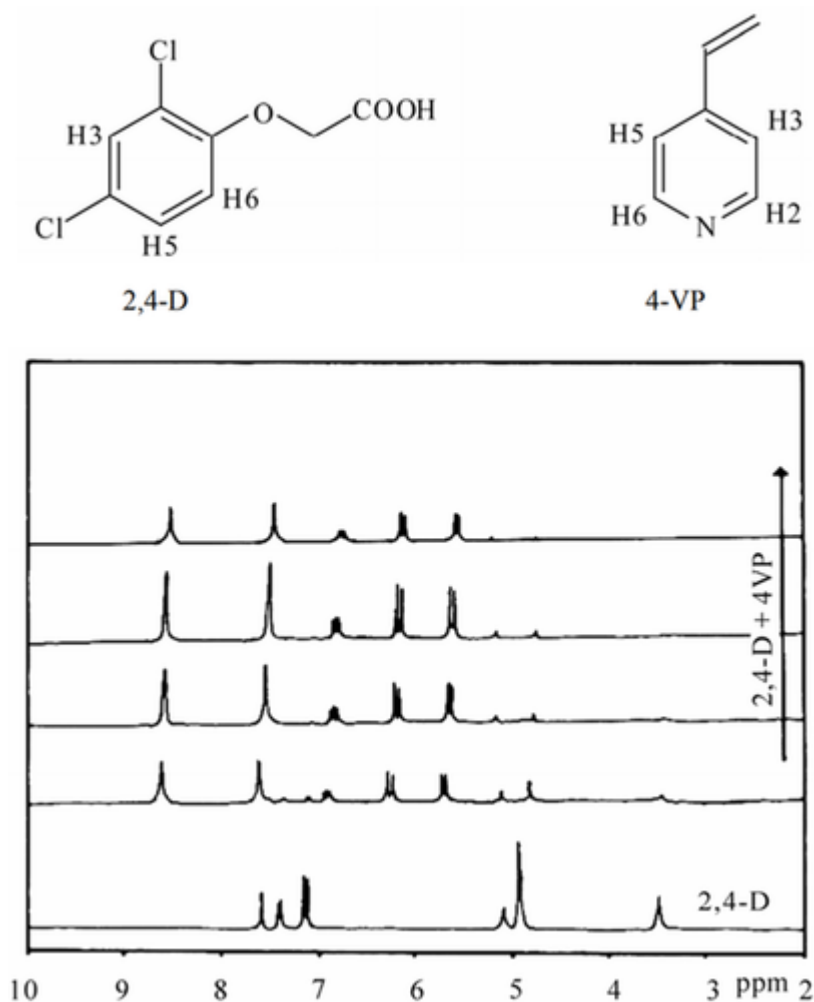


Figure 5 ¹H NMR spectra of 2,4-D with increasing concentration of 4-VP showing changes in the chemical shifts used to rationalize a low crosslinked system that allows for higher levels of specificity and selectivity. (Reproduced with permission.^[106] Copyright 2011, Springer.)

2.3 Isothermal Titration Calorimetry (ITC)

Isothermal titration calorimetry (ITC) is a microcalorimetry technique that measures the heat released or absorbed during a chemical reaction, generally used to determine binding affinity,

enthalpy changes, and stoichiometry of interactions between molecules in solutions.^[107] The advantage of this technique is that no immobilization or modification of the starting reagents is required. In addition, ITC has the ability to detect changes in the low mK range that corresponded to noncovalent interactions such as hydrogen bonds.^[108] However, ITC is not widely available in laboratories and requires expensive instrumentation, which limits the application in the field of MIPs^[109]. To the best of our knowledge, there have been no reports about the use of ITC for the characterization or rational design for MIPs produced for antibiotics. There are few reports in literature about using ITC to determine binding affinity of MIPs for small molecules^[110, 111] and predicting the optimum ratio of target-to-functional monomer.^[112, 113] Due to ITC providing thermodynamic data, it gives fundamental insight into the binding mechanism of MIPs that has been proven strongly dependent on pH,^[114, 115] showing that pH can be a considerable variable in achieving optimum MIP function. Considering ITC is routinely used in biomedical research including enzyme kinetics, it might play a crucial role in optimizing MIPs for antibiotic detection and understanding the influence of external parameters (T, pH, etc.) on binding to polymers.

2.4 Infrared Spectroscopy

Infrared (IR) spectroscopy is ubiquitously used in laboratories as it is versatile, offers fast and straightforward analysis, and is inexpensive. The main disadvantage of IR is that it is difficult to analyze complex mixtures or aqueous solutions, as the corresponding spectra provides only limited information about individual peaks of chemicals of interest. Therefore, IR is not routinely used to study interactions in the prepolymerization complex prior to MIP formation as the stretching frequency of hydrogen bond donors or acceptors is generally in the same range as that of the solvent peaks.^[116] However, IR measurements can also be collected from solid particles and this method of IR can provide useful information about the resulting solid MIP on

the expected performance of the material as the peak intensity of the carbonyl group provides quantitative information about the amount of polymer present on the surface.^[116] Thin films of poly(*N*-isopropylacrylamide) revealed systematic changes in IR peaks associated with the amide bond, that could serve to bind molecules via hydrogen bonding. In addition, the study also demonstrated that the molecular architecture can significantly vary depending on what solvent was used to cast the film.^[117] IR measurements are fast and straightforward and therefore have scope for this technique to be used for high-throughput screening of performance of solid polymeric materials.

MIP materials are often heavily crosslinked and have limited solubility, which can complicate characterization. IR is often used on solid materials to establish the presence of the polymer on surfaces and determine whether the template has been fully removed from the MIP cavities. Chen et al., reported on the separation of tetracycline antibiotics from egg and tissue samples using magnetic MIPs as the solid phase.^[116] Peaks from the carbonyl and hydroxyl group of the polymer were present in the recorded IR spectra, which confirmed presence of the polymer on the magnetic particles. Wei et al. developed dual-imprinted MIPs for the rapid determination of amphenicol antibiotics in water, serum, and food samples. The presence of the polymer was verified with IR measurements. Furthermore, IR spectra of the reference non-molecularly imprinted polymer (NIP) and its corresponding MIP were compared and significant frequency shifts in the peak corresponding to methacrylic acid were observed.^[118] It was hypothesized that the observed shift in this peak was due to hydrogen bond interactions between functional monomer and target. A similar approach was followed by the group from Mizaikoff and coworkers^[119] that developed gravimetric sensors for detection of the antimalarial drug artemether. Upon inspecting the IR spectra of the polymers, a spectral shift of the peaks corresponding to the carboxyl groups of methacrylic acid to the shorter wavelength was

reported. Besides these peaks, there was also a distinct intensity change at a wavelength of 3000 cm^{-1} that was attributed to additional interactions of functional monomers with the template.

Over recent years, there has been a move toward the use of the aforementioned “dummy” templates in Section 1.3, which avoid the use of high-cost or toxic target molecules. Zhang et al., used a simple sugar, raffinose, as a dummy template to develop MIPs for antiglycoside antibiotic detection.^[120] This molecule resembles the size and shape of the antibiotic of interest and is able to selectively extract six antibiotics from the family of antiglycoside antibiotics from environmental samples. In research by Liu et al.^[121] roxithromycin was used an example of a macrolide antibiotic to develop MIPs for the extraction of this entire family of macrolides. The interesting aspect of this work was that a simple wooden tip was used, that makes it extremely suitable for work in developing countries. IR was used to monitor extraction of the template from the MIP cavities.

IR measurements are fast and straightforward and, as shown via the earlier example, there is certainly scope for this technique to be used for high-throughput screening for the performance of MIPs.

3 MIP Morphologies

In the early years of imprinting, the most common approach involved free radical polymerization, often achieved using azobisisobutyronitrile (AIBN). The reason this method is often used is due to its simplicity as it can either be initiated with UV light or increasing the temperature; unfortunately, given the fast chain propagation and the fact that the associated termination reactions are irreversible, it yields inhomogeneous cavities and particle size.^[122] This results in MIPs with heterogeneous binding sites, with cavities directly on the surface and others that are partly inaccessible, which hinder the mass transfer and limit

selectivity. This problem has been addressed with the use of controlled polymerization techniques including reversible addition fragmentation chain transfer (RAFT) polymerization,^[123, 124] ring-opening metathesis polymerization,^[125] and atom transfer radical polymerization (ATRP),^[126] which lead to particles uniform in size with homogeneous binding sites. In this section, we will review a couple of methodologies which improve upon sensor specificity.

3.1 Use of Copolymers

One way to improve upon the specificity and selectivity of MIPs is the inclusion of more than one functional monomer, resulting in what is referred to as a copolymer.^[127, 128] Chullasat et al.^[129] demonstrated an amoxicillin detection system using a copolymer along with quantum dots (QDs). The resulting system proved capable of detecting amoxicillin in complex media such as milk and honey with a limit of detection (LoD) of $0.14 \mu\text{g L}^{-1}$, outcompeting the HPLC standards it was tested against. It was also shown that the use of copolymer MIPs can increase the accuracy of results against modern, industrial detection systems but also decrease the time taken and reduce the need for expensive infrastructure. Tunc et al.^[130] demonstrated optimizing copolymer MIPs through synthesis and comparative testing. This provided insights into optimum monomer selection for the theophylline-imprinted monomers; however, planning monomer selection via rational design, e.g., computational modeling, would lend aid as to which monomers to test. Valtchev et al.^[131] tested a vast range of MIPs, including six cofunctional monomer polymers. The study resulted in the synthesis of many significantly optimized MIPs for the detection of the antibiotic sulfamethoxazole in wastewater. Although this type of “trial by error” study is not time efficient, it does give certain, quantified values to the efficiencies of all the MIPs tested and shows the positive impact that using copolymers can have. Wang et al.^[132] developed inorganic–organic cofunctional monomer-imprinted polymers

for fluoroquinolones in milk and observed an LoD in the ng/mL range, which exceeds the standards required by the EU. As sample matrices as complex as milk have benefited from the use of copolymers, the eventual use of copolymers for detection in other sample matrices, especially simple matrices such as water, would have presumptive benefits.

3.2 Integration of Fluorescent Moiety

Fluorescence detection of antibiotics has been a crucial analytical tool for many years because of its versatility, simplicity, and accuracy.^[133-135] It can be used across a range of different recognition elements, including MIPs. However, it often requires the introduction of a secondary molecule to either bind to the target^[136] or serve as a competitor^[137] for a measurable fluorescent response to be obtained. Recent studies, therefore, have looked to develop MIPs, which are inherently fluorescent by introducing certain elements into the polymer itself.^[138, 139] This reduces the number of preparation steps needed to analyze samples and allows for the polymer to be adapted to a variety of targets. There have been two primary focuses to achieve this functionality: QDs embedded within or surrounded by the polymer matrix or a fluorescent moiety copolymerized into the backbone.^[140, 141] These integrated QDs and fluorophores typically rely on energy or electron transfer from the target molecule to achieve their fluorescence change (**Figure 6**). This transfer is strongest when the target rebinds into the imprinted sites as this is in closest proximity to the fluorescence element that can be achieved.

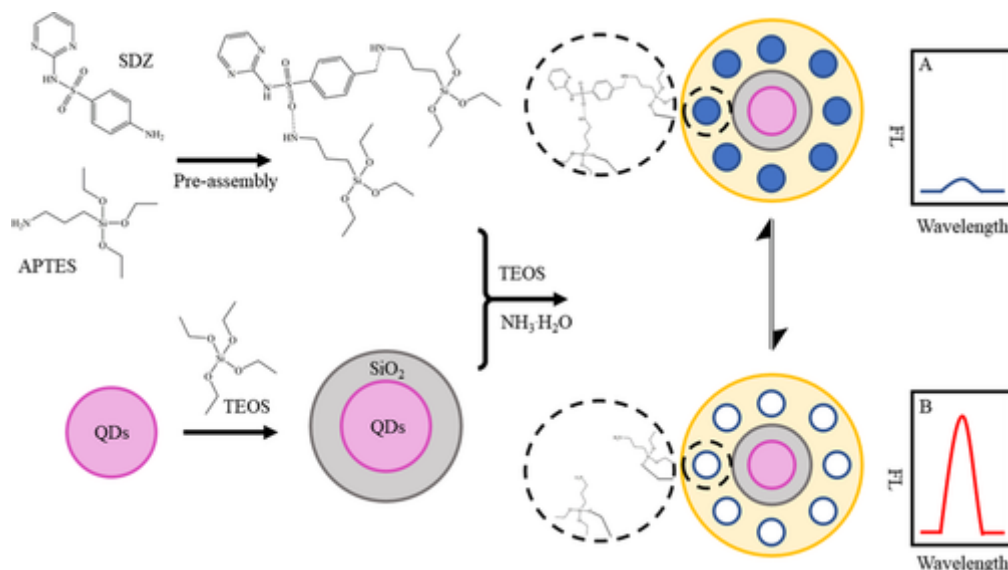


Figure 6 Formation of an MIP layer on the surface of QDs for an antibiotic, sulfadiazine (SDZ). The polymer layer can then have the target extracted, breaking the electron transfer between SDZ and the QDs, which results in a decrease in the fluorescence signal. (Reproduced with permission.^[141] Copyright 2018, Elsevier.)

Fluorescence quenching is most commonly seen in both cases, although enhancement can be facilitated by tailoring the molecular system to achieve specific interactions upon rebinding.^[60] Shi et al. utilized CdSe QDs to introduce fluorescence into a bulk MIP for kanamycin.^[142] An increase in fluorescence was seen for both NIP and MIP upon addition of kanamycin, with a greater increase seen for the latter. The fluorescence response was greatly influenced by composition, pH, temperature, and required optimization. The system was able to detect kanamycin with a detection limit of $0.013 \mu\text{g mL}^{-1}$ and a linear range of $0.05\text{--}10 \mu\text{g mL}^{-1}$ in PBS. Furthermore, it was tested with real samples (including lake water and urine) and showed good recoverability of spiked concentrations of the drug. This methodology also utilized aptamers to increase binding affinity to the polymer layer and click chemistry to provide a more simplified chemical route for polymer attachment to the QDs compared with

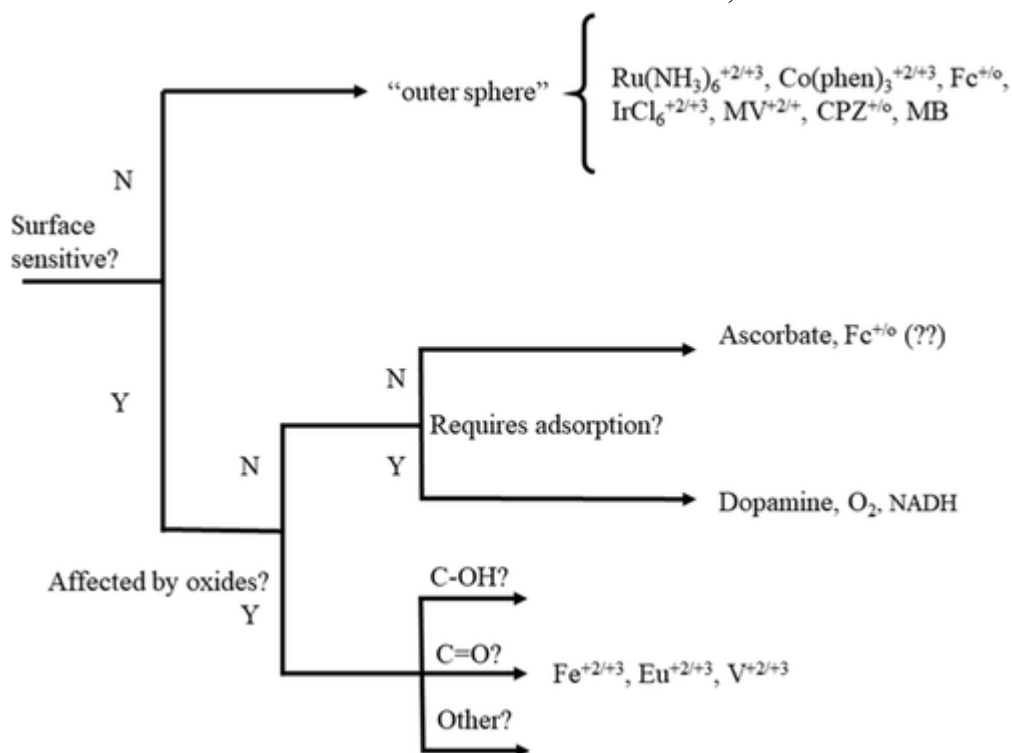
conventional methods. Zhang et al. integrated ZnS QDs into a mesoporous silica network containing an imprinted polymer for tetracycline.^[143] Quenching of the fluorescence was seen upon addition of tetracycline to the MIPs only, which they propose is due to an electron transfer between the target and the QDs. The particles showed high selectivity for tetracycline compared with similarly structured compounds, and an LOD of 15.0 ng mL⁻¹ was obtained. Similar quenching probes for antibiotics have been produced using graphene,^[144] ZnS,^[145] and CdTe QDs,^[142] yielding comparable LODs and selectivity.

Integrated fluorophores offer a unique alternative to QDs, where the interactions between the fluorescent moiety and the target can be more specifically tailored.^[146, 147] In addition, the use of heavy metal atoms can be avoided and integration into the polymer backbone significantly reduces leaching. However, these molecules often require a multistep synthesis and extensive optimization of the polymer composition as quantifying the fluorescence change requires one-to-one interactions. Niu et al. introduced an anthracene-based monomer into MIP nanoparticles for the detection of tetracycline.^[148] The fluorescence of the RAFT-polymerized nanoparticles would be quenched in the presence of the target, with the imprinted particles exhibiting a stronger change than the nonimprinted ones. The polymers were able to detect tetracycline at an LOD of 0.26 μM and were able to perform in a more complex medium (bovine serum). UV-vis analysis demonstrated that the underlying mechanism for quenching was based on electron transfer, rather than energy transfer. Sunayama et al. used attached fluorophores to explore the binding activities of a cephalexin-imprinted polymer.^[136] The template was functionalized and crosslinked into the polymer network and then removed using two different chemical reactions. This method is unconventional compared with common imprinting techniques but allows for direct functionalization of the imprinting sites; in this case, two fluorophores were introduced via Schiff base and disulfide reactions. Ampicillin was used to

monitor rebinding due to solvent constraints, and an increase in fluorescence intensity was observed with corresponding concentrations. An LOD of 5.0 μM was observed and the fluorescence change was highly specific due to the nature of the interaction. Ashley et al. were able to produce fluorescent doxycycline-imprinted microparticles using an acrylated fluorescein derivative.^[149] The moiety was introduced into a thin polymer layer surrounding FeO_x nanoparticles and would exhibit quenching upon rebinding of the target. Although the interaction between fluorophore and target appears less specific, the polymer demonstrated strong selectivity toward doxycycline compared with similarly structured antibiotics based on fluorescence readings. Recently, our group has explored the use of a fluorescein-based MIP as an optical detection platform for beta lactam antibiotics.

3.3 Using Redox Probes to Monitor MIP/Target Binding Phenomena

If the target analyte is not electrochemically active, a redox-active probe can suffice for the detection. A redox reaction involves the transfer of electrons, which is facilitated through the



working of an auxiliary (counter) electrode, whereby if an oxidation process occurs at the working electrode, the corresponding reduction process will take place at the auxiliary electrode. In electrochemistry, redox probes can be used to follow interfacial changes in a system, such as adsorption, electrode modification, and binding phenomena. There is a vast array of redox probes and care must be taken when choosing one for use in characterization of a system or for use as an indicator for sensing applications. All of these systems are classified under two main categories, outer-sphere and inner-sphere redox probes, summarized by McCreery et al. (see **Figure 7**).^[150]

Figure 7 Flow diagram showing classification of outer- and inner-sphere probes. (Reproduced with permission.^[150] Copyright 2008, American Chemical Society.)

Outer-sphere probes come close to the electrode surface, but do not directly contact it, to allow the electrons to tunnel/hop across the solvent monolayer, and as such are only influenced by the electronic structure of the electrode surface. Ruthenium hexamine (RuHex) is the best example of a near-ideal outer-sphere redox probe; it does not exhibit any variation in electron transfer rate for any changes other than the electronic structure of the electrode (density of states and the Fermi level). Alternatively, inner-sphere redox probes require contact with the electrode surface to facilitate the electron transfer; as such, they are affected by both the electronic structure of the electrode surface and the surface chemistry at play (i.e., surface functional groups and adsorption sites).^[151] When using MIPs as recognition elements, the desire is typically to record and track changes in binding phenomena between the imprinted polymers (typically on the surface of an electrode) and a target analyte (in solution that diffuses to the electrode surface and binds to the MIP). Most papers in literature combine MIPs and redox probes, where the use of an inner-sphere redox probe in solution is as an indirect detection

method, where the binding of the target to the polymer blocks the access of the redox probe to the electrode surface, producing a reduction in measured response. As such, the most common redox probe in this area of research, as an indirect detection method, is potassium ferri/ferrocyanide ($K_3/K_4 [Fe(CN)_6]^{3-/4-}$). This can be done utilizing various electro(analytical) techniques such as cyclic voltammetry (CV),^[152] electrochemical impedance spectroscopy (EIS),^[153] and differential pulse voltammetry (DPV).^[154-156] CV typically will not reach the same levels of detection as other electroanalytical techniques; however, the analytical response can be amplified by adding extra components to the system. Lian et al.^[157] accomplished this for the detection of the antibiotic kanamycin through the addition of horseradish peroxidase and H_2O_2 , where potassium ferricyanide acts as a mediator for the reaction. This reaction mechanism gives a large amplification in the measured current; therefore, when the electrode surface is blocked through the binding between kanamycin and MIP, there is large reduction in current as the reaction can no longer be mediated. These methodologies typically require two-step analysis, consisting of an incubation step in the analysis solution and a subsequent measurement step in the probe solution, which is not ideal for production, reproducibility, and analysis time.

Instead of using a free in-solution redox probe, an alternative strategy is to incorporate the redox probe directly into the polymer matrix. In this process, known as redox tagging, a redox probe such as ferrocene is attached to a moiety capable of taking part in the polymerization process. Mazzotta et al.^[158] reported this for the detection of the antibiotic vancomycin through using two ferrocene-derived monomers, vinylferrocene and ferrocenylmethyl methacrylate, in conjunction with the solid-phase synthesis approach,^[159] for the development of nanoMIPs that produce homogeneous binding sites and pseudomonoclonal binding properties. The direct anchoring of the redox probe into the polymer allows for a reduction in analysis time and a

more direct interaction between the probe and target, which does not rely on diffusion of the probe in solution. The main drawback of using ferrocene-derived redox probes covalently attached to the system is a natural reduction in the current signal when cycling. As seen from the cyclic voltammograms in the manuscript from Mazzotta, over the course of 250 scans, there is a significant reduction in the measured current; this needs to be taken into account when developing a sensor platform using this methodology and may require significant calibration steps to produce a reliable system.

4 Different MIP Production Methods

There are many different production methods for MIPs, depending on the desired function of the polymer. MIPs intended for use in chromatography are usually prepared by free-radical polymerization, which results in the production of heterogeneous microparticles. Research into other MIPs has elevated their use, such as, their synthesis via solid-phase imprinting to generate homogeneous high-affinity nanoparticles, which have the added benefit of biocompatibility. The evolution has led them to compete with their biological counterparts—antibodies. In fact, they can also offer benefits over antibodies because they are far more stable. MIPs can be stored in dry conditions and ambient temperatures for many years, without loss of recognition capability, whereas antibodies denature rapidly unless they are kept frozen. This provides advantages for manufactured MIPs sensing devices as they can have appropriate shelf life for use outside of lab settings. In addition, MIPs are able to withstand many adverse conditions (heat, cold, changes in pH, etc.), which allow them to be used for a variety of in-field, real-time sensing applications.^[156] For our interest, MIPs can easily be implemented into sensors for food and water analysis for antibiotics.

One of the biggest stumbling blocks, however, for broad-scale commercial use of MIPs as sensors has been reproducible mass manufacture. The advent and recent development of

nanoparticles, and especially core–shell and gel nanoparticles, whose solubility can finely be tuned, is promising for the next generation of sensors.^[160] Recently, photolithography has been used to pattern MIPs for the wafer-scale production of biochips. This technique allows for the control of shape and size (1.5 μm) of the patterns and the deposition of different MIPs on the same chip.^[161] Some of the advancements to mass manufacture will be discussed later.

4.1 Screen-Printing Techniques

Screen printing is a well-established methodology for the mass production of biosensors.^[162] The most common commercial example is the glucose sensor, used in the treatment of diabetes, that utilizes a screen-printed electrode (SPE) and is responsible for a billion-dollar market annually.^[163] Screen printing offers the ability to mass produce disposable platforms that offer high reproducibility, flexibility, versatility, and high sensitivity at a low production cost. This technique involves the spreading of a thixotropic fluid, containing a mixture of predominantly graphite, solvents, and binder, through a predesigned mesh that will produce a printed pattern of a defined shape and size.^[164] As such, a vast array of electrodes has been designed utilizing this methodology to produce different shapes such as microbands,^[165] shallow recessed arrays, and^[166] back-to-back sensors^[167-169] and produce electrodes containing a wide range of constituents for various applications in biosensors.^[170] MIPs can be incorporated into and used in conjunction with screen-printed platforms in a variety of ways, such as the direct formation of MIPs on the surface through processes like electropolymerization,^[171] incorporation of MIPs into the screen-printing ink,^[172-174] or depositing onto nanomaterials decorated on the surface.^[175]

Direct formation of MIPs onto the surface of an unmodified SPE was reported by Ayankojo et al.,^[156] who used computational modeling to choose *m*-phenylenediamine as their chosen monomer for the detection of erythromycin. In strategies such as this, where direct

electrochemical detection is used, the thickness of the MIP layer becomes a priority. They explain that with the thinnest MIP layer deposited, a better detection signal is acquired; however, there is lower specificity due to nonspecific interactions, such as that directly with the surface. Conversely, when the layer was too thick, there was a significant decrease in the electroanalytical signal for both the MIP and NIP regimes. Therefore, when using MIP layers on SPEs, each system must be optimized for electrochemical detection.

Electropolymerization (discussed later) is the most obvious route for MIP formation on SPE surfaces; however, this methodology can struggle from a limited selection of suitable monomers and poor scalability. Within our group, Jamieson et al.^[176] reported a sensor for amoxicillin through the direct formation of MIPs onto the SPE surface through UV polymerization. This offers better prospects in terms of mass production; however, more work has to be done to increase the synergy between the transducer, MIP, and detection methodology.

The enhancement of electroanalytical output for SPE platforms is typically done through the incorporation of nanomaterials. These materials are either incorporated in the ink, on the surface of the electrode, or on top of the MIP and help to overcome problems with poor conductivity and electroanalytical response. This can be seen in the work by Devkota et al.,^[177] who reported a sensor platform for the detection of tetracycline, in which the formation of the MIP was achieved using the conductive polymer pyrrole. Following MIP formation, the polypyrrole layer was overoxidized, a process that while stabilizing also removes the conductivity associated with the polymer layer. Therefore, to increase the efficacy of the sensor, gold nanoparticles (AuNPs) were deposited on the surface of the MIPs. Although this helps to counteract the loss of conductivity, the multiple electrochemical modification steps do not lend the system ability for simple mass production, which is a great advantage when using SPEs.

This can be further seen through the work of Moghadam et al.^[178] using a combination of gold nanourchins and graphene oxide for the detection of oxacillin. In this case, the nanomaterials were deposited onto the surface of the electrode prior to the MIP. Although the use of drop casting to modify electrodes is standard practice and scalable, using multiple drying conditions followed by electropolymerization and template removal provides difficult production steps. Instead of multiple electrochemical functionalization steps, Dechirat et al.^[155] utilized inkjet printing of a nanocomposite layer, containing AuNPs and poly(3,4-ethylenedioxythiophene)/poly(styrene sulfonate) (PEDOT:PSS), onto the surface of the SPE. This synergetic approach to the incorporation of nanomaterials onto the electrode allowed for the detection of nitrofurantoin at two orders of magnitude lower than the bare sensor platform. This sensor exhibited the advantages of using screen printing and MIPs in combination, producing a sensor platform that is both highly reproducible and stable over a long lifetime.

4.2 Electrodeposition of MIP Layers on Transducer Surfaces

The electrodeposition of MIPs is concerned with the immobilization or formation of MIPs directly onto an electrode surface using electrochemical methodology.^[179] The vast majority of MIPs that fall into this category is electrosynthesized MIPs (eMIPs). A more detailed overview of this subsection of MIPs, including their formation and application to the detection of biologically important molecules, including antibiotics, up to 2019, can be found in a recent past review.^[171] Briefly, the formation of eMIPs takes place through electropolymerization, where a polymer layer is formed upon an electrode/substrate in the presence of the desired template. This can be achieved through a variety of electrochemical techniques, such as voltammetry,^[180] potentiometry,^[181] and galvanostatic techniques.^[182] It is vital when using this methodology to define the working material, counter and reference electrodes, monomer composition, solvent, supporting electrolyte, electropolymerization methodology, and time as

these variables will greatly affect the binding affinities, layer sizes, conductivities, and surface morphologies of the polymeric films.^[183]

Good recent examples, presenting the optimization required for the production of a sensor array for the detection of β -lactam antibiotics, were reported by Moro et al.^[184] and Bottari et al.^[185] Both explain the rationale behind the design of their eMIP-based sensor platform. Moro et al. discussed the importance of utilizing a conductive polymer (4-aminobenzoic acid, 4-ABA) to synergize with their chosen squarewave voltammetric (SWV) detection method and the use of modifiers, in this example multiwalled carbon nanotubes (MWCNTs), to enhance the electroanalytical properties of the device.

The overwhelming majority of sensor platforms utilizing electrodeposition also use electrochemistry as their chosen detection method. This can be achieved either through indirect detection, such as the redox probes described earlier, or by direct detection of the binding between the target and recognition element. One such way to monitor the interfacial changes at the MIP/electrode surface is through EIS, where a change in the measured charge transfer resistance (R_{CT}) can signify the binding of a target molecule. Roushani et al.^[186] demonstrate this using a design that utilizes a combination of electrosynthesized poly(resorcinol) MIP and a silver nanoparticle (AgNP)/reduced graphene oxide (RGO)/aptamer system. Although this methodology uses a large amount of preparation steps, it was able to detect chloramphenicol (CAP) in milk samples. Another effective choice of monomer for antibiotic detection through eMIP layers, due to its ease of polymerization and favorable structure, is represented by resorcinol. This presents an improved chance of advantageous hydrogen bonding occurring between the hydroxyl groups present and the functional groups on the antibiotic molecules. Although electropolymerization techniques lend themselves toward fast single-sensor

production, it does not scale well for mass production due to the often multistep production schemes and varying conditions.^[187]

Electropolymerization offers a promising method of fast and varied single-sensor production; however, in its current form, the scalability ready for mass production of sensor platforms is not readily available. In particular, this production methodology does not lend itself to array sensor development for multiple analytes. The use and development of more conductive polymers with an array of functional groups will allow for great improvement on the sensor efficacy of eMIP-based sensor platforms for the detection of antibiotics, allowing for improvements in the sensitivity and selectivity.

4.3 Grafting from/to Core–Shell Nanoparticles

There has been considerable increase in the use of MIPs based on core–shell nanoparticles that can overcome the drawbacks generally associated with monoliths. The formation of thin imprinted polymer layers on a solid support enhances binding kinetics, mass transfer, and facilitates easy template removal. Among the materials used for MIP functionalization, Fe₃O₄ magnetic nanoparticles (MNPs) are most often used due to their paramagnetic properties. A comprehensive review on magnetic particles for MIPs in analytical chemistry, including for the extraction of antibiotics from environmental and food samples, is provided by Chen et al.^[188] The use of controlled polymerization techniques allows to devise the molecular architecture of interest. Atom transfer radical emulsion polymerization (ATREP) was used to functionalize a molecularly imprinted layer for tetracycline onto magnetic particles,^[189] leading to a material that can extract the antibiotic tetracycline with very high specificity from a food sample.

AuNPs have the advantages of excellent optical, electronic, and catalytic properties^[190] and are therefore often used for sensor applications. Gold structures combined with silica nanoparticles

were used for the specific detection of ENR. The presence of gold core branches^[191] acted as intrinsic hot spots that strongly enhance the electric magnetic field, thereby significantly augmenting the Raman scattering and thus leading to a higher specificity. It was shown that the combination of silica and AuNPs increased the signal by a factor of 2 compared with the use of AuNPs on its own.

It is expected that different cores, such as polystyrene micropsheres^[192] and chitosan microspheres, which possess excellent biocompatibility, will be explored in the future. However, it has to be noted that the use of a thin MIP layer can limit the number of recognition sites, which will hamper the sensor sensitivity. Therefore, currently, the preferred method of choice is suspension or emulsion polymerization, which has proven to yield MIPs with high adsorption capacity while maintaining excellent binding kinetics. The key issues with the current methodology include precise controlling of the thickness, as buried templates can limit the extraction process, and a multistep process that is often not scalable, even though examples of one-pot synthesis of MIP particles are present. The group of Niu developed a range of MIP particles bearing hydrophilic polymer brushes via controlled polymerization^[148] techniques. A one-pot synthesis method, based on hydrophilic macromolecular chain-transfer agent (macro-CTA)-mediated reversible addition–fragmentation chain transfer precipitation polymerization, was used to prepare fluorescent MIP nanoparticles for tetracycline. The use of hydrophilic polymers ensured that measurements are compatible with biological samples, which enabled direct quantification of tetracycline in complex biological samples.^[148]

Instead of a solid support, it is possible to use as a sacrificial support matrix. The approach chosen by Tang et al.,^[193] shown in Figure 3, demonstrates the preparation of hollow MIPs with fast absorption kinetics (≈ 10 min) for ENR. This method was used to determine the levels of this antibiotic in fish samples, with LoDs well below the legally maximum residual level.

The sacrificed support matrix, $K_2Ti_4O_9$ was chosen because of its nontoxicity, low cost, and easy removal process. Silica is one of the popular choices as sacrificial support as the polymers can be embedded into the pores of the particles. The group of Moreno-Bondi^[71] developed MIPs that were able to recognize six cephalosporin below the maximum residual levels set for these antibiotics in raw milk. Silica etching, in contrast, is a more time-consuming process and involves harsh chemicals, as the particles are treated with an ammonium hydrogen difluoride mixture for 24 h. A similar approach, where silica beads were functionalized with MIPs according to the procedure by Yilmaz et al.,^[194] was used to synthesize selective recognition elements for structurally related penicillins. The base structure of this family of antibiotics, 6-aminopenicillanic acid, as a dummy template enabled to detect the entire class of target analytes from milk with high recovery rates.^[195]

4.4 Solid-Phase Imprinting: Immobilization of the Template on a Solid Support

NanoMIPs have the potential to become cost-efficient and robust alternatives to natural antibodies in diagnostics. However, intrinsic problems associated with the imprinting technique have limited their adoption at an industry level. In particular, the most evident drawbacks are 1) the presence of residual template in the MIP; 2) high binding site heterogeneity; and 3) lengthy or labor-intensive methodologies required for MIP production.

The solid-phase imprinting approach allows to overcome these drawbacks. In this method, the template is covalently immobilized on the surface of a suitable solid support (such as solid glass beads, magnetic particles, or similar). This support bearing the immobilized template is then placed in contact with the monomer mixture, and polymerization is initiated under conditions that promote the formation of polymeric nanoparticles. After the polymerization, the solid support acts as an affinity medium: by means of a temperature-based affinity step, unreacted monomers, oligomers, and low-affinity particles are eluted. Then, the temperature of the system is increased and this leads to the disruption of the stronger interactions between high-affinity particles and template, allowing to selectively collect high-affinity nanoMIPs only (**Figure 8**).

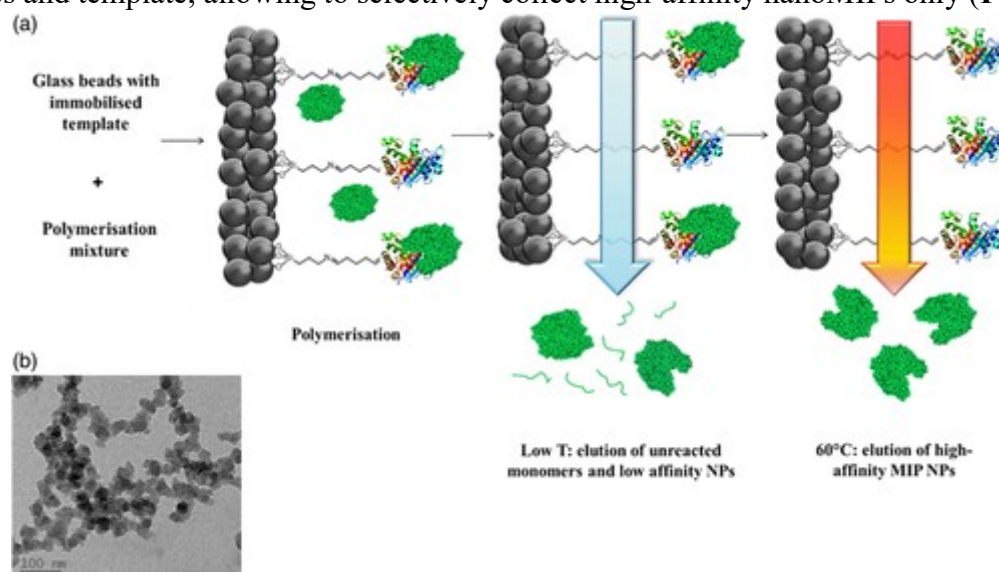


Figure 8 a) Solid-phase synthesis of nanoMIPs. In this example, a protein is shown as the template molecule. b) Representative TEM of nanoMIPs. (Reproduced with permission.^[207] Copyright 2018, Royal Society of Chemistry.)

As previously demonstrated,^[196] this process can be easily automated^[196] and executed in a matter of a few hours. Because of the affinity purification step, nanoMIPs possess high affinity and specificity toward their targets, exhibit a homogeneous distribution of binding site affinities, and do not contain any residual template (as it was covalently attached to the solid-support).

However, template leaching may occur if the bond used to immobilize the template onto the solid phase gets cleaved (usually by hydrolysis) during the elution process.

It should be noted that high-affinity nanoMIPs can also potentially be collected by means of changes in pH and/or solvent. Haupt and coworkers^[197] use the transition temperature of NIPAm to collect the high-affinity nanoMIPs, conducting imprinting at 37 °C and the elution at lower temperature (i.e., at 25 °C—which is below the lower critical solution temperature of the MIP polymer). This allows the nanoMIPs to swell, detach from the immobilized template, and be eluted. The proposed approach is generic in nature as virtually any molecule can be imprinted, and it can be conducted both in water and in organic solvents (via a UV-triggered process). However, the template is required to bear at least one functional group for immobilization on the solid phase, and this may be problematic especially for small molecules (<500 Da). Polymerization in the organic solvent has been successfully used to imprint small molecules,^[196, 198, 199] whereas aqueous polymerization has proven effective for imprinting of peptides and proteins.^[200-203]

Several works have demonstrated that nanoMIPs produced via solid-phase imprinting can be used as a direct replacement for natural antibodies in diagnostic or bioanalytical assays.^[199, 204-206]

In one such example, the solid-phase approach was used for the manufacture of these imprinted polymers against vancomycin.^[207] They were then successfully immobilized on a novel sensor type capable of measuring tiny variations in temperature upon target binding. Thanks to the high affinity, the LoD of the sensor was lowered by three orders of magnitude compared with MIP microparticles developed without solid-phase extraction. Such improvement can also be attributed to the enhanced conductivity and increased surface area. The developed thermal

sensors were capable of measuring samples with a turnaround time of a few minutes (< 5), which potentially enable real-time detection of biomolecules.

In a similar example, antivancomycin nanoMIPs produced by solid-phase synthesis were doped with ferrocene derivatives to make them electroactive.^[158] This allowed the indirect electrochemical detection of vancomycin due to the change of redox properties of the ferrocene label upon binding. The authors claimed that the observed behavior is likely due to hindering of the electron transfer process of ferrocene in the nanoMIPs by their interaction with vancomycin.

As mentioned earlier, nanoMIPs have also replaced antibodies in assays. In one such example, antigentamicin-imprinted nanoparticles were used in a pseudo-enzyme-linked immunosorbent assay in spiked milk,^[208] as a synthetic capture antibody, whereas target detection was achieved in competitive binding tests with a horseradish peroxidase–gentamicin conjugate. The developed polymers showed superior selectivity over other antibiotics (streptomycin and ampicillin) and were capable of detecting gentamicin in milk at clinically relevant concentrations.

5 Outlook on the Future of Commercial MIP Sensors for Antibiotics

The straightforward approach, ease of synthesis, and, more importantly, great chemical stability means that MIP integration within sensors is an appealing prospect as they can function in a variety of different environments. In contrast, a natural receptor that might have to be used instead often suffers from poor stability and lower specificity to the target compounds. In our research scenario, where the target/analyte is an antibiotic, an antibody or receptor might not be available,^[209] and in cases such as this, MIPs have a clear advantage over naturally occurring ligands. Due to their relative ease of fabrication, researchers have utilized imprinted polymers

for separation purposes, in the development of complex matrix pretreatment strategies,^[210, 211] and as artificial antibodies.^[196, 212-214]

While the imprinting techniques have improved greatly over the course of the years, it is easy to see how their use in combination with novel smart and nanomaterials greatly benefits the selectivity and the specificity of the sensors as the interest in exploring the integration of MIPs into chemo-^[215-218] and biosensors^[219-222] keeps rising. As a multidisciplinary technology, the use of MIPs will greatly benefit from the developments in polymer and material sciences, drug, and environmental research: in contrast, they can be tailored to get maximum advantage from the existing techniques e.g., microfluidic, nanotechnology, biotechnology, and stimuli-responsive technology among others.^[223]

In recent years, the threat of AMR has been gathering much interest as the adverse consequences of such resistance are better understood. The manufacture of cheap, reliable sensors able to monitor antibiotic presence in a variety of environments and conditions will provide an avenue of determining the level of human exposure to antibiotics in our everyday life and what implications and impacts this may present for current and future increasing antibiotic resistance. The intrinsic stability of MIPs would allow for a long shelf life and robustness regardless of the conditions they might be used in. The adaptability of MIPs toward a target of interest and their accessibility make them great candidates for this very delicate and important task.

Despite their unequivocal usefulness and practicability, a few factors limit the commercial use of MIPs, including 1) limited sensitivity of microparticles, which makes them unable to compete with commercial antibodies; 2) integration of MIPs into electrodes that is not an evident task; and 3) mass production of these sensors, which is complicated with standard methods of producing nanoMIPs including electropolymerization or lithographic techniques,

even though we have shown several examples where these problems are partially overcome. Currently, only a few companies are present in the market and the commercialization of MIPs has mostly been confined to laboratory research, mostly focused on SPE of several environmental contaminants.^[224]

MIPs are usually prepared in organic solvents (water affects mostly H-bond-driven template-functional monomer equilibrium) but it has been shown that rebinding is usually more efficient when synthesis takes place in the same solvent used for synthesis.^[225] Water and food analysis might thus be a challenge for the obvious presence of water; however, if practices such as taking hydrophilicity of monomers into consideration during monomer selection and conducting controlled radical polymerization to control surface modification are practiced, then, compatibility issues can be reduced. Another issue is the number of functional monomers available that are appropriate for their synthesis, which is a hurdle to overcome. However, this limitation has pushed several researchers to explore alternatives, including the combination of different monomers and the exploitation of amino acids. The issue can also be tackled by the design of new monomers with multiple and varied functional groups, as they can facilitate the ability to offer several interactions with the target, a highly desirable development at the current stage.^[63]

The exceptional circumstances in which the COVID-19 pandemic has significantly accelerated the recent growing interest in AMR have drawn the attention to the mass production of in-field sensors, whose main features include long shelf life, stability, and ease of use. Despite the increase in academic output recorded in the last 20 years, industrial application has not followed a similar trend mostly due to the limitations mentioned earlier. Nonetheless, the recent breakthroughs in the synthesis are likely to ignite interest in novel MIPs. Mass production of polymers imprinted with antibiotics, especially if produced using the noncovalent method and

mild temperatures, can benefit the great advantage of reusing the template and make sustainability a great selling point. The EU has banned animal-derived antibodies,^[226] which boosts the appeal of MIP usage as their design and production does not require animal exploitation, constituting a significant ethical advantage. Moreover, their low cost and robustness make them a safe bet for the construction of field-deployable and in vivo sensors.

Acknowledgements

Funding from Innovate UK (KTP reference: 11473) and EPSRC (EP/R029296/2) are acknowledged.

6. References

- [1] M. De Kraker, A. J. Stewardson, S. Harbarth, *PLoS Med* 2016, 13, 1002184.
- [2] A. Cassini, L. D. Högberg, D. Plachouras, A. Quattrocchi, A. Hoxha, G. S. Simonsen, M. Colomb-Cotinat, M. E. Kretzschmar, B. Devleeschauwer, M. Cecchini, D. A. Ouakrim, T. C. Oliveira, M. J. Struelens, C. Suetens, D. L. Monnet, R. Strauss, K. Mertens, T. Struyf, B. Catry, K. Latour, I. N. Ivanov, E. G. Dobрева, A. Tambic Andrašević, S. Soprek, A. Budimir, N. Paphitou, H. Žemlicková, S. Schytte Olsen, U. Wolff Sönksen, P. Märtin, et al., *Lancet Infect. Dis.* 2019, 19, 56.
- [3] C. L. Ventola, *Pharm. Ther.* 2015, 40, 277.
- [4] A. Misurski, D. Lipson, D. Changolkar, *Am. J. Manag. Care* 2011, 17, 601.
- [5] T. M. Rawson, L. S. P. Moore, E. Castro-Sanchez, E. Charani, F. Davies, G. Satta, M. J. Ellington, A. H. Holmes, *J. Antimicrob. Chemother.* 2020, 75, 1681.
- [6] F. Zhou, T. Yu, R. Du, G. Fan, Y. Liu, Z. Liu, J. Xiang, Y. Wang, B. Song, X. Gu, L. Guan, Y. Wei, H. Li, X. Wu, J. Xu, S. Tu, Y. Zhang, H. Chen, B. Cao, *Lancet* 2020, 395, 1054.

- [7] M. P. Stevens, P. K. Patel, P. Nori, *Infect. Control Hosp. Epidemiol.* 2020, 41, 744.
- [8] S. K. Behera, H. W. Kim, J. E. Oh, H. S. Park, *Sci. Total Environ.* 2011, 409, 4351.
- [9] P. Paíga, C. Delerue-Matos, *Mar. Pollut. Bull.* 2017, 120, 355.
- [10] N. Watanabe, T. H. Harter, B. A. Bergamaschi, *J. Environ. Qual.* 2008, 37, S.
- [11] R. P. Tasho, J. Y. Cho, *Sci. Total Environ.* 2016, 563–564, 366.
- [12] H. Willer, M. Youssefi-Menzler, N. Sorensen, *The World of Organic Agriculture Statistics and Emerging Trends 2008* (Eds: H. Willer, J. Lernoud) Frick, Switzerland 2011.
- [13] A. J. Watkinson, E. J. Murby, D. W. Kolpin, S. D. Costanzo, *Sci. Total Environ.* 2009, 407, 2711.
- [14] S. Rodriguez-Mozaz, S. Chamorro, E. Marti, B. Huerta, M. Gros, A. Sanchez-Melsi, C. M. Borrego, D. Barcel, J. Luis Balcazar, *Water Res.* 2014, 69, 234.
- [15] P. Carsten Von Der Ohe, V. Dulio, J. Slobodnik, E. De Deckere, R. Kühne, R.-U. Ebert, A. Ginebreda, W. De Cooman, G. Schüürmann, W. Brack, *Sci. Total Environ.* 2011, 409, 2064.
- [16] I. T. Carvalho, L. Santos, *Environ. Int.* 2016, 94, 736.
- [17] M. Khaskheli, R. S. Malik, M. A. Arain, A. H. Soomro, H. H. Arain, *Pakistan J. Nutr.* 2008, 7, 682.
- [18] B. G. Knecht, A. Strasser, R. Dietrich, E. Ma, R. Niessner, M. G. Weller, *Anal. Chem.* 2004, 76, 646.
- [19] H. Wang, L. Ren, X. Yu, J. Hu, Y. Chen, G. He, Q. Jiang, *Food Control* 2017, 80, 217.
- [20] M. G. Pikkemaat, *Anal. Bioanal. Chem.* 2009, 395, 893.
- [21] F. Baquero, J.-L. Martínez, R. Cantón, *Curr. Opin. Biotechnol.* 2008, 19, 260.
- [22] A. J. Smith, J. L. Balaam, A. Ward, *Mar. Pollut. Bull.* 2007, 54, 1940.
- [23] D. Bitas, V. Samanidou, *Molecules* 2018, 23, 316.

- [24] F. Horemans, J. Alenus, E. Bongaers, A. Weustenraed, R. Thoelen, J. Duchateau, L. Lutsen, D Vanderzande, P. Wagner, T. J. Cleij, *Sensors Actuators B Chem.* 2010, 148, 392.
- [25] B. Tse Sum Bui, K. Haupt, *Anal. Bioanal. Chem.* 2010, 398, 2481.
- [26] P. A. Cormack, A. Z. Elorza, *J. Chromatogr. B* 2004, 804, 173.
- [27] A. G. Mayes, K. Mosbach, *Trends Anal. Chem.* 1997, 16, 321.
- [28] L. Ye, K. Haupt, *Anal. Bioanal. Chem.* 2004, 378, 1887.
- [29] A. Bossi, F. Bonini, A. P. F. Turner, S. A. Piletsky, *Biosens. Bioelectron.* 2007, 22, 1131.
- [30] D. M. Hawkins, D. Stevenson, S. M. Reddy, *Anal. Chim. Acta* 2005, 542, 61.
- [31] J. U. Klein, M. J. Whitcombe, F. Mulholland, E. N. Vulfsen, *Angew. Chem. Int. Ed.* 1999, 38, 2057.
- [32] S. Wei, B. Mizaikoff, *J. Sep. Sci.* 2007, 30, 1794.
- [33] W.-C. Lee, C.-H. Cheng, H.-H. Pan, T.-H. Chung, C.-C. Hwang, *Anal. Bioanal. Chem.* 2008, 390, 1101.
- [34] E. Turiel, A. Martin-Esteban, *J. Sep. Sci.* 2005, 28, 719.
- [35] M. Kempe, K. Mosbach, *J. Chromatogr. A* 1995, 691, 317.
- [36] V. Remcho, Z. Tan, *Analyt. Chem.* 1999, 71, 248A.
- [37] U. Curti, R. Colombo, *Chem. Ind.* 1951, 23, 103.
- [38] A. Tiwari, U. Lokman, in *Advanced Molecularly Imprinting Materials*
(Eds: A. Tiwari, L. Uzun), John Wiley & Sons, Inc., Hoboken, NJ 2016, Chapter 1.
- [39] R. Arshady, K. Mosbach, *Die Makromol. Chemie* 1981, 182, 687.
- [40] C. Alexander, H. S. Andersson, L. I. Andersson, R. J. Ansell, N. Kirsch, I. A. Nicholls, J. O'Mahony, M. J. Whitcombe, *J. Mol. Recognit.* 2006, 19, 106.

- [41] J. Haginaka, *J. Chromatogr. B* 2008, 866, 3.
- [42] J. Yin, G. Yang, Y. Chen, *J. Chromatogr. A* 2005, 1090, 68.
- [43] J. Matsui, T. Kato, T. Takeuchi, M. Suzuki, K. Yokoama, E. Tamiya, I. Karube, *Anal. Chem.* 1993, 65, 2223.
- [44] B. Sellergren, *J. Chromatogr. A* 2001, 906, 227.
- [45] M. Monier, A. M. A. El-Sokkary, *Int. J. Biol. Macromol.* 2010, 47, 207.
- [46] Z. J. Tan, V. T. Remcho, *Electrophoresis* 1998, 19, 2055.
- [47] M. Kempe, K. Mosbach, *J. Chromatogr. A* 1994, 664, 276.
- [48] R. J. Ansell, *Adv. Drug Deliv. Rev.* 2005, 57, 1809.
- [49] C. He, Y. Long, J. Pan, K. Li, F. Liu, *J. Biochem. Biophys. Methods* 2007, 70, 133.
- [50] F. G. Tamayo, E. Turiel, A. Martín-Esteban, *J. Chromatogr. A* 2007, 1152, 32.
- [51] M. Lasáková, P. Jandera, *J. Sep. Sci.* 2009, 32, 799.
- [52] V. Pichon, *J. Chromatogr. A* 2007, 1152, 41.
- [53] E. Caro, R. M. Marcé, F. Borrull, P. A. G. Cormack, D. C. Sherrington, *Trends Anal. Chem.* 2006, 25, 143.
- [54] E. Turiel, A. Martín-Esteban, *Anal. Chim. Acta* 2010, 668, 87.
- [55] M. Baker, *Nature* 2015, 527, 545.
- [56] K. Haupt, K. Mosbach, *Chem. Rev.* 2000, 100, 2495.
- [57] W. Kusnezow, J. D. Hoheisel, *Biotechniques* 2002, 33, S14.
- [58] S. Nestora, F. Merlier, S. Beyazit, E. Prost, L. Duma, B. Baril, A. Greaves, K. Haupt, B. Tse Sum Bui, *Angew. Chem.* 2016, 128, 6360.

- [59] B. B. Prasad, A. Srivastava, M. P. Tiwari, *J. Colloid Interface Sci.* 2013, 396, 234.
- [60] W. Wan, M. Biyikal, R. Wagner, B. Sellergren, K. Rurack, *Angew. Chem. Int. Ed.* 2013, 52, 7023.
- [61] G. Guan, R. Liu, Q. Mei, Z. Zhang, *Chem. A Eur. J.* 2012, 18, 4692.
- [62] F. Lu, H. Li, M. Sun, L. Fan, H. Qiu, X. Li, C. Luo, *Anal. Chim. Acta* 2012, 718, 84.
- [63] L. Chen, X. Wang, W. Lu, X. Wu, J. Li, *Chem. Soc. Rev.* 2016, 45, 2137.
- [64] D. Spivak, *Adv. Drug Deliv. Rev.* 2005, 57, 1779.
- [65] D. S. Janiak, P. Kofinas, *Anal. Bioanal. Chem.* 2007, 389, 399.
- [66] B. Schweiger, J. Kim, Y. J. Kim, M. Ulbricht, *Sensors* 2015, 15, 4870.
- [67] L. I. Andersson, *J. Chromatogr. B Biomed. Sci. Appl.* 2000, 739, 163.
- [68] K. Smolinska-Kempisty, A. Guerreiro, F. Canfarotta, C. Cáceres, M. J. Whitcombe, S. Piletsky, *Sci. Rep.* 2016, 6, 37638.
- [69] S. A. Piletsky, E. V. Piletska, A. Bossi, K. Karim, P. Lowe, A. P. F. Turner, *Biosens. Bioelectron.* 2001, 16, 701.
- [70] X. Hu, Y. Hu, G. Li, *J. Chromatogr. A* 2007, 1147, 1.
- [71] A. N. Baeza, J. L. Urraca, R. Chamorro, G. Orellana, M. Castellari, M. C. Moreno-Bondi, *J. Chromatogr. A* 2016, 1474, 121.
- [72] E. Yilmaz, O. Ramström, P. Möller, D. Sanchez, K. Mosbach, *J. Mater. Chem.* 2002, 12, 1577.
- [73] G. Vlatakis, L. Andersson, R. Muller, K. Mosbach, *Nature* 1993, 361, 645.
- [74] U. Athikomrattanakul, N. Gajovic-Eichelmann, F. W. Scheller, *Anal.*
- [75] M. Haruki, Y. Konnai, A. Shimada, H. Takeuchi, *Biotechnol. Prog.* 2007, 0, 0.
- [76] N. T. Hoai, D.-K. Yoo, D. Kim, *J. Hazard. Mater.* 2010, 173, 462.

- [77] X. Chen, Z. Zhang, X. Yang, Y. Liu, J. Li, M. Peng, S. Yao, *J. Sep. Sci.* 2012, 35, 2414.
- [78] X. Cai, J. Li, Z. Zhang, F. Yang, R. Dong, L. Chen, *ACS Appl. Mater. Interfaces* 2014, 6, 305.
- [79] L. Guo, X. Ma, X. Xie, R. Huang, M. Zhang, J. Li, G. Zeng, Y. Fan, *Chem. Eng. J.* 2019, 361, 245.
- [80] Y. Liu, D. Wang, F. Du, W. Zheng, Z. Liu, Z. Xu, X. Hu, H. Liu, *Microchem. J.* 2019, 145, 337.
- [81] A. Rachkov, N. Minoura, *J. Chromatogr. A* 2000, 889, 111.
- [82] A. Rachkov, N. Minoura, *Biochim. Biophys. Acta – Protein Struct. Mol. Enzymol.* 2001, 1544, 255.
- [83] M. J. Abdin, Z. Altintas, I. E. Tothill, *Biosens. Bioelectron.* 2015, 67, 177.
- [84] Z. Altintas, B. France, J. O. Ortiz, I. E. Tothill, *Sensors Actuat. B Chem.* 2016, 224, 726.
- [85] Y. Lv, T. Tan, F. Svec, *Biotechnol. Adv.* 2013, 31, 1172.
- [86] L. I. Andersson, A. Paprica, T. Arvidsson, *Chromatograph* 1997, 46, 57.
- [87] K. Karim, T. Cowen, A. Guerreiro, E. Piletska, M. J. Whitcombe, S. A. Piletsky, *Glob. J. Biotechnol. Biomater. Sci.* 2017.
- [88] I. A. Nicholls, H. S. Andersson, C. Charlton, H. Henschel, B. C. G. Karlsson, J. G. Karlsson, J. O'Mahony, A. M. Rosengren, K. J. Rosengren, S. Wikman, *Biosens. Bioelectron.* 2009, 25, 543.
- [89] E. B. B. Castro, G. Ramirez, M. F. Rubio, M. J. Whitcombe, E. N. Vulfson, R. Vazquez-Duhalt, *Am. Inst. Chem. Eng. J.* 1998, 329.
- [90] S. A. Piletsky, K. Karim, E. V. Piletska, A. P. F. Turner, C. J. Day, K. W. Freebairn, C. Legge, *Analyst* 2001, 126, 1826.
- [91] L. Zhang, L. Chen, H. Zhang, Y. Yang, X. Liu, *J. Appl. Polym. Sci.* 2017, 134, 45468.
- [92] Y. Kong, N. Wang, X. Ni, Q. Yu, H. Liu, W. Huang, W. Xu, *J. Appl. Polym. Sci.* 2016, 133.
- [93] B. Gao, X.-P. He, Y. Jiang, J.-T. Wei, H. Suo, C. Zhao, *J. Sep. Sci.* 2014, 37, 3753.

- [94] L. D. Marestoni, A. Wong, G. T. Feliciano, M. R. R. Marchi, C. R. T. Tarley, M. D. P. T. Sotomayor, L. D. Marestoni, A. Wong, G. T. Feliciano, M. R. R. Marchi, C. R. T. Tarley, M. D. P. T. Sotomayor, *J. Braz. Chem. Soc.* 2015, 27, 109.
- [95] Z. Dai, J. Liu, S. Tang, Y. Wang, Y. Wang, R. Jin, *J. Mol. Model.* 2015, 21, 290.
- [96] S. J. Pace, E. Nguyen, M. P. Baria, E.-R. E. Mojica, *Microchim. Acta* 2015, 182, 69.
- [97] B. Sellergren, M. Lepistoe, K. Mosbach, *J. Am. Chem. Soc.* 1988, 110, 5853.
- [98] L. Wang, W. Fu, Y. Shen, H. Tan, H. Xu, *Molecules* 2017, 22, 508.
- [99] P. Mattos dos Santos, A. J. Hall, P. Manesiotis, *J. Chromatogr. B* 2016, 1021, 197.
- [100] L. Fielding, *Tetrahedron* 2000, 56, 6151.
- [101] J. O'Mahony, A. Molinelli, K. Nolan, M. R. Smyth, B. Mizaikoff, *Biosens. Bioelectron.* 2005, 20, 1884.
- [102] J. Sánchez-González, Á. Peña-Gallego, J. Sanmartín, A. M. Bermejo, P. Bermejo-Barrera, A. Moreda-Piñeiro, *Microchem. J.* 2019, 147, 813.
- [103] S. Akatani, R. Takemoto, T. Kitade, A. Konishi, S. Takegami, *J. Anal. Bioanal. Tech.* 2017, 08, 1.
- [104] H. S. Andersson, I. A. Nicholls, *Bioorg. Chem.* 1997, 25, 203.
- [105] Y. Zhang, X. Qu, J. Yu, L. Xu, Z. Zhang, H. Hong, C. Liu, *J. Mater. Chem. B* 2014, 2, 1390.
- [106] K. M. Annamma, B. Mathew, *Mater. Sci. Appl.* 2011, 2, 131.
- [107] V. K. Srivastava, R. Yadav, in *Handbook for Complex Biological Data Source* (Eds: G. Misra), Academic Press 2019, pp. 125–137.
- [108] M. W. Freyer, C. B. Lewis, in *Biophysical Tools For Biologists, Volume One: In Vitro Techniques*, Academic Press, Cambridge, MA 2008, pp. 79–113.

- [109] S. Wei, M. Jakusch, B. Mizaikoff, *Anal. Chim. Acta* 2006, 578, 50.
- [110] J. K. Awino, Y. Zhao, *Chem. Commun.* 2014, 50, 5752.
- [111] S. Striegler, *Anal. Chim. Acta* 2005, 539, 91.
- [112] W. P. Fish, J. Ferreira, R. D. Sheardy, N. H. Snow, T. P. O'Brien, *J. Liq. Chromatogr. Relat. Technol.* 2005, 28, 1.
- [113] R. J. Ansell, in *Advances in Biochemical Engineering/Biotechnology* (Eds: B. Mattiasson, L. Ye), Springer International Publishing, Cham, 2015, pp. 51–93.
- [114] Z. Zhang, J. Liu, *RSC Adv.* 2015, 5, 91018.
- [115] W.-Y. Chen, C.-S. Chen, F.-Y. Lin, *J. Chromatogr. A* 2001, 923, 1.
- [116] L. Chen, J. Liu, Q. Zeng, H. Wang, A. Yu, H. Zhang, L. Ding, *J. Chromatogr. A* 2009, 1216, 3710.
- [117] T. Hasegawa, S. Tatsuta, Y. Katsumoto, *Anal. Bioanal. Chem.* 2010, 398, 2203.
- [118] S. Wei, J. Li, Y. Liu, J. Ma, *J. Chromatogr. A* 2016, 1473, 19.
- [119] N. Karaseva, T. Ermolaeva, B. Mizaikoff, *Sensors Actuat. B Chem.* 2016, 225, 199.
- [120] Z. Zhang, X. Cao, Z. Zhang, J. Yin, D. Wang, Y. Xu, W. Zheng, X. Li, Q. Zhang, L. Liu, *Talanta* 2020, 208, 120385.
- [121] Y. Liu, Q. Yang, X. Chen, Y. Song, Q. Wu, Y. Yang, L. He, *Talanta* 2019, 204, 238.
- [122] Y. Fuchs, O. Soppera, K. Haupt, *Anal. Chim. Acta* 2012, 717, 7.
- [123] X. Xie, X. Liu, X. Pan, L. Chen, S. Wang, *Anal. Bioanal. Chem.* 2016, 408, 963.
- [124] F. Chen, J. Zhang, M. Wang, J. Kong, *J. Sep. Sci.* 2015, 38, 2670.
- [125] X. Wang, L. Chen, X. Xu, Y. Li, *Anal. Bioanal. Chem.* 2011, 401, 1423.
- [126] X. Li, J. Pan, J. Dai, X. Dai, L. Xu, X. Wei, H. Hang, C. Li, Y. Liu, *Chem. Eng. J.* 2012, 198–199, 503.

- [127] F. Liu, S. Zhang, G. Wang, J. Zhao, Z. Guo, RSC Adv. 2015, 5, 22811.
- [128] P. Wang, S. Chen, X. Zhu, J. Xie, J. Chromatogr. A 2009, 1216, 7639.
- [129] K. Chullasat, P. Nurerk, P. Kanatharana, F. Davis, O. Bunkoed, Sensors Actuat. B Chem. 2018, 254, 255.
- [130] Y. Tunc, N. Hasirci, A. Yesilada, K. Ulubayram, Polymer 2006, 47, 6931.
- [131] M. Valtchev, B. S. Palm, M. Schiller, U. Steinfeld, J. Hazard. Mater. 2009, 170, 722.
- [132] H. Wang, R. Wang, Y. Han, J. Chromatogr. B 2014, 24, 949.
- [133] W. Mao, L. Xia, H. Xie, Angew. Chem. Int. Ed. 2017, 56, 4468.
- [134] R. E. Hargrove, R. J. Lehman, C. A. Matthews, J. Dairy Sci. 1958, 41, 617.
- [135] H. Nakata, K. Kannan, P. D. Jones, J. P. Giesy, Chemosphere 2005, 58, 759.
- [136] H. Sunayama, T. Ohta, A. Kuwahara, T. Takeuchi, J. Mater. Chem. B 2016, 4, 7138.
- [137] E. Benito-Peña, M. C. Moreno-Bondi, S. Aparicio, G. Orellana, J. Cederfur, M. Kempe, Anal. Chem. 2006, 78, 2019.
- [138] S. Wagner, J. Bell, M. Biyikal, K. Gawlitza, K. Rurack, Biosens. Bioelectron. 2018, 99, 244.
- [139] Y. Liu, Y. Wang, L. Liu, Y. He, Q. He, Y. Ji, Anal. Bioanal. Chem. 2016, 408, 5261.
- [140] M.-R. Chao, C.-W. Hu, J.-L. Chen, Biosens. Bioelectron. 2014, 61, 471.
- [141] Y. Geng, M. Guo, J. Tan, S. Huang, Y. Tang, L. Tan, Y. Liang, Sensors Actuat. B Chem. 2018, 268, 47.
- [142] T. Shi, L. Tan, H. Fu, J. Wang, Mar. Pollut. Bull. 2019, 146, 591.
- [143] L. Zhang, L. Chen, ACS Appl. Mater. Interfaces 2016, 8, 16248.
- [144] T. Zhou, A. Halder, Y. Sun, Biosensors 2018, 8, 82.

- [145] K. Chen, R. He, X. Luo, P. Qin, L. Tan, Y. Tang, Z. Yang, *Biosens. Bioelectron.* 2017, 94, 609.
- [146] Q. Yang, J. Li, X. Wang, H. Peng, H. Xiong, L. Chen, *Biosens. Bioelectron.* 2018, 112, 54.
- [147] O. Y. F. Henry, D. C. Cullen, S. A. Piletsky, *Anal. Bioanal. Chem.* 2005, 382, 947.
- [148] H. Niu, Y. Yang, H. Zhang, *Biosens. Bioelectron.* 2015, 74, 440.
- [149] J. Ashley, X. Feng, Y. Sun, *Talanta* 2018, 182, 49.
- [150] R. L. McCreery, *Chem. Rev.* 2008, 108, 2646.
- [151] A. García-Miranda Ferrari, C. W. Foster, P. J. Kelly, D. A. C. Brownson, C. E. Banks, *Biosens.* 2018, 8, 53.
- [152] I.-A. Stoian, B.-C. Iacob, C.-L. Dudaş, L. Barbu-Tudoran, D. Bogdan, I. O. Marian, E. Bodoki, R. Oprean, *Biosens. Bioelectron.* 2020, 155, 112098.
- [153] A. R. Cardoso, A. C. Marques, L. Santos, A. F. Carvalho, F. M. Costa, R. Martins, M. G. F. Sales, E. Fortunato, *Biosens. Bioelectron.* 2019, 124–125, 167.
- [154] B. Feier, A. Blidar, A. Pusta, P. Carciuc, C. Cristea, *Biosensors* 2019, 9, 31.
- [155] D. Dechtrirat, P. Yingyuad, P. Prajongtat, L. Chuenchom, C. Sriprachuabwong, A. Tuantranont, I.-M. Tang, *Microchim. Acta* 2018, 185, 261.
- [156] A. G. Ayankojo, J. Reut, V. Ciocan, A. Öpik, V. Syritski, *Talanta* 2020, 209, 120502.
- [157] W. Lian, S. Liu, L. Wang, H. Liu, *Biosens. Bioelectron.* 2015, 73, 214.
- [158] E. Mazzotta, A. Turco, I. Chianella, A. Guerreiro, S. A. Piletsky, C. Malitesta, *Sensors Actuat. B Chem.* 2016, 229, 174.
- [159] F. Canfarotta, A. Poma, A. Guerreiro, S. Piletsky, *Nat. Protoc.* 2016, 11, 443.
- [160] A. Poma, A. P. F. Turner, S. A. Piletsky, *Trends Biotechnol.* 2010, 28, 629.
- [161] S. Guillon, R. Lemaire, A. V. Linares, K. Haupt, C. Ayela, *Lab Chip* 2009, 9, 2987.

- [162] J. P. Metters, R. O. Kadara, C. E. Banks, *Analyst* 2011, 136, 1067.
- [163] A. Heller, B. Feldman, *Chem. Rev.* 2008, 108, 2482.
- [164] E. P. Randviir, D. A. C. Brownson, J. P. Metters, R. O. Kadara, C. E. Banks, *Phys. Chem. Chem. Phys.* 2014, 16, 4598.
- [165] J. P. Metters, R. O. Kadara, C. E. Banks, *Analyst* 2013, 138, 2516.
- [166] J. P. Metters, R. O. Kadara, C. E. Banks, *Sensors Actuat. B Chem.* 2012, 169, 136.
- [167] A. P. Ruas de Souza, M. Bertotti, C. W. Foster, C. E. Banks, *Electroanalysis* 2015, 27, 2295.
- [168] J. P. Metters, E. P. Randviir, C. E. Banks, *Analyst* 2014, 139, 5339.
- [169] A. P. Ruas de Souza, C. W. Foster, A. V. Kollopoulos, M. Bertotti, C. E. Banks, *Analyst* 2015, 140, 4130.
- [170] Z. Taleat, A. Khoshroo, M. Mazloun-Ardakani, *Microchim. Acta* 2014, 181, 865.
- [171] R. Crapnell, A. Hudson, C. Foster, K. Eersels, B. Grinsven, T. Cleij, C. Banks, M. Peeters, *Sensors* 2019, 19, 1204.
- [172] M. Peeters, B. van Grinsven, C. Foster, T. Cleij, C. Banks, *Molecules* 2016, 21, 552.
- [173] S. Casadio, J. W. Lowdon, K. Betlem, J. T. Ueta, C. W. Foster, T. J. Cleij, B. van Grinsven, O. B. Sutcliffe, C. E. Banks, M. Peeters, *Chem. Eng. J.* 2017, 315, 459.
- [174] K. Betlem, I. Mahmood, R. D. Seixas, I. Sadiki, R. L. D. Raimbault, C. W. Foster, R. D. Crapnell, S. Tedesco, C. E. Banks, J. Gruber, M. Peeters, *Chem. Eng. J.* 2019, 359, 505.
- [175] R. Gui, H. Jin, H. Guo, Z. Wang, *Biosens. Bioelectron.* 2018, 100, 56.
- [176] O. Jamieson, T. C. C. Soares, B. A. de Faria, A. Hudson, F. Mecozzi, S. J. Rowley-Neale, C. E. Banks, J. Gruber, K. Novakovic, M. Peeters, R. D. Crapnell, *Chemosensors* 2020, 8, 5.
- [177] L. Devkota, L. T. Nguyen, T. T. Vu, B. Piro, *Electrochim. Acta* 2018, 270, 535.

- [178] M. Rohani Moghadam, L. Salehi, S. Jafari, N. Nasirizadeh, J. Ghasemi, *Microchim. Acta* 2019, 186, 798.
- [179] A. Florea, B. Feier, C. Cristea, in *Mip Synthesis, Characteristics And Analytical Application*, (Ed: M. Marc), Elsevier, Amsterdam 2019.
- [180] I. Losito, F. Palmisano, P. G. Zambonin, *Anal. Chem.* 2003, 75, 4988.
- [181] S. Komaba, M. Seyama, T. Momma, T. Osaka, *Electrochim. Acta* 1997, 42, 383.
- [182] Y.-M. Uang, T.-C. Chou, *Electroanalysis* 2002, 14, 1564.
- [183] *Intelligent Coatings For Corrosive* (Eds: A. Tiwari, J. Rawlins, L. Hihara), Elsevier, Amsterdam 2015.
- [184] G. Moro, F. Bottari, N. Slegers, A. Florea, T. Cowen, L. M. Moretto, S. Piletsky, K. De Wael, *Sensors Actuat. B Chem.* 2019, 297, 126786.
- [185] F. Bottari, G. Moro, N. Slegers, A. Florea, T. Cowen, S. Piletsky, A. L. N. van Nuijs, K. De Wael, *Electroanalysis* 2020, 32, 135.
- [186] M. Roushani, Z. Rahmati, S. J. Hoseini, R. Hashemi Fath, *Colloids Surf. B Biointerfaces* 2019, 183, 110451.
- [187] A. K. Prusty, S. Bhand, *Electroanalysis* 2019, 31, 1797.
- [188] L. Chen, B. Li, *Anal. Methods* 2012, 4, 2613.
- [189] J. Dai, J. Pan, L. Xu, X. Li, Z. Zhou, R. Zhang, Y. Yan, *J. Hazard. Mater.* 2012, 205–206, 179.
- [190] R. Ahmad, N. Griffete, A. Lamouri, N. Felidj, M. M. Chehimi, C. Mangeney, *Chem. Mater.* 2015, 27, 5464.
- [191] S. Carrasco, E. Benito-Peña, F. Navarro-Villoslada, J. Langer, M. N. Sanz-Ortiz, J. Reguera, L. M. Liz-Marzán, M. C. Moreno-Bondi, *Chem. Mater.* 2016, 28, 7947.

- [192] M. Niu, C. Pham-Huy, H. He, *Microchim. Acta* 2016, 183, 2677.
- [193] Y. Tang, M. Li, X. Gao, X. Liu, Y. Ma, Y. Li, Y. Xu, J. Li, *Microchim. Acta* 2016, 183, 589.
- [194] E. Yilmaz, K. Haupt, K. Mosbach, *Angew. Chem. Int. Ed.* 2000, 39, 2115.
- [195] C. Giovannoli, L. Anfossi, F. Biagioli, C. Passini, C. Baggiani, *Microchim. Acta* 2013, 180, 1371.
- [196] A. Poma, A. Guerreiro, M. J. Whitcombe, E. V. Piletska, A. P. F. Turner, S. A. Piletsky, *Adv. Funct. Mater.* 2013, 23, 2821.
- [197] P. X. Medina Rangel, S. Laclef, J. Xu, M. Panagiotopoulou, J. Kovensky, B. Tse Sum Bui, K. Haupt, *Sci. Rep.* 2019, 9, 3923.
- [198] E. Moczko, A. Poma, A. Guerreiro, I. Perez de Vargas Sansalvador, S. Caygill, F. Canfarotta, M. J. Whitcombe, S. Piletsky, *Nanoscale* 2013, 5, 3733.
- [199] A. Elbelazi, F. Canfarotta, J. Czulak, M. J. Whitcombe, S. Piletsky, E. Piletska, *Nano Res.* 2019, 12, 3044.
- [200] A. E. Ekpenyong-Akiba, F. Canfarotta, B. Abd H, M. Poblocka, M. Casulleras, L. Castilla-Vallmanya, G. Kocsis-Fodor, M. E. Kelly, J. Janus, M. Althubiti, E. Piletska, S. Piletsky, S. Macip, *Nanoscale Horiz.* 2019, 4, 757.
- [201] A. Cecchini, V. Raffa, F. Canfarotta, G. Signore, S. Piletsky, M. P. MacDonald, A. Cuschieri, *Nano Lett.* 2017, 17, 2307.
- [202] J. Xu, E. Prost, K. Haupt, B. Tse Sum Bui, *Sensors Actuat. B Chem.* 2018, 258, 10.
- [203] J. Xu, F. Merlier, B. Avalle, V. Vieillard, P. Debré, K. Haupt, B. Tse Sum Bui, *ACS Appl. Mater. Interfaces* 2019, 11, 9824.
- [204] F. Canfarotta, S. A. Piletsky, N. W. Turner, in (Eds: J. A. Gerrard, L. J. Domigan) Springer, New York 2020, pp. 183–194.

- [205] F. Canfarotta, K. Smolinska-Kempisty, S. Piletsky, in (Eds: T. Tiller), Springer, New York 2017, pp. 389–398.
- [206] K. Betlem, F. Canfarotta, R. Raumbault, C. E. Banks, K. Eersels, B. van Grinsven, T. J. Cleij, R. Crapnell, A. Hudson, M. Peeters, *Analyst* 2020, 145, 5419.
- [207] F. Canfarotta, J. Czulak, K. Betlem, A. Sachdeva, K. Eersels, B. van Grinsven, T. J. Cleij, M. Peeters, *Nanoscale* 2018, 10, 2081.
- [208] S.-P. Tang, F. Canfarotta, K. Smolinska-Kempisty, E. Piletska, A. Guerreiro, S. Piletsky, *Anal. Methods* 2017, 9, 2853.
- [209] C. Chen, J. Luo, C. Li, M. Ma, W. Yu, J. Shen, Z. Wang, *J. Agric. Food Chem.* 2018, 66, 2561.
- [210] W. Zhang, Z. Chen, *Talanta* 2013, 103, 103.
- [211] M. Bompart, K. Haupt, C. Ayela, in Springer, Berlin 2011, p. 83.
- [212] Z. Altintas, J. Pocock, K.-A. Thompson, I. E. Tothill, *Biosens. Bioelectron.* 2015, 74, 996.
- [213] M. J. Whitcombe, I. Chianella, L. Larcombe, S. A. Piletsky, J. Noble, R. Porter, A. Horgan, *Chem. Soc. Rev.* 2011, 40, 1547.
- [214] I. Chianella, A. Guerreiro, E. Moczko, J. S. Caygill, E. V. Piletska, I. M. P. De Vargas Sansalvador, M. J. Whitcombe, S. A. Piletsky, *Anal. Chem.* 2013, 85, 8462.
- [215] G. Guan, B. Liu, Z. Wang, Z. Zhang, *Sensors* 2008, 8, 8291.
- [216] Y. Wu, Y. Liu, X. Gao, K. Gao, H. Xia, M. Luo, X. Wang, L. Ye, Y. Shi, B. Lu, *Chemosphere* 2015, 119, 515.
- [217] P. Turkewitsch, B. Wandelt, G. D. Darling, W. S. Powell, *Anal. Chem.* 1998, 70, 2025.
- [218] O. Güney, F.Ç. Cebeci, *J. Appl. Polym. Sci.* 2010, 117, 2373.
- [219] Z. Uygun, H. Uygun, N. Ermise, E. Canbay, in (Eds: T. Rinken), InTech, Rijeka, 2015.

- [220] V. Tsouti, C. Boutopoulos, I. Zergioti, S. Chatzandroulis, *Biosens. Bioelectron.* 2011, 27, 1.
- [221] L. Lebogang, M. Hedström, B. Mattiasson, *Anal. Chim. Acta* 2014, 826, 69.
- [222] W. Limbut, M. Hedström, P. Thavarungkul, P. Kanatharana, B. Mattiasson, *Anal. Bioanal. Chem.* 2007, 389, 517.
- [223] R. Suedee, C. Songkram, A. Petmoreekul, S. Sangkunakup, S. Sankasa, N. Kongyarit, *J. Pharm. Biomed. Anal.* 1999, 19, 519.
- [224] M.-C. Savoy, P. M. Woo, P. Ulrich, A. Tarres, P. Mottier, A. Desmarchelier, *Food Addit. Contam. Part A* 2018, 35, 675.
- [225] G. Vasapollo, R. Del Sole, L. Mergola, M. R. Lazzoi, A. Scardino, S. Scorrano, G. Mele, *Int. J. Mol. Sci.* 2011, 12, 12.
- [226] A. C. Gray, A. R. M. Bradbury, A. Knappik, A. Plückthun, C. A. K. Borrebaeck, S. Dübel, *Nat. Methods* 2020, 17, 755.
- [227] N. W. Turner, C. W. Jeans, K. R. Brain, C. J. Allender, V. Hlady, D. W. Britt, *Biotechnol. Prog.* 2006, 22, 1474.
- [228] R. Li, Y. Feng, G. Pan, L. Liu, *Sensors* 2019, 19, 177.

Appendix H. Published paper on the detection of amoxicillin via MIP modified SPEs

Screen Printed Electrode Based Detection Systems for the Antibiotic Amoxicillin in Aqueous Samples Utilising Molecularly Imprinted Polymers as Synthetic Receptors

Oliver Jamieson¹, Thais C. C. Soares², Beatriz A. de Faria³, Alexander Hudson¹, Francesco Mecozzi⁴, Samuel J. Rowley-Neale^{4,5}, Craig E. Banks^{4,5}, Jonas Gruber³, Katarina Novakovic¹, Marloes Peeters¹ and Robert D. Crapnell^{4,*}

¹School of Engineering, Newcastle University, Merz Court, Claremond Road, Newcastle Upon Tyne NE1 7RU, UK

²Departamento de Engenharia Química, Escola Politécnica, Universidade de São Paulo, Avenida Prof. Luciano Gualberto, trav. 3, 380, CEP 05508-900 São Paulo, SP, Brazil

³Departamento de Química Fundamental, Instituto de Química, Universidade de São Paulo, Av. Prof. Lineu Prestes, 748, CEP 05508-000 São Paulo, SP, Brazil

⁴Faculty of Science and Engineering, Manchester Metropolitan University, John Dalton Building, Chester Street, Manchester M1 5GD, UK

⁵Manchester Fuel Cell Innovation Centre, Manchester Metropolitan University, Chester Street, Manchester M1 5GD, UK

Abstract

Molecularly Imprinted Polymers (MIPs) were synthesised for the selective detection of amoxicillin in aqueous samples. Different functional monomers were tested to determine the optimal composition via batch rebinding experiments. Two different sensor platforms were tested using the same MIP solution; one being bulk synthesized and surface modified Screen Printed Electrodes (SPEs) via drop casting the microparticles onto the electrode surface and the other being UV polymerized directly onto the SPE surface in the form of a thin film. The sensors were used to measure amoxicillin in conjunction with the Heat-Transfer Method (HTM), a low-cost and simple thermal detection method that is based on differences in the thermal resistance at the solid–liquid interface. It was demonstrated that both sensor platforms could detect amoxicillin in the relevant concentration range with Limits of Detection (LOD) of 1.89 ± 1.03 nM and 0.54 ± 0.10 nM for the drop cast and direct polymerisation methods respectively. The sensor platform utilising direct UV polymerisation exhibited an enhanced response for amoxicillin detection, a reduced sensor preparation time and the selectivity of the platform was proven through the addition of nafcillin, a pharmacophore of similar shape and size. The use of MIP-modified SPEs combined with thermal detection provides sensors that can be used for fast and low-cost detection of analytes on-site, which holds great potential for contaminants in environmental aqueous samples. The platform and synthesis methods are generic and by adapting the MIP layer it is possible to expand this sensor platform to a variety of relevant targets.

Keywords: beta lactam antibiotics; amoxicillin; antimicrobial resistance; biomimetic sensors; Molecularly Imprinted Polymers (MIPs), Heat-Transfer Method (HTM), Screen-Printed Electrodes (SPEs), thermal sensors

1. Introduction

The World Health Organisation has stated that antimicrobial resistant (AMR) bacteria pose a fundamental threat to human health due to the overuse and declining effectiveness of antibiotics [1,2]. Antibiotic consumption has increased 65% worldwide between the years 2000 and 2015 [3]. The use of antibiotics in veterinary or clinical practice exerts selective pressure to bacteria, which accelerates the emergence of bacteria with AMR properties due to the accumulation of pharmaceuticals in the food chain and water systems. There are also notable concerns about the discharge of antibiotic waste by pharmaceutical producers, which lead to point-source pollution. Watkinson et al. have shown that even in a first world country such as Australia, there are many water systems that have a presence of beta lactam antibiotics [4]. Recent studies from India, one of the world's leading pharmaceutical producers, has revealed excessively high concentrations of antibiotic compounds in drinking water that exceed the maximum regulatory limits (MRLs). This has a serious impact on vulnerable populations living near manufacturing facilities, with an estimate of 58,000 new-borns dying in India in these regions from multi-drug resistant infections [5,6,7]. The risk of these infections is considerably higher in developing countries, which has been attributed to the lack of optimal wastewater treatment facilities and high costs associated with vigilant monitoring of pharmaceutical waste [8]. Furthermore, while there are strict European regulations regarding MRL of pharmaceuticals in food products of animal origin, regulations for waste and surface water are yet to be implemented with currently only environmental quality standards set for a number of micropollutants [9]. Antibiotic residues that are most often found in aquatic environments belong to the classes of beta-lactams, fluoroquinolones, macrolides, sulfonamides and tetracyclines [10]. Current commercial screening tests for antibiotics in food and environmental samples either require a long response time (several hours), or are not able to selectively detect antibiotic compounds and solely provide semi-quantitative information. Thus, there is a strong need for low-cost, robust and easy to use sensors that can be used on site to determine trace

levels of antibiotics in aquatic systems. Many electrochemical sensors display promise in this respect [11,12,13]. Pellegrini et al. [14] discuss the usability of electrochemical sensors for the determination of antibiotics and promote their use for on-site testing due to their analysis time (~2 h) and small sample volume (~100 μ L). These factors combined with the lack of any pre-treatment steps required and a high level of precision give a strong indication of the appropriateness of this type of analysis for the desired purpose. Previous reports in literature have shown the ability of synthetic polymeric recognition elements, namely Molecularly Imprinted Polymers (MIPs), to improve the affinity and selectivity of electrochemical sensors [15]. Yang et al. [16] have demonstrated limits of detection in the nanomolar regime in buffered solutions and in spiked food samples can be achieved with MIP layers grown onto multiwalled carbon nanotubes. Zeinali et al. [17], use magnetic MIPs modified onto carbon paste electrodes combined with cyclic voltammetry to detect amoxicillin with a limit of detection of 0.26 nM. Betlem et al. [18] have shown the effective use for the Heat-Transfer Method (HTM) as an appropriate analysis technique for small molecules such as caffeine.

The current study was built on from this work and tailored the detection system to a beta lactam antibiotic. We used amoxicillin in this manuscript as a case study and compared the sensors characteristics of microparticle modified Screen-Printed Electrodes (SPEs) to those functionalised with a thin film. The structures of amoxicillin and nafcillin, another beta lactam antibiotic used in this study to test the selectivity of the sensors, are shown in **Figure 1**.

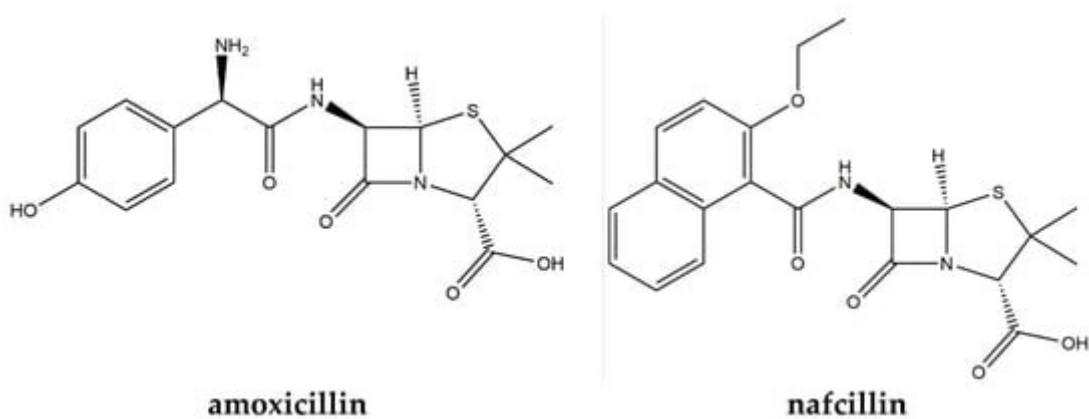


Figure 1. Structures of amoxicillin and nafcillin.

SPEs are often used in commercial sensors due to their high reproducibility, low-cost and inherent suitability for mass-production [19]. However, integration of polymer structures into SPEs is complicated due to their low resistance to traditional organic solvents such as chloroform and toluene [20].

In this paper, we explore two different electrode modification strategies and compare and contrast towards the analytical detection of amoxicillin. The SPEs are modified with MIPs in two manners; (i) surface modification via dropcasting of MIP microparticles suspended into ethanol directly onto the sensor surface along with a thin layer of polypyrrole to hold the MIPs in place; (ii) directly depositing of MIP thin films onto SPEs using UV polymerization. The disadvantage of working with MIP microparticles is the two-step (indirect) functionalisation process and the fact that the resulting electrodes are insulating and not compatible with traditional electrochemical detection. Recent work in our group has demonstrated that thermal analysis, in particular the Heat-Transfer Method (HTM), can provide an interesting alternative analysis technique that is easy to employ and provides rapid detection [21].

2. Experimental

2.1. Equipment and Reagents

Dimethyl Sulfoxide (DMSO) was sourced from TCI (Oxford, UK). Pyrrole, amoxicillin, nafcillin, azobisisobutyronitrile (AIBN), trimethylolpropane trimethacrylate (TRIM), methacrylic acid (MAA), acrylamide (AA) and 2-vinylpyridine were sourced from Sigma Aldrich (Gillingham, UK). Ethanol was sourced from Fisher Scientific (Loughborough, UK). The orbital shaker used was a Stuart mini orbital shaker SSM1 (Staffordshire, UK). All experiments were carried out in Newcastle University and Manchester Metropolitan University. Experiments were carried out at 20 ± 1 °C unless otherwise noted. UV/Vis analysis was carried out on an Agilent 8453 UV-Vis spectrophotometer (Santa Clara, CA, USA). Phosphate Buffered Saline (PBS) tablets were purchased from Sigma (Gillingham, UK) and used to maintain pH level (pH = 7.4) and the ionic strength of solutions used throughout the experimental portion of the study.

2.2. MIP and NIP Microparticle Syntheses

MIPs for amoxicillin were synthesised with varying compositions, which are listed in **Table 1**. The general functionalisation procedure includes mixing of the template (0.35 mmol) with the monomer (1.4 mmol) in 3.3 mL of DMSO. Subsequently, the crosslinker monomer TRIM (2.8 mmol) was added followed by the initiator AIBN (0.22 mmol). The mixture was sonicated and degassed with N₂. Polymerization was initiated by exposing the samples to a UV lamp (200 mW, Polytec UV LC-S, Karlsbad, Germany) for 10–15 min. The obtained polymer block was washed with water and subsequently ground to obtain a fine powder. The template was removed by continuous Soxhlet extraction with a mixture of methanol and water (50/50) until UV-Vis analysis no longer showed traces of amoxicillin in the extract. The powders were washed with water and dried overnight under vacuum. Non-Imprinted Polymers (NIPs) were synthesized in the same manner but without the addition of the template.

Table 1. The composition of the different Molecularly Imprinted Polymers (MIPs), listing the amount of template, functional monomer, crosslinker monomers, initiator and porogen used.

| | MIP-1 | MIP-2 | MIP-3 |
|---------------------------|--------------|--------------|--------------|
| Amoxicillin (mmol) | 0.35 | 0.35 | 0.35 |
| MAA (mmol) | 1.4 | - | - |
| Acrylamide (mmol) | - | 1.4 | - |
| 2-vinylpyridine (mmol) | - | - | 1.4 |
| TRIM (mmol) | 2.8 | 2.8 | 2.8 |
| Initiator (mmol) | 0.22 | 0.22 | 0.22 |
| DMSO (mL) | 3.3 | 3.3 | 3.3 |

2.3. Batch Rebinding Experiments Evaluated with Optical Detection

Batch rebinding experiments were performed and optical detection was used to evaluate the binding of amoxicillin to the MIP and NIP powders. The antibiotic concentration was determined by measuring the absorbance at $\lambda = 272$ nm. In each experiment, 10 mg of MIP or NIP powder was added to 5.0 mL of PBS solutions with amoxicillin concentrations between 0.5–1.0 mM. The resulting suspensions were placed on a rocking table (110 rpm) for 60 min and subsequently filtered. The free concentration of amoxicillin (C_f) in the filtrate was determined by comparing the absorbance to that of a pre-determined calibration curve. Subsequently, the amount of bound template (C_b) was calculated by subtracting the initial concentration added to the solution (C_i) by the free template concentration (C_f), $C_b = C_i - C_f$. The molecule of template bound per gram (S_b) was obtained by multiplying C_b by the volume in litres and then dividing this by the amount of polymer used in the experiment (10 mg). The Imprint Factor (IF) was determined by dividing S_b for a given MIP by the S_b for the corresponding NIP at a C_f value of 0.5 mM [22].

2.4. Thin Film Polymerization

A pre-polymerization mixture of MIP 2 was produced as described in **Section 2.2**. A total of 0.3 μ L of the solution was applied onto the working electrode of the SPE and subsequently exposed to UV light (365 nm) for 1 min. A cover slip was placed over the droplet and it was exposed to UV light for a further 1 min to complete the polymerization. The functionalised SPE was then washed in methanol and the template extracted in deionized water (40 mL) using an orbital shaker (160 rpm) overnight and stored in a fresh deionized water solution until use. A NIP was produced using an identical protocol without the presence of the target amoxicillin.

2.5. Electrochemical Deposition of Polypyrrole

Electrochemical experiments were performed using a standard three electrode set up. Graphite Screen-Printed macroelectrodes (SPE, Manchester Metropolitan University, UK) [23,24] were utilised as the working electrode alongside a nickel/chromium wire auxiliary

electrode and silver silver chloride (Ag AgCl) reference electrode (BASi, West Lafayette, IN, USA). These were controlled by an Ivium Compactstat (Eindhoven, The Netherlands) connected to a Desktop PC (Dell, UK). The SPEs were fabricated in-house using a stencil design to achieve a 3.1 mm diameter working electrode using a graphite ink (Product Ink: C2000802P2; Gwent Electronic Materials Ltd., Pontypool, UK) and were printed using a DEK 248 screen printer machine (DEK, Weymouth, UK) onto a polyester flexible film (Autostat, Milan, Italy, 250 micron thickness). The layer was cured in a fan oven at 60 °C for 30 min and finally, a dielectric paste (Product Code: D2070423D5; Gwent Electronic Materials Ltd., Pontypool, UK) was then printed onto the polyester substrate to cover the connections. The SPEs were then cured for an additional 30 min at 60 °C before use [25,26].

All electrochemical measurements were carried out at 20 ± 1 °C and using deionised water of resistivity ≥ 18.2 M Ω cm. Prior to all electrochemical measurements the solutions were thoroughly degassed with highly pure nitrogen for 15 min.

MIP microparticles were dispersed in ethanol (1 mg/mL), dropcast (30 μ L) onto the SPE surface and allowed to dry. Following this, a thin layer of polypyrrole was applied to the SPE surface to hold the MIPs in place. A droplet (30 μ L) of pyrrole (0.1 M) in PBS was applied to the electrode surface. Electropolymerization was performed through chronoamperometry, using the three electrode system described above and applying a potential of +0.8 V for 30 s. The electrodes were thoroughly rinsed with deionised water and the presence of MIPs on the surface confirmed by Scanning Electron Microscopy (SEM) (**Figure S1A**).

2.6. Scanning Electron Microscopy (SEM)

SEM measurements were recorded on a Supra 40VP Field Emission from Carl Zeiss Ltd. (Cambridge, UK) with an average chamber vacuum of 1.3×10^{-5} mbar and average gun vacuum of 1×10^{-9} mbar. To enhance the contrast of these images, a thin layer of Au/Pd (8 V, 30 s) was sputtered onto the electrodes with a SCP7640 from Polaron (Hertfordshire, UK).

2.7. HTM Measurements with MIP-Modified SPEs

The functionalised SPEs were cut into 1×1 cm squares, inserted into an additively manufactured/3D-printed flow cell [27] and sealed with an O-ring (RS Components, UK). Thermal measurements were carried out using the flow cell (**Figure S2**) of volume 110 μL in conjunction with the heat-transfer set-up which was designed in-house [28,29]. The flow cell is connected to a copper block which acts as a heat sink. The temperature of this block (T_1) is controlled via a Proportional-Integral-Derivative (PID) controller. A type-K thermocouple (RS Components, UK) is used to measure the temperature of the sample solution (T_2) 1.7 mm above the surface of the SPE. The thermal resistance (R_{th}) at the solid-liquid interface can be determined by dividing the measured temperature difference between the copper block and the solution ($T_1 - T_2$) by the power provided to the heat source to maintain its temperature, $R_{\text{th}} = (T_1 - T_2) / P$. The aforementioned PID parameters can affect the power signal stability and therefore the sensitivity of the developed sensor. As such, the PID parameters were set to the optimized values determined for this heat source of $P = 1$, $I = 14$, $D = 0.3$ [21].

For all experiments, the flow cell was filled with PBS solution and the copper block was heated to a pre-set temperature of 37.00 ± 0.02 °C. The cell was left to stabilise for 15 min before a first injection of PBS was added to act as the blank measurement. Sequential amounts of amoxicillin (1–500 nM) were injected into the flow cell using an automated NE500 programmable syringe pump (Prosense, Oosterhout, the Netherlands) at a flow rate of 250 $\mu\text{L} \cdot \text{min}^{-1}$. Following each injection, the temperature was allowed to stabilise for 30 min, of which the last 10 min (600 data points) were averaged out and used to calculate the R_{th} . These experiments were carried out in triplicate to prove the reproducibility of the electrodes. The calculated R_{th} values were used to produce dose-response curves and calculate the limit of detection (LoD) using the three sigma method. Specificity tests were carried out by injecting the same concentrations of amoxicillin to an electrode modified with a NIP. Selectivity studies

were carried out by injecting the same concentration of a competitive target, with a similar pharmacophore, nafcillin.

3. Results

3.1. Batch Rebinding Results

First, batch rebinding experiments with MIP1-3, that have similar compositions, but differ in the functional monomer, were performed and are presented in **Table 2**. The time of the experiments was fixed at 1 h since after this time no increase in the binding to the MIP particles was observed. In each experiment, 5 mL of amoxicillin solutions in PBS ($C_i = 0.5\text{--}1.0$ mM) were added to 10 mg of the MIP particles.

Table 2. The amount of binding for MIP and Non-Imprinted Polymer (NIP) at $C_f = 0.5$ mM.

| Polymers | S_b [$\mu\text{mol/g}$] | Imprint factor $C_f = 0.5$ mM |
|----------|-----------------------------|----------------------------------|
| MIP1 | 43.86 | 1.3 |
| NIP1 | 35.09 | |
| MIP 2 | 63.38 | 6.5 |
| NIP 2 | 9.8 | |
| MIP 3 | 2.48 | 0.3 |
| NIP 3 | 8.47 | |

The results obtained from the batch rebinding experiments are presented in **Table 2** and **Figure 2**. It was observed that MIP 2, made of acrylamide (AA) as the functional monomer, exhibited a significantly higher binding affinity for the amoxicillin target compared to MIP 1 (based on methacrylic acid) and MIP 3 (based on 2-vinyl pyridine). In addition to this,

at a C_f value of 0.5 mM the calculated Imprint Factor (IF) for MIP 2 was significantly higher than either of the other MIPs at 6.47, exhibiting the MIPs affinity efficiency compared to the corresponding NIP. The highest affinity MIP using AA as a functional monomer was most likely due to the nature of the functional groups on the monomer when compared to the structure of the target. These functional groups would allow self-assembling of monomers around the target to form the non-covalent forces necessary to hold them together [30]. On the other hand, 2-vinylpyrldine lacks these functional groups required for binding [31].

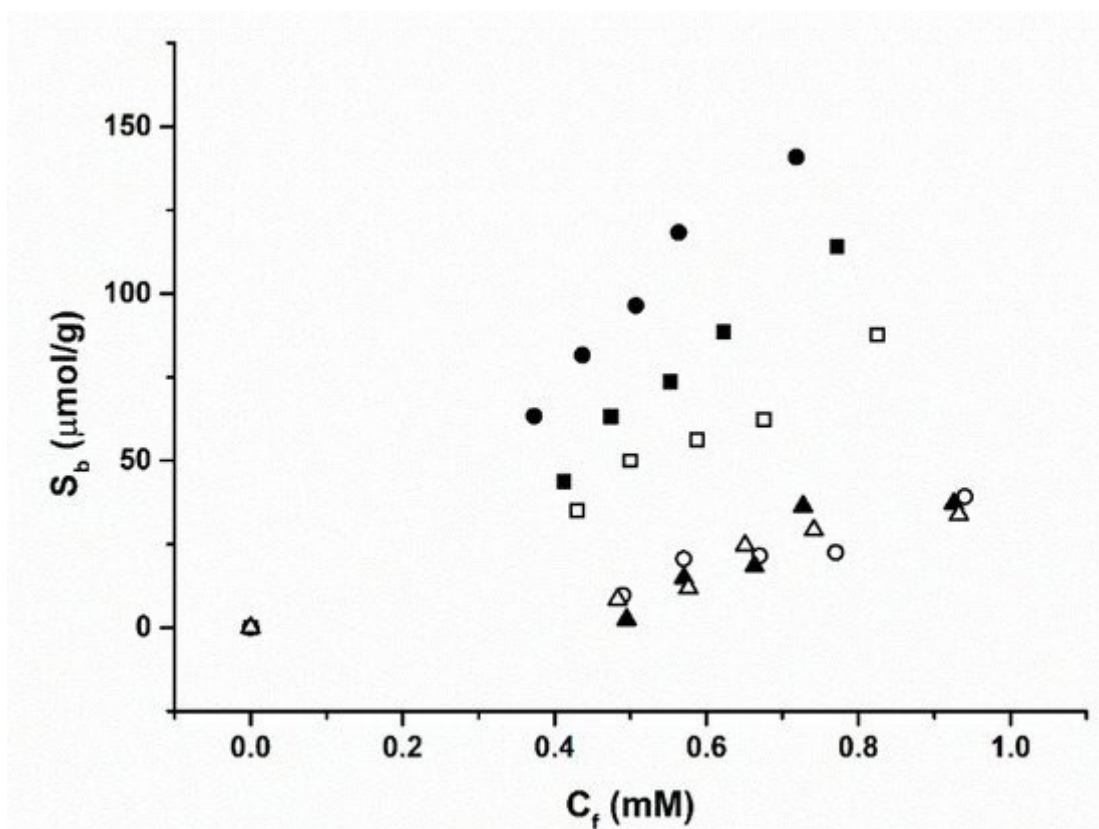


Figure 2. Binding isotherms of the polymerised MIP/NIPs upon exposure to amoxicillin solutions in Phosphate Buffered Saline (PBS). MIP 1 (**filled squares**) and NIP 1 (**hollow squares**), MIP 2 (**filled circles**) and NIP 2 (**hollow circles**) and MIP 3 (**filled triangles**) and NIP 3 (**hollow triangles**).

Time dependent experiments were performed to determine the optimal time for rebinding. Readings were taken at 30 min, 2 h and 24 h after mixing MIP with target solution, resulting in absorbance values of 1.52, 1.51 and 1.47, respectively. This shows that there is no significant change over time and that 30 min is sufficient to gain an accurate representation of batch rebinding data.

Figure 3 displays the selectivity presented by MIP 2, which exhibits a higher binding affinity towards amoxicillin than towards nafcillin. This shows that the pores in the imprinted polymer have a higher affinity towards their intended target even if a very similar pharmacophore is used, thus confirming the polymers ability to recognise the target. The NIPs have no significant difference in binding affinity as expected, since they do not possess the stereoselective cavities present in the MIP.

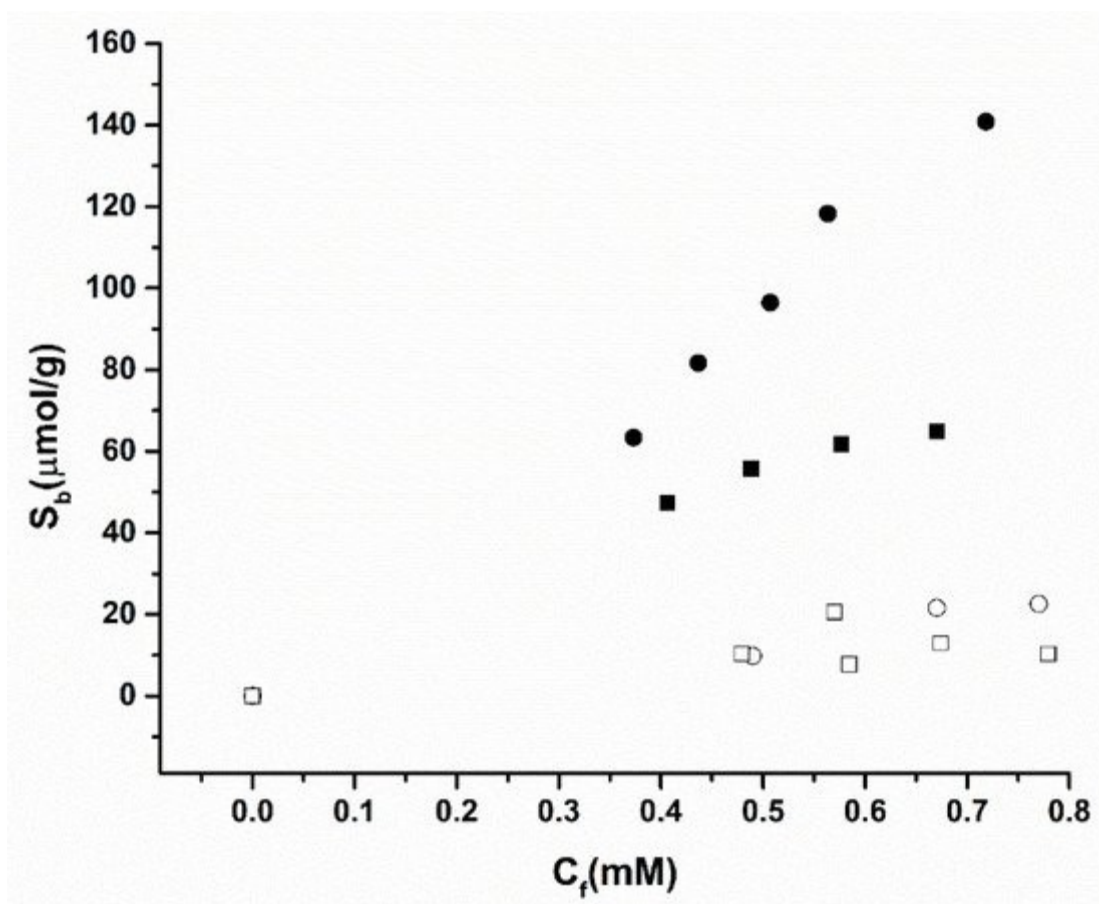


Figure 3. Selectivity batch rebinding of MIP 2 (**filled symbols**) and NIP 2 (**hollow symbols**) with amoxicillin (**squares**) and nafcillin (**circles**) in PBS.

The relevant concentration range of amoxicillin in water samples is in the low nanomolar range [32]. Therefore, it was decided to evaluate the performance of the sensor to discriminate amoxicillin from its competitor molecule in the nanomolar concentration, for which it is required to use a more sensitive read-out strategy such as HTM.

3.2. Detection of Amoxicillin Using MIP Microparticles

Bulk polymerized MIPs (MIP 2) were functionalised onto SPEs (**Figure S1A**) as explained in **Section 2.5**, fitted inside the flow cell (**Figure S2**) and connected to the HTM equipment. SPEs were used in this work because they can be used as disposable sensors. This aligns well with the use of MIPs as multiple template removals is not advised for a reproducible platform. The flow cell was filled with PBS and allowed to stabilise for 45 min. Then, sequential injections of the target analyte amoxicillin (1–500 nM) in PBS were started, allowing the system to equilibrate for 30 min after each injection. The raw data output obtained for these additions is presented in **Figure 4A**. Specific values for the thermal resistance (R_{th}) values for each concentration of amoxicillin were calculated using the last 10 min of each stabilisation period. This resulted in a value and standard deviation being calculated over 600 data points. In PBS, the R_{th} of the MIP functionalised system stabilised at a value of 5.91 ± 0.05 °C/W. Upon the addition of 1 nM of amoxicillin the R_{th} increased from this baseline value to 6.06 ± 0.05 °C/W. The R_{th} value increased further until the addition of 500 nM of amoxicillin where it stabilised at a value of 6.42 ± 0.06 °C/W. An identical experiment was performed using an SPE modified with the NIP. In this case, R_{th} of the NIP functionalised system stabilised at a value of 5.51 ± 0.06 °C/W. After the addition of 1 nM of amoxicillin the R_{th} exhibited no statistically significant deviation from the baseline value to 5.55 ± 0.06 °C/W. The R_{th} value for the addition of 500

nM of amoxicillin showed a small increase due to some non-specific binding, where it stabilised at a value of 5.61 ± 0.06 °C/W.

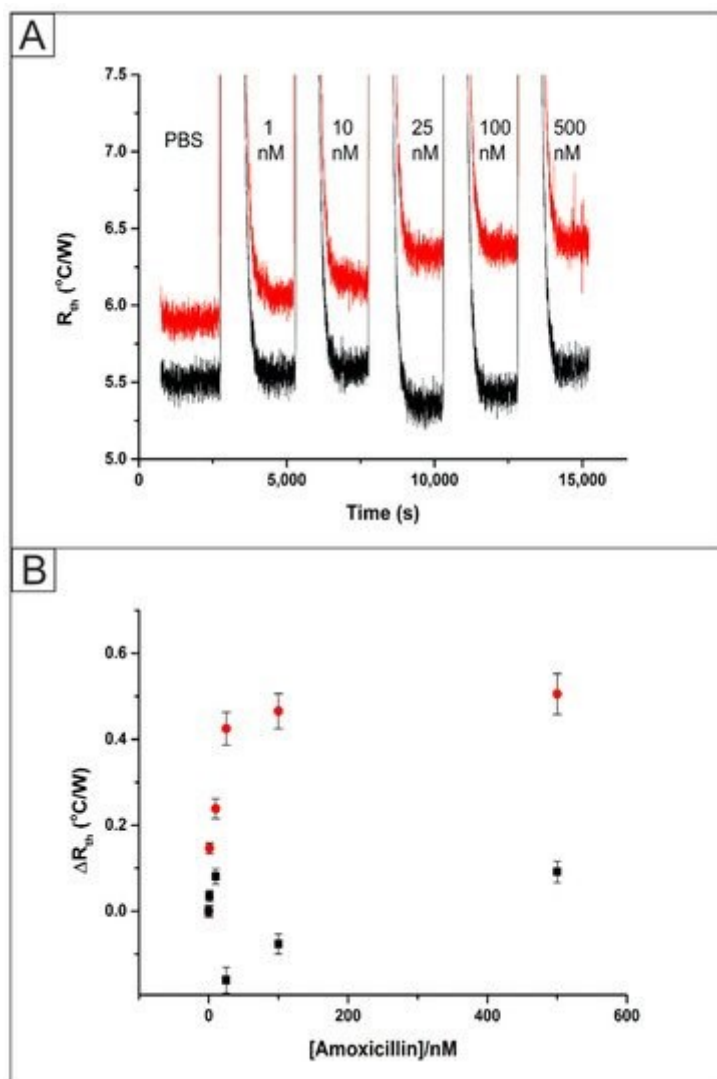


Figure 4. (A) The raw Heat-Transfer Method (HTM) data plot of R_{th} versus time for the addition of amoxicillin (1–500 nM) in PBS to an Screen Printed Electrodes (SPE) functionalised with bulk UV polymerized MIP (red) and NIP (black). (B) Comparison between the absolute R_{th} values obtained from the HTM for a MIP functionalised SPE (red circles) and NIP functionalised SPE (black).

These R_{th} values were plotted against the concentration of amoxicillin injected into the system to produce a dose-response curve, **Figure 4B**. This was used to calculate a Limit of Detection (LOD) for the bulk UV polymer system of 1.90 ± 1.03 nM. These results were found to exhibit a lower LOD and wider detection range than that observed in previous work on caffeine detection [18]. This was expected due to the limited loading of MIP when incorporated directly into the SPE ink in comparison to drop casting. Additionally, template bleeding is a problem in the use of MIP microparticles. Up to 99% of the template is removed during the extraction step; however, the remaining template can cause issues when ‘leeching’ out of the polymer matrix during measurements giving erroneous quantification [33]. The removal of MIP over time is of considerable concern when using a drop casting method, therefore the direct formation of the MIP onto the electrode surface using UV polymerisation was investigated.

3.3. Detection of Amoxicillin Using MIP Thin Films

Screen-Printed Electrodes (SPEs) were functionalised with amoxicillin MIPs via UV-Vis polymerization (**Figure S1B**) as described in **Section 2.4**. These SPEs were inserted into a flow cell (**Figure S2**) and exposed to PBS solutions containing sequential amounts of the target analyte amoxicillin. The HTM raw data obtained for the addition of amoxicillin (1–500 nM) are presented in **Figure 5A**. In PBS, the R_{th} of the MIP functionalised system stabilised at a value of 7.58 ± 0.05 °C/W. The increase in the R_{th} value compared to previous work [18,21] was expected due to the presence of a thicker layer of polymer present on the electrode surface, which in turn will increase the resistance to heat flow through the interface. Upon the addition of 1 nM of amoxicillin an increase in the absolute R_{th} value was observed from its baseline of 7.58 ± 0.05 °C/W to 7.67 ± 0.06 °C/W. The R_{th} increased until the last addition of 500 nM amoxicillin where it reached a value of 8.16 ± 0.06 °C/W and an additional injection of PBS produced no significant change in the R_{th} . An identical experiment was performed using a NIP functionalised SPE where the R_{th} stabilised at a value of 7.59 ± 0.06 °C/W. Upon the addition

of 1 nM of amoxicillin to the system there was no significant change to the R_{th} value with it remaining at 7.59 ± 0.06 °C/W. Once 500 nM of amoxicillin was added to the NIP modified SPE there was an increase in the R_{th} to 7.68 ± 0.07 °C/W. The increase in the R_{th} can be explained by some non-specific binding of the target molecule to the polymer on the surface of the SPE however, the increase is significantly less than observed for the MIP modified SPE. Both of these results were used to produce a dose-response curve (**Figure 5B**) which shows the improved response of the MIP based platform and was used to calculate the Limit of Detection (LOD) of 0.54 ± 0.10 nM.

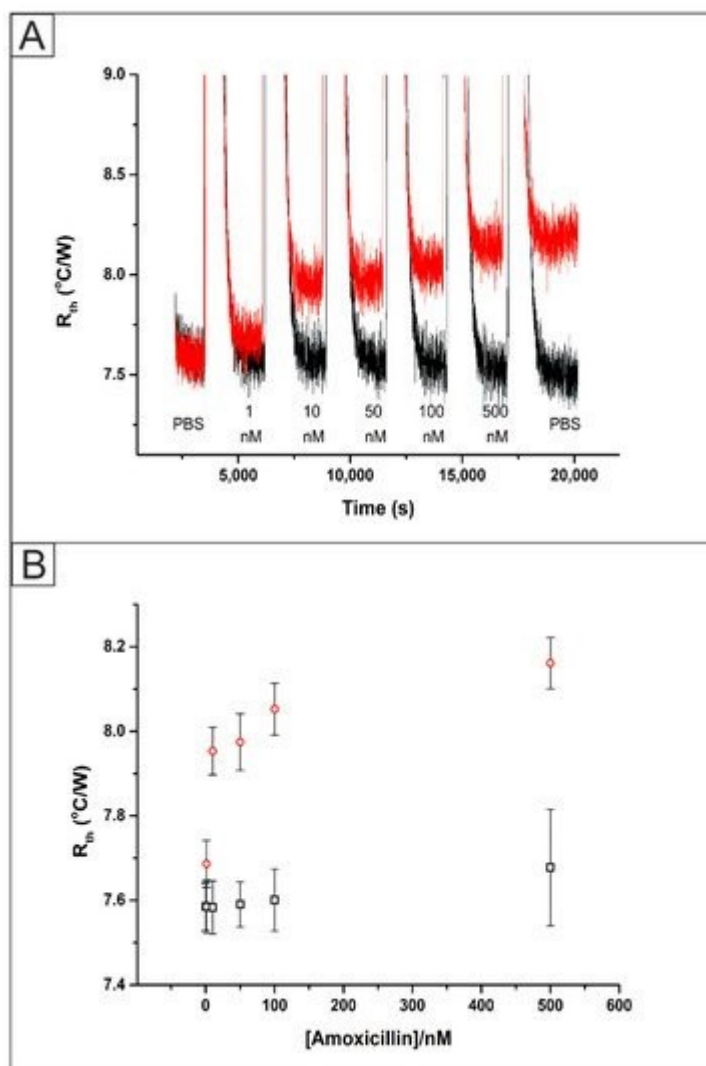


Figure 5. (A) The raw HTM data plot of R_{th} versus time for the addition of amoxicillin (1–500 nM) in PBS to an SPE functionalised with a direct UV polymerized MIP (red) and NIP (black). (B) Comparison between the absolute R_{th} values obtained from the HTM for a MIP functionalised SPE (red circles) and NIP functionalised SPE (black).

The selectivity of the MIP was assessed through repeating the experiment with additions of a molecule with the same pharmacophore and similar size, nafcillin (1–500 nM). An SPE functionalised with a MIP via UV polymerization directly onto the surface was placed inside the flow cell (**Figure S1**) and attached to the HTM equipment. The data collected from the addition of the competitor (black) was plotted alongside the previous results for the addition of the target molecules (red) to MIP functionalised SPEs.

The raw data plot that was obtained is presented in **Figure 6A** (black) where there is a clear difference between the stabilised R_{th} values. This can be explained as the Type K thermocouples used in the experiment have a temperature error of up to 2.5 °C. The R_{th} value of the system in PBS stabilised at a value of 6.47 ± 0.05 °C/W. Upon the addition of 1 nM of nafcillin, there was no observed statistically significant change in the stabilised R_{th} value at 6.46 ± 0.05 °C/W. Once 500 nM of nafcillin had been injected into the flow cell an increase in the R_{th} was observed from the baseline level of 6.47 ± 0.05 °C/W up to 6.60 ± 0.05 °C/W. These values, along with those obtained for the addition of the target molecule were used to produce dose-response curves, **Figure 6B**, showing the increase in the R_{th} from the baseline stabilised levels for both the target (red circles) and competitor (black squares). This indicated that there was some non-specific binding of the competitor antibiotic to the surface of the polymer. However, the increase was significantly lower than that observed for the injections of the target antibiotic, showing the high selectivity of the sensing platform.

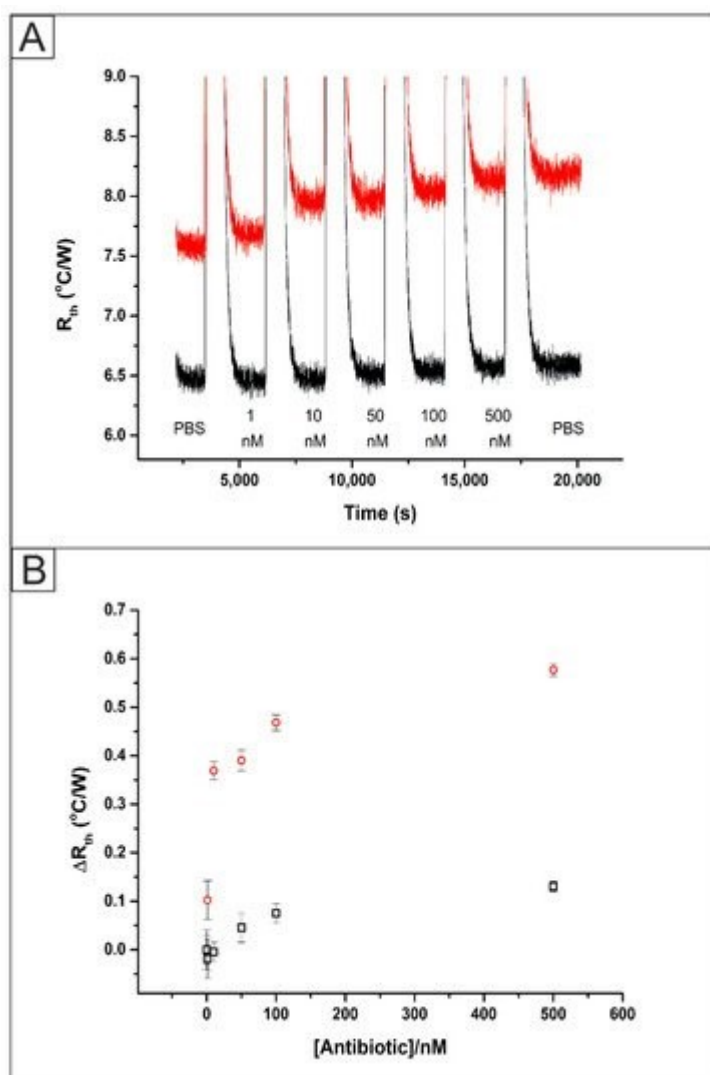


Figure 6. (A) The raw HTM data plot of R_{th} versus time for the addition of amoxicillin (1–500 nM, red) and nafcillin (1–500 nM, black) in PBS to an SPE functionalised with a direct UV polymerized MIP. (B) Comparison between the absolute R_{th} values obtained from the HTM for a MIP functionalised SPE with additions of amoxicillin (red) and nafcillin (black).

4. Conclusions

MIPs for the detection of amoxicillin were synthesized using bulk UV polymerisation with the functional monomers methacrylic acid, acrylamide (AA) and 2-vinylpyridine. Batch

rebinding experiments evaluated via spectroscopic methods determined that the MIPs using AA (MIP 2) as the functional monomer exhibited the highest recognition capability ($IF = 6.47$) for amoxicillin. Subsequently, MIP 2 was drop cast onto a SPE, fitted to the HTM and subjected to injections of increasing concentrations of amoxicillin (1–500 nM). An increase in the measured R_{th} was observed from the baseline of 5.91 ± 0.05 °C/W to 6.42 ± 0.06 °C/W after the addition of 500 nM amoxicillin for the MIP functionalised SPE; whereas, the NIP functionalised exhibited an R_{th} of 5.52 ± 0.05 °C/W and 5.61 ± 0.06 °C/W for the baseline and 500 nM amoxicillin respectively. These results were used to construct a dose-response curve and calculate a LOD of 1.89 ± 1.03 nM. This was then compared to a system where the MIP was formed directly onto the SPE surface through UV polymerisation. This methodology dramatically reduced the preparation time and increased the reliability of the sensor through the attachment of the polymer to the electrode surface. An increase in the measured R_{th} was observed for the addition of amoxicillin (1–500 nM) to the MIP functionalised SPE from the baseline value of 7.58 ± 0.06 °C/W to 8.16 ± 0.06 °C/W at 500 nM amoxicillin. The NIP produced a significantly smaller increase in the R_{th} from 7.59 ± 0.06 °C/W to 7.68 ± 0.07 °C/W after 500 nM amoxicillin. The dose-response curve for the MIP allowed for the determination of the LOD of 0.54 ± 0.1 nM which is a big improvement over the drop cast method. The direct UV polymerized SPE was also tested for interference from a competitive pharmacophore, nafcillin. This exhibited a rise in the measured R_{th} from of 6.47 ± 0.05 °C/W in PBS to of 6.60 ± 0.05 °C/W after 500 nM nafcillin, showing the excellent specificity the MIP sensing platform has for amoxicillin.

The developed sensor platform has shown the ability to detect amoxicillin at relevant concentration ranges for environmentally contaminated aqueous samples. Molecular imprinting is versatile and by adapting the MIP, other antibiotics and pollutants can be targeted. The polymerisation methodology was significantly shortened in comparison to the bulk synthesis

method and in conjunction with the thermal set-up, offers a portable and low-cost sensing platform suitable for on-site measurements.

Supplementary Materials

The following are available online at <https://www.mdpi.com/2227-9040/8/1/5/s1>, Figure S1: **(A)** SEM image (2 k magnification) of MIP 2 microparticles immobilized onto an SPE using polypyrrole. **(B)** SEM image (1 k magnification) of thin film of polymer made directly on an SPE. Figure S2: Schematic image of the flow cell used in the experiments. The SPE is placed in the central chamber, which is sealed with an O-ring. The thermocouple (T_2) is measured throughout the experiment (1 second = 1 data point). Solutions of analyte are injected into the inflow and the system is allowed to stabilise for 30 min before the next injection.

Author Contributions

Conceptualization M.P. and R.D.C.; Data curation O.J., T.C.C.S., B.A.d.F., A.H., F.M. and R.D.C.; Formal analysis O.J., M.P. and R.D.C.; Methodology A.H., S.J.R.-N., M.P., C.E.B. and R.D.C.; Resources S.J.R.-N., C.E.B., J.G., K.N. and M.P., Supervision C.E.B., J.G., K.N., M.P. and R.D.C.; Writing – Original Draft O.J., A.H., M.P. and R.D.C.; Writing – Review and Editing C.E.B., J.G., K.N., M.P. and R.D.C. All authors have read and agreed to the published version of the manuscript.

Funding

This research was funded by EPSRC grant number EP/R029296/1 and Conselho Nacional de Desenvolvimento Científico e Tecnológico (CNPq) grant numbers 306147/2016-5 and 424027/2018-6.

Acknowledgments

All authors would like to thank Heitor Valarini. MP would like to acknowledge the EPSRC for funding under grant number EP/R029296/1. JG thanks Conselho Nacional de Desenvolvimento Científico e Tecnológico (CNPq) for the financial support (grant numbers: 306147/2016-5 and 424027/2018-6). Data available from <https://data.ncl.ac.uk>.

Conflicts of Interest

The authors declare no conflict of interest.

References

1. Michael, C.A.; Dominey-Howes, D.; Labbate, M. The antimicrobial resistance crisis: Causes, consequences, and management. *Front. Public Health* **2014**, *2*, 145.
2. World Health Organization. Antimicrobial Resistance and Primary Health Care: Brief; World Health Organization: Geneva, Switzerland, 2018.
3. Klein, E.Y.; Van Boeckel, T.P.; Martinez, E.M.; Pant, S.; Gandra, S.; Levin, S.A.; Goossens, H.; Laxminarayan, R. Global increase and geographic convergence in antibiotic consumption between 2000 and 2015. *Proc. Natl. Acad. Sci. USA* **2018**, *115*, E3463–E3470.
4. Watkinson, A.; Murby, E.; Kolpin, D.W.; Costanzo, S. The occurrence of antibiotics in an urban watershed: From wastewater to drinking water. *Sci. Total Environ.* **2009**, *407*, 2711–2723.
5. Hall, W. *Superbugs: An Arms Race against Bacteria*. Harvard University Press: Cambridge, MA, USA, 2018.
6. Mutiyar, P.K.; Mittal, A.K. Risk assessment of antibiotic residues in different water matrices in India: Key issues and challenges. *Environ. Sci. Pollut. Res.* **2014**, *21*, 7723–7736.
7. Fick, J.; Söderström, H.; Lindberg, R.H.; Phan, C.; Tysklind, M.; Larsson, D.J. Contamination of surface, ground, and drinking water from pharmaceutical production. *Environ. Toxicol. Chem.* **2009**, *28*, 2522–2527.

8. Ashbolt, N.J. Microbial contamination of drinking water and disease outcomes in developing regions. *Toxicology* **2004**, 198, 229–238.
9. European Union. Directive 2008/105/EC of the European Parliament and of the Council of 16 December 2008 on environmental quality standards in the field of water policy. *O. J. Eur. Union* **2008**, 348, 84–97.
10. Kemper, N. Veterinary antibiotics in the aquatic and terrestrial environment. *Ecol. Indic.* **2008**, 8, 1–13.
11. Rezaei, B.; Damiri, S. Electrochemistry and adsorptive stripping voltammetric determination of amoxicillin on a multiwalled carbon nanotubes modified glassy carbon electrode. *Electroanal. Int. J. Devoted Fundam. Pract. Asp. Electroanal.* **2009**, 21, 1577–1586.
12. Prado, T.M.; Cincotto, F.H.; Moraes, F.C.; Machado, S.A. Electrochemical sensor-based ruthenium nanoparticles on reduced graphene oxide for the simultaneous determination of ethinylestradiol and amoxicillin. *Electroanalysis* **2017**, 29, 1278–1285.
13. Muhammad, A.; Yusof, N.; Hajian, R.; Abdullah, J. Construction of an electrochemical sensor based on carbon nanotubes/gold nanoparticles for trace determination of amoxicillin in bovine milk. *Sensors* **2016**, 16, 56.
14. Pellegrini, G.E.; Carpico, G.; Coni, E. Electrochemical sensor for the detection and presumptive identification of quinolone and tetracycline residues in milk. *Anal. Chim. Acta* **2004**, 520, 13–18.
15. Ahmad, O.S.; Bedwell, T.S.; Esen, C.; Garcia-Cruz, A.; Piletsky, S.A. Molecularly imprinted polymers in electrochemical and optical sensors. *Trends Biotechnol.* **2019**, 37, 294–309.
16. Yang, G.; Zhao, F. Molecularly imprinted polymer grown on multiwalled carbon nanotube surface for the sensitive electrochemical determination of amoxicillin. *Electrochim. Acta* **2015**, 174, 33–40.
17. Zeinali, S.; Khoshsafar, H.; Rezaei, M.; Bagheri, H. Fabrication of a selective and sensitive electrochemical sensor modified with magnetic molecularly imprinted polymer for amoxicillin. *Anal. Bioanal. Chem. Res.* **2018**, 5, 195–204.
18. Betlem, K.; Mahmood, I.; Seixas, R.; Sadiki, I.; Raimbault, R.; Foster, C.; Crapnell, R.; Tedesco, S.; Banks, C.; Gruber, J.; et al. Evaluating the temperature dependence of heat-transfer based detection: A

case study with caffeine and molecularly imprinted polymers as synthetic receptors. *Chem. Eng. J.* **2019**, *359*, 505–517.

19. Li, M.; Li, Y.-T.; Li, D.-W.; Long, Y.-T. Recent developments and applications of screen-printed electrodes in environmental assays—A review. *Anal. Chim. Acta* **2012**, *734*, 31–44.

20. Almeida, E.S.; Silva, L.A.; Sousa, R.M.; Richter, E.M.; Foster, C.W.; Banks, C.E.; Munoz, R.A. Organic-resistant screen-printed graphitic electrodes: Application to on-site monitoring of liquid fuels. *Anal. Chim. Acta* **2016**, *934*, 1–8.

21. Crapnell, R.D.; Canfarotta, F.; Czulak, J.; Johnson, R.; Betlem, K.; Mecozzi, F.; Down, M.P.; Eersels, K.; van Grinsven, B.; Cleij, T.J.; et al. Thermal detection of cardiac biomarkers h-fabp and st2 using a molecularly imprinted nanoparticle-based multiplex sensor platform. *ACS Sens.* **2019**, *4*, 2838–2845.

22. Hudson, A.D.; Solà, R.; Ueta, J.T.; Battell, W.; Jamieson, O.; Dunbar, T.; Maciá, B.; Peeters, M. Synthesis of optimized molecularly imprinted polymers for the isolation and detection of antidepressants via HPLC. *Biomimetics* **2019**, *4*, 18.

23. Peeters, M.M.; van Grinsven, B.; Foster, C.W.; Cleij, T.J.; Banks, C.E. Introducing thermal wave transport analysis (twta): A thermal technique for dopamine detection by screen-printed electrodes functionalized with molecularly imprinted polymer (mip) particles. *Molecules* **2016**, *21*, 552.

24. Foster, C.W.; Metters, J.P.; Kampouris, D.K.; Banks, C.E. Ultraflexible screen-printed graphitic electroanalytical sensing platforms. *Electroanalysis* **2014**, *26*, 262–274.

25. Cumba, L.R.; Foster, C.W.; Brownson, D.A.; Smith, J.P.; Iniesta, J.; Thakur, B.; Do Carmo, D.R.; Banks, C.E. Can the mechanical activation (polishing) of screen-printed electrodes enhance their electroanalytical response? *Analyst* **2016**, *141*, 2791–2799.

26. Blanco, E.; Foster, C.W.; Cumba, L.R.; Do Carmo, D.R.; Banks, C.E. Can solvent induced surface modifications applied to screen-printed platforms enhance their electroanalytical performance? *Analyst* **2016**, *141*, 2783–2790.

27. Casadio, S.; Lowdon, J.W.; Betlem, K.; Ueta, J.T.; Foster, C.W.; Cleij, T.J.; van Grinsven, B.; Sutcliffe, O.B.; Banks, C.E.; Peeters, M. Development of a novel flexible polymer-based biosensor

platform for the thermal detection of noradrenaline in aqueous solutions. *Chem. Eng. J.* **2017**, 315, 459–468.

28. van Grinsven, B.; Vanden Bon, N.; Strauven, H.; Grieten, L.; Murib, M.; Jiménez Monroy, K.L.; Janssens, S.D.; Haenen, K.; Schöning, M.J.; Vermeeren, V.; et al. Heat-transfer resistance at solid–liquid interfaces: A tool for the detection of single-nucleotide polymorphisms in DNA. *ACS Nano* **2012**, 6, 2712–2721.

Appendix I. Published paper on a proof-of-concept- yeast sensor based on a MIP modified SPE

Electropolymerised molecularly imprinted polymers for the heat-transfer based detection of microorganisms: A proof-of-concept study using yeast

O. Jamieson¹, K. Betlem², N. Mansouri², R. D. Crapnell², F. S. Vieira³, A. Hudson¹, C. E. Banks², C. M. Liauw⁴, J. Gruber⁵, M. Zubko², K. A. Whitehead⁴, M. Peeters¹

1 Newcastle University, School of Engineering, Merz Court, Claremont Road, NE1 7RU Newcastle Upon Tyne, United Kingdom

2 Manchester Metropolitan University, Faculty of Science and Engineering, John Dalton Building, Chester Street, M1 5GD Manchester, United Kingdom

3 Departamento de Engenharia Química, Escola Politécnica, Universidade de São Paulo, Av. Prof. Luciano Gualberto, trav. 3, 380, CEP 05508-900 São Paulo, SP, Brazil

4 Microbiology at Interfaces, Manchester Metropolitan University, John Dalton Building, Chester Street, M15GD Manchester, United Kingdom

5 Departamento de Química Fundamental, Instituto de Química, Universidade de São Paulo, Av. Prof. Lineu Prestes, 748, CEP 05508-000 São Paulo, SP, Brazil

Abstract

In this contribution, molecularly imprinted polymers (MIPs) were electropolymerised onto screen-printed carbon electrodes (SPCEs) to develop specific sensors for thermal detection of yeast. A laboratory yeast strain free of interferents was used to optimise the polymerisation

procedure, whereas yeast in a complex mixture (yeast for baking) was employed to produce the final sensors and demonstrate proof-of-application. Two different electropolymerisation methods were employed, cyclic voltammetry and chronoamperometry respectively; the electrochemical methodology allows for controlled deposition and the ability to tailor the polymer surface to the required application. Infrared spectroscopy and scanning electron microscopy confirmed that the methods led to different structures; with cyclic voltammetry a high surface area was achieved, whereas for chronoamperometry a dense film was formed. Subsequently, these functionalised electrodes were inserted into a home-made thermal device that can measure the selective binding of yeast cells to the MIP layer *via* monitoring the thermal resistance (R_{th}) at the solid–liquid interface.

The results of the measurements showed that MIP-functionalised electrodes produced, according to both methods, a significant response in thermal signal for the MIP-functionalised electrode, which was not the case for the reference Non-Imprinted Polymer (NIP)-functionalised electrode. This demonstrated that thermal analysis can be employed for the detection of yeast, even in a complex sample such as food. To our knowledge, this is the first report of MIPs electropolymerised onto screen-printed electrodes for the thermal detection of fungi.

The proposed approach enables the fast production of low-cost electrodes using a simple manufacturing procedure compatible with a portable device, implying high commercial potential. In the future, this could be adapted to a broad range of microorganisms including bacteria.

1. Introduction

Microbiological contamination presents huge concerns in a wide variety of sectors throughout the world, such as in food and drink [1], [2], sports [3], medicine [4] and even the construction industry [5]. Contamination of food and drink products specifically presents huge concerns for both health and economic reasons [6]. Even in developed economies foodborne illness is commonplace, with an estimated one third of populations suffering from a type of foodborne illness annually [7]. The quality and safety of food is best preserved by delaying the growth of specific bacteria or by reducing contamination by bacterial pathogens; therefore rapid detection and removal of infected foodstuff is vital [8]. The majority of current detection methods for microorganisms are based on microbiological techniques, analytical antibody assays and nucleic acid-based assays, such as the polymerase chain reaction (PCR) tests [9]. All these methodologies require time-consuming preparation, procedures and/or measurement protocols, thus, development of a fast, reliable, on-site sensor platform for the recognition of microorganisms is of high interest to the analytical community. Commonly, antibodies are used as a recognition element in sensor development due to the specific recognition between the antibody and the target antigen, which can be released by, (*e.g.* virulence factors) or is present on the surface of the microorganism [10], [11]. However, problems with antibody-based sensors include high cost, high batch-to-batch variation, limited stability, and the fact that some antibodies still require animals for production [12], [13], [14].

As such, for use in a portable sensor, molecularly imprinted polymers (MIPs) have gained significant interest as biomimetic recognition elements capable of replacing antibodies due to their high affinity, low production cost and superior chemical and thermal stability [15], [16], [17]. They can be produced using a wide range of monomers and synthetic methodologies, leading to a vast array of sensitive and selective recognition elements [18], [19]. They have been shown to produce highly specific sensing platforms in conjunction with

optical [20], electrochemical [21] and thermal [22] detection methodologies. MIPs epitomise versatility in respect to target sensing. With optimisation, they can be utilised for the detection of a significant breadth of targets, ranging from small molecules to proteins and cells [23]. Whilst the present study demonstrates detection of yeast, there is promise to extrapolate the protocol to other targets, potentially even antimicrobial resistant (AMR) bacteria, in a bid to fight the critical issues posed by AMR. Thermal detection strategies have been relatively unexplored; when simply measuring the temperature such as with thermistors, it is difficult to require the level of specificity required for biomarker sensing. However, there has been promise in using the Heat-Transfer Method (HTM) which detection principle is based on measuring changes in heat transfer at the solid–liquid interface due to its low-cost, fast analysis, and ability to measure different markers by changing the functionalised interface. MIPs can be combined with the HTM as a read-out technique and have been shown to produce sensor platforms suitable for the detection of small molecules [24] and proteins [25], [26], as well as for the monitoring of the growth of microorganisms such as yeast and *Staphylococcus aureus* in nutrient rich media [27], [28]. Quantitative detection of microorganisms based on analysis of heat-transfer at the solid-interface provides significant challenges due to the inherent differences in size and shape of the microorganisms within a population. The selective detection of the presence of yeast cells has been reported previously using surface imprinted polymers (SIPs) combined with HTM [29], [30]. One significant drawback of using these SIPs is the production time, which can take as long as 18 h. In this manuscript, we explore the use of electropolymerisation which significantly reduces the manufacturing process of the biosensor to minutes, in addition to forming the MIP layer directly onto the surface of the transducer [31]. There have been multiple reports on conductive and non-conductive polymer MIPs for various transducers including glassy carbon electrodes (GCE) [32], [33], [34], gold [35], [36], [37] and screen-printed carbon electrodes

(SPCE) [38], [39], [40]. The latter are attractive options due to the ability to mass produce such sensors, in addition to their reliability, flexibility and low-cost [41], [42]. Previously, we have shown that SPCEs can be used as substrates for the deposition of MIP particles for the detection of antibiotics [43] or have the MIP microparticles directly incorporated into the screen-printing ink [44]. Polypyrrole (PPy) is a commonplace monomer when considering the application of MIP synthesis in respect to electrochemical means due to its conductivity. Ramanavicius *et. al* [45] displayed the use of PPy for a detection sensor for bisphenol S through the use of functionalised glass. The produced polymers displayed sensitivity as low as 0.7–12.5 μm and displayed promising selectivity trends when compared to related compounds such as bisphenol C. The use of electrochemical polymerisation over oxidation polymerisation is favoured due to ease and speed of the synthesis process in addition to facilitating direct deposition onto conductive surfaces [46]. The imprinting of larger biomacromolecules, including proteins and microorganisms, can be complicated since these contain a myriad of potential binding sites. Hence, it is often required to use combination of monomers to achieve selective binding, which can be a time-consuming process without the use of computational modelling tools. Different strategies to develop MIPs for electrochemical sensing of biomarkers and larger macromolecules are discussed in Ref. [47].

In this manuscript we present a proof-of-concept that MIPs can be generated directly onto SPCE substrates using electropolymerisation for the detection of microorganisms, in this case yeast, using the HTM. Due to the low-cost and reproducible nature of the SPCEs, there is scope to use them as disposable sensors in the future for screening of contaminants in the food and water industry.

2. Experimental

2.1. Reagents

To optimise the synthesis procedure, we worked with *Saccharomyces cerevisiae* laboratory strain DLY640 originating from the Rothstein lab [48], [49] which has the advantages of not containing interferents such as sorbitan monostereate and ascorbic acid in commercial baker's yeast. These compounds significantly interfere with analysis and mask the yeast and/or polymer signal and therefore a "pure" laboratory strain was used to optimise the synthesis procedure and enabling analysis with infrared (IR) spectroscopy and scanning electron microscopy (SEM). For each experiment, a fresh yeast colony was grown from a yeast extract peptone dextrose (YEPD) agar plate in 250 mL of YEPD broth until an optical density (OD) of at least 1.4 at 660 nm was reached. The optical density for cell concentration was determined by UV-vis analysis which was carried out on a Jenway 7205 UV-visible 72 Series Diode Array Scanning Spectrophotometer (UK). Allinson's Easy Bake Yeast (UK), containing *Saccharomyces cerevisiae* (7 g per sachet), sorbitan monostearate as emulsifier, and ascorbic acid as flour treatment agent, was used for all thermal analysis experiments to evaluate yeast detection in a complex sample such as food. Suspensions of yeast were prepared in sterile deionised water solutions, where the concentration was estimated using the optical density at 660 nm [50]. An optimal profilometer (Omniscan, UK) which uses a MicroXAM (phase shift) surface mapping microscope with an ADE phase shift (XYZ 4400 mL system) and an AD phase shift controller (Omniscan, UK) was used to determine layer thickness. This system was coupled to image analysis software Mapview AE (Omniscan, UK).

SPCEs were produced according to a well-known procedure described in [41]. Carbon-graphite ink formulation (Product Code: C2000802P2; Gwent Electronic Materials Ltd, UK) was printed onto a standard polyester substrate and cured at 60 °C for 30 min, followed by a dielectric layer (Product Code: D2070423D5; Gwent Electronic Materials Ltd., Pontypool, United Kingdom) to cover the connections, which was also cured at 60 °C for 30 min. The pyrrole was

sourced from Acros Organics (Loughborough, UK), the yeast extract, peptone bacteriological agar bacteriological (AgarNO.1), D (+)-glucose and glycerol were all obtained from Fisher Scientific (Basingstoke, UK), while the adenine sulfate was purchased from Alfa Aesar (Heysham, United Kingdom). All other chemicals mentioned were acquired from Sigma Aldrich (Gillingham, UK). All experiments were carried out at 21 ± 1 °C (ambient temperature) unless noted differently. For polymerisation, a modified PBS solution (pH = 2) was used to ensure a constant ionic strength was maintained for all experiments. All other experiments were carried out in deionised water.

2.2. MIP and NIP syntheses

MIPs and NIPs were produced by electrodeposition. A solution of pyrrole (1 mM) in a phosphate buffered saline solution at pH = 2 was prepared as follows: 4 g of NaCl, 0.1225 g of KCl, 0.72 g of Na₂HPO₄ and 0.12 g of KH₂PO₄ were dissolved in 25 mL of deionised water (resistivity 18.2 MΩ cm). The solution was then acidified to pH 2 via the addition of dilute HCl. Yeast cells were re-suspended in 2 mL of this solution to the density of approximately 5.0×10^6 colony forming units (CFU)/mL [28]. For the “real” yeast sample, powder from Allinson’s Easy Bake Yeast was suspended into deionised water solutions and the suspension density was determined spectrophotometrically as described in item 2.1. As the yeast was specialised for use in the culinary sector, it had other additives to enhance its performance. The addition of these additives complicates determination of the yeast cell concentration. Prior to using the *Saccharomyces cerevisiae* laboratory strain DLY640 it was recovered from cryo-storage on a YEPD plate. Then a single colony was re-suspended in 250 mL of YEPD broth and grown at, 23.00 ± 0.05 °C (for approx. 48 h) to an optical density of at least 1.4 at 660 nm.

After growth, the yeast cells were washed 3 times with fresh YEPD, aliquoted into 2 mL samples containing 20% of glycerol which serves as a cryo-protector and stored at $-80\text{ }^{\circ}\text{C}$.

All electrochemical experiments were performed using a three-electrode set up controlled by a PalmSens4 Potentiostat (the Netherlands), where the working electrode was an SPCE (diameter = 3.1 mm), counter electrode was a nickel wire and the reference was an external Ag|AgCl reference electrode. The procedures were all performed at $21 \pm 1\text{ }^{\circ}\text{C}$ in solutions made with deionised water (resistivity no less than $18\text{ M}\Omega\text{ cm}$). The SPCE was placed in the acidified pyrrole PBS solution and polymerised according to two electrochemical methods. The first method was cyclic voltammetry, where the electrodes were placed in solution and cycled from -0.2 V to $+1.2\text{ V}$ at 0.1 V s^{-1} for 10 scans. The second method was chronoamperometry, where the potential was set to $+0.98\text{ V}$ and maintained for 100 s for polymerisation.

The polymerised SPCEs were placed under running hot water to remove yeast cells from the polymer complex, SEM analysis was carried out to confirm this method of extraction was sufficient (see Supporting Information S-1). SEM measurements were recorded on a Supra 40VP Field Emission from Carl Zeiss Ltd. (Cambridge, UK) with an average vacuum chamber of $1.3 \times 10^{-5}\text{ mbar}$ and average gun vacuum of $1 \times 10^{-9}\text{ mbar}$. To enhance the contrast of these images, a thin layer of Au/Pd (8 V, 30 s) was sputtered onto the electrodes with a SCP7640 from Polaron (Hertfordshire, UK). Furthermore, references (Non-Imprinted Polymers) were prepared in a similar manner except there was no addition of yeast to the pyrrole solution in PBS. Diffuse reflectance Fourier transform infrared spectroscopy (DRIFTS) was conducted to monitor polymerisation over time; the high roughness and dark colour of the electrode surfaces made them suitable for DRIFTS. A Thermo-Nicolet Nexus FTIR, (DTGS detector), fitted with a Spectra-Tech DRIFTS cell (equivalent to the current Thermo-Fisher Scientific Collector™ II Diffuse Reflectance Accessory) was used for this analysis. Spectra were made up of 164 scans with resolution set to 4 cm^{-1} . The thickness of the polymerised film (a measure

of the extent of pyrrole polymerisation) on the electrode was proportional to the absorbance of the N–H stretching band at 1600 cm^{-1} .

2.3. HTM measurements of yeast with MIP-modified SPEs

The Molecularly Imprinted Polymers polymerised SPEs (MIP-modified SPEs) were cut into squares ($1 \times 1\text{ cm}^2$) around the working electrode. These were pressed onto a copper block and mounted into a 3D printed flow cell with an inner volume of $110\text{ }\mu\text{L}$ that was designed in house, where a glass slide of the same size was used to create a seal. This cell was sealed off with an O-ring and connected to the HTM set up that is described by van Grinsven *et al.* [51]. The copper block, which serves as a heat sink, is actively steered with a Proportional-Integral-Derivative (PID) controller. PID parameters can significantly affect the response recorded and therefore were kept at constant, optimised values of $P = 1$, $I = 14$, $D = 0.3$ [26].

The thermal resistance (R_{th} – Eq. (1)) at the solid–liquid interface was calculated by subtracting the controlled input temperature of the copper block (T_1) from the temperature of the solution T_2 , measured at 1.7 mm above the electrode surface, divided by the power (P) given to the heat source to maintain the required experimental temperature. The temperature in the liquid (T_2) was measured every second with a type K thermocouple at 1.7 mm above the chip surface.

$$R_{th} = \frac{T_1 - T_2}{P}$$

Equation (1)- Description of how to calculate the thermal resistance

Previous research has shown that changes at the solid–liquid interface result in a change in R_{th} . In the case of MIPs, the “pore blocking model” [52] demonstrates how binding of the target to

the cavities in the polymer leads to an increase in R_{th} . All experiments were conducted at 37 ± 0.02 °C, except for one experiment carried out at 50.00 ± 0.02 °C to determine if higher temperatures increase binding to the surface (Supporting Information S-2). However, no significant change in the measured R_{th} was found which could be due to disintegration of the yeast at elevated temperatures [28].

The MIP-modified SPE were stabilised in PBS for at least 45 min after which a second injection of PBS was performed to establish a stable baseline. Subsequently, at 30 min intervals, suspensions of increasing yeast concentrations (1.0×10^2 , 1.0×10^3 , 1.0×10^4 , 1.0×10^5 , 1.0×10^6 and 1.0×10^7 CFU/mL) in deionised water were added into the flow cell with an automated NE500 programmable syringe pump (Prosense, Oosterhout, the Netherlands). The solutions were injected at intervals of 30 min, with an injection volume of 3 mL being injected with a flow rate of 1.975 mm/min. The thermal resistance was monitored over time and determined at each concentration. This was used to construct dose–response curves, where the limit of detection was calculated using the three-sigma method in the linear range of the sensor. To establish the specificity of the sensor platform, identical measurements were performed with a NIP-modified SPE.

3. Results

3.1. IR and SEM analyses to determine surface structure of MIP-modified SPEs

Firstly, the formation and deposition of PPy on the surface of the electrode material was investigated. The substrate of choice for the final sensor platform was a SPCE; however, this substrate is notoriously difficult to analyse due to its large, rough surface area and high absorbance. Therefore, to analyse the initial deposition technique, it was first performed using a gold substrate. PPy layers were formed on this substrate using chronoamperometry for different periods of time (0, 30, 60 and 120 s) to monitor the growth of the polymer layer. This

was achieved by placing the electrode in the solution specified above and held at + 0.98 V vs. Ag|AgCl for the specified amount of time. The FTIR spectra for the different polymerisation times is presented in Fig. 1 A, where the increase in the peak at 1600 cm^{-1} , corresponding to N–H stretching, confirms an increase in the amount of PPy on the surface of the electrode. The IR absorption bands of the electrode composition (e.g. the ester carbonyl stretch of the binder at ca. 1730 cm^{-1}) are unaffected by the PPy [53]. As expected, the longer the system was subjected to the potential, the thicker the layer of PPy formed on the surface as seen by the increase in absorbance of the peak.

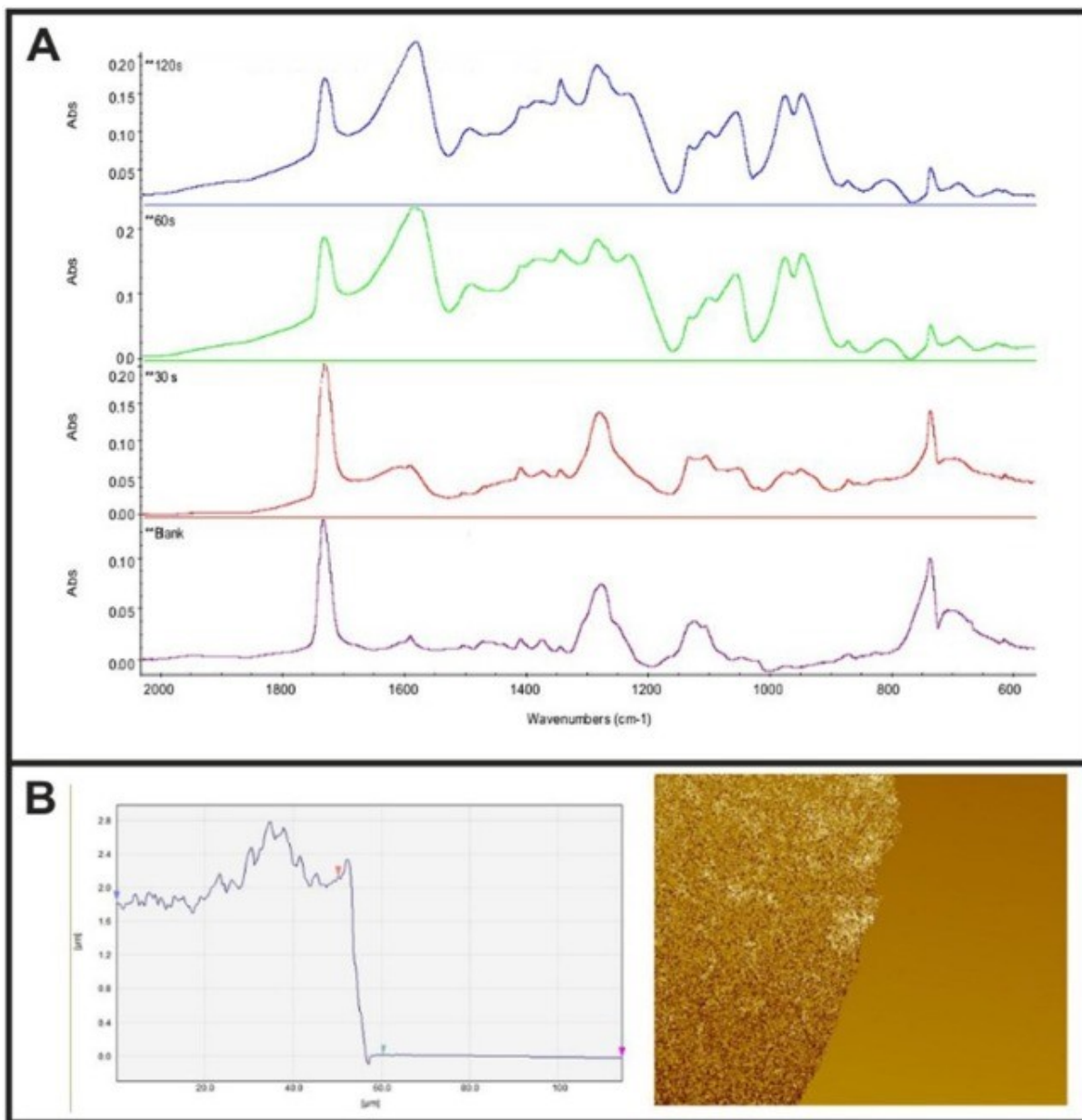
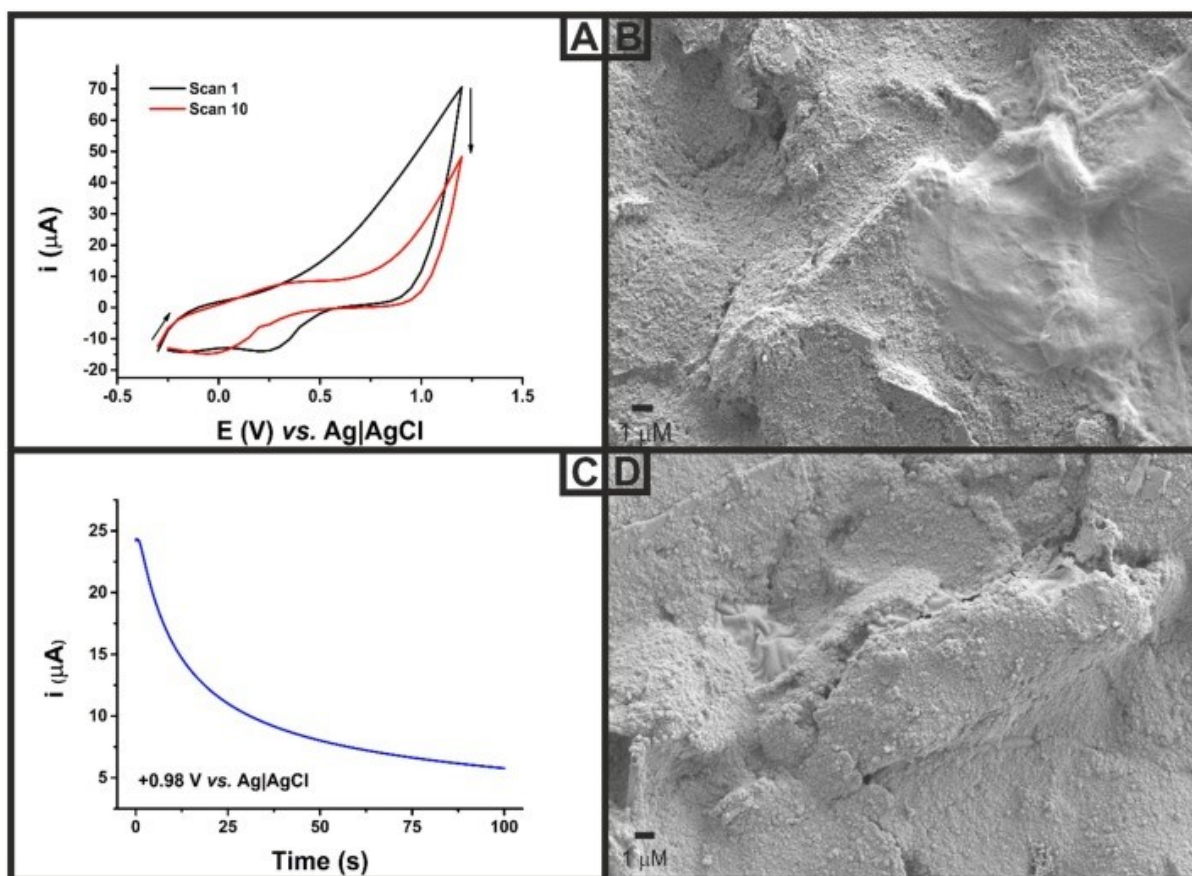


Fig. 1. A) FTIR result showing the generation of PPy on the surface of the electrode. B) White light profilometry of the PPy layer generated on the surface of the electrode.

To obtain an estimate for the thickness of the layer of PPy, an Au electrode was coated with PPy and placed under a White Light Profilometer (Fig. 1B). While the binding kinetics for

Au electrodes and SPCEs are different, this provided an indication of the layer thickness which is needed to bind the microbial cells but not too high so it hampers mass diffusion.

As seen in Fig. 1 B, the layer was non-uniform, manifesting a rough texture and an estimated thickness between 1.5 and 3 μm . It is reasonable to assume that the thickness of the layer deposited on an SPE would be thinner than this due to the slower electrode kinetics [54]. Yeast cells typically range from 5 to 10 μm in size [55], therefore a slightly longer deposition time of 100 s was chosen for sensing experiments. This would allow for the formation of cavities roughly 50% of the size of the yeast cells, suggesting that they would not be fully covered by polymer. It was important to keep the polymer layer as thin as possible, whilst still offering binding sites for yeast that were deep enough for the yeast to bind to through both size, shape



and functionality. Therefore, both cyclic voltammetric and chronoamperometric deposition methodologies were performed and compared, Fig. 2.

Fig. 2. A) Cyclic voltammograms for the formation of PPy on the surface of the SPCE performed at 100 mV s^{-1} . B) SEM image for the formation of PPy patches on the surface of the SPCE using cyclic voltammetry. C) Chronoamperomogram for the formation of a PPy layer on the surface of an SPCE at $+0.98 \text{ V vs Ag|AgCl}$ for 100 s. D) SEM image for the formation of a PPy layer on the surface of an SPCE using chronoamperometry.

As can be seen in Fig. 2, there were significant differences observed in the polymeric coverage when using cyclic voltammetry (CV) and chronoamperometry (CA). When using CV, Fig. 2A, the formation of PPy on the surface begins following the oxidation of the pyrrole monomer on the first scan. The formation of PPy can be tracked by following the decrease in the current on the oxidation scan due to the polymerisation of monomeric pyrrole into polypyrrole. This was confirmed *via* SEM, Fig. 2B, where patches of polymer can be seen although there is not a uniform coverage across the SPE surface. In comparison, when using CA, Fig. 2C, a greater coverage of polymer was observed on the surface, Fig. 2D. This was expected as while CA is run, polymer was continuously formed since it is at the oxidation potential; however, when CV was used the polymer was only formed when the potential was raised above the required oxidation potential of the monomer [56]. Both of these polymer systems were then used for the detection of yeast cells. This preparation method, whilst presently being used for thermal detection, could be suitable for electrochemical detection such as electrochemical impedance spectroscopy or differential pulse voltammetry. However, it has to be noted that thick layers are needed for microorganism detection which can hamper electrochemical detection and thermal

analysis we can make use of the full surface, including the non-conductive binder, which is expected to enhance the signal response.

3.2. Thermal resistance measurements for yeast using MIP-modified SPCEs

HTM allows for the monitoring of changes occurring at the solid–liquid interface through the change in measured thermal resistance. As such, PPy formed *via* both CV and CA imprinted with yeast cells was electrochemically deposited on the surface of SPCEs as described above; after which, the yeast cells were removed leaving specific associated cavities. SPCEs were chosen as the substrate for these sensing experiments as they offer ease of preparation for the MIPs due to the inclusion of counter and reference electrode in addition to a significant reduction in cost compared to other commonly used electrodes such as gold and glassy carbon. The functionalised SPCEs were then inserted into the flow cell presented in Fig. 3 A and sealed with a rubber O-ring and copper block. The copper block temperature was set to 37 ± 0.02 °C, in line with previous studies on proteins and real-time monitoring of organisms [26], [27]. To demonstrate proof-of-concept, a MIP-modified electrode produced with *Saccharomyces cerevisiae* laboratory strain DLY640 was measured (Supporting Information S-3). The electrode was stabilised in a buffered solution after which a suspension of *Saccharomyces cerevisiae* in PBS (1.0×10^7 CFU/mL) was added. A sharp increase in the thermal resistance was observed, which is due to binding of the yeast cells on the surface. Washing with the buffered solution did not change the signal, indicating that the yeast cells were firmly bound into cavities.

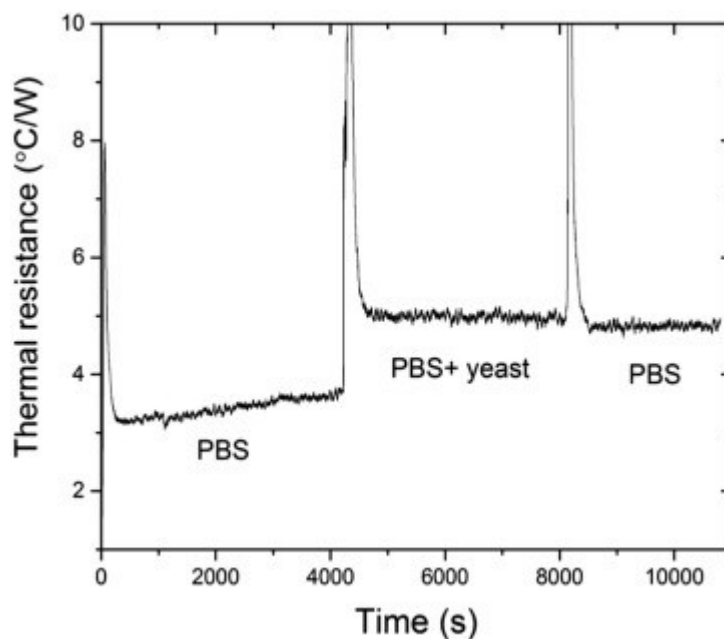


Fig. 3. A MIP-modified electrode (prepared with laboratory strain of yeast) was mounted into the HTM set up and stabilised in a standard PBS solution (pH = 7.4). While there is some minor drift in the signal, addition of a suspension of yeast (1.0×10^7 CFU/mL) in PBS led to a significant increase in the thermal resistance due to binding of yeast in the activities on the surface. This provided proof-of-concept and in following experiments, yeast from a complex mixture was considered.

Subsequently, we moved towards the yeast in a complex sample to further evaluate the specificity of the sensor platform. Initially, comparisons in the sensing proficiency for both the CV and CA MIPs were explored. An initial test was carried out to draft any initial insight to the function of the detection system. Fig. 3 displays a simplistic sample run of a single injection of complex yeast solution (followed by a PBS washing injection). A significant increase in thermal resistance gave a indication that the yeast adhered to the polymer and thus provided the first demonstration of the systems abilities.

The same procedure was used for both systems. The MIP SPE is mounted onto an O ring which upon the flow chamber, a copper block acting as the heat sink is placed on top and screwed in to consolidate the seal on the flow chamber. A blank solution of deionised water was injected to fill the flow cell, and the system allowed to reach a stable temperature for 45 min. The baseline R_{th} value was calculated from the average of the final 600 data points (10 min) prior to the injection of the first concentration of yeast cells. Following this 3 mL of the lowest concentration of yeast cells (10^2 CFU/mL) was injected into the flow cell, indicated by the sharp vertical line in the raw data plots in Fig. 4. This sharp increase in the R_{th} was due to the injection of room temperature liquid (~ 20 °C) into the system at 37 °C. After the injection was completed, the R_{th} was left to stabilise for 30 min before the next injection of analyte, thus facilitating calculation of the R_{th} from the last 600 data points of each stabilisation period.

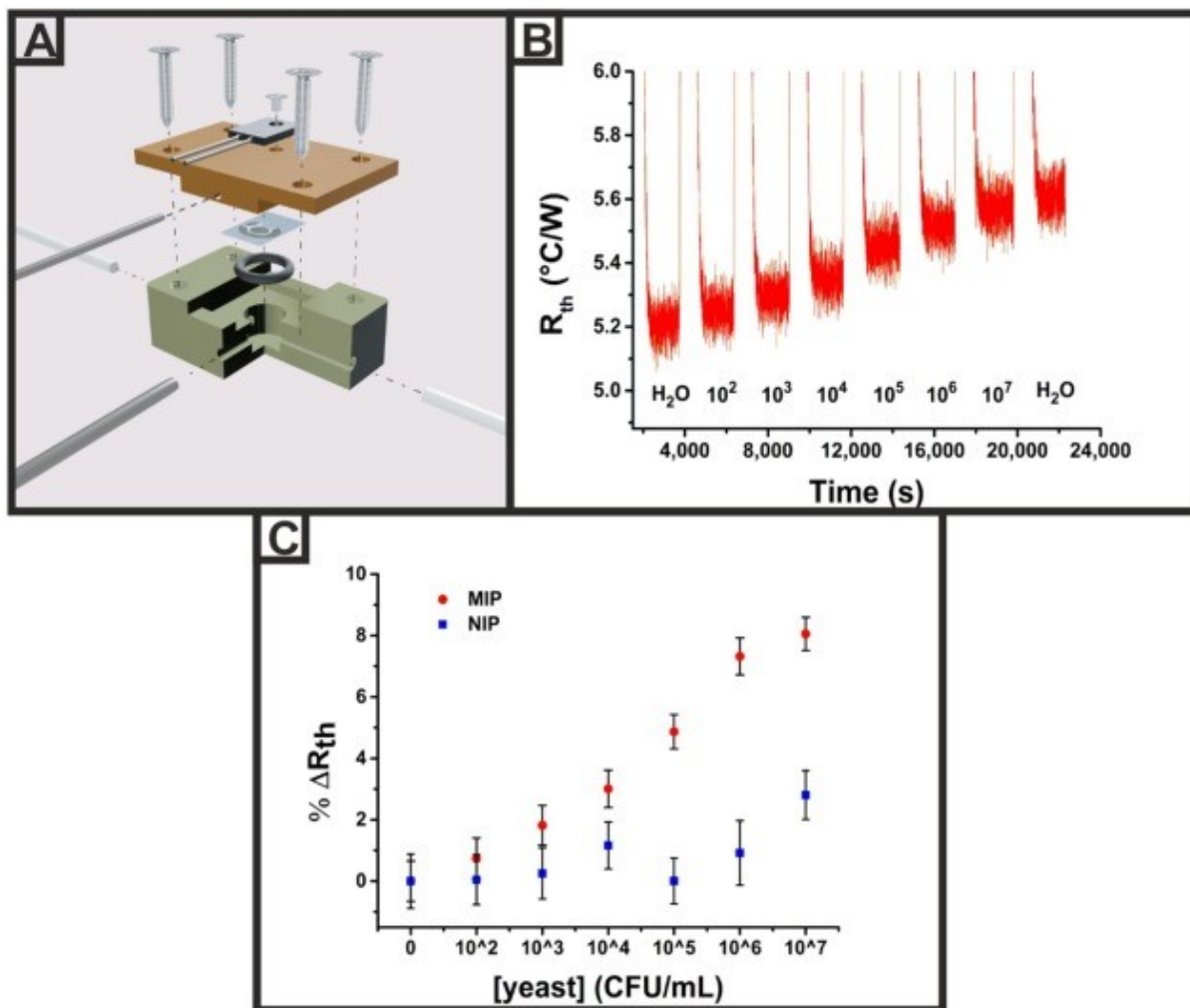


Fig. 4. A) Schematic diagram of the flow cell used throughout the thermal measurements in this work, comprising of a single thermocouple inserted into a main chamber with a flow inlet and outlet. B) HTM raw data plot of the measured R_{th} versus the time for sequential additions of yeast cells (10^2 - 10^7 CFU/mL) to a MIP-coated SPCE produced using CV. C) Plot of the change in measured R_{th} against the concentration of added yeast cells to a HTM set-up with both a MIP and NIP coated SPE.

For the CV based MIP the baseline stabilised at a value of calculated to be 5.20 ± 0.03 °C/W. After the addition of yeast cells (10^2) CFU/mL the measured R_{th} increased to 5.24 ± 0.03 °C/W. It continued to rise after further additions of yeast cells in higher concentrations, which was attributed to the binding of yeast cells to the MIP layer on the SPE surface, making transfer of heat across the interface polymer/solution more difficult. For the final addition of yeast to the system, R_{th} reached 5.61 ± 0.03 °C/W which represents an overall increase of $8 \pm 1\%$ in the R_{th} . Then, the system was injected with a blank solution of DI water and no significant increase in the measured R_{th} (5.62 ± 0.03 °C/W). This indicated that the change in the R_{th} was due to the presence of yeast cells binding to the MIP layer on the SPE and that washing with water did not cause a significant amount of yeast cells to be removed. An image obtained with the white light profilometer is shown in Supporting Information S-4, demonstrating the presence of yeast on the surface after HTM measurements with a MIP-modified electrode.

In contrast to this, the NIP-modified electrode showed little changes in the measured R_{th} for any injection of yeast into the flow cell, Fig. 3C, up to 10^6 CFU/mL. This indicated that the binding of yeast cells to the electrode surface was specific for the MIP platform and did not rely on non-specific adsorption to the surface of the polymer.

In comparison to the CV prepared platform, when CA was used the baseline stabilised at a value of 6.49 ± 0.03 °C/W, which was a higher value than that seen for CV based MIPs. This was expected due to the thicker, more uniform coverage of polymer across the SPCE surface increasing the resistance to heat-transfer across the system. For the MIP, there was an increase in the R_{th} for every addition of increased concentration of yeast until the final addition of 10^7 CFU/mL where the R_{th} stabilised at a value of 6.87 ± 0.04 °C/W. In the case of the NIP, there was an initial rise in the measured R_{th} ; however, this then reduced back to the baseline level.

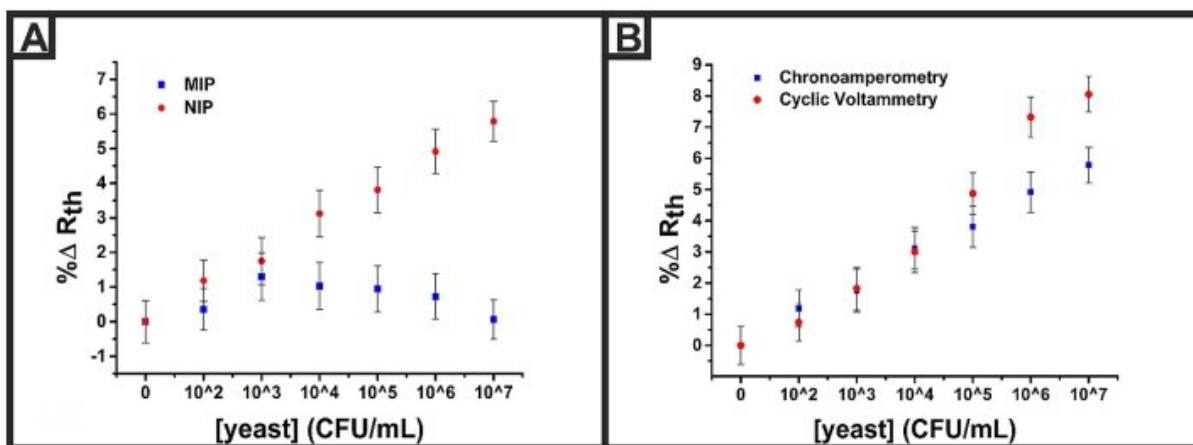


Fig. 5. A) Plot of the percentage change in the measured R_{th} against the concentration of added yeast cells to a HTM set-up with both a MIP and NIP coated SPCE using chronoamperometry. B) Plot comparing the percentage change in R_{th} for the MIP platforms produced by chronoamperometry and cyclic voltammetry. Error bars relate to the standard deviation of the experiment.

Further indication of yeast binding can be gained from Fig. 5, an image captured from a white light profilometer clearly shows yeast cells upon the surface of the MIP. This image being capture after the final injection of PBS shows that the yeast cells are not merely settled upon the surface but bonded to it.

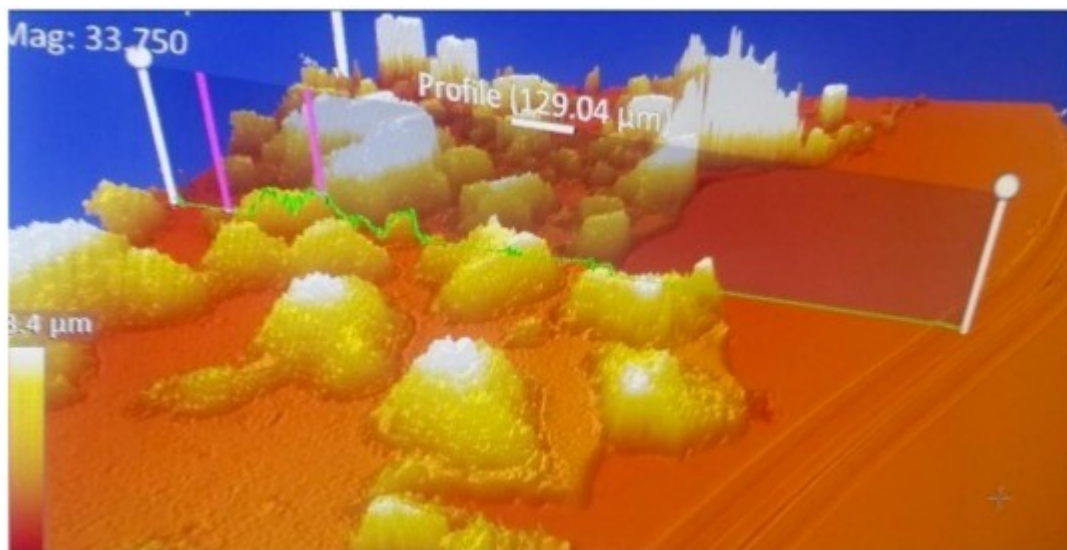


Fig. 6. Measurements with the white light profilometer of a MIP-modified electrode after HTM measurements confirmed the presence of yeast on the surface.

Both the CV and CA production methods produced a system capable of detecting the presence of yeast in the system when the MIP was present and showed minimal or no response when the NIP was present. The CV produced system exhibited a higher specificity between MIP and NIP, where the limit of detection was determined at the three-sigma method. For the system with CV, a limit of detection was determined of $10^{1.25 \pm 0.09}$ CFU/mL, whereas this compared to a limit of detection of $10^{1.12 \pm 0.07}$ CFU/mL for CA, which are well below the concentrations found in the brewing process of $\sim 10^4$ – 10^6 CFU/mL [57]. The data in Fig. 4B confirm that at low concentrations the response is similar whereas the polymers produced using CV have higher response at higher concentration, suggesting a higher binding capacity. This could be due to higher surface area of the electrodes produced in this manner, although

for detection of macromolecules it would normally be preferred to have a dense layer covering the surface to minimise non-specific binding by similar microorganisms or interferents from the matrix structure. Issues associated with MIP synthesis for larger biomolecules has been widely reported on. Whether it is the challenges faced by protein imprinting due to their poor structural resilience and restricted synthetic routes [47] or the obstacles of cell (e.g. yeast) imprinting such as the complexity and fragility of cells, coupled with their fluidity [58]. This study joins the founding insight into the future ease of application of MIPs to templates of a significantly larger size and more complex physical state. In the future, more work on understanding the surface structure of electropolymerised MIPs is needed to understand how it impacts on the specificity and selectivity of binding of macromolecules.

4. Conclusions

MIPs and reference NIPs for the detection of yeast were deposited onto SPCEs using cyclic voltammetry and chronoamperometry. To optimise the synthesis procedure, MIPs were prepared using at *Saccharomyces cerevisiae* laboratory strain DLY640 which is free from interferents, allowing to study the layer thickness and surface structure by using IR and SEM analysis. It was shown that with cyclic voltammetry a “patch-type” structure was formed, with polymer mainly forming around the ridges of the SPCEs. In contrast, if CA was used, a thick homogeneous coating was formed with an estimated layer thickness of several microns, which is sufficient to incorporate the yeast cells. SPCEs coated with both methods were mounted into our home-made thermal device, where the response of the thermal signal was used to monitor binding of yeast from a commercial baker’s yeast sample (Allinson’s Easy Bake) to demonstrate proof-of-concept. A significant response in the thermal resistance was observed from the MIP, contrary to reference NIP electrodes, demonstrating the change in signal was due to binding of yeast in the imprinted cavities.

Electrodeposition of MIPs onto the SPCEs led to sensors with similar levels of detection attained,; however, the polymers produced using CA had a higher binding capacity. These levels of detection are within the relevant range in the brewing industry, suitable for in-situ monitoring in fermenters, or to determine the yeast presence in food samples [59]. This preparation method could be suitable for electrochemical detection such as EIS (along with pore blocking theory) or using DPV. The change in electrochemical impedance or reduction in obtained signal using other methods will be highly dependant on many factors not only layer thickness (electrolyte, deposition method, electrode, adhesion all play roles). This means the thermal detection method Is more flexible and requires less optimisation. Could just mention that a comparison could be interesting for future work. The advantage of the method proposed in this project is that it is fast, low-cost, and portable, providing it with high commercial potential, and demonstrating that analysis of heat-transfer analysis can play a vital role in the biosensor community. Due to the versatility of the molecular imprinting technology, in the future this can be expanded to other relevant objects such as macromolecules, bacteria and eukaryotic cells which will open many other applications beyond the food industry.

Declaration of Competing Interest

The authors declare that they have no known competing financial interests or personal relationships that could have appeared to influence the work reported in this paper.

Acknowledgements

I would like to acknowledge the EPSRC (EP/R029296/1) for salary of Dr Hudson and Dr Foster for production of the SPEs. JG thanks Conselho Nacional de Desenvolvimento Científico e Tecnológico (CNPq) (Proc. n° 424027/2018-6 and 307501/2019-1) for financial support.

References

- [1] S. Pedley, G. Howard, The public health implications of microbiological contamination of groundwater, *Q. J. Eng. Geol. Hydrogeol.* 30 (2) (1997) 179–188.
- [2] Y. Wadamori, R. Gooneratne, M.A. Hussain, Outbreaks and factors influencing microbiological contamination of fresh produce, *J. Sci. Food Agric.* 97 (5) (2017) 1396–1403.
- [3] C. Dacarro, A. Picco, P. Grisoli, M. Rodolfi, Determination of aerial microbiological contamination in scholastic sports environments, *J. Appl. Microbiol.* 95 (5) (2003) 904–912.
- [4] L. Kallings, O. Ringertz, L. Silverstolpe, Microbiological contamination of medical preparations, *Acta Pharmaceutica Suecica* 3 (3) (1966) 219.
- [5] N.S. Geweely, Evaluation of ozone for preventing fungal influenced corrosion of reinforced concrete bridges over the River Nile, Egypt, *Biodegradation* 22 (2) (2011) 243–252.
- [6] S. Magnússon, H. Gunnlaugsdo'ttir, H. van Loveren, F. Holm, N. Kalogeras, O. Leino, J. Luteijn, G. Odekerken, M. Pohjola, M. Tjihuis, State of the art in benefit–risk analysis: food microbiology, *Food Chem. Toxicol.* 50 (1) (2012) 33–39.
- [7] S. Akhtar, M.R. Sarker, A. Hossain, Microbiological food safety: a dilemma of developing societies, *Crit. Rev. Microbiol.* 40 (4) (2014) 348–359.
- [8] J. Gruber, H.M. Nascimento, E.Y. Yamauchi, R.W. Li, C.H. Esteves, G.P. Rehder, C. C. Gaylarde, M.A. Shirakawa, A conductive polymer based electronic nose for early detection of *Penicillium digitatum* in post-harvest oranges, *Mater. Sci. Eng., C* 33 (5) (2013) 2766–2769.
- [9] P.D. Skottrup, M. Nicolaisen, A.F. Justesen, Towards on-site pathogen detection using antibody-based sensors, *Biosens. Bioelectron.* 24 (3) (2008) 339–348.

- [10] F.S. Felix, L. Angnes, Electrochemical immunosensors—a powerful tool for analytical applications, *Biosens. Bioelectron.* 102 (2018) 470–478.
- [11] O.A. Sadik, J.M. Van Emon, Applications of electrochemical immunosensors to environmental monitoring, *Biosens. Bioelectron.* 11 (8) (1996) i–x.
- [12] S. Banta, K. Dooley, O. Shur, Replacing antibodies: engineering new binding proteins, *Annu. Rev. Biomed. Eng.* 15 (2013) 93–113.
- [13] A.C. Gray, A.R. Bradbury, A. Knappik, A. Plückthun, C.A. Borrebaeck, S. Dübel, Animal-derived-antibody generation faces strict reform in accordance with European Union policy on animal use, *Nat. Methods* 17 (8) (2020) 755–756.
- [14] J. Wackerlig, P.A. Lieberzeit, Molecularly imprinted polymer nanoparticles in chemical sensing—synthesis, characterisation and application, *Sens. Actuators, B* 207 (2015) 144–157.
- [15] M. Jia, Z. Zhang, J. Li, X. Ma, L. Chen, X. Yang, Molecular imprinting technology for microorganism analysis, *TrAC, Trends Anal. Chem.* 106 (2018) 190–201.
- [16] J.W. Lowdon, H. Diliën, P. Singla, M. Peeters, T.J. Cleij, B. van Grinsven, K. Eersels, MIPs for commercial application in low-cost sensors and assays—an overview of the current Status Quo, *Sens. Actuators B: Chem.* (2020) 128973.
- [17] K. Haupt, K. Mosbach, Molecularly imprinted polymers and their use in biomimetic sensors, *Chem. Rev.* 100 (7) (2000) 2495–2504.
- [18] J.J. Bel Bruno, Molecularly imprinted polymers, *Chem. Rev.* 119 (1) (2018) 94–119.
- [19] B. Sellergren, A.J. Hall, Molecularly imprinted polymers, *Supramolecular chemistry: from molecules to nanomaterials*, (2012).
- [20] A. Rico-Yuste, S. Carrasco, Molecularly imprinted polymer-based hybrid

materials for the development of optical sensors, *Polymers* 11 (7) (2019) 1173.

- [21] R. Gui, H. Jin, H. Guo, Z. Wang, Recent advances and future prospects in molecularly imprinted polymers-based electrochemical biosensors, *Biosens. Bioelectron.* 100 (2018) 56–70.

- [22] H. Diliën, M. Peeters, J. Royakkers, J. Harings, P. Cornelis, P. Wagner, E. Steen Redeker, C.E. Banks, K. Eersels, B. van Grinsven, Label-free detection of small organic molecules by molecularly imprinted polymer functionalized thermocouples: toward in vivo applications, *ACS Sens.* 2 (4) (2017) 583–589.
- [23] S. Ansari, Combination of molecularly imprinted polymers and carbon nanomaterials as a versatile biosensing tool in sample analysis: recent applications and challenges, *TrAC, Trends Anal. Chem.* 93 (2017) 134–151.
- [24] K. Betlem, I. Mahmood, R. Seixas, I. Sadiki, R. Raimbault, C. Foster, R. Crapnell, S. Tedesco, C. Banks, J. Gruber, Evaluating the temperature dependence of heat-transfer based detection: a case study with caffeine and Molecularly Imprinted Polymers as synthetic receptors, *Chem. Eng. J.* 359 (2019) 505–517.
- [25] F. Canfarotta, J. Czulak, K. Betlem, A. Sachdeva, K. Eersels, B. Van Grinsven, T. Cleij, M. Peeters, A novel thermal detection method based on molecularly imprinted nanoparticles as recognition elements, *Nanoscale* 10 (4) (2018) 2081–2089.
- [26] R.D. Crapnell, F. Canfarotta, J. Czulak, R. Johnson, K. Betlem, F. Mecozzi, M.P. Down, K. Eersels, B. van Grinsven, T.J. Cleij, Thermal detection of cardiac biomarkers heart-fatty acid binding protein and ST2 using a molecularly imprinted nanoparticle-based multiplex sensor platform, *ACS Sens.* 4 (10) (2019) 2838–2845.
- [27] K. Betlem, A. Kaur, A.D. Hudson, R.D. Crapnell, G. Hurst, P. Singla, M. Zubko, S. Tedesco, C.E. Banks, K. Whitehead, Heat-transfer method: a thermal analysis technique for the real-time monitoring of *Staphylococcus aureus* growth in buffered solutions and digestate samples, *ACS Appl. Bio Mater.* 2 (9) (2019) 3790–3798.

- [28] K. Betlem, S. Hoksbergen, N. Mansouri, M. Down, P. Losada-Pérez, K. Eersels, B. Van Grinsven, T.J. Cleij, P. Kelly, D. Sawtell, Real-time analysis of microbial growth by means of the Heat-Transfer Method (HTM) using *Saccharomyces cerevisiae* as model organism, *Phys. Med.* 6 (2018) 1–8.
- [29] D. Yongabi, M. Khorshid, P. Losada-Pérez, K. Eersels, O. Deschaume, J. D’Haen, C. Bartic, J. Hooyberghs, R. Thoelen, M. Wübbenhorst, Cell detection by surface imprinted polymers SIPs: a study to unravel the recognition mechanisms, *Sens. Actuators, B* 255 (2018) 907–917.
- [30] O. Hayden, F.L. Dickert, Selective microorganism detection with cell surface imprinted polymers, *Adv. Mater.* 13 (19) (2001) 1480–1483.
- [31] R.D. Crapnell A. Hudson C.W. Foster K. Eersels B.v. Grinsven, T.J. Cleij, C.E. Banks, M. Peeters, Recent advances in electrosynthesized molecularly imprinted polymer sensing platforms for bioanalyte detection *Sensors* 19(5) (2019) 1204.
- [32] V.K. Gupta, M.L. Yola, N. Özalp, N. Atar, Z. Üstündağ, L. Uzun, Molecular imprinted polypyrrole modified glassy carbon electrode for the determination of tobramycin, *Electrochim. Acta* 112 (2013) 37–43.
- [33] E. Mathieu-Scheers, S. Bouden, C. Grillot, J. Nicolle, F. Warmont, V. Bertagna, B. Cagnon, C. Vautrin-UI, Trace anthracene electrochemical detection based on electropolymerized-molecularly imprinted polypyrrole modified glassy carbon electrode, *J. Electroanal. Chem.* 848 (2019), 113253.
- [34] Y. Wu, P. Deng, Y. Tian, Z. Ding, G. Li, J. Liu, Z. Zuberi, Q. He, Rapid recognition and determination of tryptophan by carbon nanotubes and molecularly imprinted polymer-modified glassy carbon electrode, *Bioelectrochemistry* 131 (2020), 107393.
- [35] L. Li, L. Yang, Z. Xing, X. Lu, X. Kan, Surface molecularly imprinted

- polymers-based electrochemical sensor for bovine hemoglobin recognition, *Analyst* 138 (22) (2013) 6962–6968.
- [36] S. Menon, S. Jesny, K.G. Kumar, A voltammetric sensor for acetaminophen based on electropolymerized-molecularly imprinted poly (o-aminophenol) modified gold electrode, *Talanta* 179 (2018) 668–675.
- [37] T. Wang, C. Shannon, Electrochemical sensors based on molecularly imprinted polymers grafted onto gold electrodes using click chemistry, *Anal. Chim. Acta* 708 (1–2) (2011) 37–43.
- [38] R.A. Couto, S.S. Costa, B. Mounsef Jr, J.G. Pacheco, E. Fernandes, F. Carvalho, C. M. Rodrigues, C. Delerue-Matos, A.A. Braga, L.M. Goncalves, Electrochemical sensing of ecstasy with electropolymerized molecularly imprinted poly (o- phenylenediamine) polymer on the surface of disposable screen-printed carbon electrodes, *Sens. Actuators, B* 290 (2019) 378–386.
- [39] V.M. Ekomo, C. Branger, R. Bikanga, A.-M. Florea, G. Istamboulie, C. Calas- Blanchard, T. Noguier, A. Sarbu, H. Brisset, Detection of Bisphenol A in aqueous medium by screen printed carbon electrodes incorporating electrochemical molecularly imprinted polymers, *Biosens. Bioelectron.* 112 (2018) 156–161.
- [40] H. Zhang, G. Liu, C. Chai, A novel amperometric sensor based on screen-printed electrode modified with multi-walled carbon nanotubes and molecularly imprinted membrane for rapid determination of ractopamine in pig urine, *Sens. Actuators, B* 168 (2012) 103–110.
- [41] C.W. Foster, J.P. Metters, D.K. Kampouris, C.E. Banks, Ultraflexible screen-printed graphitic electroanalytical sensing platforms, *Electroanalysis* 26 (2) (2014) 262–274.
- [42] R.O. Kadara, N. Jenkinson, C.E. Banks, Characterization and fabrication of disposable screen printed microelectrodes, *Electrochem. Commun.* 11 (7) (2009) 1377–1380.

- [43] O. Jamieson, T.C. Soares, B.A.d. Faria, A. Hudson, F. Mecozzi, S.J. Rowley-Neale, C.E. Banks, J. Gruber, K. Novakovic, M. Peeters, Screen printed electrode based detection systems for the antibiotic amoxicillin in aqueous samples utilising molecularly imprinted polymers as synthetic receptors, *Chemosensors* 8 (1) (2020) 5.
- [44] S. Casadio, J. Lowdon, K. Betlem, J. Ueta, C.W. Foster, T. Cleij, B. van Grinsven, O. Sutcliffe, C.E. Banks, M. Peeters, Development of a novel flexible polymer-based biosensor platform for the thermal detection of noradrenaline in aqueous solutions, *Chem. Eng. J.* 315 (2017) 459–468.

- [45] R. Viter, K. Kunene, P. Genys, D. Jevdokimovs, D. Ertz, A. Sutka, K. Bisetty, A. Viksna, A. Ramanaviciene, A. Ramanavicius, Photoelectrochemical bisphenol S sensor based on ZnO-nanoroads modified by molecularly imprinted polypyrrole, *Macromol. Chem. Phys.* 221 (2) (2020) 1900232.
- [46] S. Ramanavicius, A. Ramanavicius, Conducting polymers in the design of biosensors and biofuel cells, *Polymers* 13 (1) (2021) 49.
- [47] R.D. Crapnell, N.C. Dempsey-Hibbert, M. Peeters, A. Tridente, C.E. Banks, Molecularly imprinted polymer based electrochemical biosensors: Overcoming the challenges of detecting vital biomarkers and speeding up diagnosis, *Talanta Open* (2020), 100018.
- [48] J.S. Wood, L.H. Hartwell, A dependent pathway of gene functions leading to chromosome segregation in *Saccharomyces cerevisiae*, *J. Cell Biol.* 94 (3) (1982) 718–726.
- [49] L. Maringele, D. Lydall, EXO1-dependent single-stranded DNA at telomeres activates subsets of DNA damage and spindle checkpoint pathways in budding yeast *yku70Δ* mutants, *Genes Dev.* 16 (15) (2002) 1919–1933.
- [50] D. Burke, D. Dawson, T. Stearns, *Methods in Yeast Genetics: A Cold Spring Harbor Laboratory Course Manual*, 2000 Edition, Cold Spring Harbor Laboratory Press. [Google Scholar], Plainview, NY, 2000.
- [51] B. Van Grinsven, N. Vanden Bon, H. Strauven, L. Grieten, M. Murib, K.L. Jim'enez Monroy, S.D. Janssens, K. Haenen, M.J. Scho'ning, V. Vermeeren, Heat-transfer resistance at solid–liquid interfaces: a tool for the detection of single-nucleotide polymorphisms in DNA, *ACS Nano* 6 (3) (2012) 2712–2721.
- [52] M. Peeters, P. Csipai, B. Geerets, A. Weustenraed, B. Van Grinsven, R. Thoelen,

- J. Gruber, W. De Ceuninck, T. Cleij, F. Troost, Heat-transfer-based detection of L nicotine, histamine, and serotonin using molecularly imprinted polymers as biomimetic receptors, *Anal. Bioanal. Chem.* 405 (20) (2013) 6453–6460.
- [53] A. Yussuf, M. Al-Saleh, S. Al-Enezi, G. Abraham, Synthesis and characterization of conductive polypyrrole: the influence of the oxidants and monomer on the electrical, thermal, and morphological properties, *Int. J. Polymer Sci.* (2018).
- [54] E.P. Randviir, A cross examination of electron transfer rate constants for carbon screen-printed electrodes using Electrochemical Impedance Spectroscopy and cyclic voltammetry, *Electrochim. Acta* 286 (2018) 179–186.
- [55] M. Zakhartsev, M. Reuss, Cell size and morphological properties of yeast *Saccharomyces cerevisiae* in relation to growth temperature, *FEMS Yeast Res.* 18 (6) (2018) foy052.
- [56] P.K. Sharma, G. Gupta, V.V. Singh, B. Tripathi, P. Pandey, M. Boopathi, B. Singh, R. Vijayaraghavan, Synthesis and characterization of polypyrrole by cyclic voltammetry at different scan rate and its use in electrochemical reduction of the simulant of nerve agents, *Synth. Met.* 160 (23–24) (2010) 2631–2637.
- [57] F.B. Pilo', E.J. Carvajal-Barriga, M.C. Guama'n-Burneo, P. Portero-Barahona, A.M. M. Dias, L.F.D.d. Freitas, F.d.C.O. Gomes, C.A. Rosa, *Saccharomyces cerevisiae* populations and other yeasts associated with indigenous beers (chicha) of Ecuador, *Braz. J. Microbiol.* 49 (4) (2018) 808–815.
- [58] J. Pan, W. Chen, Y. Ma, G. Pan, Molecularly imprinted polymers as receptor mimics for selective cell recognition, *Chem. Soc. Rev.* 47 (15) (2018) 5574–5587.
- L.R. Beuchat, Media for detecting and enumerating yeasts and moulds, *Int. J. Food Microbiol.* 17 (2) (1992) 145–158

[59] .

